QATAR UNIVERSITY

COLLEGE OF ARTS AND SCIENCES

The development of novel composite materials of modified roasted date pits using ferrocyanides for the recovery of valuable metal ions from seawater reverse osmosis brine.

BY

Rana Said Alabsi

A Thesis Submitted to

the College of Arts and Sciences

in Partial Fulfillment of the Requirements for the Degree of

Masters of Science in Master of Science in Environmental Sciences

June 2021

COMMITTEE PAGE

The members of the Committee approve the Thesis of
Rana S. Alabsi defended on [Defense Date].

Prof. Mohammad Al-Ghouti
Thesis Supervisor

Prof. Mohammed Abu-Dieyeh
Co-supervisor

Dr. Radhouane Ben-Hamadou
Committee Member

Dr. Mustafa Nasser
Committee Member

Approved:

Ibrahim AlKaabi, Dean, College of Arts and Sciences

ABSTRACT

Alabsi, Rana, S. Masters: June : 2021, Master of Science in Environmental Sciences

Title: The development of novel composite materials of modified roasted date pits using ferrocyanides for the recovery of valuable metal ions from seawater reverse osmosis brine.

Supervisor of Thesis: Mohammad, A, Al-Ghouti.

In this project, novel composite materials from modified roasted date pits using ferrocyanides were developed and investigated for the recovery of valuable metal ions (Li^{+} and Sr^{2+}) from seawater reverse osmosis (RO) brine. Three adsorbents were prepared, namely roasted date pits (RDP), potassium copper hexacyanoferrate, and potassium nickel hexacyanoferrate – date pits composites (RDP-FC-Cu and RDP-FC-Ni). The physicochemical characteristics of the RO desalination brine and the adsorbents were determined. Various analytical techniques were used such as Inductively coupled plasma atomic emission spectroscopy (ICP-AES), Scanning Electron Microscopy (SEM) with Energy Dispersive X-Ray Analysis (EDX), X-ray powder diffraction (XRD), Fourier-transform infrared spectroscopy (FTIR) as well as pH, salinity, conductivity, particle size distribution test, Brunauer–Emmett– Teller (BET) surface area, and pore size distribution. The RO brine was found to be highly saline, have a crystal structure, and contain a variety of metals as well as salts. RDP-FC-Cu and RDP-FC-Ni exhibited enhanced chemical and physical characteristics than RDP. The optimum pH, metal-ion initial concentration, and temperature for all adsorbents were pH 6, 100 mg/L, and 45°C, respectively. The RDP-FC-Cu and RDP-FC-Ni achieved higher adsorption capacities and efficiencies towards lithium ions than RDP at all the studied pH, concentration ranges as well as temperatures. The RDP-FC-Cu was found to be more selective towards lithium than strontium with higher

adsorption capabilities than RDP-FC-Ni. To compare, RDP-FC-Ni was more selective towards strontium. All the prepared adsorbents showed high selectivity towards lithium and strontium from the reverse osmosis brine. The adsorption thermodynamics such as Gibbs free energy (ΔG^o), enthalpy (ΔH^o), and entropy (ΔS^o) revealed that the adsorption process of lithium and strontium onto RDP, RDP-FC-Cu, and RDP-FC-Ni were endothermic, spontaneous, and favorable. Furthermore, the adsorption mechanism was well-fitted to Langmuir and Freundlich adsorption isotherms.

DEDICATION

I dedicate my thesis to the dreamers, and the doers, the believers, and the thinkers and especially to those who saw greatness in me even when I did not see it myself. To my beloved husband, mother, father, siblings, and the many friends who supported, believed in me and made this achievement possible: love and unlimited gratitude.

ACKNOWLEDGMENTS

First and foremost, praise and thanks to Allah for his showers of blessings throughout my research work to complete the research successfully.

I would like to express my deep and sincere gratitude to my thesis supervisor, Prof. Mohammad Al-Ghouti, for giving me the opportunity to do this research and providing valuable guidance and support throughout this research. His dynamism, vision, sincerity, and motivation have deeply inspired me. He has taught me the methodology to carry out the research and to present the research works as clearly as possible. It was a great privilege and honor to work and study under his guidance. I am also thankful for the continuous guidance and advice that I received from my committee members, Prof. Mohammad Abu-Dieyeh, Dr. Radhouane Ben-Hamadou, and Dr. Mustafa Nasser.

I would like to thank my friends and colleagues in the MSc Environmental Science program, Ghaida Odeh, Sara Wahib, and Lubna Zarif who provided me with valuable knowledge and were always there to help, advise and motivate me. Special thanks go to the research assistances, Ms. Dana Da'ana and Mariam Khan, for their guidance and assistance in carrying on the experiments of this research.

Finally, I am extending my thanks to the Gas Processing Center (GPC), Materials Science Center (MSC), and the Central Laboratories Unit (CLU) at Qatar University as well as Qatar Environment & Energy Research Institute (QEERI) for providing the necessary equipment and analysis for the results of this research.

TABLE OF CONTENTS

LIST OF TABLES

LIST OF FIGURES

CHAPTER 1: INTRODUCTION

1.1 Introduction

Water availability on earth is greatly impacted by natural causes like aridity, seasonal changes, climate change as well as topographic and geographic locations (Habiyaremye, 2020; Mvulirwenande and When, 2020). The environmental health, population densities, development, efficiency of wastewater treatments, use of water resources, and the implementation of water management, policies, and regulations differ from country to country and contribute to the overall water supplies (Rahman and Zaidi, 2018; Honarparvar et al., 2019). As a global trend, there has been a continuous increase in population and economic growths, development, urbanization, and industrialization. These are considered human-derived factors that contribute to the overall amounts of water that are available for human use in countries. As a result, water demands in the world are increasing substantially. Consequently, many countries in Asia and Africa are experiencing increased pressures on water availability and supply (Preez and Huyssteen, 2020; Damkjaer and Taylor, 2017; Rahman and Zaidi, 2018; Pangarkar et al., 2011).

The Gulf council countries (GCC) are characterized as semi-arid to arid where rainfall and freshwater resources such as groundwater reservoirs are limited. Besides, population growths, urbanization, industrialization, improper policy implementations, intense groundwater extractions, climate change, saline intrusions, and water pollutions have been reported in the GCC (Mannan et al., 2019). However, most of these countries are surrounded by sea, which comprises the majority of their water resources (Rahman and Zaidi, 2018). One of the main reasons behind these scenarios is the continuous development of their fossil fuel industries as well as its related economic level growths (Baaloucha and Ouda, 2017).

A well-established method for providing freshwater for the countries experiencing water availability and supply issues is seawater desalination, which is a process that produces freshwater from seawater. Nowadays, seawater desalination is employed all over the world and accounts for the main or sole source of domestic and industrial freshwater in many countries. This is evident in the Gulf region where the high economic status along with the aridity would pave the way for the implementation of seawater desalination to produce potable water. Many countries like Qatar invest substantial amounts annually of their technological and financial resources in desalination research, training, and implementation to overcome their water scarcity problems (Nassrullah et al., 2020; Mannan et al., 2019; Rahman and Zaidi, 2018). Zheng and coworkers (2020) reported that during the last two decades, a major worldwide trend in employing desalination technologies to overcome the water availability issues by producing freshwater has been noticed. In the year 2000, desalination technologies were applied by around 136 regions to provide people with potable water. Most of these countries were located in the Middle East, Europe, and the United States (Schorr, 2011; Baaloucha and Ouda, 2017). The number of countries relying on desalination to a great extent remained to increase continuously after that. For example, it was estimated that in the year 2011, more than 30 million m^3/d of desalinated potable water was produced globally. Also, the economic trends of the world's spending on desalination technologies revealed that by the year 2015 the desalination industry would reach 30 billion US dollars globally (Schorr, 2011; Baaloucha and Ouda, 2017; Nassrullah et al., 2020). In the year 2015, it was reported that around 18,426 desalination plants existed around the world, which provided more than 150 countries with more than 86.8 million m^3 of freshwater. Interestingly, the North African and Middle Eastern countries compromised around 45% of the

desalination freshwater capacity provided then (Gude, 2017). Specifically, seawater desalination accounts for 99% of Qatar's accessible water, whereas groundwater meets the remaining 1%. The water per capita consumption rates in Qatar are among the highest in the world at about 500 Liters per day (Baaloucha and Ouda, 2017; Mannan et al., 2019). This could be due to many reasons like economic stability, wealth, high standards of living, availability of desalination energy and technologies, and population growth. These consumption rates are met by increasing the number of desalination plants and capacities throughout the years. For example, in 2014, the production of desalinated potable water in Qatar was around 493 million m^3. In 2017, the amount of desalted water in Qatar was estimated to be 540 million m^3 (Baaloucha and Ouda, 2017; Mannan et al., 2019; Rahman and Zaidi, 2018). In the year 2017, the number of countries that applied desalination technologies increased to reach 231 countries. One of the most important driving forces to this trend is the fact that water demand is also increasing (Zheng et al., 2020). Like any industrial process, desalination technologies not only vary in their working principles but also in the produced outcomes. To be more specific, all desalination plants are based on the principle of de-salting or removing salts from seawater or brackish waters to produce freshwaters as a mainstream and brine solution as a secondary stream. However, their process requirements, as well as environmental impacts vary from being extremely inefficient and harmful to being efficient with the least harm to the environment (Castro et al., 2020). Selecting the most suitable desalination technology for a given country or place depends on many factors like cost, land space, outcome needed, environmental parameters, and many others. Reverse osmosis (RO) considered to be the leading membrane-based desalination technology in the GCC due to the ease of maintenance, simpler design, low cost, and environmental impacts as well as flexibility compared to other popular thermal

desalination technologies like multistage flash desalination (MSF) (Ahmadvand et al., 2019; SeaWater Desalination - Key Issues, 2020; Honarparvar et al., 2019; Castro et al., 2020). RO works by employing a high pressure over a semi-permeable membrane, which results in the separation of salts from seawater (Ahmadvand et al., 2019; Reverse Osmosis - Lenntech, 2020). However, almost all current desalination plants nowadays pose many effects on the environment, produce harmful emissions and contribute to the environmental pollution of the world (Nassrullah et al., 2020). For example, entrainment and entrapment of ecologically important marine species in the desalination plants could alter food webs and the ecosystem in which these species live (Honarparvar et al., 2019). Also, the current conventional desalination plants employ various and numerous types of pre-treatment chemicals such as coagulants and flocculants which could significantly harm the environment through leaks or improper disposal of waste streams like brine (Amy et al., 2017). This stream is a concentrated by-product salt stream from desalination technologies, which contains various substances such as pre-treatment chemicals, salts, metals, and others. A typical brine stream would be characterized by high temperatures, altered pH values, and high salinity (ElSaid et al., 2020). Today, many countries seek the direct environmental disposal of brine streams into lakes, rivers, land, oceans, and others. These methods are extremely dangerous to the environment as well as living organisms (Jones et al., 2019). Other brine management methods include conventional zero discharge brine treatment, which aims at minimizing and concentrating the volume of brine streams while recovering freshwater from them (Alnouri et al., 2018; Al-Anzi et al., 2020). Examples of these methods include forward osmosis (FO), membrane crystallizers (MCr), and multi-stage flash distillation (MSF). These methods are successful today; however, they suffer from many technical, economic, as well as environmental issues. Consequently,

the world is in desperate need of water sustainability as well as environmentally friendly approaches in meeting the freshwater needs of the ever-growing populations and protecting the environmental resources (Kim and Min, 2020). This could be achieved by employing the technique of adsorption to remove, remediate and recover harmful and valuable substances from desalination brine streams. The adsorption technique is based on the use of a solid material referred to as an adsorbent that receives the target mineral known as adsorbate on its surface (Vardhan et al., 2019). The surface of adsorbents should contain pores known as adsorption active sites, which the adsorbate material bonds chemically or physically. The chemical bonding between the adsorbate and adsorbent is characterized by the formation of strong irreversible covalent bonds. On the other hand, the forces of attraction between the adsorbent and adsorbate molecules that occur in a physical adsorption bonding are due to the weaker van Der Waals forces (Al-Ghouti and Al-Absi, 2020). Many factors like adsorbate characteristics, concentration, adsorbent surface area, and others can significantly affect the level of adsorption capacity and achieving an efficient removal of pollutants and valuable materials from brines. Also, the presence of many metals of competing nature to the target metal could greatly affect the adsorption process (Li et al., 2020; Gao et al., 2009). This is due to the fact that some metals, due to their characteristics and the surrounding conditions, would be more attracted to the adsorbent material in terms of the formation of chemical or physical bonds (Fotoohi and Mercier, 2014; Gao et al., 2009). There are a variety of well-established adsorbents for the remediation of pollutants like dyes, gases, metals, and others from brines. Examples of these adsorbents include chitosan, alumina, and activated carbon. Many of these adsorbents must undergo a variety of modification processes in order to show high adsorptive capacities towards pollutants, which could make them as pollutants. Therefore, their

worldwide application remains challenging (Al-Saad et al., 2019). Scientists are seeking natural-based effective adsorbents that do not pose risks to the environment and cost-friendly. Examples of such adsorbents could be natural agricultural wastes such as maize cob, coconut sawdust, silk cotton hull, and fruit pits (Yadav et al., 2021). Qatar is one of the leading countries in the production of dates and this sector produces massive amounts of date pits as waste annually. Date pits could demonstrate great adsorptive potentials towards many pollutants and in particular valuable metals from brines due to their carbonaceous compositions and porous structures (Al-Saad et al., 2019). As mentioned previously, Qatar relies heavily on desalination in order to meet its national freshwater needs. Therefore, date pits could be sustainably used to remediate the reverse osmosis brine streams produced from Qatari desalination plants (Al-Ghouti et al., 2019). This would facilitate the effective, cost-efficient, and environmentally friendly remediation of two of the major waste products in Qatar brines and date pits. Utilizing fruit pits for adsorption processes could provide countries with flexibilities in terms of their usage in order to obtain efficient adsorption of pollutants. For example, simple roasting of fruit pits has been proven by studies to be effective adsorbents toward a variety of pollutants. Roasting of agricultural wastes would enhance their adsorptive properties due to enhanced carbonaceous composition, structure, surface area, and pore sizes (Al-Ghouti and Al-Absi, 2020). Also, fruit pits could be used as support materials for more effective adsorbents like metal hexacyanoferrates, which are coordination polymers that contain coordinated bridges of C≡N and a transition metal ion like Cu^{2+}, Fe^{3+}, Co^{2+}, and Ni^{2+} (Oliveira et al., 2018). Metal hexacyanoferrates (MHCFs) have a unique cubic lattice structure that would facilitate the adsorption of pollutants like valuable metals by an ion-exchange mechanism between the transition metal and the target pollutant (Wang et al., 2018).

These materials are commonly applied in metal extraction, recovery, and adsorption due to their insolubility, high selectivity, and adsorptive capacities. Almost all the synthesis methods of MHCFs are cost-effective and simple, with the most employed method is initiating a precipitation reaction between the precursors of hexacyanoferrate and the transition metals (Kim et al., 2017).

1.2 Research focus and rationale

Utilizing date pits in the recovery of valuable metals from reverse osmosis desalination brines has a great sustainability potential, especially in Qatar. However, according to the current study, combining the adsorptive capabilities of date pits with metal hexacyanoferrates could further provide a more efficient and cost-friendly approach in decreasing date pit waste, brine streams as well as recovering valuable metals from brine. Nowadays, lithium is used in a variety of fields like lithium-ion batteries, greases, polymers, ceramics, and metal additives (Gaztañaga et al., 2020). On the other hand, strontium is an alkaline earth metal that could be used in the pharmaceutical industry and manufacturing glass and ceramics (Liu et al., 2019). Due to the high demands on lithium and strontium-containing products, their extraction from hard rock ores or brine is becoming more expensive. However, the extraction of lithium and strontium from brines remains cheaper and simpler (Wang et al., 2019). Therefore, extracting these two metals from reverse osmosis desalination brine using date pits would bring forward many advantages to Qatar and other countries with water scarcity issues.

1.3 Research hypothesis

It is anticipated that the modified date pits using hexacyanoferrates (II)] of (Cu and Ni) will achieve high recovery of Li^{+} and Sr^{2+} from reverse osmosis concentrated brine.

1.4 Research questions and objectives:

In this project, the synthesis of composite materials by modification of roasted date pits using ferrocyanides was investigated. The elucidation of the composites by spectroscopic methods and the evaluation of their adsorption capacity for valuable Li^+ and Sr^{2+} from a reverse osmosis brine concentrate were studied. The main objectives of the study are the followings:

i. Study the physicochemical characterizations of the collected concentrated brine. Various analytical techniques were used, namely: inductively coupled plasma optical emission spectrometry (ICP-OES), ion chromatography (IC), pH, salinity, conductivity, and total dissolved solids (TDS), scanning electron microscopy (SEM) with energy-dispersive X-ray spectroscopy (SEM-EDX), Fourier- Spectroscopy (FTIR), and X-ray diffraction (XRD) analysis.

ii. Prepare the roasted date pits (RDP) from raw date pits (Raw-DP) as well as the composite materials by modification of roasted date pits using ferrocyanides (potassium copper hexacyanoferrate, and potassium nickel hexacyanoferrate – date pits composites (RDP-FC-Cu and RDP-FC-Ni)).

iii. Perform the physiochemical characterizations of the prepared roasted date pits and composite materials. The adsorbents were characterized using SEM, particle size distribution, Brunauer–Emmett– Teller (BET) surface area, pore size, and volume distribution test, carbon and nitrogen elemental analysis, XRD, FTIR, and Thermogravimetric analysis (TGA).

iv. Evaluate the adsorption capacity, recovery behavior, mechanism(s) of Li^+ and Sr^{2+} binding for the prepared composites (RDP-FC-Cu and RDP-FC-Ni).

v. Apply the Langmuir and Freundlich adsorption isotherm models to study the adsorption mechanisms and interactions between the adsorbates (Li^{+} and Sr^{2+}) and the adsorbents (RDP, RDP-FC- Cu, and RDP-FC-Ni).

vi. Perform statistical analysis.

CHAPTER 2: LITERATURE REVIEW

2.1 Water as a fundamental property of life: availability and resources on earth

The sustenance and development of human civilizations are dependent on water as a fundamental property of life on earth. Water resource availability and distribution on earth are largely linked to the distribution of animals and humans' distributions as their survival are dependent on water. Achieving economic and industrial development requires that water resources are available and adequate. This is because many industrial activities as well as food production activities like agriculture are largely dependent on water (Sun et al., 2021). Therefore, sustainable development in terms of maintaining social well-being for the current and future generations cannot be achieved without sufficient and adequate water resources. This was discussed in the sustainable development conference that was held by the United Nations in 2012. The conference examined the emerging environmental challenges and specified water scarcity as a major one that needs urgent action (D'Odorico et al., 2017). Water scarcity on earth could be due to many direct and indirect natural as well as human-derived causes. The natural-based driver for water scarcity in many parts of the world stems from the water resource patterns, availability, and distributions on earth. The hydrological cycle is a balanced water cycle that circulates water between oceans, air, and land through physical processes like evaporation, condensation, and precipitation (Omer et al., 2020). Despite the balance of the hydrological cycle and the fact that the hydrosphere contains approximately 1388 million km^3 of water, available freshwater resources like rivers, lakes, and reservoirs compromise 1% only. The remaining water is contained in forms of ice or groundwater that are inaccessible or contaminated and require pre-treatment before consumption or use. Therefore, freshwater is important for ensuring life on earth; however, they are finite. Additionally, there is an uneven distribution of

freshwater resources between countries. For example, Jordan's freshwater resources are around 0.88 km^3/year while in Brazil they are around 8,233 km^3/year (D'Odorico et al., 2017). In the Middle East and North Africa region, water scarcity is a major issue nowadays due to uneven water distributions and fluctuating water production patterns due to many human-derived factors like increased air pollution, industrialization wastes, and unsustainable energy consumption. Qatar has been ranked by the World Resources Institute (2019) as the topwater-scarce country in the world. It has been estimated that around 99% freshwater needs of Qatar like municipality are met by desalinating seawater (World Resources Institute, 2019). Moreover, Qatar experiences a production of around 197 million m^3/year of treated municipal wastewater and significant quantities of treated wastewaters to perform industrial processes and irrigation activities. Qatar is also an arid country where land is considered to be infertile and temperatures could be extremely elevated for several months a year, this leads to the high annual evapotranspiration of water (Around 2200 mm). Therefore, the cultivation of land is as low as 1% of the total land in the country (Lahlou et al., 2020). Therefore, water scarcity is based on the availability of accessible water and the sustainable usage of this water. Other major indirect contributors to the water availability problems are the continuously increasing human populations and development in the world. These factors lead to unsustainable water use and overexploitation of water resources in order to meet the demands (Mohammadpour et al., 2019). Despite the great economic and social benefits of development and industrialization, environmental pollution and ultimately are leading to the phenomena of climate change. The environment is interlinked and any alteration or pollution of one reservoir (Land, water, or air) could significantly result in significant results in others. For example, climate change has been proven to be one of the main causes of disrupting

the natural balance of the hydrological cycle on earth (Kummu et al., 2016). For these reasons, in many countries around the world, people are facing extreme water and food scarcities and pollution, which is significantly harming people's and animals' health and the sustainability of the environment (Sun et al., 2021). Seawater and saline water desalination have emerged throughout the years as a solution for countries that lack freshwater resources, however, the technologies implemented today could have many challenges like cost, feasibility, harmful emissions, and wastes to the environment (Ahmadvand et al., 2019). Consequently, there is an urgent need for improving the management of water resources at a global level to achieve sustainable development and water security for all generations (Müller et al., 2020).

2.2 Desalination technologies principles

The main working principle of desalination technologies is the separation of salts from seawater, brackish waters, or brine. After the desalination is complete, the production of two main streams is notable. These streams are freshwater that is suitable for human use and consumption as well as brine. The latter is a concentrated stream that contains high amounts of salts, various types of metals, pretreatment chemicals, additives, wastes, and other substances. Moreover, brine streams are characterized by their higher salinity, conductivities, and temperatures than the seawater that they are extracted from (Nassrullah et al., 2020; Castro et al., 2020). There are two main approaches to desalination technologies, which are thermal desalination and membrane desalination (Table 1). Thermal desalination technologies employ evaporation latent heat to evaporate freshwater from the remaining concentrated brine stream. These processes are known to be more energy-intensive than membrane-based desalination technologies (Rahman and Zaidi, 2018; Castro et al., 2020; Honarparvar et al., 2019; Amy et al.,

2017). Thermal-based desalination technologies are known to be more costly, require more maintenance, slower in terms of production, and less flexible in production capacities. On the other hand, membrane desalination technologies are based on the separation of salts from seawater by its passage through semi-permeable membranes by applying different types of energies or pressures. During the process, freshwater would pass through the membranes while salts would retain on the other side (SeaWater Desalination - Key Issues, 2020; Rahman and Zaidi, 2018). Due to the mentioned challenges and extra requirements of thermal-based desalination technologies, they have been replaced by membrane desalination technologies in many parts of the world. For example, reverse osmosis (RO) is a leading membrane-based desalination technology in the GCC due to the ease of maintenance, simpler design, low cost, and environmental impacts as well as flexibility compared to other popular thermal desalination technologies like multistage flash desalination (MSF) (Ahmadvand et al., 2019; SeaWater Desalination - Key Issues, 2020; Honarparvar et al., 2019; Castro et al., 2020). RO (Figure 1) works by employing a high pressure over a semi-permeable membrane, which results in the separation of salts from seawater (Ahmadvand et al., 2019; Reverse Osmosis - Lenntech, 2020). Specifically, the name of the reverse osmosis desalination technology comes from the fact that the process depends on applying a higher pressure than the osmotic pressure. The higher pressure would force the movement of water molecules through the semi-permeable membrane, leaving behind a concentrated salty brine solution (Castro et al., 2020; Ahmadvand et al., 2019). In an RO desalination technology, four stages are considered important for the efficient production of freshwater from seawater. These four stages are known as pre-treatment, application of high-pressure pumps, separation, and post-treatment (Reverse Osmosis - Lenntech, 2020; Rahman and Zaidi, 2018).

Table 1. Common Desalination technologies

		Brine separation mechanism	Energy Requirement	References
Thermal desalination				
	Solar distillation (active and passive) Multi-effect evaporation (boiling or distillation) Multistage flash distillation Thermal vapor compression Mechanical vapor compression	Phase change processes that involve evaporating freshwater from seawater and condensing the brine solution	Latent heat and electric power	Rahman and Zaidi, 2018; Ahmadvand et al., 2019; Kaplan et al., 2017; Gude, 2011; Gude 2016; Gude, 2017; Castro et al., 2020; ElSaid et al., 2020
Membrane desalination				
	Electrodialysis Nano-filtration Forward osmosis resverse osmosis	Non-phase change processes that involve the separation of brine solution from seawater using semi-permeable membranes	Electric, mechanical and chemical energies	Rahman and Zaidi, 2018; Ahmadvand et al., 2019; Kaplan et al., 2017; Gude, 2011; Gude 2016; Gude, 2017; Elimetech and Phillip, 2011; Castro et al., 2020;

				ElSaid et al. 2020
Combination of Both	Membrane distillation Reverse osmosis combined with multistage flash or multi-effect distillation	Hybrid processes that combine membrane and thermal processes in a single plant or in consecutive stages to produce freshwater	latent heat, electric, chemical, and mechanical energies	Kaplan et al., 2017; Gude, 2011; Gude 2016; Gude, 2017; ElSaid et al., 2020

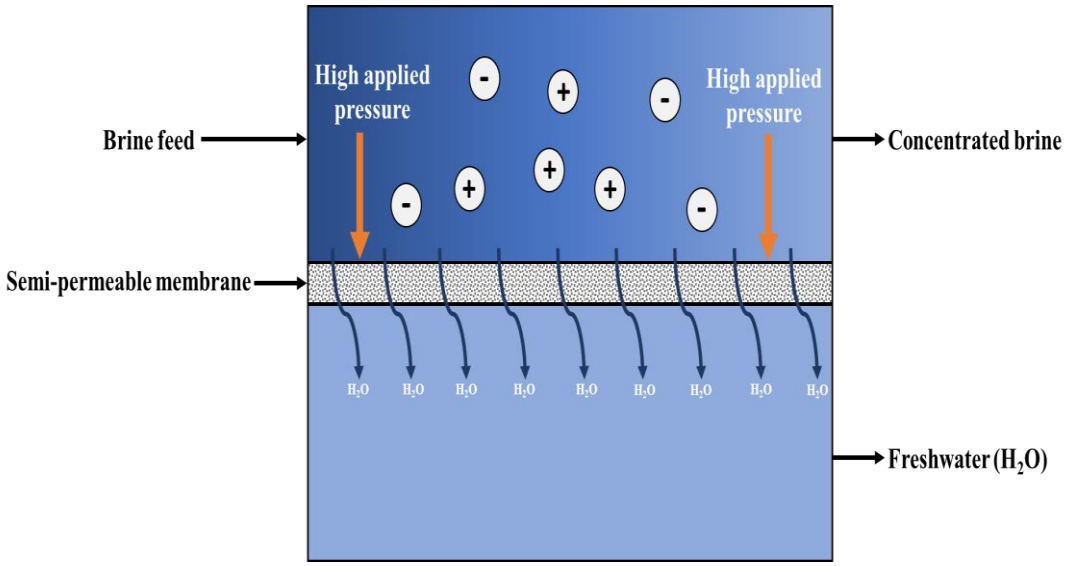

Figure 1. The common schematic diagram of RO. Adapted from: Shi et al., 2020; Panagopoulos et al., 2019.

2.2.1 Environmental and health impacts of desalination technologies

Despite the wide use, reliance, efficiency, and reliability of RO and other desalination

technologies in producing freshwater, many environmental and health impacts need to be properly addressed (ElSaid et al., 2020). For example, many small-sized marine organisms could get entrained in the different parts of the desalination plant while the seawater passes through the units. It is proven that small marine organisms greatly affect and control food webs, sea structure, benthic communities, and the health of entire sea communities. Thus, their removal from their natural habitats could lead to deleterious ecological effects. Moreover, intermediate-sized and larger marine organisms may get entrapped or injured and killed by the desalination plant's screens as the seawater passes through. This would lead to the loss of communities and impaired ecosystems (Honarparvar et al., 2019; Amy et al., 2017; ElSaid et al., 2020). Other major challenges related to many desalination technologies include low recovery rates, high costs due to energy requirements, and limited capacities (Gude, 2017). Another major concern to desalination technologies is their requirement for pre-treatment stages that include the addition of many chemicals to the feedwater (Table 2). Indeed, these chemicals would enhance the desalination process in terms of production, duration, durability as well as decrease the amount of scaling, fouling, corrosion, and required maintenance (Brine Treatment ZLD, 2020; Honarparvar et al., 2019; Panagopoulos et al., 2019). Examples of desalination pre-treatment chemicals include corrosion inhibitors, cleaning agents, flocculants, antiscalants, disinfectants, coagulants, and others (Amy et al., 2017). Furthermore, all desalination technologies require energy in order to operate, however, some require higher energies than others. This would result in a brine solution that contains various chemicals, a high concentration of salts and metals such as iron, lithium, rubidium, cesium, strontium, and others as well as high temperatures (ElSaid et al., 2020). Panagopoulos and others (2019) reported that a typical desalination brine solution would have a concentration of salts higher than

55,000 mg/L whereas the average salinity of seawater is typically around 35,000 mg/L. It must be noted that the application of energy and pre-treatment chemicals are often vital to produce high-quality freshwater for human consumption. However, the amount and types of pre-treatment chemicals greatly affect the overall quality of the produced brine stream. Therefore, it is of great importance to select the most appropriate and balanced method of desalinating seawater to obtain potable water of considerable quality as well as a brine solution that has the least amount and risky chemicals (Gude, 2017; ElSaid et al., 2020; Nassrullah et al., 2020). The quantity of produced brine could be as high as the produced water. However, brine quantity can be controlled by enhancing the recovery rate of desalination technologies or selecting the desalination technology with the highest recovery rate, such as RO. A high recovery rate of a desalination process means that the production of brine would be less than the produced freshwater (Panagopoulos et al., 2019; Gude, 2017; Amy et al., 2017). Furthermore, it is not surprising that desalination technologies, especially thermal desalination would contribute to the worsening of climate change by greenhouse emissions. This is because of the high-energy requirements of desalination technologies (Nassrullah et al., 2020; ElSaid et al., 2020; Gude, 2016).

Table 2. Desalination plants common pretreatment chemicals

Chemicals category	Common chemicals	Purpose of application	References
Antiscalant	Phosphonates, acids, and bases	Enhance the solubility of salts, polyvalent anions, and cations.	Brine Treatment ZLD, 2020; Panagopoulos et al., 2019; Ariono et al., 2016; Gude, 2016; Gude, 2011; Amy et al., 2017; Xu et al., 2007; Kavitha et al., 2019
Flocculants and coagulants	polymeric aluminum chloride, aluminum sulfate, Ferric chloride, and cationic polymers	Prevent fouling of membranes and enhances the removal of suspended solids	Wu et al., 2006; Panagopoulos et al., 2019; Ariono et al., 2016; Gude, 2016; Gude, 2012; Amy et al., 2017; Xu et al., 2007; Kavitha et al., 2019
Strong bases and acids	Hydrochloric acid, sodium hydroxide, and sulfuric acid	pH adjustments to prevent the precipitation of metals, and salts	Panagopoulos et al., 2019; Ariono et al., 2016; Gude, 2016; Gude, 2012; Amy et al., 2017; Kavitha et al., 2019
Disinfectants (Oxidizing agents)	Chloramines, Chlorine, and sodium hypochlorite	To control and prevent biofouling and membrane bacterial growth.	Panagopoulos et al., 2019; Ariono et al., 2016; Gude, 2016; Gude, 2012; Xu et al., 2007; Kavitha et al., 2019

2.3 Brine management strategies and their impacts

The well-recognized challenges and impacts of desalination industries have resulted in the development of some brine management strategies (Pramanik et al., 2017). This is because of the common interests between governments and nations to ensure the safety of humans, environments, and economic stabilities. There are two main categories for brine management strategies, which are direct environmental disposal as well as brine treatment and recovery technologies (Giwa et al., 2017; Panagopoulos et al., 2019).

2.3.1 Direct environmental disposal of brine

After the desalination of seawater and the production of brine, the most commonly used brine direct disposal methods are surface water discharge, deep-well injection, sewer discharges, land applications, and evaporation ponds (Jones et al., 2019;). Typically, many factors play a role in selecting the most appropriate brine disposal method. These factors include composition, quantity, and quality of the brine stream, the option's permissibility, receiving site availability, acceptance of the public, availability of the disposal site's geographic location, operating and capital and operational costs, and the ability to expand the facility (Schorr, 2011; Giwa et al., 2017). All the mentioned brine disposal methods are widely used globally and do not involve the treatment or modification of the brine solution (Ariono et al., 2016). Surface water direct discharge and sewer discharge involve either the direct release of the brine into water bodies (e.g., rivers, lakes, oceans, and others) or wastewater collection systems (sewers). Moreover, the injection of brine into deep wells is not as famous as surface water and sewer discharges because of the longer-term risks of groundwater contamination. On the other hand, the evaporation of brine in constructed lined ponds has been widely applied in countries with high solar energy. Lastly, low volumes of brine solutions could be used to irrigate salt-tolerant grasses and plants as a land application ("Brine Treatment ZLD", 2020).

The most cost-effective and practical brine direct disposal method is the surface water direct discharge or sewer discharges. This is relatively true if the brine stream has suitable characteristics to the receiving water body and if the discharge point is close to the plant (Panagopoulos et al., 2019). Therefore, the brine characterization assessments, transportation, outfall construction systems, and environmental monitoring are all cost factors for the brine surface water and sewers discharge methods. This means that surface water direct brine discharge is a feasible option for offshore or near-sea

desalination plants. This is because transportation costs due to constructing pipelines or outfall systems would be significantly reduced (Giwa et al., 2017; Ziolkowska, 2014). Moreover, sewer discharge would be a feasible option if the concentration of the brine is similar to the receiving wastewater and if current wastewater treatment is sufficient (Giwa et al., 2017). Deep-well injection of brine streams is more costly than surface water and sewer discharge; however, it is mostly suitable for inland desalination plants where surface water and sewer discharges are not feasible. The high costs for deep-well injection of brine are due to long pipeline systems, monitoring, brine conditioning, and geological assessments of the site. The selection of a suitable site for deep wells is vital to prevent any leakages into groundwater due to earthquakes or seismic activities (Thomas and Benson, 2015). Furthermore, a suitable brine disposal option for inland desalination plants located in arid, semi-arid, dry, and hot regions could be evaporation ponds (Morillo et al., 2014; Jones et al., 2019). Parameters such as pond size, depth, lining material, and monitoring affect the feasibility of evaporation ponds due to costs (Morillo et al., 2014; Ariono et al., 2016). Applying a proper lining system such as polyethylene, polyvinyl chloride, or butyl rubber is costly; however, it might significantly reduce potential groundwater and surrounding contamination. Also, brine evaporation ponds are based primarily on weather conditions, which makes their application unreliable (Panagopoulos et al., 2019; Morillo et al., 2014). The irrigation of certain salt-tolerant plants called halophytes using brine solutions is currently very limited. This is because halophyte species grow in extremely arid and semi-arid places where temperatures are very high, therefore, they are rare to find (Morillo et al., 2014; Ariono et al., 2016). Therefore, land application of brine solutions depends largely on local climates, as well as land and salt-tolerant plant availability (Ariono et al., 2016). Also, researches have shown that irrigating plants with brine could limit evaporation

and soil infiltration. These results in low water absorption by plants, which leads to low crop production and accelerates their welting. Moreover, risks to groundwater reservoir contamination by brine solutions should be avoided. Therefore, it is suggested that brine treatment prior to land application is necessary to achieve sufficient crop production (Morillo et al., 2014; Ariono et al., 2016).

2.3.1.1 Impacts of direct environmental disposal of brine

Although the mentioned brine disposal methods can be effective and are being widely implemented worldwide, they greatly threaten the receiving environment and living organisms (Al-shammari et al., 2018; Giwa et al., 2017; Belatoui et al., 2017). Brine disposal is associated with several concerns/disadvantages (Mannan et al., 2019). Some of the major concerns include esthetic issues, harmful impacts of desalination chemicals and toxic metals, as well as elevated salinity and temperature of receiving soils and water bodies, which may disturb and affect plants and marine organisms (ElSaid et al., 2020; Panagopoulos et al., 2019; Ariono et al., 2016; Pramanik et al., 2017). Studies have shown that desalination brine disposal into water bodies could elevate the salinity to 85 g/L and the temperature to 50 °C, which is extremely higher than the conditions that most animals could tolerate (ElSaid et al., 2020; Zhou et al., 2013; Tarnacki et al., 2012; Alharbi et al., 2012). Also, direct brine disposal methods such as surface water discharge may lead to eutrophication, toxicity, altered pH, and oxygen levels. These outcomes can significantly harm living organisms (Panagopoulos et al., 2019; Mannan et al., 2019). Many studies have demonstrated the dangers of increasing the natural salinity levels of oceans. It was shown that as the salinity of the environment changes, the osmotic balance between marine organisms and the surrounding water is disrupted. As a result, turgor pressure would decrease, and cell dehydration would occur. In the

long run, a change in the salinity of a water body might lead to species extinction (Roberts et al., 2010; Ariono et al., 2016; Pramanik et al., 2017). Petersen and others (2018) showed that the coral's visual appearance and physiology were disrupted due to increased salinity of 10% above ambient. Corals that have been exposed to polyphosphate antiscalants in addition to increased salinity were more significantly influenced. As mentioned earlier, these mentioned pollutants and salinity levels are characteristics of desalination brine. Furthermore, corrosion of the heat exchangers alloys employed in desalination processes may release various heavy metals, such as Ni and Cu into the brine stream. This was shown by Alshahri (2016) when the concentrations of Fe, Cu, and Cr were significantly high in the Arabian Gulf's desalination plants brine disposal region. Furthermore, a study was done at the northern Red Sea on the impacts of the chemicals employed in RO desalination. The study has found that the highly toxic anti-biofouling agents; copper and chlorine, were accumulated in the sediments. They have also reported on the low degradability dangers of anti-scaling agents in brine streams as they can bioaccumulate in living organisms and pose serious health impacts due to their toxicity. Another study conducted by Mohamed and others (2005) reported that the direct discharge or brine into pits or ponds could have soil and groundwater risks if the lining system is not properly managed. Some of these risks include groundwater contamination and soil deterioration. Increasing the salinity of soils may negatively impact soil, microorganisms, and plant productivity. One more example of the effect of brine disposal on the quality of seawater is a study done by Al-Shemmari and Ali (2018) which found that brine disposal has an effect on seawater temperature. The study revealed an increase of 4 °C or 6 °C above ambient temperature due to brine disposal. Moreover, there was a potential effect on salinity with a 2-4 ppt range beyond the mean salinity of seawater.

The study also showed that brine disposal decreases the dissolved oxygen level (DO) in seawater due to the sodium sulfide added inside the plants to inhibit corrosion. The latter was also found by another study done by Jones and others (2019). Rodríguez-Rojas and others (2020) investigated the impacts of desalination brine discharges on the cellular and Eco-physiological responses of the brown microalgae Ectocarpus. The study involved transplanting the brown algae at 30 m and 10 m from a desalination plant brine discharge point located at Antofagasta, Chile. The results revealed that all the transplants at both locations suffered from disrupted photosynthesis capabilities, unregulated enzyme encoding genes, accumulation of ascorbate, decrease in important functional antioxidants, and enhanced peroxidation of lipids. This shows the sensitivity of the brown microalgae Ectocarpus as coastal species. Such destructive effects of brine discharge on microalgae could affect the entire food webs of coastal areas if abundances decrease as microalgae form the basis of food webs. This was demonstrated by another study done by Riera and others (2011) where the effects of desalination brine on subtidal meiofauna were investigated. The results demonstrated that the assemblage structure of the meiofauna located near the desalination plant was altered. The abundance of the copepods and nematodes was significantly reduced near the brine discharge point.

2.3.2 Conventional brine treatment and recovery technologies

As mentioned earlier, seawater and specifically desalination brine contains numerous minerals that could be useful in industrial processes. These minerals could also be expensive and rare to find in their non-aqueous forms (Mavukkandy et al., 2019). Therefore, many efforts are done to recover the minerals and valuable metals contained in the brine streams of desalination processes by brine treatment and recovery

technologies. This is because there are well-recognized issues that could be easily mitigated. These issues are reducing the environmental effects of brine discharges, mineral scarcity, and decreasing the costs of desalination processes. Providing industries with valuable metals that could be used in many productions would decrease the overall cost of desalination and add revenues to the desalination industry. Also, a substantial decrease of pressure could be observed on land ore mining if minerals could be extracted from seawater desalination brine streams (Loganathan and others 2017). Due to the well-recognized environmental impacts of brine disposal and discharge methods, there has been ongoing research and implementation of various other brine management, recovery, and treatment technologies. The conventional brine treatment and recovery technologies are based on a zero-liquid discharge (ZLD) treatment system, where the recovery of freshwater is increased and the production of brine is decreased (Alnouri et al., 2018). Moreover, a ZLD system is described as a combination system of many desalination technologies that aim at eliminating brine waste while producing pure water from the plant (Alnouri et al., 2018). Other studies have shown that ZLD produces a highly compressed brine waste, which can be further processed and used as a useful industrial material or disposed of in eco-friendly methods (Xiong and Wei, 2017). Moreover, brine treatment could serve several industrial and commercial purposes. Conducting a conventional brine minimization technology may help in several or one beneficial uses such as the recovery of pure water, salt concentration, energy regeneration, and ultimately valuable metal recovery from brines that could be used in various industrial processes (Ariono et al., 2016).

There are many brine treatment and recovery technologies that are well-accepted and established today. Below is a discussion of the main principles, benefits, and challenges of some of the most common thermal and membrane-based brine recovery technologies

(Al-Anzi et al., 2020; Panagopoulos et al., 2019; Kim and Min, 2020; Ali et al., 2020; Abdelrazeq et al., 2020; Wenten et al., 2020; Nannarone et al., 2017).

i. Brine concentrator and crystallizer (BC and BCr)

The BC and BCr are famous in their application as thermal-based ZLD technologies for the treatment of brine solutions (Panagopoulos et al., 2019). The most common design of a brine concentrator (BC) consists of a falling film evaporator or a vertical tube. However, the usage of plate-type evaporators or horizontally placed spray films is also well known. The treatment process of brine in a BC involves the elevation of the feed solution's temperature to its boiling point using a heat exchanger. Then, the non-condensable gases are removed from the brine solution as it moves to a deaerator. An evaporator sump receives the brine where the recirculating slurry is mixed with it. This forms a brine slurry, which is moved to a concentrator, then an assortment of tubes for heat transfer receives it. A thin film of brine forms on the surface of the tubes which leads to the evaporation of water from the brine. After that, more heat is added to the evaporating brine solution due to the insertion of a vapor compressor and mist eliminators (Spellman, 2015). As a consequence, the vapor present in the compressor flows through the evaporator tubes to the outside where the temperature drops. This loss of heat from the vapor results in the formation of freshwater through condensation. Finally, the heat in the freshwater produced is transferred to the feed brine solution as it gets pumped to the feed heat exchanger (Figure 2). This technology has an SEC between 15.86 and 26 kWh/m^3 (Mickley, 2008). According to Panagopoulos and others (2019), BC is characterized by the $CaSO_4$ slurry crystals that circulate in the system and function as seeds. Numerous different brine streams could be effectively treated by this BC system technology. The addition of certain amounts of $CaSO_4$ could take place

prior to the treatment of brine solutions that do not contain sufficient amounts of the slurry. Interestingly, a commercial and typical BC system could be used to treat brine streams that contain TDS concentrations as high as 250,000 mg/L and could have a freshwater recovery of up to 99%. The generated water is usually of very high quality, as it would typically contain TDS concentrations as low as 5 mg/L to 20 mg/L. A downside to commercial BC systems is their high capital costs due to the application of expensive materials like titanium and stainless steel that is super duplex (Veolia Water Technologies, 2018). These expensive materials are usually needed to prevent corrosion due to brine heating and boiling (Shaffer et al., 2013). On the other hand, the design of brine crystallizers (BCr) consists mainly of cylindrical vertical vessels and a vapor compressor or steam source, which transfers heat into the vessels. The forced circulation crystallizer is the most well-known kind of brine treatment crystallizer. This technology works by pumping brine stream into a collection container within the crystallizer, which mixes with another incoming brine stream (Panagopoulos et al., 2019). The mixture is then boiled as it is fed to a heat exchanger. Evaporation of the brine stream does not occur because of the underlying pressure due to the submergence of the tubes of the heat exchanger. Thus, the brine recirculates and enters the crystallizer's vapor body at an angle, which causes a swirling motion to happen. This swirling in a vortex motion leads to the evaporation of a small part of the brine stream and the formation of crystals (Stanford et al., 2010). A filter or a centrifuge is then used to remove any extra water molecules from the formed crystals. The recirculating brine is heated by the compressed vapor from the vapor compressor and then is condensed on the heat exchanger. The final products are freshwater and dried solid crystals of salt (Spellman et al., 2015, Panagopoulos et al., 2019). The main disadvantage of BCr technology is the higher energy and cost demands than a typical BC technology with

equal capacity. In these terms, it is estimated that employing BC for brine treatment requires 1.11 US dollars per cubic meter, while BCr requires around 1.22 US dollars per cubic meter. Moreover, BCr requires an SEC amount of around 52 to 70 kWh/m^3. However, BCr technology is suitable for treating brine solutions with TDS concentrations as high as 300,000 mg/L (Fluid Technology Solutions Inc., 2016; Mickley, 2008). This makes BCr a more efficient technology than BC in terms of treating highly concentrated brine streams. However, this is only true for countries or regions that have a high capital investment for employing such technologies.

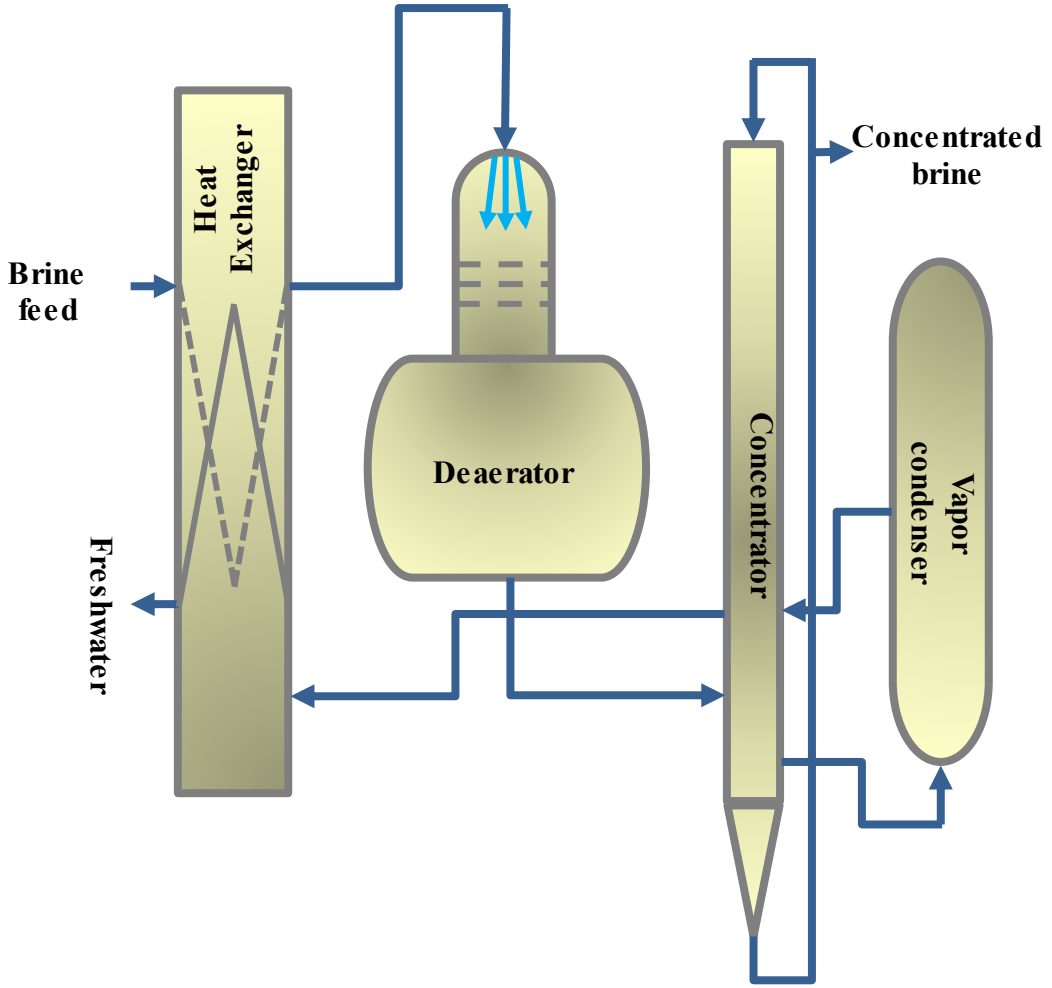

Figure 2. The common schematic diagram of a BC. Adapted from: Panagopoulos et al., 2019.

ii. Multistage-flash (MSF) and multiple effect distillation (MED)

MSF and MED are the most popular and leading thermal desalination technologies. These two technologies are mainly applied to desalinate seawater or brackish waters; however, brine treatment could also be achieved (Mabrouk and Fath, 2015). In MSF technology (Figure 3), the flash units produce condensing vapors to preheat the feed brine stream. Along with the flash units, a peripheral brine heater would raise the brine stream's temperature to around 110 - 120 °C. Then, the heated brine stream is pumped through a series of flash units with lower temperature and vapor pressure (Panagopoulos et al., 2019; Mabrouk and Fath, 2015). This would result in the

evaporation and condensation of a portion of the brine stream. Consequently, the water vapor corresponds to freshwater. The remaining portion of the brine stream is concentrated and exits in a liquid form from the last flash unit (Khoshrou et al., 2017). To compare, MED technology is different from MSF technology in two ways. Firstly, a heat exchange occurs between the vapor pressure and liquid leading to vapor condensation in a subsequent distillation effect. Secondly, the maximum temperature of heating is between 70 and 75 °C (ElSayed et al., 2018). According to Panagopoulos and others (2019), the application of MSF and MED in ZLD systems is not as popular as their application in the desalination of seawater and brackish water. The reason for this could be that the materials used in the MSF and MED design are more suitable for less concentrated streams (i.e seawater and brackish water) and not highly TDS concentrated brine as corrosion would be a challenge. These materials that compromise the system design of MSF and MED are mainly stainless-steel grades (Deyab, 2019; Nada, 2010). In order to prevent corrosion while treating highly concentrated brine streams using MSF and MED, materials such as high nickel alloys, super duplex stainless steel grades or titanium must be employed (Boillot and Peultier, 2014; Chail and Kangas, 2016; Ho et al., 2018). However, employing high-strength and resistant materials comes with an extra cost. Unfortunately, the energy requirements of MSF and MED are usually high. Therefore, the special materials along with the existing constraints of energy requirements make their application for brine treatment quite challenging. According to the literature, the SEC for MED is around 7.7 kWh/m^3– 21 kWh/m^3, while for MSF it is around 12.5 – 24 kWh/m^3 (Ihm et al., 2016; Filippini et al., 2018). Similarly, the cost for employing MED for brine treatment is around 1.10 US dollars per cubic meter while for MSF it is around 1.40 US dollars per cubic meter (Kesieme et al., 2013). These conditions of high quality and super-strength materials

combined with high energy inputs would indicate the main advantage of employing MSF and MED technologies in brine treatment. The advantage that comes with a high cost is the high quality of the produced freshwater with less than 10 mg/L TDS concentration (Chua and Rahimi, 2017).

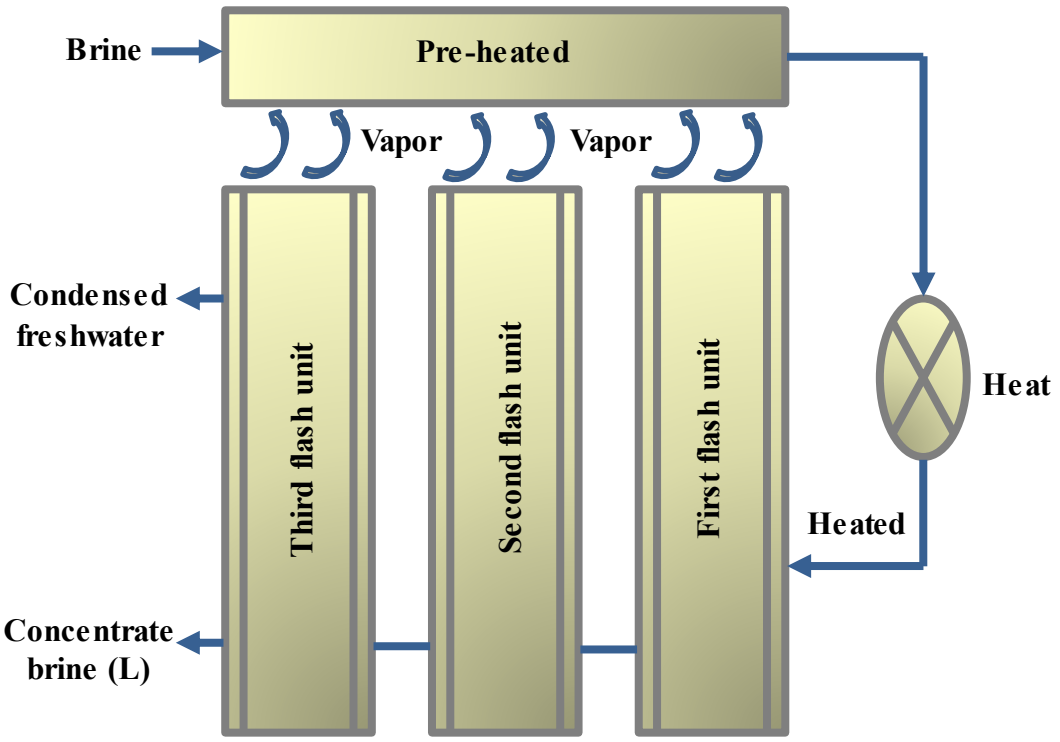

Figure 3. The common schematic diagram of MSF. Adapted from: Nannarone et al., 2017; Akram et al., 2013; Lian-ying et al., 2012.

iii. Forward osmosis (FO)

FO is different from RO in which FO uses osmotic pressure instead of the applied pressure as a driving force for transporting elements across the membrane (Figure 4) (Zhao et al., 2019). FO is used for both brine waste management and water desalination (Giwa et al., 2017). Although it does not produce large pollutants, does not require large energy, it is simple and accountable; it requires the installation of special membranes

and draws solutes (Morillo et al., 2014; Zhao et al., 2019). The draw solution in FO technology is of great importance as its high substantial concentration is responsible for producing an osmotic pressure. The osmotic pressure produced results in the transportation of water from a feed brine solution of less concentration to the draw solution of higher concentration (Amjad et al., 2018). After that, a separation of the draw solution and freshwater occurs to recycle the draw solution back to the FO system (Bell et al., 2017; Giwa et al., 2017; Tang and Ng, 2008). This was discussed by many studies where a successful and efficient FO brine treatment can be achieved if the draw solution's concentration is higher than the feed solution (Johnson et al., 2018; Giwa et al., 2017). The recycling of the draw solution is also called draw solution recovery or regeneration. RO and high-pressure reverse osmosis (HPRO) technologies are more energy-efficient and cost-effective than FO technology because they do not require the usage of a draw solution or its regeneration (Bell et al., 2017). Panagopoulos and others (2019) mentioned that FO could be applied without the usage of a draw solution in order to make it a more energy-efficient brine treatment technology than RO and HPRO. However, the main working concept, efficient brine concentration, and treatment, as well as maximum water recovery of FO technology, depends on the osmotic pressure generated by the draw solution. Therefore, it would be more ideal to apply RO or HPRO to achieve the desired maximum efficiency of the membrane brine treatment technology. Bell and others (2017) discussed that fouling in the FO membrane is one of the challenges of the technology, especially for modules working at reasonable commercial flow like 15 L/m^2h -20 L/m^2h. Zhao and others (2016) mentioned that the characteristics of an ideal draw solution and FO system are many, which makes it hard to implement the technology easily. For example, the ideal draw solution must be available commercially, have low fouling risks, provide high water

flux, inexpensive, have low or no toxicity to microorganisms, low diffusion of reverse solute, and easily recovered or regenerated. These requirements make FO an expensive membrane brine treatment technology. Therefore, according to Zhao and others (2019), the development of a FO technology that is cost-effective is not achieved till now. These two findings are three years apart and it shows that at least from 2016 till 2019, implementing an efficient, energy and cost-effective FO technology was still a challenge. On the other hand, other studies discussed that an ideal FO draw solution does not exist because there are advantages and disadvantages for every draw solution available nowadays (Gao et al., 2014; Johnson et al., 2018). This shows that an ideal draw solution and FO technology is also dependent on the economic state, availability of resources, technological aspects, working conditions, and state of the country implementing the FO technology. Also, the final goal to be achieved from the FO technology plays a major role in selecting the draw solution with the least disadvantages for the country's interests. Studies have shown that draw solutes could be inorganic salts (Roy et al., 2016; Ahmed et al., 2018), organic (Cui and Chung, 2018; Yu et al., 2017), volatile (Stone et al., 2013), and nano-particles based (Na et al., 2014; Guo et al., 2014; Zhou et al., 2015). Some of the common disadvantages of FO technology include the requirement of energy for the recovery of draw solutions, external concentration polarization (ECP), internal concentration polarization (ICP), reverse salt flux as well as the absence of specifically designed stable and enhanced membranes (Gao et al., 2014; Johnson et al., 2018). There have been recent research efforts for eliminating or reducing the mentioned FO issues and challenges. For instance, modifying FO membranes could be done by adding nanoparticle-decorated nanosheets of graphene oxide or polydopamine. Also, increasing the surface hydrophilicity and improving the antifouling issues could be done by coating the active thin-film

composite membrane layer with the mentioned materials. This results in higher water flux and reduced ICP (Guo et al., 2018; Soroush et al., 2016). Other research showed that membranes that have sulfonated carbon nanotubes in the active layer are novel FO membranes. Polymerizing FO membranes using graphene quantum dots are promising FO-modified membranes (Li et al., 2018; Xu et al., 2018).

McGinnis and others (2013) revealed that using NH_3/CO_2 draw solution to treat a brine solution of 73,000 mg/L ± 4,200 mg/L TDS in a composite thin film FO membrane produced a water recovery of 64% ± 2.2% and a concentrated brine TDS concentration of 180,000 mg/L ± 19,000 mg/L. This water recovery flux is great, however, and as with other studies, contamination of the feed stream with ammonia from the diffusion of the reverse solute is a problem that was observed (Li et al., 2015; Seker et al., 2017; Shaffer et al., 2015). This shows the efficiency of the draw solution that is to be selected as well as the potential disadvantage/s that could be associated with it. Therefore, it is important to examine the advantages and disadvantages of each draw solution in order to optimize FO technology. Eusebio and others (2016) tested different concentrations of a NaCl draw solution for the optimization of the brine FO treatment system. The draw solution's concentrations were 50 g/L, 75 g/L, 100 g/L, and 200, and the feed brine solution had a TDS concentration of 41 g/L. The study revealed that the draw solution having a concentration of 100 g/L achieved the most optimized reverse solute and permeate fluxes of 0.24 $mol/m^2.h$ and 3.46 $L/m^2.h$ respectively. As mentioned earlier, FO technology depends largely on the concentration and osmotic pressure of the draw solution. The variation of the results of this study shows this important parameter for optimizing an FO system and achieving efficient brine treatment and water recovery. A more recent study by Liden and others (2019) challenged the effectiveness of a hollow thin-film fiber composite FO membrane in the treatment of a

variety of highly concentrated brine solutions. The feed brine solutions employed in the study had concentrations between 16,000 mg/L and 210,000 mg/L. Their astonishing results revealed the effectiveness of the FO membrane to treat and concentrate all the brine concentrations investigated in their study. Therefore, finding a brine membrane treatment system that could be used to concentrate and treat a variety of brine feed concentrations is extremely useful. This is mostly useful in countries where desalination processes produce a range of highly saline brine solutions. However, according to Panagopoulos and others (2019), there are not many commercially available FO systems that could effectively treat brine solutions with high TDS concentrations. Fluid Technology Solutions Inc. (2019) has developed FO systems that could treat brine solutions of a TDS concentration of 65,000 mg/L. Additionally, a thermal pilot-scale hybrid FO membrane was developed by Oasys Water Inc. This hybrid FO system is currently available for treating brine feed solutions with a TDS concentration of 70,000 mg/L. According to Tiraferri (2020), the developed brine treatment FO system has shown it is adequate in producing an acceptable quality of freshwater as well as water recovery of 60%. In terms of SEC, FO could require much lower energy (0.1-0.85 kWh/m^3) than RO and HPRO if no draw solution is applied. However, the unique nature of FO processes and their efficiency is dependent on the draw solutions, which makes the process consume higher specific energy than RO and HPRO (13 kWh/m^3) (McGinnis et al., 2013; Kolliopoulos et al., 2018). All the mentioned requirements of FO brine treatment technology attribute to its high cost of around 0.63 US dollars per m^3 (Valladares Linares et al., 2016).

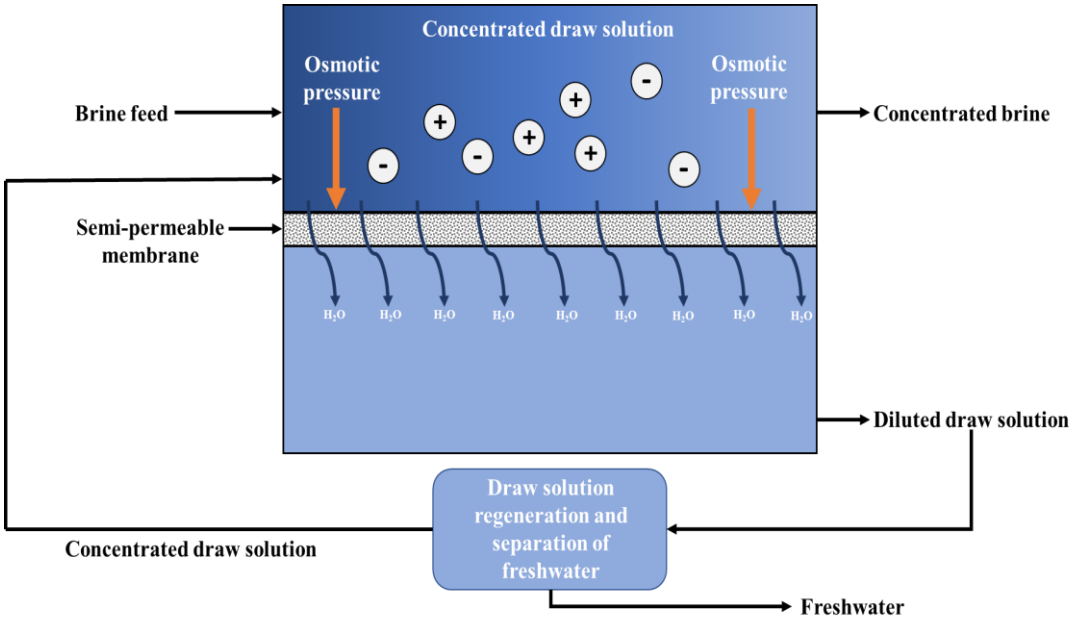

Figure 4. The common schematic diagram of FO. Adapted from: Wenten et al., 2020; Lee et al., 2020; Pham et al., 2020; Mahto et al., 2020.

iv. Membrane distillation (MD)

MD is used for brine consisting of a high concentration of salts. According to the literature, MD is efficient in treating brine solutions of concentrations as high as 350,000 mg/L TDS. This technology mostly employs the principles of membrane brine treatment processes with the combination of thermal evaporation processes (Panagopoulos et al., 2019). MD uses hydrophobic membranes where the vapor pressure gradient across the membrane controls the proceeding of the process. More specifically, the hydrophobicity of the MD membranes only allows vapor molecules to cross while preventing any liquid membranes to pass through the pores. This nature of MD membranes accounts for a clean separation, a rejection rate as high as 99%, and the recovery of freshwater of high quality (Ashoor et al., 2016; Panagopoulos et al., 2019). MD can achieve 50% - 99% treated water recovery if the precipitation and flux

challenges are handled properly. MD process is applicable even when low-quality energy sources are available to be used (Panagopoulos et al., 2019). Interestingly, there are four major MD configurations available. These configurations are known as air gap MD (AGMD), direct contact MD (DCMD), sweeping gas MD (SGMD), and vacuum MD (VMD). According to the literature, the most commonly applied brine membrane distillation process is direct contact MD (Figure 5) (Ji et al., 2010; Eykens et al., 2016; Ali et al., 2015). The DCMD treats brine solution by the principle of heating the feed brine solution prior to reaching the membrane. Once the feed brine solution is heated on one side, the vapor generated flows through the pores of the membrane where it undergoes a condensation process to result in a cold freshwater distillate. On the other hand, the brine solution does not pass through the membrane due to its hydrophobicity and subsequently is concentrated and retained (Park et al., 2019; Karam et al., 2017; Wang and Chung, 2015). Generally, all MD configurations have the advantage of requiring lower working temperatures (40-80 °C) than most other distillation processes. This allows the use of waste heat streams or low-grade heat streams (Abdelkader et al., 2018; Panagopoulos et al., 2019). This is of significant importance for countries where energy resources are limited and it allows countries to have options when it comes to the choice of a heat stream for MD processes. On the contrary, issues and challenges of FO like the unavailability of developed fabrications for the membranes as well as low permeate fluxes are common with MD technology. In addition, limited thermal efficiencies and membrane pore wetting are other problems with MD technology (Fortunato et al., 2018). This shows the similarity of challenges between MD and FO technology and the operating constraints of each that need to be well studied and dealt with prior to the construction of an MD brine membrane treatment process. Although MD can produce 99-100% quality distillate, it can have problems such as scaling, high-

energy requirements when compared to RO but lower than MCr and traditional evaporation methods (Panagopoulos et al., 2019). The complexity of the disadvantages and advantages of the different brine membrane treatment technologies is demonstrated by these interlinked issues. The types of hydrophobic membranes that MD technology employs are polymeric in their nature. For example, the most famous MD membranes are polytetrafluoroethylene (PTFE), polypropylene (PP), polyethylene (PE), and poly (vinylidene fluoride) (PVDF) (Liu et al., 2018; Zuo et al., 2016; Abdel-karim et al., 2019). The nature of their hydrophobic surfaces, low costs, and the controllable, as well as flexible characteristics of mass transfer, make polymeric membranes a very popular choice for MD processes. The downside of polymeric membranes for MD processes is their somewhat low robustness towards highly concentrated brine solutions or extreme working conditions. For example, the abrasion of the polymeric membranes may occur due to highly concentrated solutions of brine. In addition, the degradation of polymeric MD membranes might occur due to extreme pH ranges, high temperatures, solvent solutions, and others (Schnittger et al., 2020). According to the literature, recent advancement of MD membranes is the ceramic membranes that are modified chemically. Their great potential in being efficient MD membranes stems from their unique and attractive physical and chemical characteristics. These characteristics are improved lifetime, resistance to heat, and great mechanical strength (Hubadillah et al., 2018; Yang et al., 2017). Compared to polymeric membranes, ceramic MD membranes can work under extreme conditions efficiently. Interestingly, the cleaning of ceramic MD membranes can take place under vigorous and extreme methods to overcome fouling effects on their properties. For example, the use of high-pressures, hot steam, or aggressive chemical solutions are all possible options for cleaning ceramic MD membranes. The application of ceramic MD membranes might be of high costs,

however, their several decades' potential life span compensates for their high costs, making their application attractive for long-term applications (Schnittger et al., 2020; Liu et al., 2018; Zuo et al., 2016). This is true for countries that rely heavily on desalination and have a desire for effective and long-term brine treatment technology while protecting the environment. On the other hand, the manufacturing high costs of ceramic MD membranes, great thermal conductivity, and less hydrophobicity than polymeric membranes have slowed down their investigation and use. For example, it was reported that only 20% of studies tested and utilized ceramic MD membranes for brine treatment. Moreover, the hydrophobic modified ceramic MD membranes made from zirconia, alumina, or titanium have proven to have high salt rejection. However, the permeate fluxes of ceramic MD membranes are shown to be much lower than polymeric MD membranes (Kujawa et al., 2017; Nagasawa, 2020; Hubadillah et al., 2019). Therefore, it can be assumed that the development of tough hydrophobic ceramic membranes could solve the mentioned challenges by treating highly concentrated saline solutions or wastewaters. This provides an enhanced alternative for the usage of polymeric membranes that cannot handle high concentration brines. Furthermore, adapting ceramic MD membranes that are robust, energy-efficient, and have good permeate fluxes requires a full understanding of their characteristics. The characteristics like layer design, conductivity, and pore size are of great importance due to their effects on the MD process performance (Ramlow et al., 2019; Schnittger et al., 2020). A study done by Kujawa and others (2017) tested the performance of grafted titanium dioxide and aluminum oxide ceramic membranes with a variety of hydrophobic agents. The results of the study showed that the permeate flux was efficient and the retention coefficient of salts was above 98%. The treatment of a highly concentrated salt solution (250,000 mg/L) was successfully achieved with great anti-

scaling properties by a recent study conducted by Xiao and others (2019). The study involved the development of a novel porous superhydrophobic ceramic MD membrane by the technique of micro-molding phase separation. This shows the need for advancements in the ceramic MD membranes in order to enhance their performance in brine treatment and recovery.

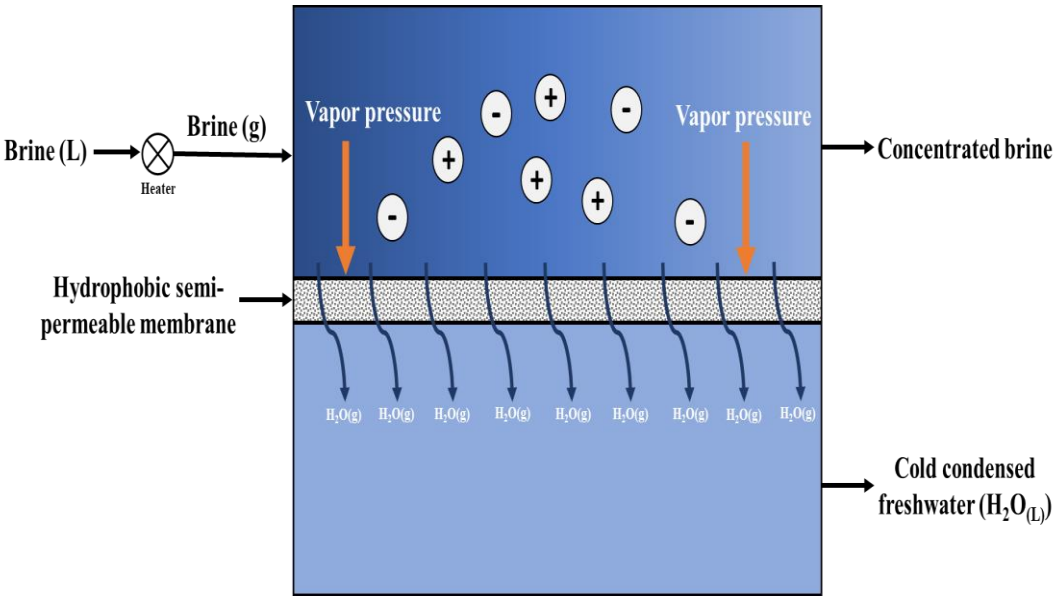

Figure 5. The common schematic diagram of DCMD. Adapted from: Abdelrazeq et al., 2020; Naidu et al., 2020; Yan et al., 2017.

v. Membrane crystallization (MCr)

MCr is emerging as a novel and promising technique for the separation and purification of many solutions and waste streams in many fields (Figure 6). MCr can be used to treat brine solutions to recover valuable metals and minerals. According to Macedonio and others (2013), the MCr process concentrates feed solutions (i.e. brine) beyond their saturation limits through the evaporation of volatiles through hydrophobic microporous membranes. This results in the formation and growth of crystals in a supersaturated environment. Furthermore, Das and others (2019) mentioned that MCr is a significantly

important emerging technology that produces solid crystals, which could serve important roles in a range of industries such as pharmaceuticals, food, and sugar processing. Therefore, the purification and separation of feed solutions, as well as downstream production, can all be achieved with MCr technology. According to the literature, the evaporation of water and other volatile compounds in the feed solution occurs due to the vapor pressure gradient across the sides of the MCr membrane. Also, condensation occurs on the other side, called the distillate side. The duration of this process proceeds until a condition of supersaturation is reached, where the induction of solid crystals occurs (Ji et al., 2010). Osmotic dewatering or concentration and pressure-induced dewatering are the two main MCr technology categories. The osmotic dewatering approach involves the synthesis and use of a draw solution, which applies a higher osmotic pressure than the feed solution (Das et al., 2019). The separation between the feed and draw solution by a semi-permeable membrane results in an osmotic gradient due to the concentration differences. As a consequence, a steady and continuous concentration of the feed solution occurs due to the induced movement of the solvent to the draw solution side (Sparenberg et al., 2020). On the other hand, the pressure-induced approach works on the size exclusion principle. This means that the process relies on an external pressure to dewater and gradually concentrate the feed solution as it passes through the semi-permeable membrane (Ye et al., 2015; Sparenberg et al., 2020).

As membrane crystallization is an emerging brine management technology, there are many process configurations. Freezing crystallization and vacuum crystallization are two of the well-known approaches of MCr. As the name implies, freezing crystallization involves the preferential freezing of the solvent, while vacuum crystallization employs vacuum suction to evaporate the solvent. As a result, the

solubility of the feed solution decreases, which aids in its salting out and concentration. Moreover, these harsh and specific working conditions would require high energy and cost expenditure (Das et al., 2019; Liu et al., 2017). It can be concluded from the working behavior of MCr that it is an advancement over MD processes due to the possibility of producing freshwater and concentrating the valuable solids as crystals (Ji et al., 2010). The growth kinetics and nucleation of crystals in MCr are well controlled which leads to very high rates of crystallization. Research has been ongoing regarding an emerging technology known as membrane distillation-crystallization. This technology has numerous advantages as it employs the combination of MD and MCr principles in the treatment of seawater, brine, and wastewaters (Sparenberg et al., 2020; Das et al., 2020). For example, the processing of streams of high concentrations, operation at ambient temperatures, the possibility and flexibility of scaling up as well as it can offer supersaturation, nucleation, and crystal growths in a well-controlled manner (Lu et al., 2017; Ruiz Salmón and Luis, 2018). Moreover, membrane contactors are employed in membrane distillation-crystallization, which prevents the two phases from contact using a hydrophobic membrane. The evaporation of water occurs due to a chemical potential difference caused by temperature, activity, or pressure gradients (Sparenberg et al., 2020; Das et al., 2020). As soon as the supersaturation of the feed solution occurs, crystallization takes place as heterogeneous nucleation. The solution flow results in the movement of the crystals towards a crystallizer, which allows for crystal growth. Lastly, the continuous recycling of the mother liquor is possible from the crystallizer to the contactor (Ji et al., 2010). Compared to other crystallization techniques, MCr offers better control over the levels of supersaturations, higher mass transfer specific area, shorter crystallization time, formation of organized and well-structured crystals with defined sizes, and selective crystallization (Macedonio et al.,

2013). According to Panagopoulos and others (2019), despite MCr being a promising brine treatment technology with numerous advantages, it has been neglected for study by literature. Quist-Jensen and others (2017) showed that MCr and MD are processed for the treatment of industrial wastewaters that contain high Na_2SO_4. Also, MCr and MD technologies are more appropriate for the efficient treatment of unfiltered wastewater than nanofiltration pre-treated wastewater. Moreover, the treatment cost and SEC for the MCr technology are higher than MD technology. For example, the treatment cost per m^3 of freshwater produced for the MCr process is 1.24 US dollars, while the SEC is generally between 39-73 kWh/m^3 (Lokare et al., 2018; Ali et al., 2015).

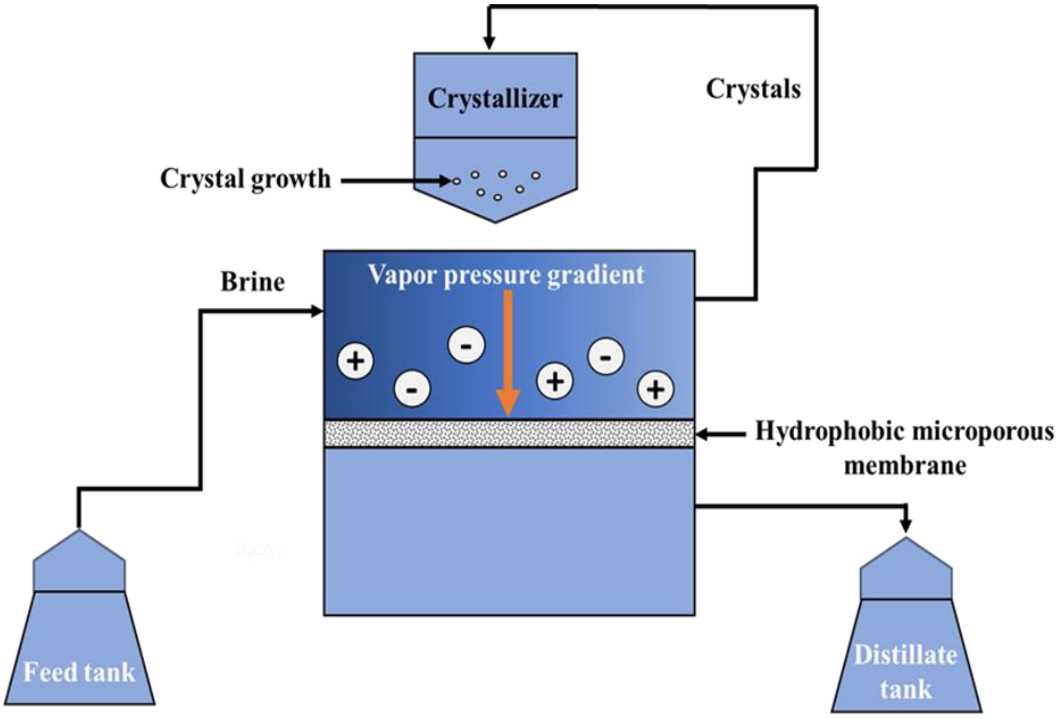

Figure 6. The common schematic diagram of Mcr. Adapted from: Panagopoulos et al., 2019; Ali et al., 2020.

vi. Osmotically assisted reverse osmosis (OARO)

OARO is a membrane-based brine treatment process that incorporates the brine treatment principles of FO and RO. The high recovery of freshwater from highly saline brines can be achieved efficiently by implementing OARO. Similar to RO, the transportation of water across a semi-permeable membrane in OARO is based on the application of hydraulic pressure against the difference of the osmotic pressure between the feed brine and permeate water. Opposite to RO, reducing the difference in osmotic pressure across the membrane is possible through a lower saline sweep in the permeate side (Figure 7) (Panagopoulos et al., 2019). This is of significant importance as it allows the transportation of water despite higher feed osmotic pressure than the membrane burst pressure. As a result, the expansion of water recovery from the maximum TDS is

possible with OARO when compared to RO. Moreover, OARO is a hydraulic pressure membrane process that can be implemented in a series of stages linked together to recover freshwater from highly saline brines (Bartholomew et al., 2017; Panagopoulos et al., 2019). An advantage of OARO is that anticipating equipment's cost savings is possible because the modules and pipes of the technology do not require the use of pressure-resistant materials (Peters and Hankins, 2019). However, as in FO technology, it is a disadvantage that OARO is a serial brine dilution treatment process that works in consecutive stages and not a direct desalination process (Bartholomew et al., 2017). Peters and Hankins (2019) investigated the desalination of brine using five arrangements of OARO technology. The investigation revealed that the desalination of a brine stream of 70,000 mg/L TDS required the consumption of 6.37 kWh/m^3 specific energy to recover 44% freshwater. Bartholomew and others (2017) noted that the treatment of a brine stream of 100,000-140,000 mg/L TDS using OARO technology is possible with the requirement of 6 kWh/m^3 specific energy. The study revealed that this could result in the recovery of 35-50% of freshwater. Moreover, Hyrec has successfully developed a commercial multi-stage OARO process that could concentrate seawater reverse osmosis brine solution to a final concentration of 250,000 mg/L. The average specific energy consumption of the multi-staged OARO system is 5.8 kWh/m^3 (WDR, 2018). The MIT Boston (Lienhard group) developed a similar approach to OARO known as Counter-Flow Reverse Osmosis (CFRO) while an Osmotically Mediated Reverse Osmosis (COMRO) technology was developed by Columbia University's Yip group. The core principles of these two technologies are the same as OARO, however, the configuration arrangements of their stages or modules are different (Bouma and Lienhard, 2018; Chen and Yip, 2018). In general, it was reported by studies that the treatment cost (US$2.4/$m^3$) and SEC (6-19 kWh/$m^3$) of OARO processes are higher

than other processes that are osmosis related. However, due to the mentioned current interest and development in OARO processes, it is anticipated that the costs and SEC would decrease in the near future (Panagopoulos et al., 2019).

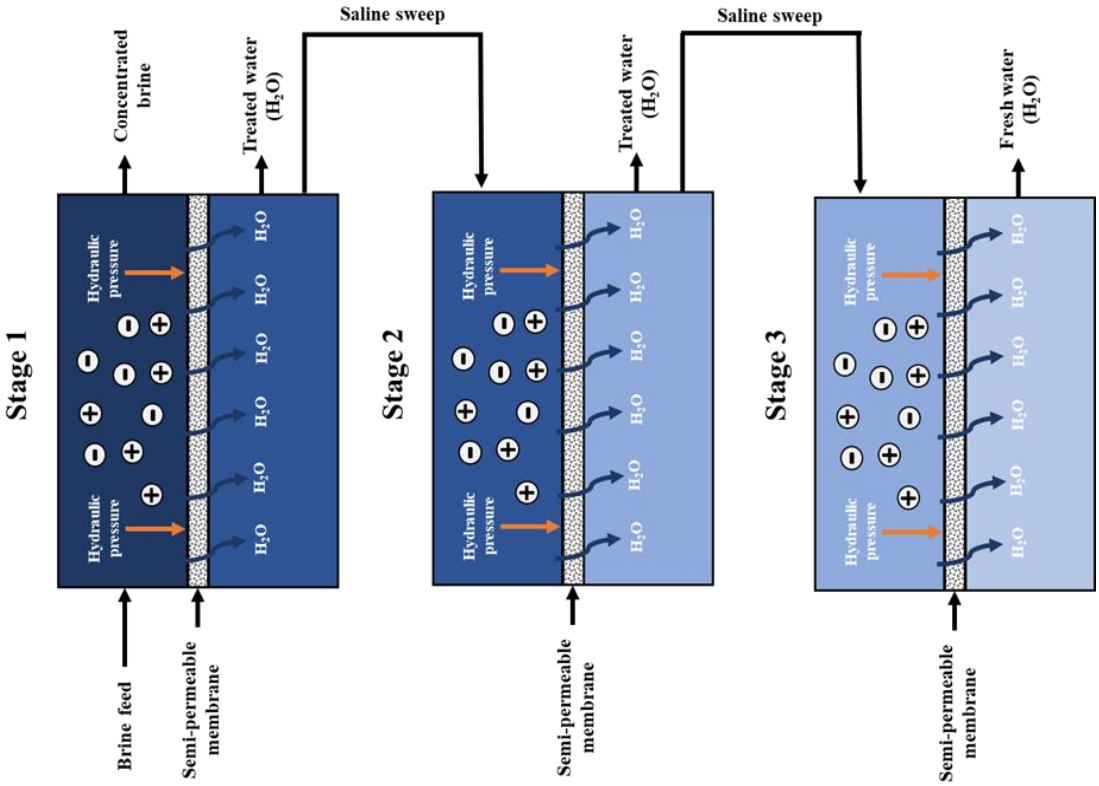

Figure 7. The common schematic diagram of OARO. Adapted from: Kim and Min, 2020; Bartholomew et al., 2017.

vii. Electrodialysis (ED), and electrodialysis reversal (EDR)

ED/EDR are developing techniques, which are membrane processes that work by voltage power (Kaplan et al., 2017). In these processes, an electric current separates inorganic ions across a semi-permeable membrane (Zhao et al., 2019). ED works by selectively transporting ions present in solutions like brine through the application of

an electrical voltage gradient to move anions and cations across semi-permeable membranes in opposite directions. The configuration of ED involves the presence of alternating cation exchange membranes (CEM) in alternating series. Also, ED contains anion exchange membranes (AEM) between an anode and a cathode. This results in the movement of anions towards the anode of positive charge and the movement of cations towards the cathode of negative charge. Untimely, this leads to the separation of brine solutions containing concentrated salts from freshwater (Figure 8) (Tado et al., 2016). Similarly, the electrochemical principles of ED are present in EDR; however, in EDR the DC voltage is reversed three to four times every hour. This occurs to minimize fouling and scaling issues by reversing the ions' transportation (Asraf-Snir et al., 2018; Qureshi and Zubair, 2016). According to Ahmad and Williams (2012), ED/EDR can recover up to 50% of the treated water, there are still some challenges faced when using such a technique. ED/EDR is highly energy consumptive but scaling membranes is not as problematic as for RO. To compare, a study done by Zhao and others (2019) discussed that the energy consumption of ED and EDR is moderate when compared to its ability to remediate highly saline feed water. Moreover, the same study reported that the anti-fouling properties of ED and EDR are somewhat efficient in comparison to other treatment technologies. McGovern and others (2014) reported that when the voltage is optimized in ED/EDR while treating high TDS-brine, the costs could be reduced by 30%- 50%. Furthermore, they suggested using ED in combination with RO to treat high saline brine. The recovery of salt and freshwater from synthesized RO brine containing a TDS concentration of 107 g/L was performed by Jiang and others (2014) using a three-stage semi-batch ED system. The concentration of the RO brine to 271.3 g/L TDS and recovery of freshwater of 67.78% was successfully achieved. However, extremely low freshwater purity was produced as TDS of 2.7 g/L, which was

similar to brackish waters. Another study done by McGovern and others (2014) showed that a ten-stage ED system could treat a brine solution containing 195 g/L NaCl concentration with producing extremely pure freshwater of 0.24 g/L TDS concentration. This shows the significant importance of the number of ED stages in the production of pure water. Therefore, scientists should choose the ED process that involves an optimum number of stages in order to obtain highly concentrated brine as well as highly pure freshwater for use. It is important to note that the number of ED stages has a direct effect on the process's cost, which would increase with the number of stages employed. The cost of ED stages employed is demonstrated by many studies. For example, Yan and others (2019) employed a three-stage ED technology for the treatment of a brine solution. They were able to concentrate the brine solution from a TDS concentration of 3.5 g/L to 20.6 g/L. Also, a seawater reverse osmosis brine solution was successfully concentrated to a TDS concentration of 45,000 mg/L while recovering 82% freshwater by Zhang and others (2017). An interesting observation was common between the two studies. The researchers observed that employing the third stage on the ED system resulted in more expenditure of energy than the first two stages. This would ultimately raise the process cost. Moreover, Reig and others (2014) tested a pilot ED plant for the treatment of seawater reverse osmosis brine solution containing a TDS concentration of 70,000 mg/L. The study involved the application of full-scale plant conditions. The results of the study indicated the successful concentration of the brine solution to a TDS concentration of 245,000 mg/L. They observed that increasing the temperatures, led to the production of less concentrated brine solution. At the same time, the study showed that increasing the inlet temperatures resulted in lower consumption of energy and higher production flow. General Electric company has developed a commercial EDR system known as the non-thermal brine contractor which

is capable of treating brackish water reverse osmosis brine solutions and achieve a recovery of freshwater as high as 99% (General Electric company, 2013). Similarly, a variety of commercial EDR systems were developed by Saltworks Technologies Inc., which could be employed to treat and concentrate reverse osmosis brine solutions to a TDS concentration as high as 180,000 mg/L (Saltworks Technologies Inc., 2019). Furthermore, fouling of ED and EDR membranes is a common issue that has to be solved by pretreatment. For instance, the presence of some compounds in the feed solution like sulfates or organic matter are common precursors for membrane fouling problems (Mikhaylin and Bazinet, 2016; Asraf-Snir et al., 2016).

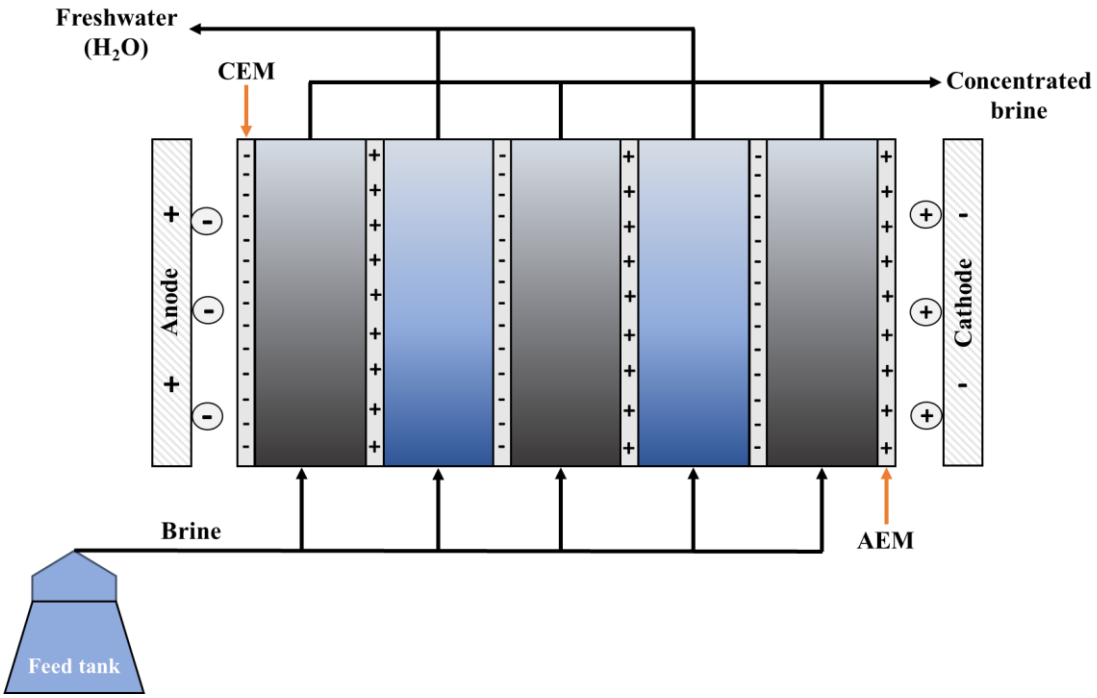

Figure 8. The common schematic diagram of ED. Adapted from: Al-Anzi et al., 2020; Panagopoulos et al., 2019.

2.3.2.1 Impacts of conventional brine treatment and recovery technologies

Similar to the case of the direct environmental disposal brine methods, the ZLD treatment technologies have many implementation challenges. Thermal brine treatment technologies were developed more than 60 years ago, however, they suffer from requiring high capital and energy costs, specific complex designs, as well as pre-treatment chemicals and stages. Similarly, membrane desalination technologies require intensive pre-treatment and/or post-treatment stages in order to limit emissions of volatile compounds, scaling, and fouling (Mavukkandy et al., 2019). Also, many of the mentioned conventional brine treatment and recovery technologies suffer from low thermal efficiencies and membrane fluxes, membrane wetting, fouling, scaling, constant maintenance, undesired recovery rates, and high costs. All these challenges pose economic constraints and environmental risks, which if not handled properly, would accumulate greenhouse gases as well as pollution and harm living organisms (Mavukkandy et al., 2019). Therefore, it is necessary to find methods to recover valuable metals from brines and overcome the mentioned constraints and challenges related to the brine disposal methods and the treatment technologies.

2.4 Adsorption as a novel brine recovery process

Many studies have investigated the great potentials of adsorption processes in the recovery of valuable minerals and resources from a variety of streams like seawater and brine (Yang et al., 2019; Liu and Gao, 2019; Ryu et al., 2019). Adsorption is a mass transfer process that is efficient, economic, simple, and selective towards specific pollutants and is widely applied for the removal of many targeted substances from seawaters, wastewaters, and brine streams (Tang et al., 2019). Like any recovery process, adsorption processes efficiency and capacities towards the full removal of

minerals and metals from brine depend on the process design, and operation specifications as well as flexibilities (Haifa et al., 2021; Lakherwal, 2014). Adsorption (Figure 9 (A)) is based on the use of a solid material referred to as an adsorbent that receives the target mineral known as adsorbate on its surface (Xing et al., 2021). The surface of adsorbents should contain pores known as adsorption active sites, which the adsorbate material bonds chemically or physically. The chemical bonding between the adsorbate and adsorbent is characterized by the formation of strong irreversible covalent bonds. On the other hand, the forces of attraction between the adsorbent and adsorbate molecules that occur in a physical adsorption bonding are due to the weaker van der Waals forces (Al-Ghouti and Al-Absi, 2020). Scientists are usually interested in adsorption processes that occur due to physical bonding, as it is easier and simpler to regenerate the adsorbent after the adsorption process is completed in a process known as desorption (Figure 9 (B)). This allows for the re-use of the adsorbent, which is a cost-effective and environmentally friendly approach in any waste removal or mineral recovery adsorption process (Vardhan et al., 2019).

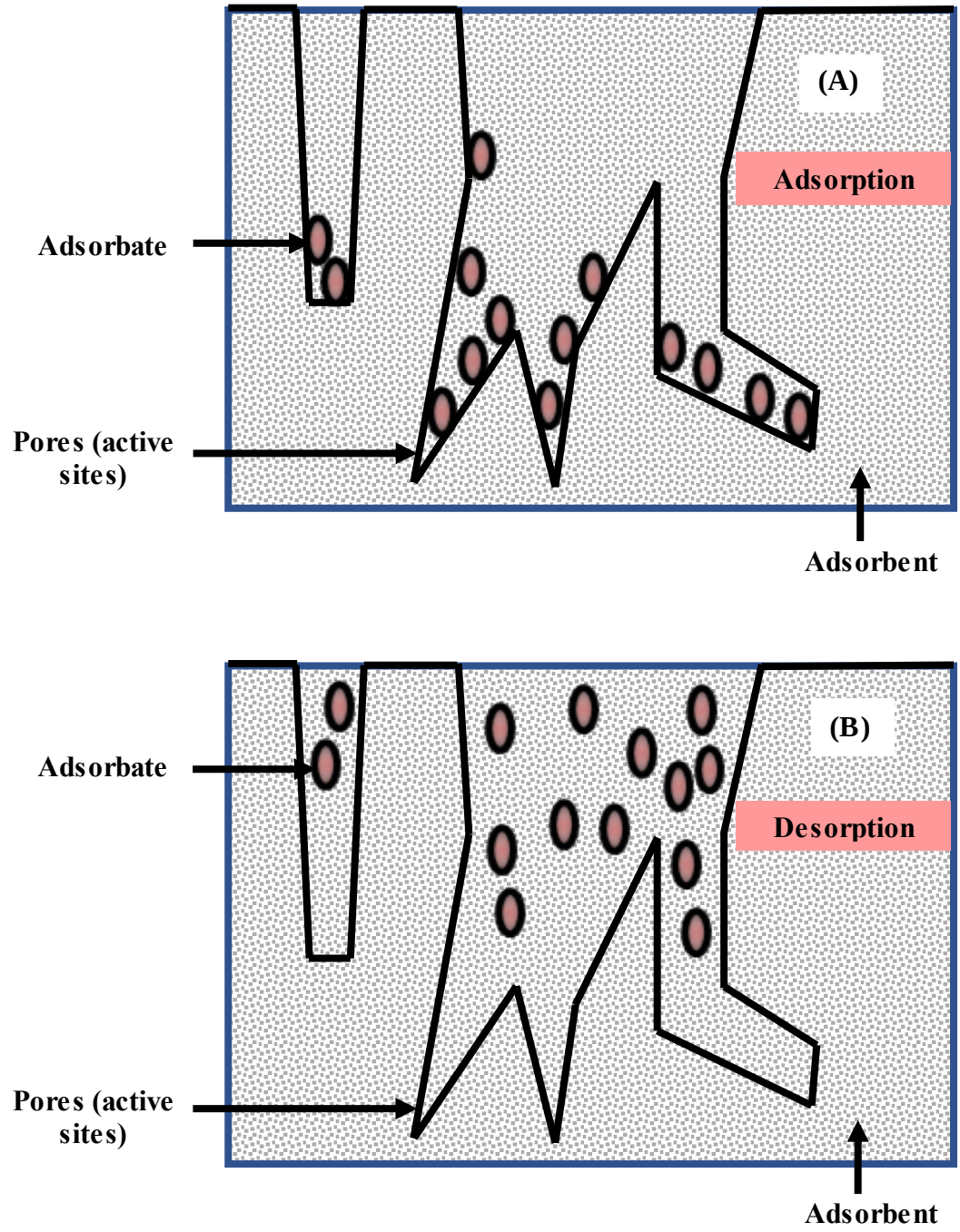

Figure 9. Diagram presenting the adsorption (A) and desorption (B) of adsorbate molecules onto the active sites of an adsorbent.

The technologies implemented in recovering valuable metals and minerals from brine streams are recognized as fixed bed and batch adsorption. A fixed bed adsorption technology (Figure 10) employs a fixed adsorbent material on a column that receives contaminated solutions continuously (Biswas and Mishra, 2015; Albroomi et al., 2017). In contrast, batch adsorption technology (Figure 11) involves the addition of a known adsorbent amount to a known volume of contaminated solution. After that, the adsorption process is left to reach an equilibrium state. Generally, batch adsorption technology is implemented when the concentration of contaminants or valuable substances is high due to its efficient performance. Additionally, batch adsorption is cheaper than fixed-bed adsorption technology and requires less maintenance due to its simplicity (Albroomi et al., 2017).

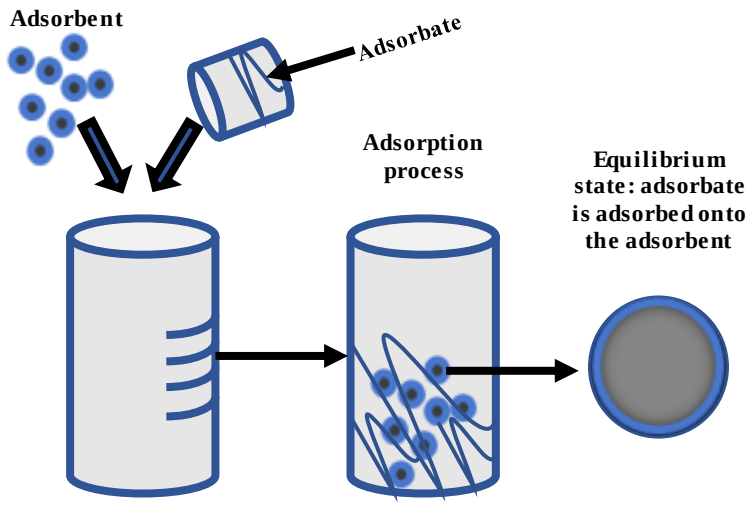

Figure 10. Diagram presenting the main stages in a batch adsorption process.

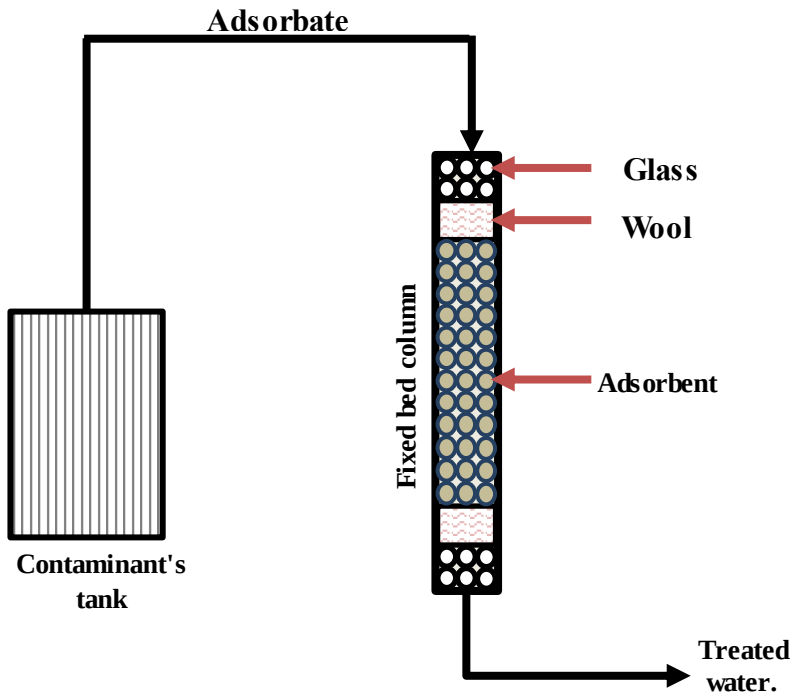

Figure 11. The common schematic diagram of a fixed bed adsorption process. Adapted from: Fallah and Taghizadeh, 2020; Henrique et al., 2020.

The quantity of adsorbate that an adsorbent can carry per unit mass is known as the adsorption capacity (qe). The adsorption capacity is usually calculated and determined through a mathematical formula shown in equation 1 (Chowdhury et al., 2020; Rojas-Mayorga et al., 2020).

$$\text{Equation 1: } qe = \frac{(C_i - C_e)V}{m}$$

Where C_i and C_e are the initial and equilibrium concentration (ppm) of the metal ion, respectively. V is the volume (L) of the solution and m is the mass (g) of the material used.

Moreover, the percentage removal of pollutants from a waste stream is calculated as

the adsorption efficiency, which gives insights regarding the capability of an adsorbent in adsorbing a given pollutant in terms of a whole percentage. The percentage removal/efficiency of adsorbents for pollutants is calculated and determined by equation 2 (Pelalak et al., 2021):

$$\text{Equation 2: \% Removal} = \frac{C_o - C_e}{C_o} \, x \, 100$$

Where C_o is the concentration in mg/L of the adsorbate before adsorption, C_e is the concentration of the adsorbate after adsorption is completed in mg/L.

The adsorption capacity of adsorbents is largely affected by many factors. Some of the major factors include the adsorbate characteristics, adsorbent surface area, reaction time, polarity, adsorbent shape and pore size, temperature, presence of functional groups on the adsorbent, initial solution pH, and others. In addition, the presence of many metals of competing nature to the target metal could greatly affect the adsorption process (Li et al., 2020; Gao et al., 2009). This is due to the fact that some metals, due to their characteristics and the surrounding conditions, would be more attracted to the adsorbent material in terms of the formation of chemical or physical bonds (Fotoohi and Mercier, 2014; Gao et al., 2009).

2.4.1 Adsorption isotherm models

Furthermore, the adsorption isotherm models can achieve an understanding of the quantity of adsorbed and non-adsorbed adsorbate molecules as well as the distributions of the adsorbate molecules at different equilibrium concentrations ref. The adsorption isotherms take into account the adsorption capacity (qe) of the adsorbent. Several

models have been developed with the most studied ones being Langmuir and Freundlich (Can et al., 2016; Núñez-Gómez et al., 2019).

The Langmuir adsorption isotherm model describes adsorbents as having identical, equivalent, finite and definite adsorption active sites. The model assumes that adsorbates form a homogenous monolayer on the surface of the adsorbent, where the adsorbate molecules on the adjacent active sites would not interact with each other (Al-Ghouti and Al-Absi, 2020; Apolinario and Pires, 2020). To analyze Langmuir's adsorption model for a given adsorption process, the linear equation could be used (Equation 3):

$$\text{Equation 3: } \frac{C_e}{q_e} = \frac{C_e}{C_m} + \frac{1}{K_L C_m}$$

Where C_e is the equilibrium concentration (mg/L) of the adsorbate, the equilibrium adsorption capacity (mg/g) is q_e, the constant for the adsorption capacity for the formation of a monolayer in mg/g is C_m and the constant describing the adsorption sites affinity towards the adsorbate in L/mg is K_L. The Langmuir plot between $\frac{C_e}{q_e} Vs. C_e$ provides the necessary values for the calculation of the Langmuir constants (K_L and C_m) through the slope and intercept (Kaur et al., 2013; Ezzati, 2020; Apolinario and Pires, 2020).

On the other hand, the Freundlich adsorption isotherm model was the first model to be developed that would provide explanations regarding adsorption process mechanisms ref. Opposite to Langmuir's adsorption isotherm model, the Freundlich model does not assume the formation of a monolayer of adsorbate molecules on the surface of the adsorbent. The Freundlich model assumes the formation of a non-uniform multilayer

of adsorbate molecules on the adsorbent's surface through a reversible and non-ideal adsorption mechanism (Terangpi and Chakraborty, 2017).

This leads to the conclusion that the adsorbate molecules would compete for the available adsorption active sites and that the molecules with higher affinities towards the active sites would occupy them first until an equilibrium state is achieved between the adsorbent and adsorbate molecules (Nnadozie and Ajibade, 2020).

Similar to Langmuir's adsorption isotherm model, the linear equation of the Freundlich model is shown in equation 4 below. The model is plotted as ln (q_e) vs. ln (C_e) (Abbas, 2020).

Equation 4: $$\log Q_e = \log K_f + \frac{1}{n}\log C_e$$

Where q_e is the adsorption capacity in mg/g, the K_f is the model's constant in terms of mg/g, the level of deviation from linearity is n, and C_e is the equilibrium concentration of the adsorbate in mg/L (Uddin et al., 2017).

2.4.2 Adsorption thermodynamics

The temperature at which adsorption systems are employed largely contributes to the overall adsorption capacities, efficiencies, and behaviors (Yang et al., 2019). This is because adsorption is either a chemical or a physical reaction that largely depends on energy. Some adsorption systems require high energy while others occur with the release of energy. Adsorptions that require energy are referred to as endothermic while adsorptions that heat the surroundings are called exothermic (Humelnicu et al., 2020). Moreover, adsorption reactions could be characterized as reversible or irreversible through studying their thermodynamic aspects. Reversible reactions take place at fixed

rates known as equilibrium states and do not dissipate energy (Wadhawan et al., 2020). On the other hand, irreversible reactions are spontaneous, finite, and do not need external factors to take place. Many important adsorption parameters like entropy, enthalpy, and Gibbs free energy are defined by thermodynamics science. These parameters help scientists in defining adsorption systems as spontaneous, favorable, endothermic, or exothermic (Yadav et al., 2021). Temperature provides heat energy to adsorption systems and either facilitate the diffusion of pollutants onto the surface of adsorbents or decreases it. Heat energy (q) is calculated as the molar heat capacity (C) multiplied by the amount of a substance and temperature rise (ΔT). The amount of internal energy that a system holds and needed to be created is known as enthalpy change ($\Delta H°$) which is expressed in the unit of kJ/mol. Interestingly, if the enthalpy change value holds a positive sign, the adsorption reaction is endothermic. On the other hand, a negative enthalpy change value indicates an exothermic reaction (Konicki et al., 2017). Moreover, the likelihood and favorability of a reaction are determined by entropy change ($\Delta S°$) in the unit of J/K.mol. Entropy change provides ideas about the spontaneously of reactions and their level of disorder. The idea is that favorable and spontaneous reactions take place at a higher disorder degree than non-spontaneous reactions ref. Thus, spontaneous and favorable reactions would have positive entropy change values, while non-favorable reactions would hold negative ones. A third and important thermodynamic aspect of reactions is Gibbs free energy or change in Gibbs free energy ($\Delta G°$). This parameter takes into account entropy, enthalpy, and temperature in kelvins to indicate the tendency of a reaction to occur. Gibbs free energy aspect is based on the assumption that reactions (adsorption) would preferably occur in a way that would maximize entropy and minimize enthalpy (Aljerf, 2018; Yadav et al., 2021). These thermodynamic aspects of reactions are vital in studying and optimizing

an adsorption clean-up or recovery process. This is because thermodynamics provides significant insights regarding the adsorption tendencies, behaviors, and energy requirements as well as cost and overall sustainability. The calculation of Gibbs free energy for adsorption systems can be done through the following equation 5:

Equation 5: $\Delta G° = -RT\ lnkL$

Where R is the universal gas constant of the value of 8.314 J/mol.K, T is the absolute temperature in kelvins, and k_L is Langmuir isotherm constant, which can be expressed as standard enthalpy and entropy changes of adsorption as functions of temperature (Yadav et al., 2021).

The relationship between temperature and k_L is shown in the following formula known as Van't Hoff equation 6:

Equation 6: $LnkL = -\Delta H°RT + \Delta S°R$

Where a plot of lnk_L Vs. $1T$ can be used to determine the values of $\Delta H°$ and $\Delta S°$ from the slope and intercept (Yadav et al., 2021; Konicki et al., 2017).

2.5 Date pits as novel and efficient brine metal recovery adsorbents

Conventional adsorbents like chitosan, alumina, activated carbon, silica gels, ion exchange resins, and zeolites can be effective in remediating or recovering valuable substances and metals from brine streams (Wu et al., 2020; Borja-Urzola et al., 2021). However, many studies have reported that the modification and production requirements, complexity, durability, and high cost, of these conventional adsorbents, add challenges to their successful and environmentally friendly application (Al-Saad et

al., 2019; Deliyanni Eleni et al., 2015). Therefore, and recently, scientists are investigating the application of natural agricultural wastes such as maize cob, coconut sawdust, silk cotton hull, banana pith, sago waste, and various kinds of fruit seeds or pits their great recovery and treatment potentials of pollutants or valuable substances from different kinds of streams like brine (Burakov et al., 2017). Many GCC like Qatar are home countries for the growth of palm-trees. In Qatar, the annual date fruit production can be as high as 8,460,443 metric tons. This makes date pits an abundant by-product or waste of date production in Qatar as well as many GCC. Studies have shown that 960,000 tons of date pits are discarded yearly by the global palm-tree sector. Interestingly, date pits possess all the previously mentioned properties of an efficient, adequate, readily available, cheap, and selective adsorbent for recovering valuable metals from brine streams (Al-Saad et al., 2019). The composition of date pits is mainly 55-65% carbohydrates, 57% protein, 10-20% fibers, 5-10% moisture, 1-2% ash, and 7-10% oils. This composition makes date pits a novel adsorbent for many pollutants in the environment and metals from brine. Raw, roasted, or burnt, chemically modified date pits are some of the forms employed in this context (Aldawsari et al., 2017). Al-Ghouti and others (2019) revealed the efficiency of roasting and modifying date pits (in the forms of sulfur-modified roasted date pits and silane-modified roasted date pits) in adsorbing mercury from an aqueous media. Another study performed by Al-Saad and coworkers (2019) showed that burning date pits prior to the adsorption process enhanced their adsorption capacity towards Cu (II) due to the formation of rich carbonaceous material. Al-Ghouti and coworkers (2014) investigated a comparison between the adsorption efficiency of roasted date pits and activated charcoal towards bromide. The results of the study demonstrated that modifying the surface of the date pits increased their adsorptive capacity by 27%. Moreover, the presence of oxygen

functional groups on the surface of the roasted date pits allowed a significant removal of bromide. Both adsorbents in the study achieved similar adsorptive capacities towards bromide, however, roasted date pits are a more cost-effective option. A more recent study done by Mangwandi and coworkers (2020) studied the adsorptive capacities of chemically modified olive stones and date pits towards hexavalent chromium (Cr (VI)) in an aqueous solution. The study found that the chemically modified date pit achieved higher adsorption capacity (82.63 mg/g) than the chemically modified olive stone (53.31 mg/g) under the same experimental conditions. These studies, among many others, show the great efficiency of date pits in the removal of metals from aqueous media.

2.5.1 Metal hexacyanoferrates (MHCFs) as novel date pits modifiers for brine metal recovery and adsorption

Moreover, metal hexacyanoferrates (MHCFs) are coordination polymers that contain coordinated bridges of C≡N and a transition metal ion like Cu^{2+}, Fe^{3+}, Co^{2+}, and Ni^{2+}. Another well-known name for MHCFs is Prussian blue or iron hexacyanoferrate (Figure 12 (A) and (B)). Prussian blue and many of its analogs are used in many fields nowadays such as batteries, dyeing, corrosion protection, energy and information storage, and biomedicine as well as in environmental cleanup and remediation of pollutants (Oliveira et al., 2018; Loos-Neskovic et al., 2004; Wessells et al., 2011). Interestingly, MHCFs are considered to be novel adsorbents for many pollutants from a variety of streams like wastewaters, brackish waters, seawater, and brine streams. These materials are commonly applied in metal extraction, recovery, and adsorption due to their insolubility, high selectivity, and adsorptive capacities. In general, MHCFs have a unique open zeolite-like morphology and a structure of a face-centered cubic lattice (Figure 12 (B)) (Wang et al., 2018).

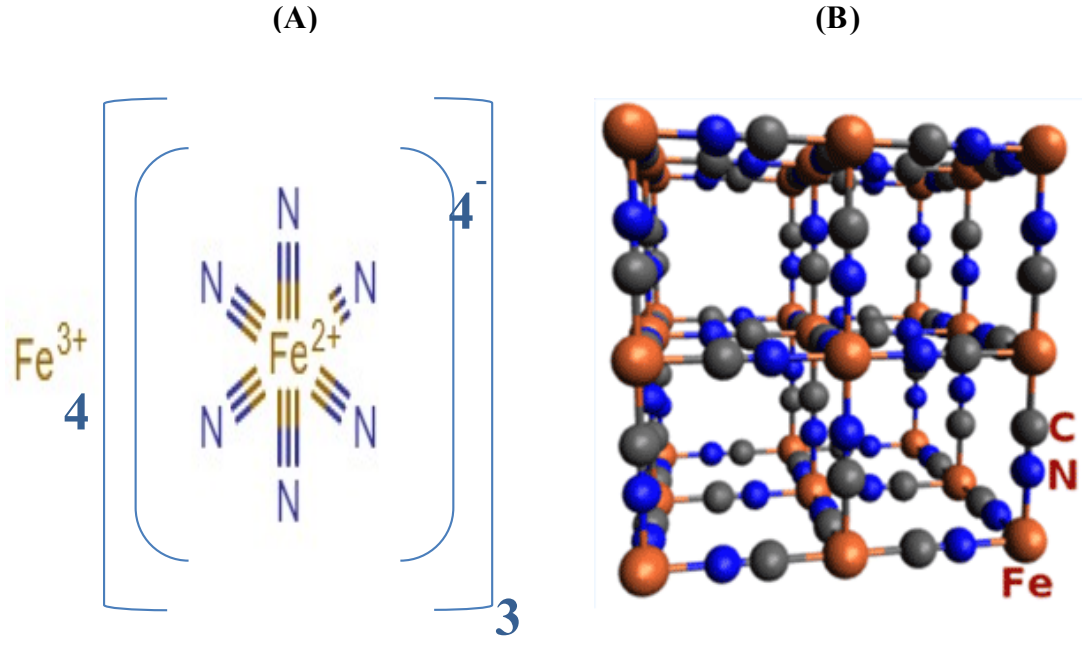

Figure 12. (A) Chemical structure of Prussian blue or iron hexacyanoferrate and (B) its cubic lattice structure. Adapted from: Yi et al., 2020; Prussian blue - American Chemical Society, 2017.

Interestingly, hexacyanoferrates that could be effectively used as metal adsorbents can be synthesized into a variety of structures, compositions, and characteristics. The unique structure of metal hexacyanoferrates gives them the adsorptive capabilities towards metals through ion exchange mechanisms. Different compositions of MHCFs that contain the same transition metal could be prepared by altering their structural arrangements. For example, it was reported that some of the structures of metal hexacyanoferrates include compact and trigonal, zeolitic rhombohedral with cavities, and cubic lattices with iron vacancies (Loos-Neskovic et al., 2004; Wessells et al., 2011). This gives a significant note regarding the flexibility in the preparation of MHCFs for adsorption purposes. As mentioned previously, the effectiveness of adsorption processes depends largely on the characteristics of the adsorbents, adsorbates, and surrounding conditions. Therefore, when scientists deal with the

preparation of MHCFs for adsorbing a target metal, they could have a variety of options in terms of their preparations, cost, feasibility, and effectiveness. Almost all the synthesis methods of MHCFs are cost-effective and simple, with the most employed method is initiating a precipitation reaction between the precursors of hexacyanoferrate and the transition metals (Kim et al., 2017). This provides more chances for countries with limited resources to utilize MHCFs for environmental cleanup and metal recovery purposes. For example, MHCF's could be synthesized with potassium to form potassium hexacyanoferrates (Figure 13). These materials exhibit high adsorptive capacities towards metals as the mechanism of adsorption could involve ion exchange with the potassium ion. As a result of an exchange between the hydrated target metal and potassium, the target metal would be effectively caged through adsorption within the matrix of the MHCFs, which causes structural changes. Many publications reported that during batch adsorption experiments that involve MHCFs as adsorbents for metals, the target-hydrated metal would be mobilized and exchanged with potassium ions within the thin layers of the cubic structure of the MHCF's (Moloney et al., 2020; Kim et al., 2017; Loos-Neskovic et al., 2004; Wessells et al., 2011). Furthermore, the selectivity of MHCFs is ought to the transition metal applied as well as the target metal to be adsorbed. The affinity of the target metal for ion exchange, largely depends on its characteristics, in terms of polarity, hydration, atomic size, and ionic size as well as the structure and chemical properties of the MHCFs employed (Moloney et al., 2020; Zhuang and Wang, 2019).

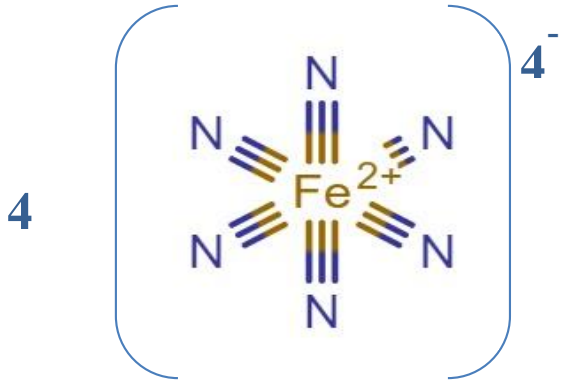

Figure 13. The chemical structure of a common potassium hexacyanoferrate.

Despite the low cost, selectivity, high adsorption capacities, and simplicity of the synthesis and utilization of metal hexacyanoferrates, their regeneration or recovery could be a complex process due to their submicron sizes. Therefore, many studies have investigated the synthesis of MHCFs with support materials. The process of combining MHCFs with support materials is usually simple and involves either encapsulation with polymers or grafting onto the materials. Various polymers have been employed in the encapsulation of MHCFs such as polyacrylic acid, polyacrylonitrile, chitin, and alginate. Similarly, many porous materials have been used for the grafting of MHCFs like carbon allotropes and silica. This combination of MHCFs to various supporters has been reported to enhance their adsorptive properties, capacities due to enhanced surface area and active sites, functionality, as well as selectivity due to unique chemical compositions and electrostatic attractions (Kim et al., 2017; El-Bahy et al., 2018). A study done by El-Bahy and others (2018) studied the adsorption of cesium onto copper hexacyanoferrate combined with carbomer. The results of the study revealed the rapid, selective, and high adsorption capacity of the composite adsorbent at pH 9, metal concentration of 9 mmol/L, and 25 °C. This means that the adsorbent was highly efficient in adsorbing cesium at room temperature, which indicates the simplicity of its utilization. Another study mentioned that copper hexacyanoferrate has been widely

used for metal adsorption due to its highly beneficial and environmentally friendly characteristics. Some of these characteristics include open channels, cubic framework, stability, and low toxicity (Long et al., 2020; Li et al., 2018). Moreover, Kim and coworkers (2017) showed the exceptional adsorption capacity, selectivity, and dispersion capability of a potassium copper hexacyanoferrate composite towards cesium adsorption from seawater. A cellulose-based hydrogel of hydroxyethyl cellulose and carboxymethyl cellulose was used as an immobilizer for the potassium copper hexacyanoferrate. The results of the study revealed that the adsorption mechanism of cesium onto the composite was through ion exchange in the adsorption sites. Furthermore, Martin and coworkers (2019) investigated the adsorption of different concentrations of cesium onto potassium nickel hexacyanoferrate composite. The study revealed that the composite was highly effective in terms of adsorption capacity and encapsulation of cesium ions from the solution. The solution pH was found to largely affect the structure of the adsorbent and its adsorptive mechanisms.

2.6 Analytical techniques for the physicochemical characterizations of brine streams as well as roasted and composite date pits as novel metal adsorbents

As mentioned previously, reverse osmosis concentrated brine contains various salts, metals, and minerals such as Ca^{2+}, K^{+}, Na^{+}, Mg^{2+}, Li^{+}, Rb^{+}, Cs^{+}, and many others. These minerals and valuable substances contained in desalination brine can be effectively removed and recovered using adsorbents such as date pits. The main reason for the recovery of the mentioned substances is that they can be used in industries, medicine, agriculture, and environmental remediation (Loganathan et al., 2017). Prior to performing a successful adsorption process for the valuable substances contained in brine streams, it is important to examine and understand the physical and chemical characteristics of the brine stream as well as the adsorbents involved in the process

(Wang et al., 2018; Tourino et al., 2018). Once a full understanding of the components of the brine is achieved, scientists can target the removal and recovery of specific substances. This could be accomplished through the optimization of certain process parameters and increasing the adsorption capacity of the adsorbent towards the targeted substance (Li et al., 2020; Al-Ghouti and Al-Absi, 2020). As mentioned previously, the selection of a selective adsorbent towards a pollutant or substance is extremely important, as it would save additional costs, lessen the process duration, and most importantly, achieve full recovery of valuable substances from brine. It is important to note that the selection of an effective adsorbent for a brine recovery and management process through adsorption depends on the physical and chemical characteristics of the brine stream as well as the adsorbents. There are many analytical physical and chemical tests and analyses that are involved in the characterization of brine streams and date pits (Naeimi and Faghihian, 2017; Gringer et al., 2014; Arshad et al., 2014; Al-Saad et al., 2019).

2.6.1 Physical and chemical characterizations of brine streams

Brines from desalination plants as well as brackish waters could be physically analyzed using various developed analytical techniques. The pH is often measured and determined for brines to determine the alkalinity, which as mentioned previously, could significantly pose various impacts on the environment and human health. Another reason for determining the pH of brines is to optimize an adsorption process where the brine is to be treated or recovered. The pH is one of the most important parameters that affect the adsorption capacity and efficiency. When targeting charged pollutants such as dyes and metal ions, it is necessary to study the electrostatic attraction and repulsion forces that may arise between the adsorbent and the adsorbate. This is because scientists

often aim at increasing the electrostatic attraction forces between the pollutant and the adsorbents, in order to achieve an efficient and high adsorption capacity, treatment process, and recovery (Pramanik et al., 2020). Moreover, it is important to note that the pH will vary significantly depending on the original source of the brine stream. Therefore, examining and optimizing the adsorption process pH working condition is vital. This was shown by many studies that have investigated the pH of brine streams. For example, a study done by Zaman and coworkers (2015) found that the pH of the reverse osmosis brine was lower than the pH of the reverse osmosis feedwater pH. The brine involved in the study was alkaline with a pH value of 8.842. Another study performed by Ali Osman and others (2014) investigated the pH of six different types of brine solutions originating from the production process of fish. The results revealed that the pH ranged from acidic (pH 4) to slightly basic (pH 6.96). Moreover, Kasedde and coworkers (2014) measured the pH value of brines sourced from different locations at Lake Katwe. The pH of the brines collected from the 15 locations ranged from 9.7 to 10 showing high alkalinity. Maxwell and others (2020) tested the pH for one staged and two stages reverse osmosis brine samples and found that the pH changed from an initial value of 7.8 to 6.9 for the two-staged brine while it reached to 7.9 for the one staged brine sample. Therefore, to enhance the adsorptive mass transfer and capacity for specific valuable metals or pollutants from brine streams, it is important to study and adjust the pH for the brine in a way that would increase the electrostatic attraction forces between the adsorbent and adsorbate.

Another important physical parameter that is often studied for brines involved in an adsorption process is salinity. As mentioned previously, brines are a concentrated by-product of a desalination process. This leads to the expectation that the salinity of brines is usually higher than seawater (the feed to a desalination plant). The salinity of

seawater is found to be equal to 35 Practical Salinity Unit (psu) on average (Xu et al., 2020). However, the salinity of brines is usually much higher depending on the desalination technology employed, process parameters, and conditions (Wu et al., 2020). For example, a study done by Sola and others (2020) found that the salinity of the discharged brine from a seawater reverse osmosis desalination brine was on average equal to 68 psu, which is more than double the salinity of seawater. The salinity greatly affects the conductivity of the brine stream as well as gives indications regarding the ion quantities in the brine stream. As one would expect, the higher the salinity of a brine stream, the higher presence of competing ions for adsorption. As mentioned previously, adsorption processes are very specific towards a certain charged molecule, pollutant, or metal ion of interest. Therefore, the presence of other metals of higher quantities than the targeted metal that represents very similar characteristics could significantly affect the adsorption capacity and efficiency towards the target metal of interest. However, it could be possible to enhance the adsorptive selectivity towards the target metal of interest through the enhancement of the chemical and physical characteristics of the adsorbent. This was shown by a study done by Petersková and others (2012) on the adsorption of cesium onto two different adsorbents from a reverse osmosis brine. The results revealed that the adsorption capacity of zirconium phosphate-based material adsorbent towards cesium decreased with the increase in the salinity of the brine. This means that the presence of other competing ions than cesium increased with the increase in salinity, which indicates the significant negative impact on the adsorption of the target metal. The competing ions would occupy the available active sites on the adsorbent and prevent the high adsorption of cesium. However, interestingly, another adsorbent; hexacyanoferrate-based extractant, which exhibits highly selective chemical and physical characteristics towards cesium, was not impacted by the increase in the

salinity of the brine. Li and others (2020) demonstrated that the salinity significantly affected the carbon dioxide adsorption in brine onto silica gel. The sequestration of carbon dioxide onto the silica gel in brine favored lowered salinity levels than higher levels due to solubility trapping.

Similar to the physical characterization tests for brine streams, chemical characterization is vital to optimizing a valuable resource recovery or treatment through adsorption. As mentioned previously, adsorption processes could be selective towards a specific substance, which accounts for their novelty in resource recovery and pollutant treatment from an aqueous media. Therefore, scientists often seek the chemical characterization of their media to fully understand and determine its composition prior to adsorption. Brine streams could be chemically analyzed by ion chromatography (IC), inductively coupled mass spectrometry (ICP-MS), and/or inductively coupled plasma atomic emission spectrometry (ICP-OES), also referred to as inductively coupled plasma atomic emission spectrometry (ICP-AES), for the determination of ionic species such as valuable metals. The separation of charged molecules and ions present in a liquid sample according to the affinity of their charged groups to an ion exchanger can be done using a simple ion chromatography analytical technique (Chan et al., 2020). This allows for the chemical analysis of liquid samples through the quantification and determination of the major cations and anions present in the sample. Metals are either positively or negatively charged; therefore, brine samples involved in an adsorption process could be chemically characterized for major metallic constitutes using ion chromatography (Bruckner, 2020; Dovidauskas et al., 2020). On the other hand, ICP-OES and ICP-MS analytical techniques are capable of detecting trace cationic and anionic species in a liquid sample. To compare, the detection limit for the ICP-MS technique is lower than ICP-OES. This means that ICP-MS allows for the quantification

and detection of metals present at lower concentrations (parts per trillion) than with the ICP-OES analytical technique (parts per billion). The reason behind this difference between the two chemical characterization techniques stems from their operation principles. ICP-MS operates by the application of mass spectrometry in order to measure the charged molecules or ions masses. On the other hand, ICP-OES operates by the application of wavelengths that are specific towards the target element or metal to excite ions or atoms and eventually quantify and determine the concentration of the target metal (Comparison of ICP-OES and ICP-MS for Trace Element Analysis, 2020). A recent study done by Xu and others (2020) on the adsorption of cesium from brines extracted from salt lakes sought the chemical characterization of the brine using ICP-OES. The brine sample involved in the study was found to contain 2 mg/L Cesium, 20 mg/L Rubidium, and higher concentrations for sodium (19.39 g/L), magnesium (28.38 g/L), and potassium (2.772 g/L). Another study done by Liu and others (2020) investigated the extraction of rare earth metals using an adsorption process onto core-shell nanoparticles from geothermal brine. The study is of particular importance as many of the metals such as neodymium, dysprosium, scandium, yttrium, holmium, europium, and others are characterized by the department of energy is critically important for the clean energy economy. Some of the applications of these metals include enhancing the efficiency of fuel cells, hydropower, and wind turbines, as well as electric motors, thus, they help in reducing the world's reliance on fossil fuels and decrease greenhouse gas emissions. The study involved the application of ICP-OES and ICP-MS to precisely characterize the brine sample. Some of the metals were found in the parts per million range such as zinc, magnesium, calcium, sodium, and lithium, while the rare earth metals were found to exist in the parts per billion range such as dysprosium, europium, cerium, yttrium, and neodymium. Thus, the application of both

analytical methods (ICP-MS and ICP-OES) gives assurances regarding the presence of metal ions found in trace amounts. Wang and others (2017) demonstrated that a brine sample that was involved in an adsorption process for the recovery of lithium contained considerable concentrations of lithium, sodium, magnesium, potassium, and calcium. The study involved the application of ICP-OES for the chemical characterization of metals in the brine sample prior to adsorption. The same metals were found by another study conducted on the characterization of brine prior to adsorption. The study examined the metal constitutes in the brine using ICP-OES (Gu et al., 2018).

2.6.2 Physical and chemical characterizations of adsorbents

The physical characterizations of adsorbents involved in a metal recovery or pollutant removal from aqueous media such as brine streams are important. This is because it is equally beneficial to characterize adsorbents as adsorbates to select the most efficient working parameters for an adsorption process. There are many physical characterization methods for studying adsorbents such as particle size distributions, Brunauer–Emmett–Teller (BET) surface area, and pore size analysis, and scanning electron microscopy (SEM) (Al-Saad et al., 2019; Al-Ghouti et al., 2010). On the other hand, the chemical characterization tests for adsorbents include carbon and nitrogen elemental analysis, X-ray diffraction (XRD) analysis, Fourier-transform infrared spectroscopy (FTIR) analysis, and thermogravimetric analysis (TGA) (Sarfraz et al., 2020; Dou et al., 2021).

i. Particle size distribution (PSD) test

One of the most influential factors to the efficient and high adsorptive properties of a given adsorbent is particle size. It is well accepted and established that the particle sizes

of adsorbents largely contribute to their overall surface area, which affects their adsorption capacities (Lu et al., 2020). In other words, the smaller the particle size of an adsorbent, the larger surface area it will exhibit. This results in an overall enhancement in its adsorption capacities towards pollutants of different kinds and natures and particular interest, the adsorption and recovery of valuable metals from solutions. Therefore, there is a great link between the particle size of an adsorbent and the available adsorption binding sites on its surface (Li et al., 2021). A useful analytical technique that can precisely and accurately measure the particle sizes of adsorbents is known as the particle size distribution (PSD) test. This technique presents the full distribution pattern of the different particle sizes present in a homogenous sample of an adsorbent. Through this technique, one can view the different particle sizes a sample holds in different proportions in terms of percentage. Thus, this technique is based on the assumption that the total amount of particles in a sample is 100% (Arslanoglu, 2021). Scientists are most interested in determining the distribution of the various particle sizes for an unknown size adsorbent. The PSD test is beneficial for confirming the particle size distributions present in a synthetically prepared adsorbent sample (Kumar et al., 2019). There are two commonly established and used working principles for particle size distribution analyzers. The first working principle is based on the dispersion of a small amount of the sample into a receiving compartment where it is dispersed in water. Then monochromatic laser light is passed through the sample where it gets scattered at different angles and subsequently measured by a detector made from multi-elements. The scattering pattern of the laser light is then transformed into numerical values that are ultimately turned into the proportion of the total volume of the sample to the various particle sizes using mathematical and optical models. The second well-known working principle of PSD analyzers is based on the application of

a dynamic light through the sample compartment. The calculation of the particle size distribution is done in multiple steps. The particles of different sizes do Brownian motion inside the sample's compartment at different speeds, which leads to the fluctuation of the diffracted light by the particles. This fluctuation of light is sensed by a detector and the particle size distribution data is presented through a computer screen (Arslanoglu, 2021; Buyang et al., 2019). A study done by Kumar and others (2019) investigated the particle size distribution of four different adsorbents and their effect on the adsorption time and isotherms for phosphate from aqueous solution. The study revealed that the small-sized adsorbents achieved faster adsorption equilibrium status (7 days) than the medium and large-sized adsorbents (60-90 days). The authors suggested that the small particle size of adsorbents allows for faster internal diffusion of the adsorbate into the adsorption binding sites due to the shorter distance associated with small-sized particles. This has also resulted in the higher adsorption capacities of the smaller-sized adsorbents at the study. Another study done by Buyang and co-workers (2019) revealed the significant effect that the adsorbent's particle size poses on the adsorption capacity towards lead, zinc, and copper. The study involved five different particle size groups of <5 µm, 5-10 µm, 10-30 µm, 30-50 µm, and 50-150 µm. The results showed that the adsorption of these metals increased with the decrease in the adsorbent's particle size.

ii. Brunauer–Emmett–Teller (BET) surface area, pore size, and volume analysis

The physical analysis of the surface area, pore size, and volume of adsorbents is of significant importance for optimizing adsorption processes (Awwad et al., 2013 Naeimi and Faghihian, 2017). As mentioned previously, adsorption is a selective process where

an adsorbate would be physically or chemically adsorbed onto the active sites known as adsorption sites on an adsorbent. The mechanism of any adsorption process could be explained through various adsorption isotherm models. Therefore, the surface area, pore size, and volume of adsorbents give insights regarding the overall adsorption potential area, which helps in making conclusions regarding the efficiency of the adsorbents in terms of the availability of active sites (pores) for adsorption. The Brunauer–Emmett–Teller (BET) surface area analysis is a well-known physical characterization technique that is used to analyze adsorbents for their specific surface area as well as their pore size and volume distribution (Yu et al., 2017). The main principle of the technique is the application of nitrogen adsorption (inert gas) onto the adsorbents at a standard temperature of 77 kelvins. The quantity of the adsorbed nitrogen gas corresponds to the surface area that is available for adsorption. For example, Awwad and coworkers (2013) prepared activated carbon adsorbents from date pits through chemical and physical activation methods. The study aimed at the adsorption and removal of various heavy metals such as Co(II), Fe(III), Pb(II), Zn(II), and some metal ions like Zn^{2+}, Pb^{2+}, Fe^{3+}, and Co^{2+}. The BET analysis showed a high specific surface area of the adsorbents for adsorption. The specific surface area ranged from 290 to 702 m^2/g while the pore volumes were between 0.248 mL/g – 0.321 mL/g. This enabled the high adsorption removal percentage (above 95%) towards the heavy metals and metal ions from the aqueous samples. Another study synthesized the two adsorbents as MOF/KNiFC and MOF/Fe_3O_4/KNiFC nano-particles for the adsorption of cesium from aqueous solutions. The BET surface area and pore size distribution were done for the two adsorbents as well as MOF, KNiFC, and Fe_3O_4 nanoparticles. The results revealed that MOF/KNiFC had a surface area of 47.74 m^2/g while MOF/Fe_3O_4/KNiFC had a surface area of 111.7 m^2/g. Moreover, the MOF showed a

surface area of above 1000 m^2/g, while for KNiFC the surface area was found to be 53.76 m^2/g and 114 m^2/g for Fe_3O_4. Interestingly, the higher surface area of MOF compared to KNiFC and Fe_3O_4 gave indications regarding the successful modification and pore filling of MOF by them. This resulted in the lower surface area and pore volumes of the final products of the MOF/KNiFC and MOF/Fe_3O_4/KNiFC Nano-particles (Naeimi and Faghihian, 2017). Furthermore, Kiener and others (2019) studied the BET surface area and pore volume of activated carbon, nickel hexacyanoferrate, indium hexacyanoferrate, and copper hexacyanoferrate for the adsorption of cesium from aqueous solutions. The surface area was in the descending order of nickel hexacyanoferrate > activated carbon > copper hexacyanoferrate > indium hexacyanoferrate. The pore volume was the highest for activated carbon followed by nickel hexacyanoferrate, copper hexacyanoferrate then indium hexacyanoferrate. Interestingly, the adsorption results showed that copper hexacyanoferrates and activated carbon achieved the highest adsorption capacities towards cesium compared to the other nanoparticles. This was due to the porosity, high surface area, and functional groups of the composites; therefore, surface chemistry plays a significant role in the adsorption mechanism and capacity as well as porosity. Furthermore, Forghani and others (2020) indicated the high surface area and adsorptive capacity of synthesized metal-organic framework adsorbent towards lead and chromium present in aqueous solution. The surface area of the adsorbent was reported to be equal to 1843.9 m^2/g.

iii. Carbon and nitrogen elemental analysis

Generally, novel and efficient adsorbents are characterized by having high carbon and nitrogen contents ref. Therefore, the determination of the specific contents of carbon

and hydrogen in an adsorbent is of particular importance for the optimization of a given adsorption system. This can be done through the application of a carbon and nitrogen elemental analysis for the adsorbent at study, which is a simple, but destructive analytical technique for the chemical characterization of adsorbents (Moloukhia et al., 2016). A common carbon and nitrogen elemental analyzer work by oxidizing and decomposing the organic adsorbent sample, which mostly results in the formation of nitrogen and sulfur oxides. The oxidation reactions are usually facilitated by oxygen sources (doners) such as SnO_2, MnO_2, and CuO. The resulting oxides then form pure sulfur and carbon dioxides as well as elemental nitrogen and water as final products by reduction reactions (Bagheri et al., 2020). From this, one can conclude that determining the specific carbon and nitrogen contents present in an adsorbent sample would give indications regarding its purity, composition, and adsorptive properties towards a pollutant or a valuable metal from solutions such as brines. Furthermore, the determination of the carbon and nitrogen contents in different potential adsorbents for a given pollutant allows for the accurate comparison between the chemical characteristics, compositions, and potential adsorptive properties of these adsorbents. For example, a study done by Al-Ghouti and Al-Absi (2020) involved the carbon and nitrogen elemental analysis for two adsorbents namely green and black olive stones. The study revealed that black olive stones contained higher percentages of carbon and nitrogen than green olive stones, which revealed predictions regarding their high adsorptive properties. Moreover, Mallesh and others (2020) prepared three types of adsorbents from Waste Entada Rheedii shell (ERS) for the remediation of CO_2. In short, the three types of adsorbents were prepared from either treating the ERS with base, acid, or water. The results showed the major differences in the carbon and nitrogen contents between the three adsorbents. The authors discussed that the alkali-treated

adsorbent obtained the lowest carbon content possibly due to the fact that organic matter and specifically carbon, reacts and decomposes upon reactions with NaOH in the solution. Moreover, the results of the study showed that there are potential nitrogen-based adsorption functional groups in the three adsorbents.

iv. Thermogravimetric analysis (TGA)

Another powerful analytical technique for the chemical characterization of adsorbents is known as thermogravimetric (TGA) analysis. This technique gives valuable information regarding the thermal stability of adsorbents as well as thermal decomposition patterns as a function of time or temperature. In short, the adsorbents' weight loss could be measured using two main ways. The first and most widely used working principle of TGA analysis relies on raising the temperature of the sample at a constant heating rate and pressure while observing the weight loss. The second working principle of TGA analysis is based on maintaining a constant temperature and pressure while measuring the weight loss of the sample with time (Parameshwaran et al., 2018). The weight change of a sample is precisely and accurately measured during a TGA analysis by a scale of extreme sensitivity. The heating rate of the sample is done and controlled through the application of a programmable furnace. The main structure of a TGA analyzer consists of a thermally isolated balance, which is located above a programmable furnace. The measurement of the sample's weight occurs by placing a sample pan at the end of a high-precision hang-down wire from the balance to the furnace. The thermal isolation of the measuring balance accounts for its high sensitivity, precision, and accuracy. The weight loss percentage of a sample is calculated and presented to the examiner using a computer (Inan, 2017; Ebnesajjad, 2011). As a general trend, organic and inorganic materials would lose fractions of their weight upon

a temperature rise. This occurs as the samples degrade, oxidize, lose moisture, volatile substances, impurities, and others. Therefore, a loss in weight for an adsorbent that is involved in an environmental cleanup or recovery process is a major challenge (Sarfraz et al., 2020; Polini and Yang, 2017). This is because some adsorbents might lose valuable adsorptive characteristics when a fraction of their weight is lost. This might occur as a loss of quantity of adsorbent as well as loss of modification chemicals characteristics. Also, as mentioned previously, temperature plays a significant role in the adsorptive capacities and efficiencies of adsorbents, which is a parameter that scientists often seek to optimize in order to select and operate the most efficient adsorption process for the targeted pollutant. In other words, the successful industrial application of adsorption processes largely depends on the process's working temperature and the thermal stability as well as durability of the applied adsorbent (Hildal and Perepezko, 2018). Furthermore, high temperatures could lead to the shortening of life expectancy as well as the thermal and oxidative stability of adsorbents. If the adsorption of a pollutant favors increasing temperatures, then it becomes vital to select an appropriate adsorbent that shows high thermal and oxidative stabilities and durability's in order to achieve a great adsorption capacity (Polini and Yang, 2017; Gomes et al., 2018).

A study done by Oh and coworkers (2013) revealed that the weight percentage of mesoporous silica-based adsorbents decreased sharply at a temperature of around 350 °C and maintained a constant and gradual decrease till the temperature reached 700 °C. This could mean that the adsorbents at study lose their thermal stability and possibly their adsorptive properties at a temperature of 350°C. A more recent study applied TGA analysis to study the thermal stability of three different adsorbents. The results revealed that all the adsorbents were thermally stable until a temperature of 200 °C, which was

discussed as a temperature suitable for most industrial adsorption processes. Moreover, the three adsorbents began to lose considerable amounts of their overall weight at a temperature of 280 °C and above (de la Cruz et al., 2020). Another study done by Kumar and others (2021) compared the thermal stability change in cross-linked and grafted chitosan adsorbents. The results showed that the grafted chitosan adsorbents had lower thermal stability than the cross-linked chitosan adsorbents. This was justified by the fact that the cross-linked chitosan adsorbents degraded in two steps while the grafted ones degraded in three steps. The results revealed that the first step of thermal decomposition occurring at around 120 °C was attributed to the loss of water from the samples while the second step degradation occurring between 200°C-325°C was due to the loss of pendant groups. The authors discussed that the cross-linked chitosan was associated with higher degradation temperatures than the grafted chitosan adsorbents. This shows that the cross-linked chitosan has much more thermal durability and stability than the grafted analog.

2.6.3 Physical and chemical characterizations of brines and adsorbents

i. *Scanning electron microscopy (SEM) and SEM with energy-dispersive X-ray spectroscopy (SEM-EDX)*

The scanning of an adsorbent's sample by an electron beam emitted from an electron microscope is the basis of the scanning electron microscopy technique for the physical characterization of adsorbents. In short, as the electron beam strikes the sample's surface, it get backscattered and detected to result in images of high resolutions. This is of particular use as SEM provides visual information regarding the sample's topography, morphology, surface characteristics such as the presence of pores ref. It is useful to visualize the presence of pores on an adsorbent's surface because they

represent adsorption active sites and give an indication regarding the adsorptive properties of an adsorbent. Scientists that seek adsorbent modifications to enhance their adsorption capacities could use SEM to visualize and confirm any morphological changes. Additionally, studying the morphological changes to adsorbents prior to and after adsorption is extremely beneficial to confirm and understand the adsorptive efficiency of adsorbents (Scanning Electron Microscopy Working Principle, 2019; Zhang et al., 2020). For example, a recent study was done to study the adsorption of malachite green dye and heavy metals on a chemically modified activated carbon adsorbent derived from Chrysopogon zizanioides roots. The authors conducted an SEM analysis to study the surface morphology and surface structure of the prepared adsorbent before and after adsorption. The results revealed that the adsorbent had many heterogeneous pores (adsorption active sites), which were occupied and filled with the heavy metals and dye effectively (Thanarasu et al., 2020). Another study conducted on the adsorption of lead from gold mining wastewater onto adsorbents made from cotton hulls applied SEM to study the physical appearance of the adsorbent. The authors reported through the obtained SEM images that the surface structure changed after the adsorption process was completed. Prior to adsorption, the adsorbent showed a smooth surface with crevices and microscopic pores. However, the SEM images showed that after adsorption, white layers appeared on the adsorbent's surface. Also, the adsorbent's surface became irregular and unsmooth after adsorption. This gave initial indications that lead ions (white layers) were adsorbed onto the cotton hulls and led to their irregular appearance (Yahya et al., 2020). Furthermore, Ventura and coworkers (2020) studied the surface morphology of laboratory prepared lithium manganese oxide (LMO) nanostructured adsorbent for the recovery of lithium from geothermal brines. The authors compared the SEM images of the LMO with manganese oxide to confirm

the successful modification required. The results showed the morphological changes due to the formation of LMO. These changes were the appearance of needle-like structures on the surface of manganese oxide that has a length of less than 1 micron and a width of 100 nanometers. This would provide significant indications regarding the accomplished modification and insights regarding the adsorption process.

SEM with energy-dispersive X-ray spectroscopy (SEM-EDX) is a non-destructive analytical morphological characterization technique that was developed in order to provide scientists with a chemical characterization along with the physical characterization that SEM provides. Therefore, SEM-EDX is considered to be an enhancement of the SEM-EDX technique as it provides insights regarding the elemental composition of materials such as adsorbents and adsorbates. An SEM-EDX analyzer can provide information regarding the surface morphology, types of elements present in the sample as well as their distribution within the sample being analyzed (Nanakoudis, 2019). Similar to a typical SEM analyzer, the first step of sample analysis in SEM-EDX involves the ejection of an electron beam towards the sample. This electron beam would strike an inner shell electron and cause it to be exited and lead to its ejection from the nucleus of the sample. As a result, an electron from an outer shell (higher energy) would replace the vacant site that was left in the inner shell (lower energy) of electrons. This movement of electrons and difference in energy leads to the emission of characteristic X-ray that is specific and unique to an element. Finally, the emitted characteristic X-ray would be measured and detected using a detector and the result viewed on a computer screen (Vengatesh and Sundaravadivelu, 2019; Abd Mutalib, 2017). An example of the useful characterization information that SEM-EDX provides is represented by a study done by Buthiyappan and others (2019). The study involved the synthesis of an adsorbent from the impregnation of sugarcane bagasse

using iron oxide. The SEM-EDX results of the synthesized adsorbent revealed that carbon, iron, and oxygen existed on the surface. This provided significant insights regarding the successful synthesis and impregnation of iron oxide onto the surface of the sugarcane bagasse.

ii. Fourier-transform infrared spectroscopy (FTIR) analysis

Another equally beneficial and important chemical characterization analytical method for brines and adsorbents is Fourier-transform infrared spectroscopy (FTIR). This analytical technique is of particular use when the aim of the characterization is to determine the functional groups, chemical structure, and its changes upon modifications or adsorption, as well as chemical composition of the adsorbent or adsorbate (Madejova, 2003; Li-Xu et al., 2019). Attaining the mentioned information regarding a brine sample involved in an adsorption process would demonstrate the specific functional groups that could chemically react or form bonds with the adsorbent (Hu et al., 2019; Mqehe-Nedzivhe et al., 2018). Any structural changes to the chemical composition of the brine sample due to adsorption or process parameters would be determined (Mqehe-Nedzivhe et al., 2018; Berthomieu and Hienerwadel, 2009; Nguyen and Lee, 2015).

FTIR technique is based on the absorption of an infrared spectrum by the material being analyzed. It is well understood that substances can absorb, transmit, reflect, scatter, or photoluminescence when electromagnetic radiation is applied. These interaction behaviors would provide scientists with data regarding the energy level as well as the molecular structure of the substance being studied. In short, the working principle of FTIR relies on the absorbed and transmitted wavelength light by a substance when an infrared beam is applied (Iftekhar et al. 2018; Munajad et al., 2018). The output result

of an FTIR is a graph that shows the absorption in percentage against wavenumber. The specificity of analyzing exact chemical bonds in a sample comes from the fact that each chemical bond would vibrate as a result of the infrared radiation at a characteristic specific frequency that represents its bond angle, structure, and length (Du et al., 2020; Munajad et al., 2018; Berthomieu and Hienerwadel, 2009).

As mentioned previously, many parameters affect adsorption processes such as contact time, pH, adsorbate concentration, and temperature. These operating conditions for an adsorption process could significantly impact the overall adsorption capacity and efficiency by impacting the chemical composition and bonding behaviors between the adsorbate and adsorbent. Therefore, scientists are usually interested in studying the chemical characteristics and structural changes due to adsorption processes in order to select the optimum conditions that result in the highest adsorption efficiency. Similarly, conducting an FTIR analysis for an adsorbent involved in the recovery of pollutants or valuable metals from a brine sample is important. This is because of two main reasons. Firstly, an FTIR analysis would give insights regarding successful adsorbent modification processes, as the functional groups' changes could be specifically determined. Secondly, the functional groups responsible for an enhanced adsorption capacity through adsorbate- adsorbent interactions could be easily determined and selected by conducting an FTIR analysis for an adsorbent involved in the recovery of valuable metals or pollutants from brine streams (Bang et al., 2017; Kaminski, 2017). For example, a study done by Yin and others (2017) performed an FTIR analysis to characterize synthesized Amidoxime silica adsorbents. The adsorbents were involved in the adsorption and recovery of uranium from a salt-lake brine stream. Upon the FTIR analysis, the authors were able to identify multiple functional groups that were characteristic of the prepared adsorbents. The identification of the potential responsible

functional groups for the adsorption of uranium from the brine stream was accomplished through the FTIR analysis. A more recent study done by Goyal and others (2020) revealed the structural changes and the functional groups involved in the adsorption of cesium and strontium onto a nanostructured chitosan/molecular sieve-4A. The structural changes included the accumulation of new peaks, broadening of some peaks, and other changes in the peak's shapes at new wavelengths. The adsorption of cesium involved the presence of a new sharp peak that indicated the presence of cesium-oxygen bonding. For strontium, the results showed a sharper and deeper peak than the one present before adsorption at 1500 cm^{-1}. This structural change indicates the involvement of C-O-C functional groups in the adsorption of strontium on the adsorbent. Another study done by Gibert and others (2010) investigated the adsorption of uranium from seawater brine onto adsorbents that contain amidoxime groups. The conducted FTIR analysis prior and after adsorption revealed that $UO_2(CO_3)^{-4}$ decomposes to UO_2^{2+} and then complexes with four main amidoxime groups. A study done by Petersková and coworkers (2012) on the adsorption of the same metal; uranium from brine onto a sulphonic and phosphonic acid functional groups containing cation exchange resin revealed the higher adsorption capacity compared to a resin that contained amidoxime groups. They were able to fully characterize and understand the adsorption mechanism of uranium through conducting an FTIR analysis. The results indicated the high adsorption capacity of uranium was due to its strong attraction and affinity towards the negatively charged sulphonic and phosphonic acid functional groups. Moreover, a study reported through performing an FTIR analysis for the adsorption of strontium onto alginate microspheres the process mechanism. The results showed that alginate has hydroxyl and carboxylate functional groups, which cross-link with the metal upon adsorption (Hong et al., 2016). Another study investigated the

adsorption of uranium from a saline lake brine onto silica that is amidoximated. The study involved the synthesis of the adsorbents; therefore, an FTIR for the characterization and confirmation of the desired result was done. The FTIR showed the presence of amidoxime groups by the conversion of cyano groups through the addition of hydroxylamine treatment (Yin et al., 2017).

iii. X-ray diffraction (XRD) analysis

Similar to FTIR and many other characterization techniques for adsorbates and adsorbents, XRD is among the most informative analytical techniques that help to analyze a wide range of materials in a non-destructive manner. A particular and important use of XRD analysis is the characterization of crystal materials, which are typically regular atomic arrays. XRD provides information regarding the elemental analysis of materials as well as their crystallinity. The analytical technique is applied in a variety of ways such as identifying the polymorphic forms of materials, distinguishing between crystalline and amorphous materials, and quantifying the percentage of crystallinity of materials. To be specific, scientists can explain the crystalline material's 3D atomic structure, which gives insights regarding their properties and possible functions. Through this, the adsorptive properties of materials, confirmations of modifications, and the chemical compositions of adsorbents and adsorbates can be determined using XRD analysis (Nasrollahzadeh et al., 2019; Nasrazadani and Hassani, 2016). For this reason, it is beneficial to characterize adsorbents and adsorbates with the XRD technique to obtain ideas regarding their structures as well as compositions and possible adsorptive interactions. For example, a study done by Naidu and coworkers (2016) studied the adsorption of rubidium onto a regular potassium copper hexacyanoferrate and polyacrylonitrile encapsulated with potassium copper

hexacyanoferrate based adsorbents. The study involved the analysis of different metal-based potassium hexacyanoferrates and the two adsorbents using XRD. The results revealed that the metal potassium hexacyanoferrates showed characteristic peaks that confirmed the crystallinity of these materials as well as their cubic face-centered structure. The XRD analysis of the adsorbents showed that the encapsulation modification of the adsorbent did not have an effect on the crystal structure. This was established as the XRD patterns for the regular potassium copper hexacyanoferrate and the encapsulated adsorbent were similar. A more recent study performed by Pires and others (2021) involved the preparation and characterization of an activated carbon cobalt hexacyanoferrate composite using XRD analysis. The application of an XRD analysis for the prepared composite was of great use as it confirmed the successful composite preparation. This is because the established XRD patterns were similar to the well-known XRD patterns for cobalt hexacyanoferrate. The authors were able to ensure the absence of any impurities in the prepared composite through the fact that no other XRD patterns were found for other chemicals or substances.

2.7 The importance and potential recovery of valuable lithium and strontium from a reverse osmosis desalination brine stream

As mentioned previously, reverse osmosis concentrated brine contains various salts, metals, and minerals such as Ca^{2+}, K^{+}, Na^{+}, Mg^{2+}, Li^{+}, Sr^{2+}, Cs^{+}, and many others. These minerals and valuable substances contained in desalination brine can be effectively removed and recovered using date pits. The main reason for the recovery of the mentioned substances is that they can be used in industries, medicine, agriculture, and environmental remediation (Loganathan et al., 2017). In this study, the recovery of Lithium (Li^{+}) and strontium (Sr^{2+}) from reverse osmosis concentrated brine using ferrocyanide modified roasted date pits will be investigated. Li^{+} belongs to alkali metals

in the periodic table. These metals are mostly found in nature bonded to other elements due to their high reactivity (Gaztañaga et al., 2020). Nowadays, lithium is used in a variety of fields like lithium-ion batteries, greases, polymers, ceramics, and metal additives. On the other hand, strontium is an alkaline earth metal that could be used in the pharmaceutical industry and manufacturing glass and ceramics. Due to the high demands on lithium and strontium-containing products, their extraction from hard rock ores or brine is becoming more expensive. However, the extraction of lithium and strontium from brines remains cheaper and simpler than hard rock (Flexer et al., 2018; Wang et al., 2019; Liu et al., 2019). Moreover, as with the previously mentioned conventional brine treatment systems based on ZLD systems, the conventional methods of extracting metals have drawbacks. Some of the drawbacks of conventional brine metal extraction methods include the complexity of brines, metal low concentrations, and low selectivity of extraction media and agents (Huang et al., 2018; Petersková et al., 2012). Consequently, the efficient, economical, simple, practical, and highly selective method for the recovery of lithium and strontium from concentrated brines could be through its adsorption onto date pits. Qatar relies on desalination for the majority of its freshwater resources; massive amounts of brine are generated daily. Qatar's date and date pit production are among the largest in the world. This calls for immediate action where a largely produced by-product (brine) can be effectively recovered for valuable minerals using a largely produced waste material (date pits). Moreover, using simple, safe, and cheap modifications on the date pits using simple roasting techniques and ferrocyanides of two transition metals (hexacyanoferrates (II) of (Cu and Ni) would enhance their surface area for adsorption, high selectivity, and adsorption capacity towards Li^{+} and Sr^{2+} ions. This is because of enhanced electrostatic attractions, immobilization, dispersion as well as the formation of metal complexes due

to high affinities towards the surface of roasted and modified date pits (Zhang et al., 2017; Vincent et al., 2017; Naemi and Faghihian, 2017; Baaloucha and Ouda, 2017; Al-Saad et al., 2019).

CHAPTER 3: MATERIALS AND METHODS

3.1 Physical and chemical characterization of the collected brine

It is important to investigate the physicochemical characteristics of the brine solution prior to adsorption to optimize the removal of the target metal (Wang et al., 2018). The rejected brine samples were collected from a reverse osmosis desalination plant in Qatar. To ensure homogenous and precise measurements, replicate samples were collected from the reverse osmosis desalination plant at different periods. After collection, the samples were mixed to create a representative homogenous sample of the Qatari RO brine. Moreover, the collected brine samples were stored in plastic bottles in a dry, clean and dark area to prevent any contaminations or reactions with the surroundings. Prior to any physiochemical analysis test, the brine sample was filtered through a 20μm filters to remove any suspended matter. Since some physiochemical analysis tests require the samples to be in a solid form, a part of the collected brine samples was dried at 100 °C for 24 hrs. to obtain solid crystals (Touriño et al., 2019).

The physical and chemical characteristic of the collected concentrated brine from reverse osmosis plant was thoroughly investigated for pH, salinity, conductivity, total dissolved solids (TDS) using HQ440d multi (Ames, lowa, USA). The functional groups' analysis was done by the FTIR technique (FTIR Perkin Elmer Model 2000) (Pramanik et al., 2020). The determination of metals was performed using an inductively coupled plasma optical emission spectroscopy (ICP-OES) (Perkin-Elmer Optima 3000V, or Shimadzu ICPS-7510 Sequential Plasma Spectrometer, Japan) and ion chromatography (IC) (METROHM model 850 professional) (Xu et al., 2020). The supernatants from isotherm experiments were filtered through 0.2 μm to separate the date pits prior to analysis. In addition, scanning electron microscopy (SEM) and SEM with energy-dispersive X-ray spectroscopy (SEM-EDX) technique (NovaTM Nano

SEM 50 Series, from FEI Company) was performed in order to study the morphological and elemental composition of the brine sample (Dovidauskas et al., 2020). Also, an x-ray diffraction (XRD) analysis for the collected brine was done to determine the chemical composition. The XRD instrument used was PANanalytical Empyrean/Netherland and the scan for the samples was run from 5 to 85 (2- theta-scale) (Bruckner, 2020).

3.2 Supporting material for the modification purposes

Date pits were collected from Qatari local markets and were used as supporting material for ferrocyanide modification. After collection, the date pits were washed with distilled water to remove any impurities and dried at 100°C for 24 hrs. The date pits were then be roasted on a hot plate with continuous mixing at 100°C for 6 mins or till they obtained a golden-brown color (Erabee et al., 2017). The roasting process converts most of the raw material into a rich carbonaceous material that supports high adsorption capabilities (Al-Saad et al., 2019). After that, the roasted date pits (RDP) were ground and sieved into different particle sizes (100–250 µm, 250–500 µm, and 500–750 µm). The date pits were then stored in glass bottles for the batch adsorption experiments (Al-Saad et al., 2019).

3.3 Ferrocyanide-date pits modification

A mix between Cu-K or Ni–K ferrocyanide and roasted date pits were used in this study. This is because Cu-K or Ni–K ferrocyanide would have high selectivity towards lithium and strontium due to ion exchange, metal complexation, and electrostatic attractions (Wang et al., 2018; Zhang et al., 2017). The roasted date pits-composite ferrocyanide adsorbents with Cu–Kor Ni–K was prepared according to the literature as follows: First, 1 molar of $K_4[Fe(CN)_6]$ (Riedel-deHaen, Germany), $CuSO_4$ (Scharlau,

Scharlab S.L, Spain) and $NiCl_2$ (Riedel-deHaen, Germany) were prepared. Then 1:1 molar ratio of $K_4[Fe(CN)_6]$ and ($CuSO_4$ or $NiCl_2$) were thoroughly mixed (Figure 14). A NaOH (RESEARCH-LAB FINE INDUSTRIES, Mumbai 400002 (India)) solution of date pits was added into the resulting suspension in sequence with strong stirring (Zhang et al., 2017; Vincent et al., 2017). The NaOH solution prepared was 0.1 molar and 100 mL of the solution was added to 50 grams of each date pit type. The NaOH date pits solution was added into the resulting suspensions of copper ferrocyanide and nickel ferrocyanide in sequence with strong stirring (Figure 15). The suspension was centrifuged at 5500 rpm for 20 mins, removing the supernatant, and centrifuge again for 20 mins. Then the supernatant was removed then drying the precipitate at 100°C for 3 hrs using an oven. Different particle sizes were obtained. The samples were denoted as RDP-FC-Cu and RDP-FC-Ni; respectively (Naemi and Faghihian, 2017; Abbas and Marji, 2005).

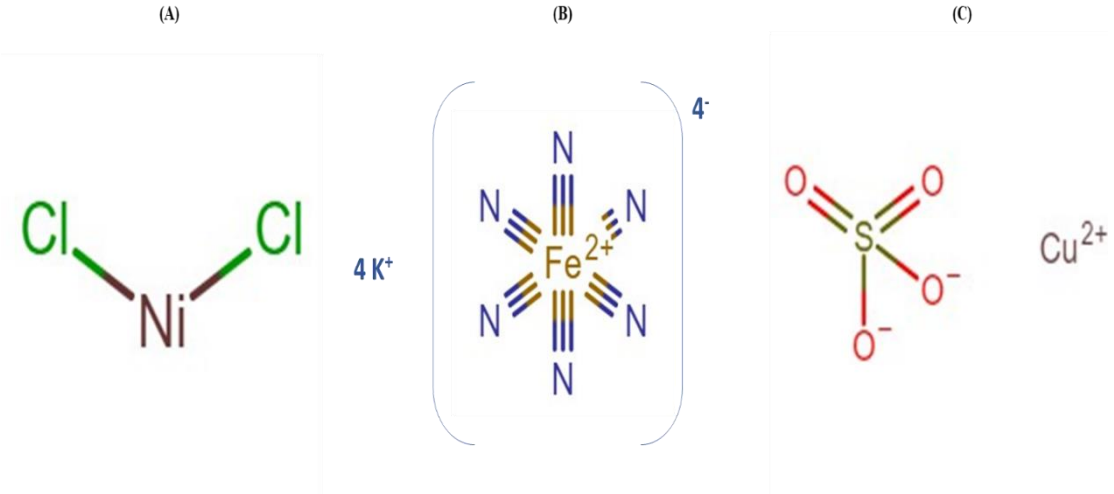

Figure 14. The chemical structures of (A) nickel chloride, (B) potassium hexacyanoferrate, and (C) copper sulfate for the preparations of potassium copper and nickel hexacyanoferrate through mixing of 1:1 molar ratio of each chemical.

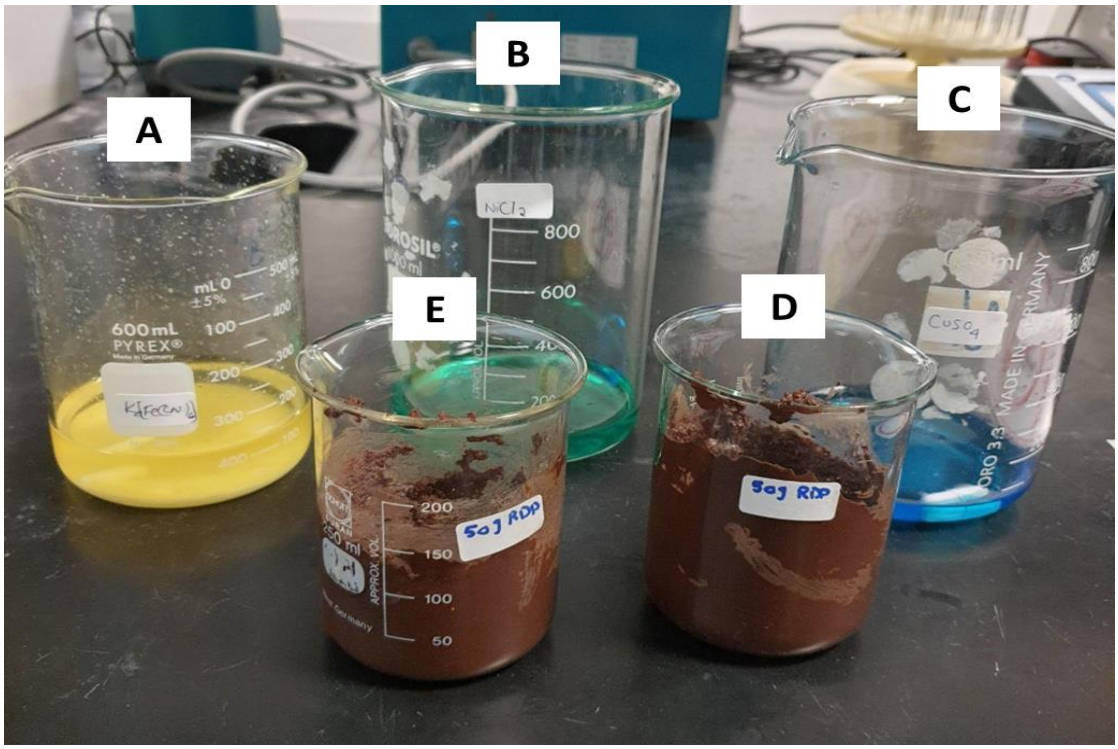

Figure 15. The prepared solutions of each (A) K4[Fe (CN)6], (B) NiCl2, (C) CuSO4, (D), and (E) 50 g of RDP mixed with 0.1M of NaOH.

3.4 Characterization of the materials

The date pits, roasted date pits, and the prepared composites were physiochemically characterized using various analytical techniques to investigate their adsorptive capabilities and characteristics (Kara and Rabbani, 2019). The physical characterization tests involved scanning electron microscopy to evaluate the surface morphology of the materials prior to and after adsorption using the NovaTM Nano SEM 50 Series, from FEI Company (Al-Ghouti and Al-Absi, 2020). A particle size distribution test was conducted for the adsorbents to analyze their size range and its role in the adsorption process. The analytical machine used for determining the particle size distributions for the adsorbents was FRITSCH'S ANALYSETTE 22 NanoTec. The surface area and pore size distribution were found using Brunauer–Emmett– Teller (BET) from

Quantachrome Corporation, Nova 3000 (Akpome et al., 2015; El-Azazy et al., 2019). The chemical characterization tests included the elemental analyzer to determine the chemical composition of the materials in terms of carbon and hydrogen, X-ray diffraction (XRD) (PANalytical Empyrean/Netherland) analysis as well as the Fourier-Transform Infrared Spectroscopy (FTIR) analysis using FTIR Perkin Elmer Model 2000. The FTIR analysis was carried out to interpret the functional groups, which occurred in the roasted, and the modified form as well as changes due to adsorption. The FTIR measurements will be performed over 4000–400 cm^{-1} (Al-Ghouti and Al-Absi, 2020; Zhang et al., 2017). Furthermore, the thermal stability of the adsorbents was determined using Thermogravimetric analysis (TGA) (PerkinElmer, Pyris 6 TGA) to investigate the durability of the adsorbents in industrial applications and large-scale adsorption processes. The TGA was done by applying argon gas and heating the samples from 25°C to 800 °C (El-Azazy et al., 2019).

3.5 Adsorption isotherms studies

As Li^{+} and Sr^{2+} exist in a complex media of brine solution, which could most probably contain other metals and chemicals. This makes the extraction capacity more reliable for the selected materials, synthetic solutions the ions were prepared (Loganathan et al., 2017). This was done to mimic lithium and strontium concentrations to the concentrations available in the collected brine. This was accomplished by dissolving appropriate amounts of LiCl (RESEARCH-LAB FINE INDUSTRIES, Mumbai 400002 (India)) and $SrCl_2$ (BDH Laboratory Supplies, England) salts in distilled water. The final concentration of the metals was in the range of 5 mg/L –100 mg/L for each batch experiment. The following general procedure was used from literature: 0.05 g of the material [roasted date pit, or modified form (prepared composites)] were placed into

100 mL of the metal solution of known initial concentration using a polycarbonate Erlenmeyer flask. The mixture was agitated at 160 rpm in an incubator shaker for 24 hrs. at room temperature (25 °C) to reach the equilibrium adsorption state (Mangwndi et al., 2020). The adsorbent was then be filtered out using filters (0.2 µm). The residual metal concentration in the solution was analyzed using ICP-OES analytical technique (Naemi and Faghihian, 2017; Al-Ghouti et al., 2010). Different key parameters were also performed such as the effect of initial solution pH and the solution temperature. The initial solution pH ranges tested were 2, 4, 6, 8, and 10 while the different temperatures tested were 35 °C and 45°C. The pH of the solutions was adjusted using minute amounts of 0.5M HCl and NaOH solutions. The batch experiments were set at the desired temperature using an incubator shaker (Al-Ghouti and Al-Absi, 2020). Furthermore, the zeta potential test was performed at pH of 2, 6, and 8 in order to examine the stability as well as the surface charge of the adsorbents in the solution at different pH values. The zeta potential was tested using Malvern ZETASIZER Nano series (Ryu et al., 2020). The adsorption capacity and adsorption efficiency were obtained using equations 1 and 2 above. The data were fit in the Langmuir and Freundlich models as previously described. These models are commonly used in metal adsorption studies with various materials; therefore, they will be investigated in this study. The adsorption parameters for the Langmuir and Freundlich fit were estimated by equations 3 and 4 above.

3.6 Desorption studies

The recovery of lithium and strontium and regeneration of the spent adsorbents (RDP, RDP-FC-Cu, and RDP-FC-Ni) would allow the multiple usage of the adsorbents. In order to recover the adsorbed metals from the adsorbents, 0.5M and 1M HCL solutions

will be used to determine the concentration that would achieve the highest desorption percentage (Cid et al., 2020). The spent adsorbents from previous adsorption experiments (Section 3.5) will be dried on filter papers and collected for the desorption experiments. Specifically, all the spent adsorbents that were involved in the adsorption of the metals at the optimum found pH, the regular temperature of 25 °C, and metal concentrations of 5, 10, 15, 20, 25, 30, 35, 50, 70, and 100 mg/L (Section 3.5) were dried and collected. Then, the collected date pits were put in polycarbonate Erlenmeyer flasks with 50 mL of 0.5M and 1M HCl solution. The solutions were put in an incubator shaker at 35 °C for 24 hrs. at 160 rpm. to reach the equilibrium desorption state. The adsorbent was then be filtered out using filters (0.2 µm). The residual metal concentration in the solution was analyzed using ICP-OES analytical technique. After that, the percentage desorption was calculated based on the initial average adsorbed metal concentrations that were determined in previous experiments (Section 3.5). Statistical analysis was done to test if there is a significant difference between the percentages of desorption achieved by the two acid concentrations. Equation 7 below shows the calculations of the percentage desorption for each metal at different HC concentrations (Ivanets et al., 2020).

Equation 7: $\frac{Average\ adsorbed\ metal\ concentration - desorbed\ concentration}{average\ adsorbed\ metal\ concentration} x100$

The concentrations in equation 7 above are in the unit of mg/L.

3.7 Selectivity adsorption studies

The selectivity of the adsorbents (RDP, RDP-FC-Cu, and RDP-FC-Ni) towards the target metals of this study (lithium and strontium) was tested by two experiments. The first experiment involved the preparation of mixture solutions of both metals and testing the adsorptive capacities of the adsorbents towards the metals (Gao et al., 2020). Equal concentrations of each metal were prepared as the previously found optimum concentration of 100 mg/L. Moreover, the pH was set to the optimum pH of 6 and temperature of 25 °C. An adsorbent (RDP, RDP-FC-Cu, and RDP-FC-Ni) mass of 0.05g was applied to the mixture solutions. After applying the adsorbents into the mixtures, they were agitated at 160 rpm for 24 hrs on a mechanical shaker to reach equilibrium. The adsorbents were then filtered out using filters (0.2 µm). The residual metal concentrations in the solutions were analyzed using ICP-OES analytical technique (Section 3.5).

The second experiment involved applying adsorption experiments to the collected reverse osmosis brine. This would give an understanding of the adsorbent's adsorptive capabilities towards the target metals in the presence of other metals as a matrix (Rohmah., 2020). As with previous experiments (Sections 3.5 and 3.6), the selectivity experiments were done by adding 0.05 g of each adsorbent into a 50 ml of the brine sample in polycarbonate Erlenmeyer flasks. The solutions were then kept in an incubator shaker at 35 °C for 24 hrs at 160 rpm. The adsorbents were then filtered out using filters (0.2 µm). The residual metal concentrations in the solutions were analyzed using ICP-OES analytical technique. The temperature was chosen as 35 °C for two main reasons. First and as mentioned previously, reject brine streams are characterized by their warm temperatures. Therefore, if the results demonstrate high adsorption capacities, the adsorption process could be performed without extra modifications on

the brine sample (In the form of adding or reducing adsorption process temperatures). Secondly, experiments (Section 3.5) showed that a temperature of 35 °C achieved high lithium and strontium adsorption onto the three adsorbents.

CHAPTER 4: RESULTS AND DISCUSSION

4.1 Physiochemical characterization of the collected reverse osmosis brine

4.1.1 Elemental analysis of the collected reverse osmosis brine

To establish a complete understanding of the major and trace metal composition of the brine at study, ion chromatography (IC) and inductively coupled plasma optical emission spectrometry (ICP-OES) analytical techniques were performed. As mentioned previously, ICP-MS, IC, and ICP-OES are valuable analytical techniques for the chemical characterization and determination of various major and trace metal concentrations in various solutions (Cha-umpong et al., 2021). Due to the fact that the ion chromatography technique can detect major ions in solutions and its availability, it was used to determine the major cations and anions present in the collected reverse osmosis brine sample at study (Rohrer, 2019). Furthermore, the ICP-OES was utilized in order to accurately and precisely measure the trace elements in the brine solution (Mudalige et al., 2019). Figure 16 represents the IC results while figure 17 and table 3 show the ICP-OES results of the brine at study. According to the IC results, the order of the major cations present in the brine solution in terms of decreasing concentration is as follows: calcium, sodium, magnesium, and potassium. On the other hand, the brine sample contained three major anions in the decreasing concentration order as chloride, sulfates, and bromide. These results are predictable for a reverse osmosis seawater desalination brine solution. This is because seawater is characterized by its salinity, which corresponds to the presence of high salt content. Salt in this context is known as calcium and sodium chloride, and as seawater is desalinated to produce freshwater, the calcium and sodium chloride should be removed in the form of brine. Therefore, the highest concentrations of cations and anions were calcium, sodium, and chloride, respectively. Other types of salts in the forms of potassium and magnesium chlorides may be present in seawater and brine solutions as well, which explains their presence

in the brine solution at study (Díaz Nieto et al., 2019; Jeong et al., 2017; Cui et al., 2020; Cha-umpong et al., 2021).

(A)

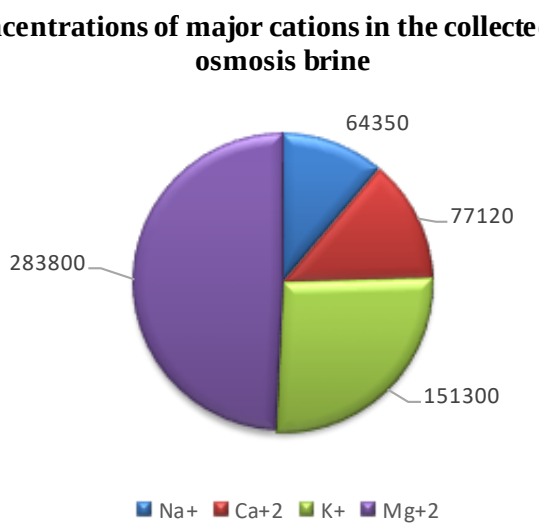

(B)

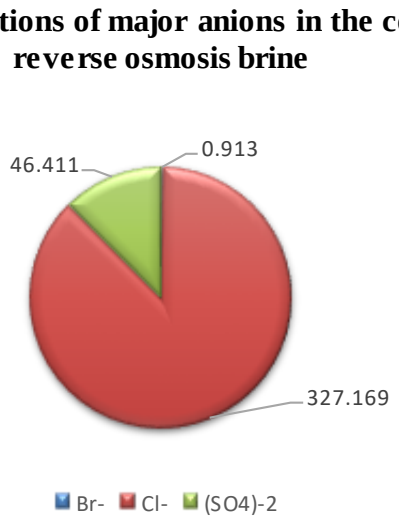

Figure 16. The IC results of (A) the major cations and (B) major anions concentrations (mg/L) present in the collected reverse osmosis brine.

The ICP-OES results (Table 3 and Figure 17) of the collected reverse osmosis brine show the presence of various trace, rare, and industrially valuable elements. These elements are (in a decreasing concentration order) strontium, zinc, vanadium, lithium, iron, lead, lanthanide, cesium, and barium. Several factors control the concentration

behavior of the trace metals in the brine. These factors can be the desalination technology employed along with the process chemicals added, and the geological setting as well as chemical characteristics of the seawater region (Loganathan et al., 2017; Panagopoulos et al., 2019; Ariono et al., 2016). The presence of strontium in the brine at study can be explained by the fact that it is the 15th most abundant element in the earth's crust and mostly in soils and rocks. Therefore, chemical and physical weathering of the local rocks around the area can also be one of the reasons for the existence of strontium trace metals in the brines. This was demonstrated by a study done by Höllriegl (2019) where it was reported that strontium is considered to be one of the five most abundant trace metals found in global seawaters. Similar to strontium, zinc is considered an abundant earth crust element, which can be released into seawater through chemical and physical weathering as well as leaching of rocks and soils (Onwuka et al., 2019). Interestingly, zinc in seawater is often found to be associated with other metals like lead, which explains the presence of lead in the brine sample at study (Cámara-Martos and Moreno-Rojas, 2016). Moreover, vanadium presence in the collected reverse osmosis brine could be due to natural reasons like soil erosion and weathering of rocks as well as anthropogenic sources such as the burning of fossil fuels (Pantapasis and Grumezescu, 2017; Vincent et al., 2019). The relatively high concentration of lithium in the brine at study is expected as previous studies demonstrated that the seas are major reserves for lithium around the world (Díaz Nieto et al., 2019; Yang et al., 2018; Cha-umpong et al., 2021; Ruan et al., 2021). As mentioned previously, desalination plants often employ various kinds of chemical treatments during the desalination process, which may be a great contributor to the presence of various kinds of trace metals like iron, lanthanide, cesium, and barium. Kasedde and others (2014) studied the characterization of brine lake in Uganda and

found that the lake dominated with Na^+, K^+, Cl^-, CO_3^{2-}, SO_4^{2-} and HCO_3^- ions while Mg^{2+}, Ca^{2+}, Br^- and F^- are present in smaller concentration. The study explained the high concentration of CO_3^{2-} and SO_4^{2-} was primarily due to the geological setting such as high trona, thermonatrite, and burkeite.

Table 3. ICP-OES trace metal concentrations of the collected reverse osmosis brine.

Trace metal	Concentration (mg/L)
Ba	3.3
Cs	3.4
Ln	4.5
Fe	30.5
Pb	10.1
Li	44.2
V	68.7
Zn	256.4
Sr	447

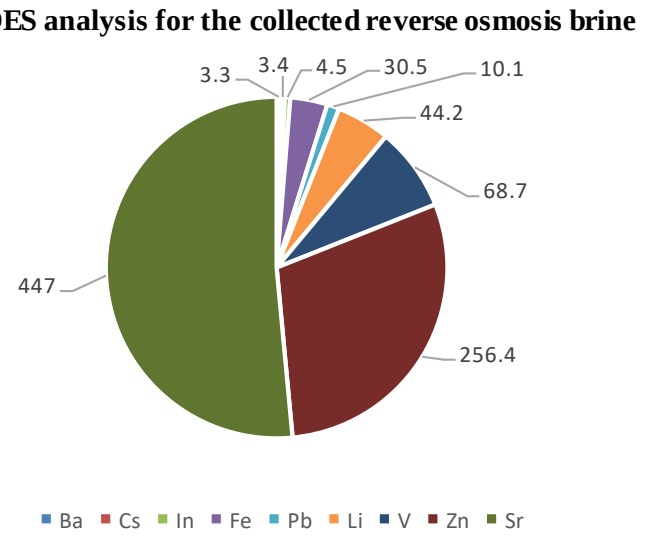

Figure 17. ICP-OES analysis for the trace metal concentrations in the collected reverse osmosis brine.

4.1.2 Physical characterization of the collected reverse osmosis brine

Determining the physical characteristics like pH, salinity, conductivity, and total dissolved solids (TDS) of brine samples involved in an adsorption of metals process is considered to be one of the initial important steps in optimizing the recovery. This is because of the previously mentioned effects that pH plays on the level of adsorption. In addition, salinity, conductivity, turbidity, and dissolved solid contents give important indications regarding the concentrations of various metals present in the brine sample, which could give hints regarding the presence of valuable metals to recover via adsorption (Pramanik et al., 2020). Therefore, these physical parameters were determined for the collected reverse osmosis brine sample and presented in table 4.

The brine was observed to be slightly alkaline as indicated by the pH which was around 8. This result was found to be similar to other studies done by Liu and coworkers (2021) and Naidu and co-workers (2019) on seawater brine. Petersková and others (2012) on reverse osmosis brine found a similar pH of around 7.8. Moreover, the salinity and electrical conductivity of the brine at the study were found to be 61.4 ppm and 99.5 mS/cm respectively. It is important to note that the salinity of the brine is significantly higher than the average salinity of the seawater of the gulf region, which was reported to be around 45 ppm on average (Ibrahim et al., 2020; Zhao et al., 2017; Dawoud and Mulla, 2012). Conductivity measures the water tendency to pass through the electrical flow. This ability is influenced by the presence of ions present in the water. The conductive ions usually come from dissolved salts and inorganic materials such as alkalis, chloride, sulfides various other compounds (Langland and Cronin, 2003). The higher the ion concentration the higher the conductivity of water. Similarly, sodium and chlorine ions are the main charge carriers for the electrical conduction in brine water along with other ionic-derived species. As observed from elemental analysis sodium

and chloride both are present in a very high amount in the brine water. While on the other hand, the salinity of a solution is considered an ambiguous term. The electrolytes dissolve in water to form ionic particles with either positive, negative, or no charge. Thus, salinity is considered a vital contributor that influences the conductivity of the solution. Additionally, it is not possible to perform a complete chemical analysis to determine the salinity of brine. The brine cannot be simply dried to obtain dry mass, as it will lose chloride contents from the mass. Therefore, brine or seawater salinity is measured indirectly, from the conductivity measurements. The salinity of brine is usually dependent on various major ions, alkali, and alkaline earth metals salts including calcium, magnesium, sodium, and various carbonates making up the highest percentage of the ionic composition. It is important to point out the high salinity of Qatar's brine can also be influenced by the high evaporation that takes place due to the high temperature observed in the country. It is important to measure the salinity of brine or seawater as it affects the dissolved oxygen solubility. Hence, the high salinity indicates low dissolved oxygen concentration. Aquatic and land animals are sensitive to change in salinity and can only tolerate a specific salinity range. This tolerance is dependent on the osmotic processes within an organism ref. Therefore, alternating the conductivity of the water will increase or decrease the salt level of the water, which will negatively affect the metabolic abilities of the organisms. This was discussed earlier as the direct disposal of brine into the environment could pose significant adverse effects on the well-being of many animals. Similarly, total dissolved solids (TDS) can also have an adverse impact on aquatic life and overall water quality. It is one of the parameters, which determines the conductivity of the water along with temperature and salinity. In a study by Bindel and others (2020), TDS and conductivity of seawater reverse osmosis brine samples were found to be similar to the results of this study.

Table 4. The physical parameters of the collected reverse osmosis brine.

Parameter	Result
pH	7.8
Salinity (ppt)	61.4
Conductivity (S/m)	99.5
Total dissolved solids (TDS) (g/L)	113.17

4.1.3 SEM with energy-dispersive X-ray spectroscopy (SEM-EDX)

An SEM-EDX analyzer can provide information regarding the surface morphology, types of elements present in the sample as well as their distribution within the sample being analyzed (Nanakoudis, 2019). This is of particular use when analyzing brine solutions that are involved in a metal recovery adsorption process because scientists could understand the morphology of the solid brine crystals, approximate sizes as well as the presence of certain metals. The morphology of the brine solid crystals could give initial predictions regarding the capability of adsorption with a given adsorbent with a known morphological structure (SEM for adsorbents discussed in the following sections). Therefore, figure 18 below shows the SEM image and EDX analysis for the collected reverse osmosis brine at study. It is important to note that the brine sample was dried at 100 °C for 24 hours prior to the SEM-EDX analysis in order to obtain the surface morphology and chemical characteristics of the crystals. The SEM image of the collected reverse osmosis brine sample shows that the morphology of the brine crystals is somewhat cubic, agglomerated, non-smooth, and contains few cavities or cracks. A study done by Quilaqueo and others (2015) showed similar SEM morphological results for various types of salts. The EDX analysis revealed that the collected reverse osmosis brine crystals contained mainly chlorine and sodium, which was shown previously by the IC and ICP-OES analysis. Moreover, some of the elements if present in minute amounts may be lost or evaporated during the drying process of the brine, which explains the remaining 3.13% by weight from the brine sample.

SEM for the collected reverse osmosis brine

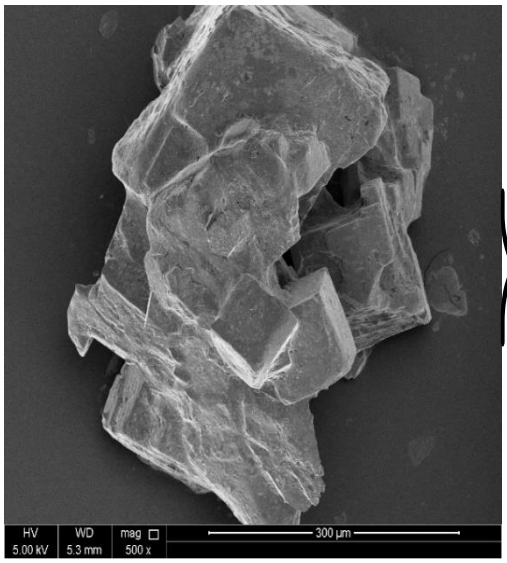

Element	Weight (%)
Carbon	1.9
Oxygen	14.52
Sodium	25.55
Magnesium	2.65
Chlorine	48.67
Calcium	1.88
Rubidium	0.95
Strontium	0.75

Figure 18. The SEM (Left) and EDX (Right) of the collected reverse osmosis brine.

4.1.4 Fourier-Transform Infrared Spectroscopy (FTIR) analysis

FTIR analytical technique is considered to be one of the most beneficial and important chemical characterization methods for adsorbates and adsorbents that are involved in an adsorption system. Through an FTIR test, scientists can obtain significant information regarding the present functional groups, chemical structures as well as the composition of adsorbates and adsorbents (Madejova, 2003; Li-Xu et al., 2019). In other words, attaining the mentioned information regarding a brine sample involved in an adsorption process would demonstrate the specific functional groups that could chemically react or form bonds with the adsorbent (Hu et al., 2019; Mqehe-Nedzivhe et al., 2018). Moreover, and as mentioned previously, adsorption processes depend largely on many working parameters such as solution pH, pollutant concentrations, temperature as well as time, and other factors relating to the chemical and physical characteristics of the adsorbents employed for a given adsorbate. These operating factors could significantly affect the functional groups that could be part of the adsorption process and lead to either enhanced adsorption or decreased adsorption.

Some specific functional groups on the adsorbate surface could indicate certain interactions with the functional groups in the adsorbent (Goyal et al., 2020). For these reasons, it was necessary to perform an FTIR analysis for the collected reverse osmosis brine at study as well as for the adsorbents to investigate the possible functional groups present as well as their involvement in the adsorption and recovery of lithium. The FTIR spectrum for the brine sample is shown in figure 19 below. As a general observation of figure 19, it can be noticed that 5 distinctive peaks were obtained for the brine sample through FTIR analysis. The broad strong peak at 3,336 cm^{-1} corresponds to an OH stretching due to the presence of, secondary amines, and alcohol respectively. The weak peak at around 1,636 cm^{-1} could be due to the presence of C=C bondage related to alkenes in the collected reverse osmosis brine sample. Moreover, the somewhat narrow and intense peak at around 1,408 cm^{-1} indicates the presence of S=O bondage in the brine sample, which could correspond to the presence of sulfonyl chlorides or sulfates as indicated by the ICP-OES results shown previously (Al-Saad et al., 2019; Al-Ghouti et al., 2019; Mangwandi, 2020). Furthermore, the peaks at 991 cm^{-1} and 874 cm^{-1} are related to C=C bending due to alkene compounds and C-C stretching respectively (Asyana et al., 2016).

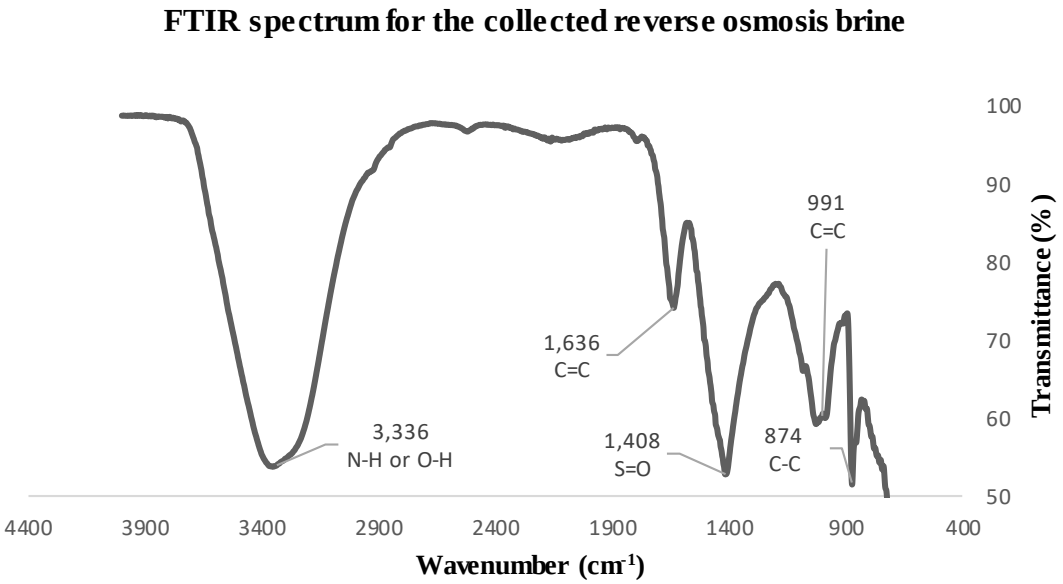

Figure 19. The FTIR spectrum of functional groups present in the collected reverse osmosis brine sample.

4.1.5 X-ray diffraction (XRD) analysis

Similar to the previously discussed material characterization techniques, x-ray diffraction (XRD) gives scientists valuable information regarding a sample's purity, crystallinity as well as morphology (ACS Nano, 2019; Zhou et al., 2018). The XRD analysis for the collected reverse osmosis brine sample was performed as well as for the adsorbents. This is because learning the characteristics of both, the material that holds the valuable metals (brine) as well as the materials that could potentially recover these valuable metals could help in achieving an understanding of the compatibility of these materials for adsorption processes. As a general principle, the spacing between the atoms or crystals of the sample is represented by the 2θ values of an XRD graph. The degree of the crystallinity of the sample could be understood from the peak intensity in the XRD graph (Figure 20), where lower intensity corresponds to lower crystallinity and vice versa. Moreover, the width of the graph's peak represents the size

of the crystals in the sample being tested (Seekaew et al., 2019). From figure 20, eight XRD peaks can be observed for the collected reverse osmosis brine sample at the study. Interestingly, one peak at 2θ of 31.7° is significantly more intense than the other seven peaks obtained, while all the eight peaks are extremely narrow. This means that at 2θ of 31.7°, the crystallinity of the atoms is significantly high with small-sized crystals. The peaks observed at 2θ of 45.5°, 56.4°, and 66.3° are almost similar in their width's (narrow) and intensities. The intensity of the peak at 2θ of 45.4° is equal to 6439 a.u. and the intensity of the peak at 2θ of 56.4° is 6767 a.u. While the intensity of the peak at 2θ of 66.3° was found to be equal to 6789 a.u. This shows that at these 2θ phases or spacing between the sample's atoms, the sizes, as well as the degree of crystallinity of the brine sample, is almost the same, low number of small-sized crystals. The lowest degree of crystallinity could be observed for the collected reverse osmosis brine sample at 2θ of 26.6°, 27.5°, 74.8°, and 84.5°. Abdou and Moharam (2019) on the characterization of marine salt samples involved the application of an XRD analysis. The peaks obtained for the sample were very similar to the peaks obtained by this study for the characterization of the reverse osmosis brine sample. Interestingly, the peaks obtained by both studies correspond to the same characteristic peaks of the NaCl standard, which demonstrates the salt nature of the sample at the present study.

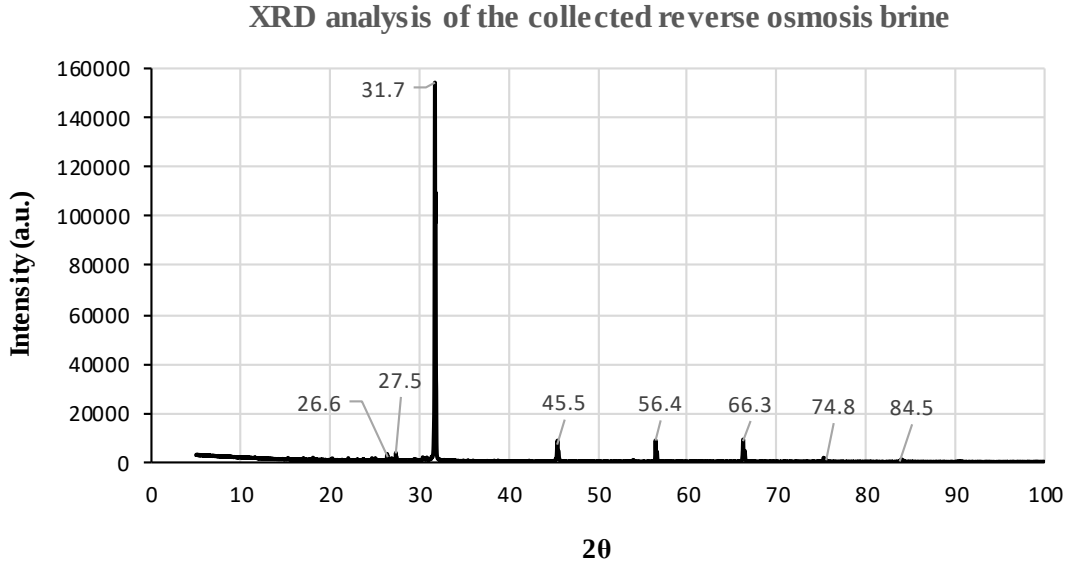

Figure 20. The XRD peak results of the collected reverse osmosis brine sample.

4.2 Physiochemical characterization of the prepared adsorbents

4.2.1 Scanning electron microscopy (SEM)

Studying the surface morphology of adsorbents is one of the most important aspects of selecting an efficient adsorbent for a given pollutant. This is because adsorbents with microporous morphologies indicate the presence of adsorption active binding sites. As mentioned previously, visualizing the surface morphology of adsorbents could be done using SEM analysis (Zhang et al., 2020). For these reasons, the adsorbents at study were analyzed for morphological characteristics using SEM and the results are shown in figure 21 (A-G). The figure shows the SEM images for the raw date pits as well as the three adsorbents prior to and after the adsorption of lithium. Similarly, figure 22 (A-F) represents the SEM morphological characteristics of the three adsorbents before and after the adsorption of strontium. As can be seen from figure 21 (A), the raw date pits prior to roasting showed a smooth somewhat flattened surface with few scattered small-sized elevations. To compare, the RDP pits prior to the adsorption of lithium (Figure

21 (B)) demonstrate a rugged dense mass structure with elevated formations of varying shapes and sizes and visible cavities throughout. The great morphological change can be seen on the RDP after the adsorption of lithium (Figure 21 (C)) at the temperature that achieved the highest adsorption capacity (From the effect of temperature on the lithium adsorption experiment). The adsorption of lithium onto the RDP along with the working temperature of 45 °C led to the formation of more pronounced similar-sized protrusions on the surface. This could be due to the high temperature, which resulted in the cracking of the surface as well as the accumulation of lithium ions on the surface of RDP. Moreover, there is a major enhancement in the surface morphologies and topographies of RDP-FC-Ni and RDP-FC-Cu in terms of numbers of cavities and pores due to the modification with potassium metal hexacyanoferrate. The prepared composite date pits reveal the rougher, denser, more compact, and smaller-sized formations and micro-fractures on their surface (Figure 21 (D-G)). To be more specific, RDP-FC-Ni before the adsorption of lithium (Figure 21 (D)) appears to have smaller formations, pores, and cavities than RDP-FC-Cu (Figure 21 (F)). These results indicate that roasting date pits would significantly alter and enhance their surface morphological characteristics in terms of porosity, which could significantly result in higher adsorptive capacities for metals and pollutants. Furthermore, modifying the roasted date pits into potassium metal hexacyanoferrates provides scientists with a great opportunity to synthesize more structured and porous adsorbents for metals. This could be due to the double action of roasting as well as chemical deposits and fracturing of the date pits. After the adsorption of lithium, RDP-FC-Ni (Figure 21 (E)) showed significant morphological change where the surface appeared to be more flattened, which indicates the filling of the available active sites (pores) of the adsorbent. For RDP-FC-Cu (Figure 21 (G)), the adsorption of lithium has also led to changes in the morphology in terms

of the formation of denser smaller-sized pronounced protrusions (Zhang and Chen, 2020; Ogungbenro et al., 2017).

Along with the mentioned morphological changes that took place upon roasting the raw date pits as well as modification to the two-potassium metal hexacyanoferrate date pits, figure 22 (A-F) shows the morphological changes that occurred on the surface of the adsorbents after the adsorption of strontium at the optimum temperature of 45 °C (Section 4.5). From figure 22 (A and B), it can be noticed that a pore filling has occurred on the surface pores of the RDP from the adsorption process of strontium at the temperature that obtained the highest adsorption capacities (45°C). This is shown by the disappearance of most of the pores and cavities upon the adsorption of strontium. The same result is obtained with the RDP-FC-Ni adsorbent (Figure 22 (C and D) where its surface became smoother with much fewer formations, microfractures, cavities, and pores upon the adsorption of strontium. However, it can be seen that a bigger-sized cavity formed on the surface of RDP-FC-Ni after strontium was adsorbed. This could be due to the effect of temperature on the structure of the adsorbent. Furthermore, RDP-FC-Cu (Figure 22 (E and F) shows similar results to the other two adsorbents with pore-filling and smooth morphology. However, the surface of RDP-FC-Cu after the adsorption of strontium appears to be rougher than the other two adsorbents with fewer changes. This shows that RDP-FC-Cu did not experience significant structural changes but did show adsorption potentials through the pore filling of strontium.

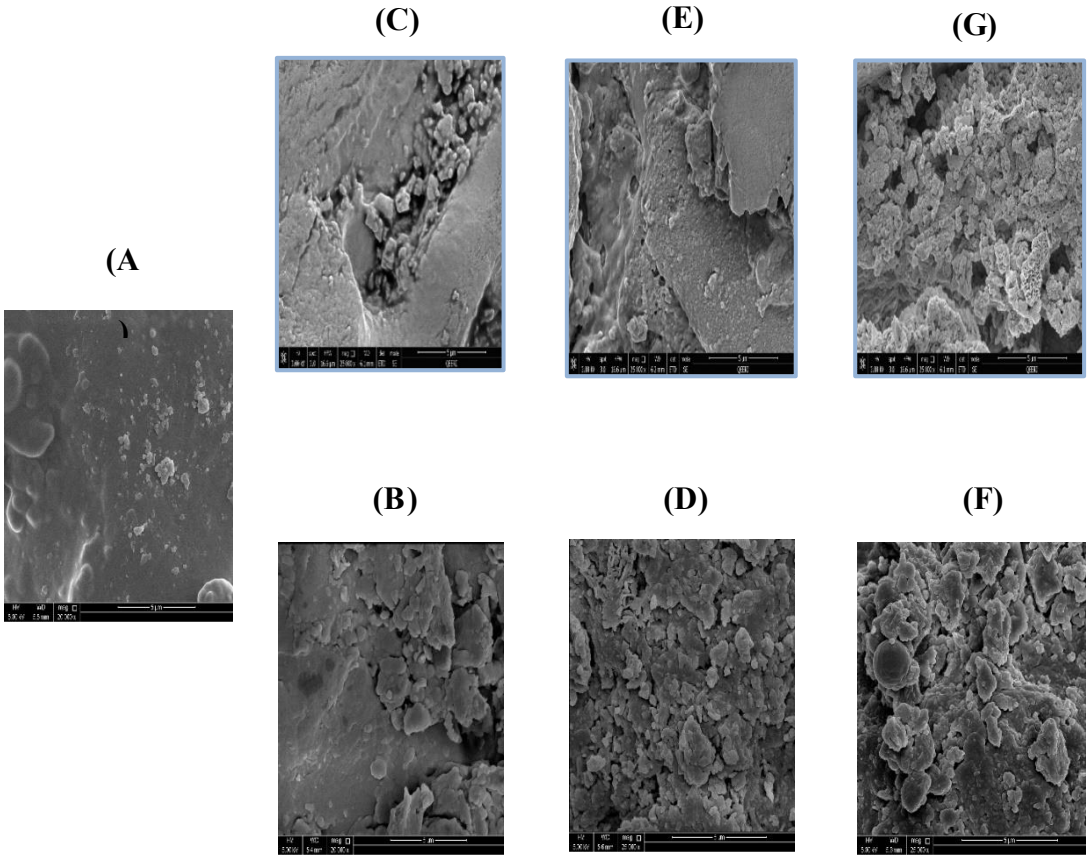

Figure 21. The SEM morphological images for the Raw-DP and the three adsorbents before (Original material) and after the adsorption of lithium at 45°C, 50 ml volume, 100 mg/L lithium-ion concentration, shaking time of 24 hrs. at 160 rpm, and 0.05 g adsorbent mass. (A) Raw-DP, (B) RDP before lithium adsorption, (C) RDP after lithium adsorption, (D) RDP-FC-Ni before lithium adsorption, (E) RDP-FC-Ni after lithium adsorption, (F) RDP-FC-Cu before lithium adsorption, and (G) RDP-FC-Cu after lithium adsorption.

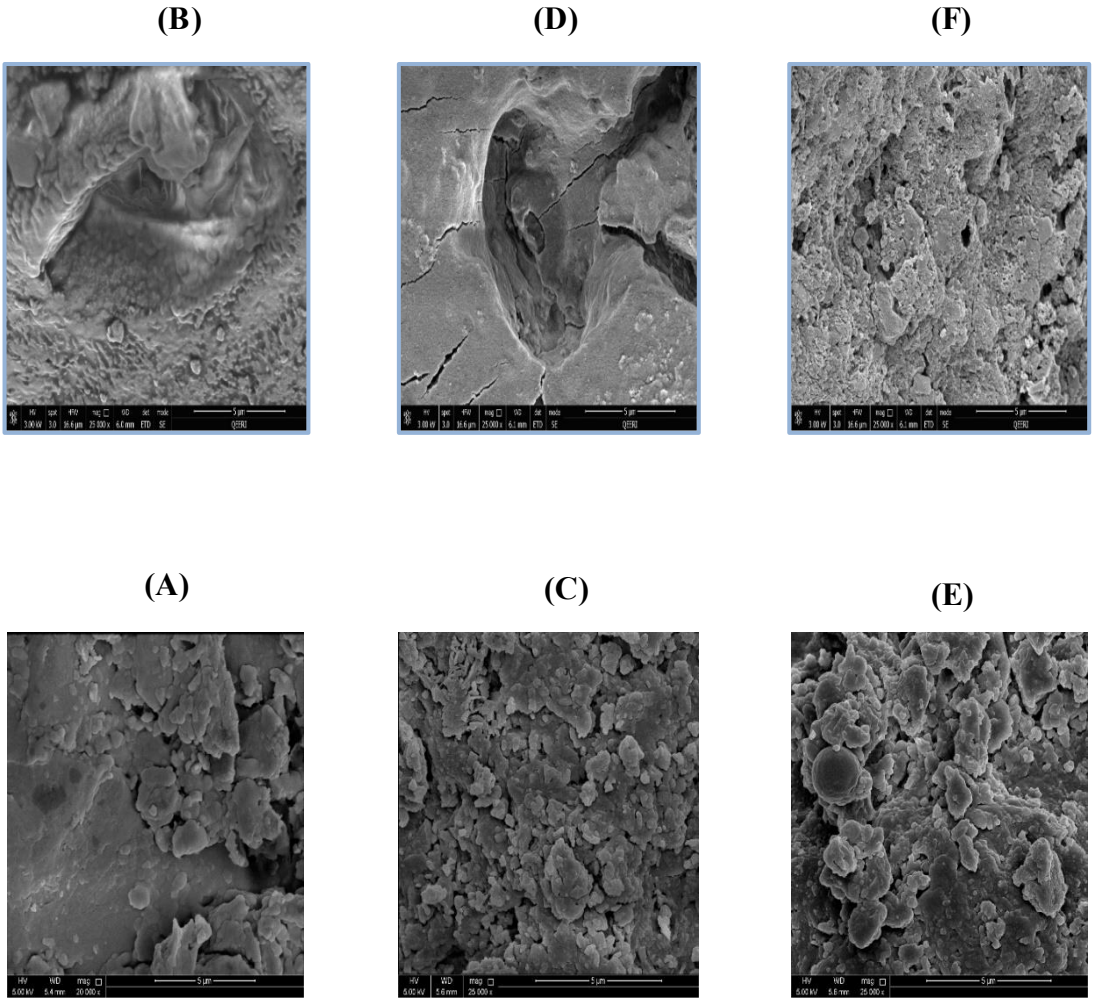

Figure 22. The SEM morphological images for the three adsorbents before (Original material) and after the adsorption of strontium at 45°C, 50 ml volume, 100 mg/L strontium-ion concentration, shaking time of 24 hrs. at 160 rpm, and 0.05 g adsorbent mass. (A) RDP before strontium adsorption, (B) RDP after strontium adsorption, (C) RDP-FC-Ni before strontium adsorption, (D) RDP-FC-Ni after strontium adsorption, (E) RDP-FC-Cu before strontium adsorption, and (F) RDP-FC-Cu after strontium adsorption.

4.2.2 Particle size distribution (PSD) test

In an adsorption system, the adsorbent's particle size distribution largely contributes to its adsorption capacity towards the targeted pollutant or valuable substance (Arslanoglu, 2021). As mentioned previously, lithium and strontium are valuable metals that could be recovered from aqueous media and brine through the adsorption technique. Therefore, the particle size distribution (PSD) test was done to examine the different sizes that compromise the three adsorbents at the study. Table 5 below represents the D10, D50, and D90 for the RDP, RDP-FC-Cu, and RDP-FC-Ni. Upon observation of the values presented in table 5, it can be noticed that the largest D10, D50, and D90 are achieved for RDP while the smallest values are obtained for RDP-FC-Ni. For RDP, 10% of the sample has a particle size less than 33.9 µm, 50% of the sample is smaller than 751.1 µm and 90% of the sample is smaller than 1,159.6 µm. The RDP-FC-Cu showed particles smaller than 29.1 µm for 10% of the sample, while 50% of the sample was less than 195.5 µm and 90% of the sample's particle size was less than 906 µm. Interestingly, the largest portion of the RDP-FC-Cu sample (90%) is below 1000 µm while the largest portion of the RDP was still in the range of 1000 µm. This means that most of the particles of the RDP-FC-Cu are smaller than most of the particles of RDP. Moreover, 10% of the RDP-FC-Ni sample has particle sizes less than 1 µm while 50% of the sample showed particle sizes less than 26.6 µm and 90% of the sample had particle sizes less than 804.3 µm. These results indicate that the majority of the RDP-FC-Ni sample had particle sizes less than the other prepared composite (RDP-FC-Cu) and the initial adsorbent material (RDP). These results are predictable as the preparation process of the prepared composites involved the addition of potassium hexacyanoferrate, sodium hydroxide, strong stirring, centrifuging, and heating in the oven. All these steps were not done for the simple preparation of the

RDP. It must be noted that the RDP-FC-Cu and RDP-FC-Ni composite adsorbents were originally RDP that was further chemically, physically, and mechanically modified. The stirring and centrifuging of the composite materials during their preparations could have led to their further breakage into smaller particle sizes. Moreover, the addition of the potassium hexacyanoferrate could have led to a decrease in the particle sizes of the composites due to alteration of the structures (formation of cubic crystal lattices), and breakage of particles. It is well-established that sodium hydroxide is a strong base, which may lead to the reduction of powder-like materials like RDP. A study done by Koutu and others (2016) demonstrated that the addition of NaOH to zinc oxide nanoparticles resulted in the subsequent decrease in their particle size distributions. A recent study done by Park and co-workers (2020) revealed that a decrease in the added NaOH concentration led to a decreased crystallinity and particle size of FeCo nanoparticles. The smaller particle size of the RDP-FC-Ni compared to RDP-FC-Cu could be attributed to the fact that the atomic mass and radius of nickel are smaller than the atomic mass and radius of copper. The atomic mass and radius of nickel are 58.693 and 124 pm (covalent radius) respectively. On the other hand, the atomic mass and radius of copper are 63.546 pm and 124 pm, respectively. This leads to less space occupied for nickel in the potassium hexacyanoferrate lattice than copper and ultimately, the smaller particle size of the composite adsorbent.

Table 5. Particle size distribution of three adsorbents for the adsorption of Li+ and Sr2+ from RO brine.

Adsorbent	D10	D50	D90
RDP	33.9	751.1	1,159.6
RDP-FC-Cu	29.1	195.5	906
RDP-FC-Ni	1	26.6	804.3

4.2.3 Brunauer–Emmett– Teller (BET) surface area, pore size, and volume distribution test

The surface area, pore sizes, and volumes of adsorbents are of great importance to adsorption systems as they could contribute largely to the effectiveness and adsorption capacities of the adsorbents towards a pollutant (Ngueagni et al., 2020). Therefore, the BET surface area, pore size, and volume distribution test were conducted for the RDP, RDP-FC-Cu, and RDP-FC-Ni that were involved in this study. The BET results are presented in Table 6. The results demonstrate the increase in the surface area upon the modification of the roasted date pits into the two composites (RDP-FC-Cu and RDP-FC-Ni). The surface area of RDP-FC-Ni was found to be the highest (5.262 m^2/g) but close to the value obtained for RDP-FC-Cu (4.758 m^2/g). This is expected as a bigger portion of RDP-FC-Ni was shown to have fewer particle sizes than the other two adsorbents (Section 4.2.2). Many of the conventional adsorbents could exhibit higher BET surface area values than the RDP, RDP-FC-Cu, and RDP-FC-Ni. For example, a study has shown that activated carbon could have a BET surface area value of around 2223 m^2/g upon activation using 600°C (Kumar and Jena, 2016). Another study revealed that activated carbon has a BET surface area of 2388 m^2/g when a temperature of 800°C is applied for activation (Zhang et al., 2017). Despite the fact that the three adsorbents in the study showed much lower BET surface areas than conventional activated carbon, they exhibited extremely high adsorption capacities for lithium and strontium (Sections 4.3, 4.4, and 4.5). Also, the three adsorbents were found to be

highly selective towards the two metals from the RO brine and a mixture solution of the two metals (Section 4.8). This means that the prepared adsorbents could be effectively utilized to recover the target metals in an environmentally friendly and cost-effective manner which does not require the added challenges of activation energies. Another study showed that nano-sized green olive stones have a BET surface area value of around 10.55 m^2/g. the nano-green olive stones were effectively used to remediate methylene blue from textile effluent. Interestingly, the prepared RDP-FC-Cu and RDP-FC-Ni in this study showed a BET surface area value of almost half the value of the nano-green olive stones. This means that the prepared composites were capable of achieving significantly high adsorption removals for the target metals despite having half the surface area of the nano-green olive stones (Al-Ghouti and Dib, 2020). Moreover, the pore size distribution shows that RDP-FC-Cu obtained the highest pore size of 138.6 A compared to 82 A for RDP-FC-Ni and 39.2 A for the RDP. Interestingly, there was a slight difference between the pore volumes of RDP and RDP-FC-Ni while RDP-FC-Cu showed the largest pore volume distribution of around 0.033 cubic centimeters per grams. The increase in the surface area and pore sizes of the potassium metal hexacyanoferrates could be due to heating, reagents depositions and/or shape modifications, pore collapses, metal complexations, formation of cubic lattice, or other factors (Dou et al., 2021; Yu et al., 2017). These modifications and enhancements of the prepared composites are expected to facilitate the adsorption activity. As the high surface area, pore size, and volume will be able to larger area for the high adsorption of lithium onto the surface and pores of the composites. Furthermore, the large pore radius and volume of RDP-FC-Cu could lead to its higher adsorptive capacities for lithium when compared to the RDP and RDP-FC-Ni. As mentioned previously, the pore radius and volumes represent the available active binding sites for adsorbates. The BET

results can be also supported by previous findings of this study where the particle size distribution was found to decrease from RDP to the prepared composite adsorbents. This would typically enhance the surface area of the adsorbents and could lead to increased pore sizes and volumes (Al-Ghouti and Al-Absi, 2020).

Table 6. BET surface area, pore size, and volume distribution test for three adsorbents

Adsorbent	Surface area (m^2/g)	Pore size (A^o)	Pore volume (cc/g)
RDP	2.518	39.2	0.010325
RDP-FC-Cu	4.758	138.6	0.032964
RDP-FC-Ni	5.262	82.0	0.010306

4.2.4 Carbon and nitrogen elemental analysis

The purity and composition of adsorbents in terms of total carbon and nitrogen can be determined analytically by conducting a carbon and nitrogen elemental analysis. Carbonaceous materials are commonly recognized as potentially highly adsorptive towards pollutants (Liu et al., 2021). Therefore, it was important to determine the composition of the Raw-DP, RDP, RDP-FC-Cu, and RDP-FC-Ni in order to obtain an overall idea regarding their carbon and nitrogen contents as a percentage of the total weight. The results of the elemental analysis are presented in table 7. It is clear from the results that the carbon content of the materials is increasing upon roasting and modification using potassium metal hexacyanoferrates. On the other hand, the nitrogen content decreased upon roasting of the date pits and modifications. The enhanced carbon contents could be due to the addition of the hexacyanoferrates, heating, and roasting. The loss of nitrogen upon roasting and modification could be attributed to the fact that roasting and heating usually lead to the loss of nitrogen gas (Dou et al., 2021; Kamil et al., 2019; Alves et al., 2020).

Table 7. The carbon and nitrogen elemental analysis of Raw-DP and three adsorbents for the adsorption of Li^{+} and Sr^{2+} from RO brine.

Material/Adsorbent	Carbon (%)	Nitrogen (%)
Raw-DP	36.12	7.32
RDP	37.42	5.04
RDP-FC-Cu	45.75	1.10
RDP-FC-Ni	46.04	1.07

4.2.5 X-ray diffraction (XRD) analysis

The analysis of the crystallinity adsorbents is of great importance when it comes to their characterization for an effective adsorption process (Hosseini et al., 2021). Similar to the achieved understanding of the chemical composition of the brine at study, an understanding of the crystallinity of the adsorbents was one of the objectives of this study. This is because the adsorption of the valuable metals from the brine solution on the adsorbents is a process that relies on the properties of both materials. Figure 23 (A-C) represents the XRD of RDP, RDP-FC-Cu, and RDP-FC-Ni before the adsorption of lithium and strontium from the brine stream involved in this study. From a general perspective, it can be noticed that the XRD of RDP (Figure 23 (A)) differs from the XRD's of the prepared composites in figure 23 (RDP-FC-Cu (B) and RDP-FC-Ni (C)), while the composites obtained more similarities in the XRD trend and peaks. For RDP (Figure 23 (A)), there are two major intense peaks at 2θ of 16° and 20°. The 2θ values represent a certain spacing between the atoms or crystals in the sample being tested. The intensity of the peaks in an XRD analysis corresponds to the degree of the crystallinity of the samples, where higher intensity means higher crystallinity and vice versa. To be more specific, the peak obtained for RDP at 2θ of 16° is more intense (intensity of 9014) than the peak obtained at 2θ of 20° (intensity of 8605). This means that at the 2θ 16° phase spacing between the atoms, there were more crystals in the

samples than at the 2θ 20° spacing. Moreover, the size of the crystals present in the sample can be determined from the obtained widths of the peaks in an XRD. Moreover, the size of the crystals is inversely proportional to the width of the XRD peaks. Moreover, for RDP, the peak at 2θ 16° is narrower than the peak at 2θ 20°. This means that at 2θ 16°, the crystals of the samples are bigger in size than the ones obtained at 2θ 20° phase or spacing (Seekaew et al., 2019). For RDP-FC-Cu (Figure 23 (B)), the XRD shows 4 distinctive sharp and intense peaks at 2θ of 17°, 25°, 30°, and 35°. These peaks indicate the high crystallinity of the sample along with the presence of smaller size crystals than RDP. In particular, it appears that the crystals in the RDP-FC-Cu adsorbent are similar in size. Also, the XRD peaks were similar to other studies that reported that the structure is an F-centered cubic unit cell (Martin et al., 2019; Wu et al., 2015). The XRD peaks obtained for RDP-FC-Cu were significantly different from the XRD peaks obtained for RDP. This shows that the modification done to the RDP to prepare the RDP-FC-Cu was effective. Interestingly, the peaks obtained for RDP-FC-Cu were consistent with other studies that involved copper-based hexacyanoferrates (El-Bahy et al., 2018; Kim et al., 2017). The XRD pattern obtained for RDP-FC-Ni (Figure 23 (C)) shows the same peaks that were obtained for RDP-FC-Cu. This shows that both composites involved in the study have similar crystalline and structural characteristics and that the modification was successful. However, a peak at 2θ 30° disappeared for the RDP-FC-Ni adsorbent, which, according to studies, was found to be a characteristic peak for copper potassium hexacyanoferrate composites (Martin et al., 2019; Michel et al., 2015).

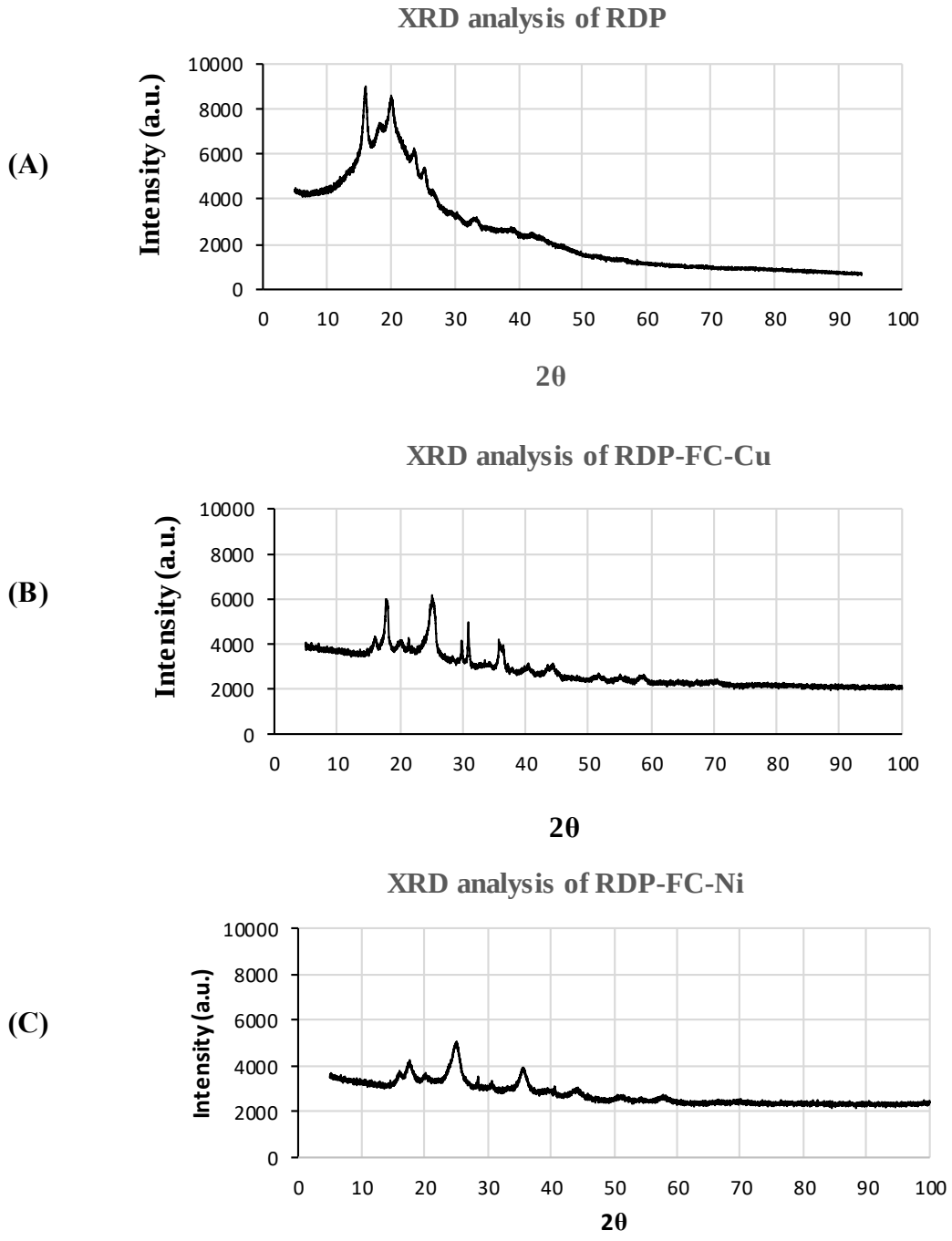

Figure 23. The XRD peak results for the three adsorbents involved in the study before the adsorption of lithium and strontium. (A) RDP, (B) RDP-FC-Cu, and (C) RDP-FC-Ni.

4.2.6 Fourier-Transform Infrared Spectroscopy (FTIR) analysis

Studying and determining the specific chemical bonds, individual compounds, functional groups as well as the atomic and molecular structure of adsorbents is

important in any treatment or recovery adsorption system. Fourier Transform Infrared Spectroscopy (FTIR) is a well-established analytical technique that provides scientists the tool for functional group analysis and optimization of adsorption systems (Zhang and Liu, 2020). Therefore, FTIR was conducted for the analysis of the RDP as well as the RDP-FC-Cu and RDP-FC-Ni composites before and after the adsorption of lithium and strontium.

The figures below (Figure 24 – Figure 29) show the FTIR spectrum for the three adsorbents involved in the study prior and after the adsorption of lithium and strontium at the optimum temperature of 45°C (Section 4.5). From a general observation of all figures, it is clear that each adsorbent shows its unique and different functional groups before the adsorption of the metals. However, the RDP (Figure 24 and 27) are more similar to RDP-FC-Ni (Figure 26 and 29) in terms of functional groups than to RDP-FC-Cu (Figure 25 and 28). RDP-FC-Cu shows the least number of functional groups compared to the RDP and RDP-FC-Ni composite. For RDP before adsorption, the medium band at around 3312 cm^{-1} corresponds to the O-H bond or N-H stretching (secondary amine). The medium bands at 2923 and 2853 cm^{-1} are for C-H stretching vibrations such as CHO, and $–CH_3$ >CH_2. In addition, the strong peak at 1743 cm^{-1} represents the C=O bondage of esters (Mangwandi et al., 2020; Al-Saad et al., 2019). Also, the RDP contains a C=C stretching bond that represents conjugated alkenes at 1609 cm^{-1}. Furthermore, the RDP demonstrated a band at around 1026 cm^{-1}, which according to studies, belongs to polysaccharides mainly hemicelluloses, and functional groups like functional groups such as C-O, C-C, C-O-P, and C-O-C vibrations (Al-Ghouti and Al-Absi, 2020; Naeimi and Faghihian, 2017). After the adsorption of lithium onto the RDP (Figure 24), considerable changes to the bands on the FTIR of the original RDP can be noticed to occur. All of the observed bands are seen to become

more intense in terms of increased absorbance and decreased transmittance. This indicates that all of the mentioned functional and characteristic groups of RDP played significant roles in the uptake, recovery, and adsorption of lithium. The broadband at 3312 cm^{-1} became less broad and more intense after lithium adsorption. The peak at around 1026 cm^{-1} had a slight shift to a wavenumber of around 1007 cm^{-1} upon the adsorption process. These observations indicate that the chemical structure of the RDP as well as the surrounding environment around the RDP changed due to the adsorption of lithium (Al-Ghouti and Al-Absi, 2020). Similar patterns were obtained for the FTIR spectrum for the adsorption of strontium onto RDP (Figure 26). However, it must be noted that an overall less transmittance and more absorbance was achieved for the RDP that was involved in the adsorption of strontium when compared to the RDP involved in lithium adsorption.

Moreover, the FTIR spectrum for the original RDP-FC-Cu composite (Figure 25 and 28) demonstrates the functional changes that occurred due to the modification of the RDP. These functional changes are represented by the broadening of the O-H or N-H stretching peak which is shown at 3209 cm^{-1} (Mangwandi et al., 2020; Naeimi and Faghihian, 2017). Also, the peak that was present for the RDP at 2923 cm^{-1} (C-H bondage) can be seen to become less intense and shifted for the RDP-FC-Cu (2907 cm^{-1}) when compared to RDP. This could be due to the chemical change that occurred on the overall cellulosic mass of the RDP upon modifications. Moreover, the peaks that were present for RDP at 2853 cm^{-1}, 1743 cm^{-1}, 1609 cm^{-1}, and 1026 cm^{-1} disappeared for the modified RDP-FC-Cu. This further confirms the chemical modification and change on the roasted date pit. Furthermore, a strong sharp peak appeared for the RDP-FC-Cu at 2078 cm^{-1} which corresponds to the C≡N bond indicating the presence of $K_4[Fe(CN)_6]$ and the modification by the potassium hexacyanoferrate (Shen et al.,

2020; Naeimi and Faghihian, 2017; Zhang et al., 2017). Another characteristic functional group is shown on the FTIR spectrum of the modified RDP-FC-Cu at 1107 cm^{-1}. This wavelength belongs to the C-O stretching bond of secondary alcohols (Al-Saad et al., 2019). The formation of a Fe-O bond due to the modification of the roasted date pits into RDP-FC-Cu is shown by the peak at 592 cm^{-1}, which confirms the presence of iron in the date pits. Major changes occurred to the FTIR bands of RDP-FC-Cu after the adsorption of lithium (Figure 24) where all the bands, except for the characteristic band of C≡N, became more intense (less transmittance and more absorbance). This shows the significant chemical and structural changes that the adsorption of lithium-induced in the RDP-FC-Cu composite. For the adsorption of strontium onto RDP-FC-Cu (Figure 28), similar results were obtained; however, overall higher transmittance (less absorbance) took place than the bands obtained for the adsorption of lithium. This means that the original FTIR spectrum for the composite before adsorption is more similar to the FTIR spectrum of the composite after adsorption. Which indicates fewer chemical changes occurring due to the adsorption of strontium than lithium onto RDP-FC-Cu (Margenot et al., 2017; Wang et al., 2018).

The FTIR spectra for the original RDP-FC-Ni composite (Figures 26 and 29) show the highest number of functional groups. This means that the modification of the RDP to RDP-FC-Ni mostly led to an enhancement of the functionality of the adsorbent. However, the modified RDP-FC-Ni still represents most of the functional groups found on the original roasted date pits. For example, the peak that corresponds to O-H or N-H bondage is less broadened (3336 cm^{-1}) than the peak for RDP-FC-Cu (Mangwandi et al., 2020; Naeimi and Faghihian, 2017). The medium peaks that represent C-H stretching at 2923 and 2853 cm^{-1} can be found for the modified RDP-FC-Ni (Al-Saad et al., 2019). Interestingly, the strong sharp peak that represents C≡N bond and indicates

the presence of $K_4[Fe(CN)_6]$ modification, is also found for the modified RDP-FC-Ni as for the modified RDP-FC-Cu (Shen et al., 2020; Naeimi and Faghihian, 2017; Zhang et al., 2017). However, the peak is less sharp and strong as well as can be seen at a slightly different wavelength of 2090 cm^{-1}. The higher intensity of the C≡N peak for RDP-FC-Cu compared to RDP-FC-Ni is attributed to more concentration of C≡N bonds in the sample. Also, copper is highly electronegative, which gives rise to strong bonds. Additionally, copper has a higher molecular weight than nickel, which takes up larger space in the formed metal hexacyanoferrate complexation. These factors result in the formation of strong and sharp peaks in an FTIR spectrum. The shift of the peak from a lower wavelength (2078 cm^{-1}) for RDP-FC-Cu to a higher wavelength (2090 cm^{-1}) for RDP-FC-Ni is due to the fact that the mass of the complex is lower than RDP-FC-Cu. In FTIR principles, the mass of the vibrating molecule is inversely proportional to the frequency of vibration (Guo et al., 2019; Iftekhar et al. 2018; Munajad et al., 2018). Moreover, the modified RDP-FC-Ni has C=O, C=C, polysaccharides, and Fe-O bonds at 1742 cm^{-1}, 1609 cm^{-1}, 1027 cm^{-1}, 591 cm^{-1}, respectively (Al-Saad et al., 2019; Al-Ghouti et al., 2019). The adsorption of lithium and strontium onto the RDP-FC-Ni composite (Figures 26 and 29) have demonstrated similar FTIR results obtained for RDP-FC-Cu, which are discussed above.

Furthermore, similar results were obtained from other studies done on metal hexacyanoferrates. For example, Long and coworkers (2020) aimed at the synthesis of copper hexacyanoferrates nano-particles film for the recovery of cobalt. The functional groups for the adsorbent were determined using FTIR technology. The results revealed the presence of a C≡N bond through the appearance of an FTIR band at 2099 cm^{-1}. Also, the authors found that the synthesized adsorbent had a Fe-C bond through the presence of bands at around 596 cm^{-1}. These bonds illustrate and confirm further the

modification of the nanoparticles by hexacyanoferrates. Another study performed by Chong and others (2019) on the synthesis of potassium nickel hexacyanoferrate cathodes for batteries investigated the functional groups by FTIR. As with the previous study, the results revealed the presence of a C≡N bond as well as an O-H bond through the peaks of the FTIR spectrum. The authors suggested that potassium nickel hexacyanoferrate adsorbent is characterized by a high surface area, mesoporous/microporous structure, and coordinated molecules of water. This was confirmed by the presence of stretching and bending modes of O-H bondage. Similar results were discussed by a study conducted by Ma and others (2019) on the production of copper hexacyanoferrates nanoflakes as sodium-ion batteries cathodes.

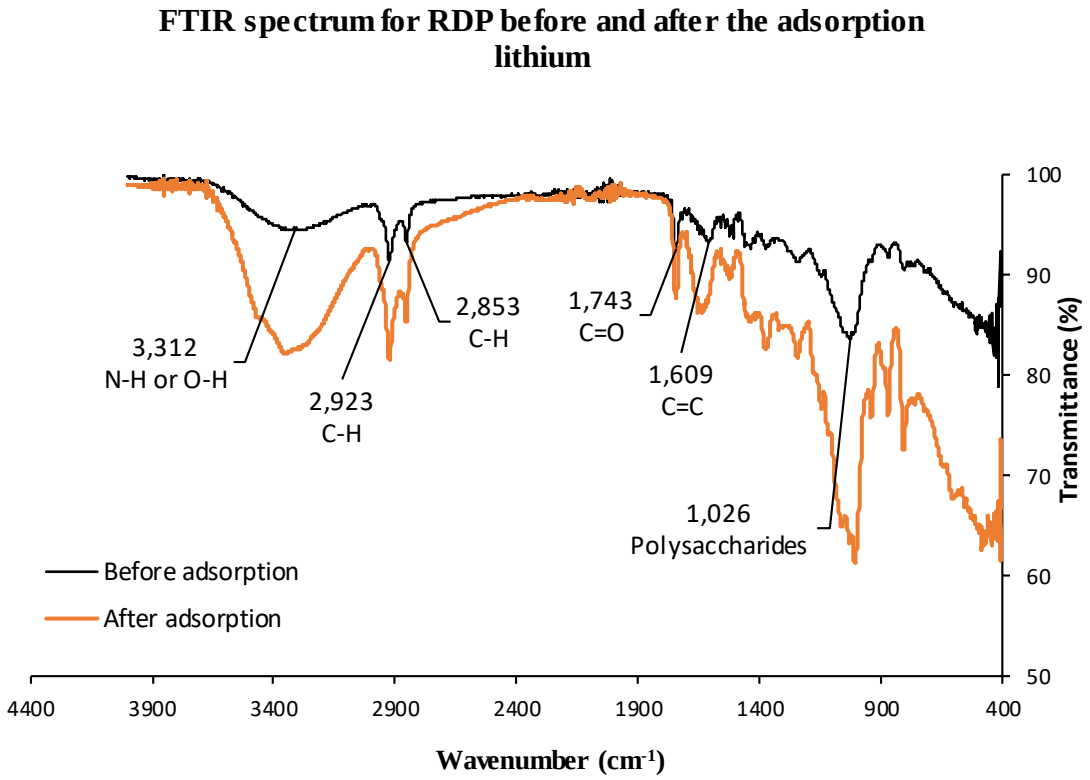

Figure 24. The FTIR analysis before and after the adsorption of lithium onto RDP. The experimental conditions were as follows: 45 °C, 50 ml volume, 100 mg/L lithium-ion concentration, shaking time of 24 hrs. at 160 rpm, and 0.05 g RDP mass.

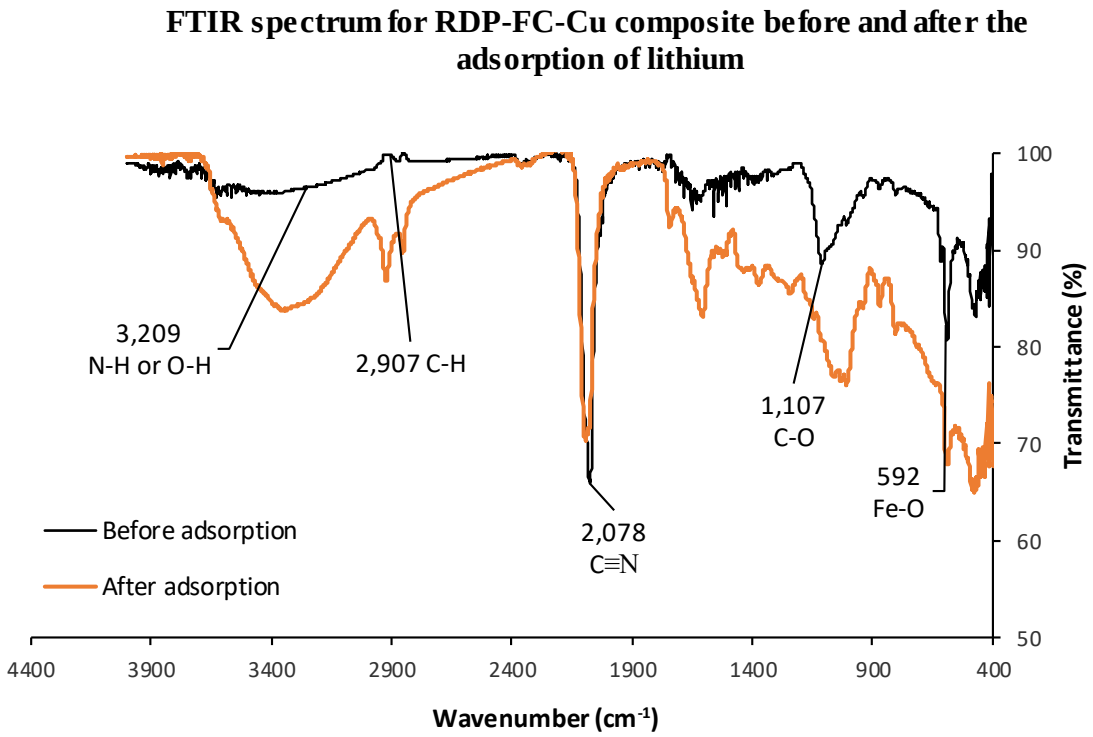

Figure 25. The FTIR analysis before and after the adsorption of lithium onto RDP-FC-Cu. The experimental conditions were as follows: 45 °C, 50 mL volume, 100 mg/L lithium-ion concentration, shaking time of 24 hrs. at 160 rpm, and 0.05 g RDP-FC-Cu mass.

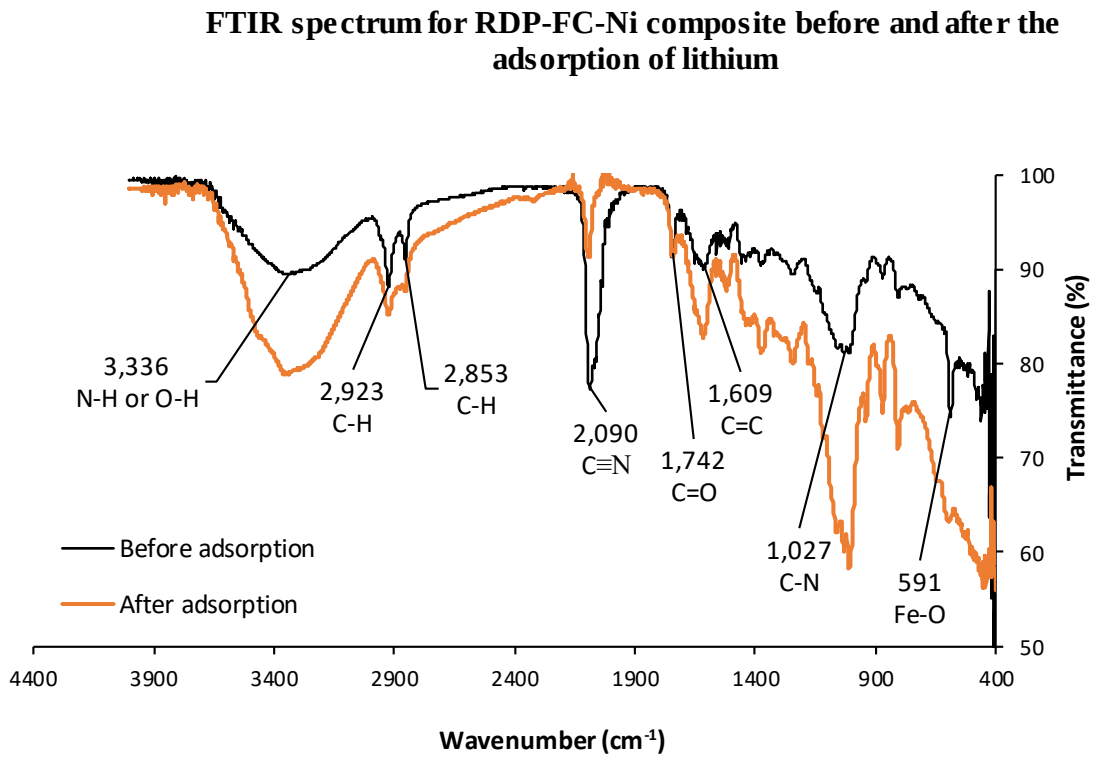

Figure 26. The FTIR analysis before and after the adsorption of lithium onto RDP-FC-Ni. The experimental conditions were as follows: 45 °C, 50 ml volume, 100 mg/L lithium-ion concentration, shaking time of 24 hrs., at 160 rpm, and 0.05 g RDP-FC-Ni mass.

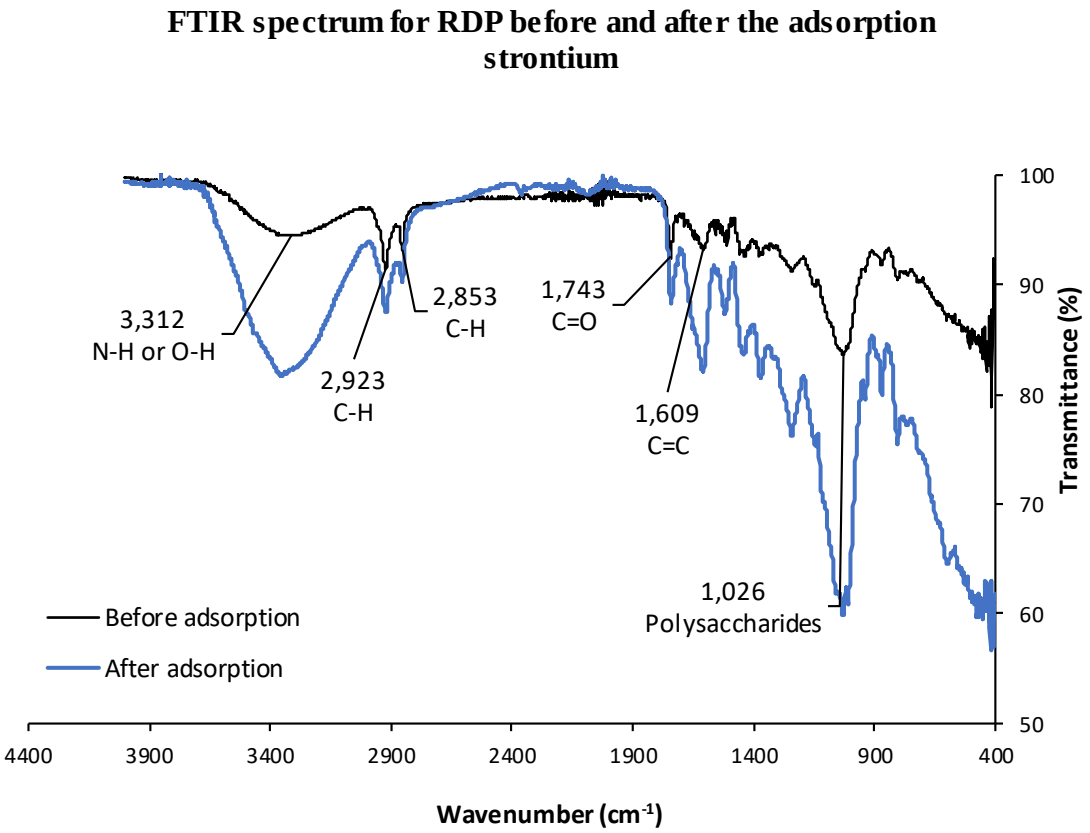

Figure 27. The FTIR analysis before and after the adsorption of strontium onto RDP. The experimental conditions were as follows: 45 °C, 50 ml volume, 100 mg/L strontium-ion concentration, shaking time of 24 hrs. at 160 rpm, and 0.05 g RDP mass.

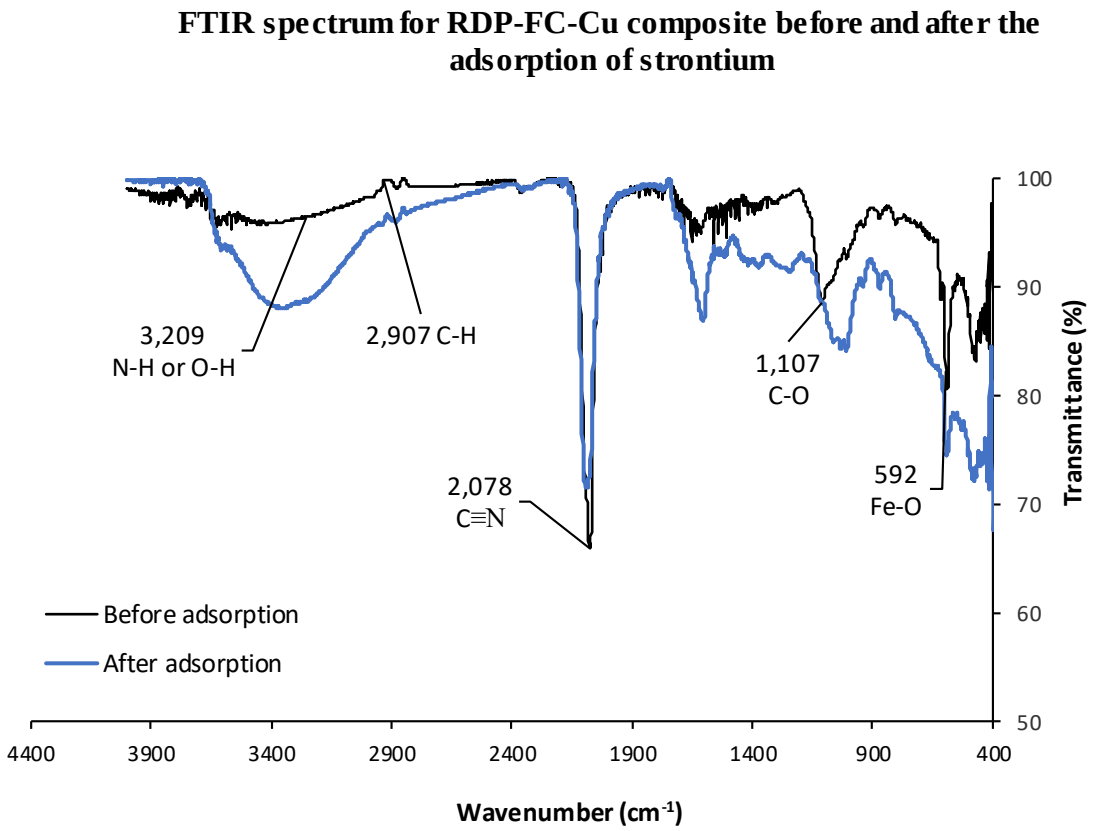

Figure 28. The FTIR analysis before and after the adsorption of strontium onto RDP-FC-Cu. The experimental conditions were as follows: 45 °C, 50 ml volume, 100 mg/L strontium-ion concentration, shaking time of 24 hrs. at 160 rpm, and 0.05 g RDP-FC-Cu mass.

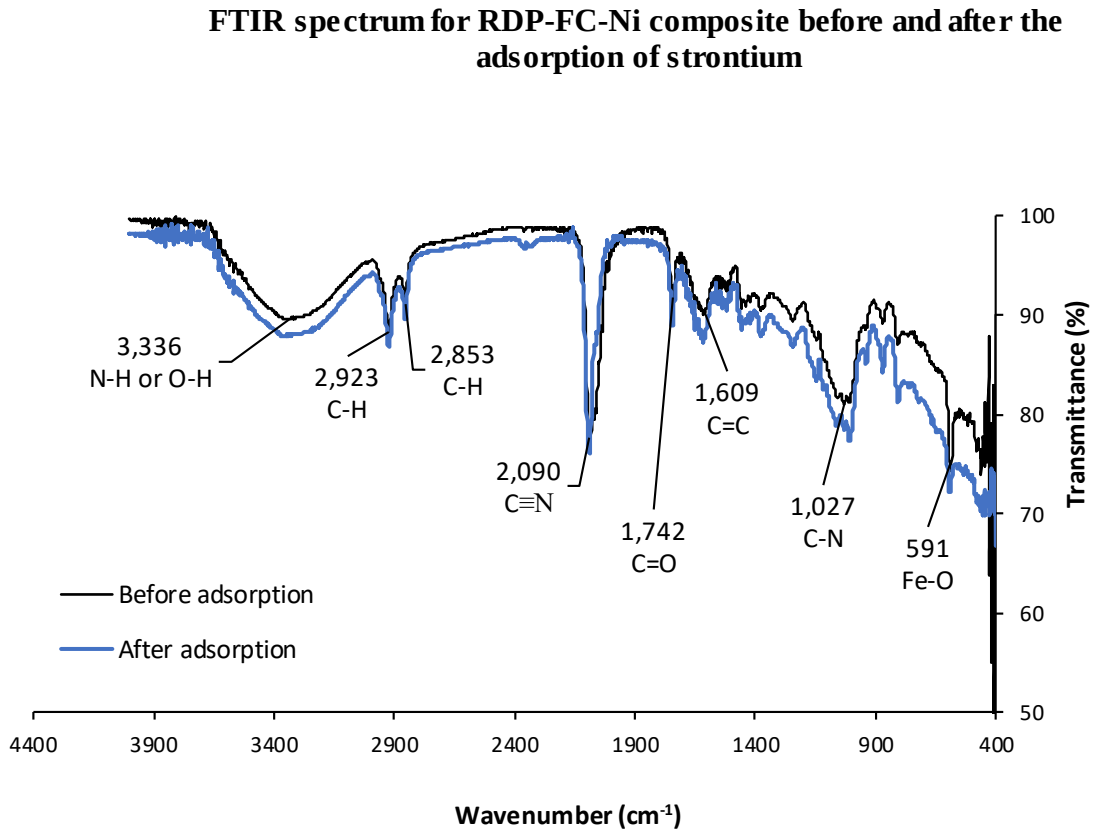

Figure 29. The FTIR analysis before and after the adsorption of strontium onto RDP-FC-Ni. The experimental conditions were as follows: 45 °C, 50 ml volume, 100 mg/L strontium-ion concentration, shaking time of 24 hrs. at 160 rpm, and 0.05 g RDP-FC-Ni mass.

4.2.7 Thermogravimetric analysis (TGA)

Temperature plays a significant role in the thermal stability and durability of adsorbents that are involved in the adsorption of pollutants or the recovery of valuable metals and materials from aqueous solutions. The thermal stability characteristics of adsorbents can be identified precisely and accurately through performing a thermogravimetric (TGA) analysis. Therefore, the RDP, RDP-FC-Cu, and RDP-FC-Ni adsorbents involved in this study for the recovery of lithium and strontium were examined through a TGA analysis test and shown in figure 30. The TGA results of the RDP reveal that an

initial weight loss was observed to occur at a temperature of around 65 °C. At this temperature and till a temperature of around 250 °C, the RDP experienced a somewhat constant weight loss. However, beyond the temperature of 250 °C, a sharp followed by a gradual decrease in the weight of RDP took place. On the other hand, RDP-FC-Cu and RDP-FC-Ni obtained similar TGA results where they follow almost the same trend in their thermal decomposition with temperature. RDP-FC-Ni showed a gradual and minute decrease in its weight percentage at a temperature of around 37 °C, followed by a stabilization trend between 116 °C and 211 °C. Above this temperature, gradual and constant degradation of the RDP-FC-Ni is observed. RDP-FC-Cu obtained a minute decrease in its weight percentage at around 38 °C followed by a stabilization in its weight between temperatures of 110 °C and 175 °C. Above 175 °C, gradual and constant degradation trends can be seen for RDP-FC-Cu with temperature. Interestingly, the constant thermal degradation observed for RDP-FC-Ni occurred at around 300 °C, while for RDP-FC-Cu it took place at around 344 °C. The initial minute decreases in the weight percentages of the three adsorbents at lower temperatures could be due to the loss of moisture and volatile content. The following stages of weight loss can be attributed to the loss of celluloses, hemicelluloses, and main compounds, as well as breaking of chemical bonds, and lastly carbonization (Dou et al., 2020; Erabee et al., 2017). From the results, it appears that RDP achieved moisture and volatile contents loss at a higher temperature than the prepared composites. This could be due to its rigid carbonaceous and lignocellulosic characteristics as well as the fact that no solvents were used to prepare the roasted date pits. It is more probable that as the prepared composites compromise a cubic lattice structure, it is much easier for moisture to evaporate at lower temperatures. Moreover, the almost constant degradation of RDP at a wide range of temperatures (65 °C - 250 °C) corresponds to their possible prolonged thermal stability.

The RDP-FC-Ni showed prolonged thermal stability of its weight between temperatures of 116 °C and 211 °C, which is a wider range of temperatures than the stabilization trend that was observed for RDP-FC-Cu (Temperatures between 110 °C and 175 °C). However, the final stage of the thermal degradation of RDP-FC-Cu was noticed at higher temperatures than RDP-FC-Ni, which indicates its durability to a wider overall range of temperatures than RDP-FC-Ni. All in all, it can be noticed from the figures that the three adsorbents exhibit similar overall weight loss profiles, which confirms the modification of the original starting material (RDP) into the prepared composites without the complete loss of the initial characteristics (Misra et al., 2020). These results demonstrate the sufficient thermal stabilities and durability's of the three adsorbents involved in this study. Despite the high thermal stability qualities for RDP, the prepared composites showed more stabilization and rigidity in terms of weight loss. Similar results were obtained by Misra and others (2020) where a TGA was done to study the thermal stabilities of three materials. The study involved the synthesis of grafted cellulose adsorbent using 4-vinyl benzene sulfonic acid sodium salt (VBSA). The initial cellulose material exhibited a short weight loss step between 50 °C and 150 °C followed by a steep weight loss step between 270 °C and 450 °C. The authors attributed the first short weight loss step to water loss while the second being due to the thermal decomposition of cellulosic bonds. The VBSA material showed a longer water loss step followed by constant, slow, and gradual thermal decomposition steps after the temperature of 450 °C. The grafted cellulose adsorbent obtained similar TGA results to both; the starting cellulose material as well as the VBSA, which is a confirmation of the grafting of the prepared adsorbent. Another study involved the application of calcium alginate carbon adsorbents in the adsorption of total organic acids from Diglycolamine solvents. The TGA results revealed that the calcium alginate carbon

adsorbent undergoes a dehydration step until a temperature of around 151.7 °C. Beyond this temperature, the adsorbents experienced a weight loss due to the production of calcium carbonate through the evaporation of carbon dioxide from the polysaccharide backbone. Similar results of multiple achieved weight loss steps for walnut shell-based adsorbents for lead ions were achieved by Rasoulpoor and coworkers (2020).

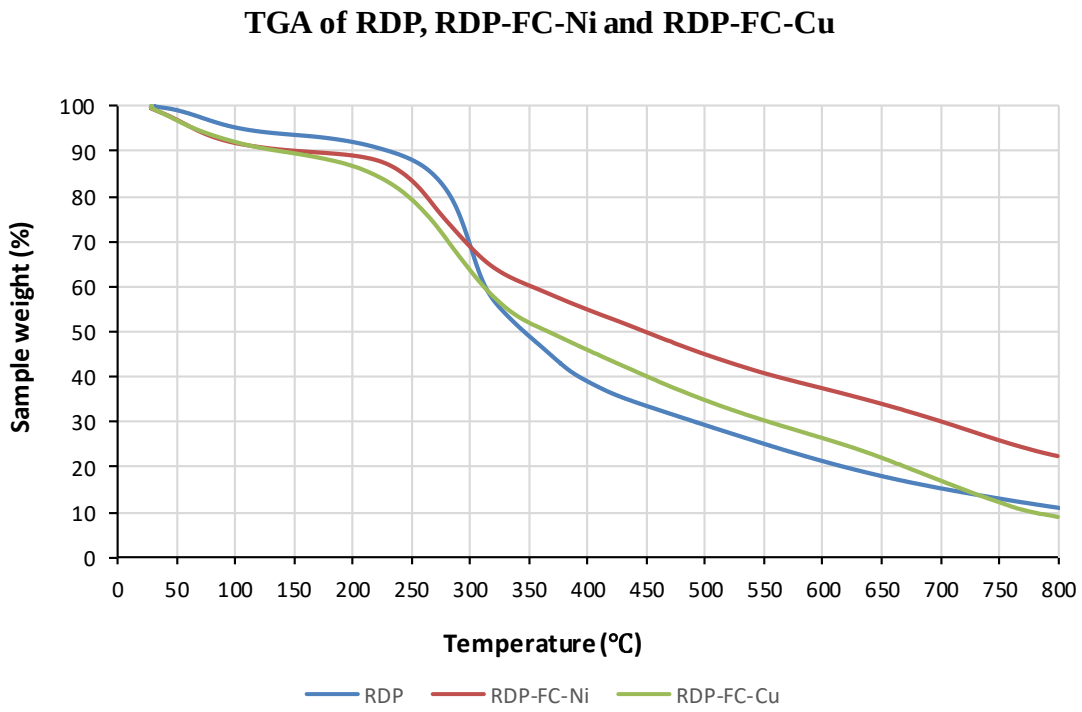

Figure 30. The TGA results for the three adsorbents (RDP, RDP-FC-Cu, and RDP-FC-Ni) involved in the adsorption of lithium and strontium.

4.3 Effect of solution pH and zeta potential on the adsorption of lithium and strontium onto roasted date pits and composites

Studying the effect of pH on the adsorption of lithium and strontium onto the date pits involved in the study is vital. This is because changing the solution pH would significantly alter the adsorption mechanisms and efficiencies of date pits towards metals. The types and amounts of electrostatic charges present in the adsorption solution will determine the extent and efficiency of the environmental clean-up and recovery of metals (Zhao et al., 2020). As shown by the ICP-OES results for the reverse osmosis brine, lithium exists at an amount of 44.2 mg/L, while strontium existed at an amount of 447 mg/L. Lithium is among the commercially valuable metals that could be harnessed and used in a variety of industrial applications and products like batteries, vehicles, pharmaceuticals, and ceramics (Ryu et al., 2020; Wang et al., 2017). Surprisingly, the ICP-OES analysis for the characterization of the reverse osmosis brine showed a high concentration of the rare metal strontium. This metal is usually used in the pharmaceutical industry and manufacturing glass and ceramics (Ryu et al., 2020; Shahmansouri et al., 2015).

Therefore, the first parameter investigated for the adsorption of Li^+ and Sr^{2+} was the solution pH. Figures 31 and 32 below show the adsorption capacities of RDP as well as the two composite materials denoted as RDP-FC-Cu and RDP-FC-Ni towards Li^+ and Sr^{2+} at a variety of pH values. The examined pH values were 2, 4, 6, 8, and 10 while the concentration of the metal ion was fixed to 100 mg/L. According to studies, changing the solution pH may have several common effects on the adsorption capacity of alkali metals in aqueous solutions (Chen et al., 2020; Huang et al., 2020; Lin et al., 2020). Alkali metals exist in aqueous solutions in a protonated form. Therefore, at low pH values, where H^+ exists at high concentrations in the solution and on the adsorbent surface, electrostatic repulsion forces are usually high. These forces prevent the high

adsorption of protonated metals onto the adsorbents. As the solution pH increases and becomes less protonated with H^+, electrostatic repulsion forces decrease and become dominated by electrostatic attraction forces between the protonated metals and the lesser protonated adsorbent surface. As a result, the adsorption capacity of the adsorbent would increase till it reaches an equilibrium point. At this point, the available active sites on the adsorbent surface decrease, which might result in a decrease in the adsorption capacity of metals. At highly basic pH values, metals start to precipitate and form metal hydroxides with a high concentration of OH^- in the solution. This behavior of metals is common and usually mimics a high adsorption capacity (Zhao et al., 2020; Chen et al., 2020; Jiang et al., 2020; Maneechakr and Mongkollertlop, 2020). A study done by Banat and others (2002) investigated the effect of solution pH on the adsorption of Cu^{2+} and Zn^{2+} onto activated and non-activated date pits. The results revealed that the adsorption for both metals favored higher pH ranges and the non-activated date pits. A more recent study done by Al-Ghouti and coworkers (2010) studied the adsorption mechanism of Cu^{2+} and Cd^{2+} onto raw date pits under the influence of different pH values. The study discussed the significant effect of solution pH on the uptake behaviors of metals onto the raw date pits. The optimum pH value range for the two metals was found to be between 4 and 6 where the adsorbent appeared to be less protonated. Also, the study emphasized that above pH 6, most metals tend to precipitate instead of getting adsorbed onto the adsorbent. Similar results were found by Huang and others (2018) for the adsorption of Rb^+ and Cs^+ onto 18-crown-6 from brine solutions. Martin and others (2019) studied the adsorption of cesium ions in solution onto potassium nickel hexacyanoferrate composite. The study involved investigating the effect of solution pH on the structure of the adsorbent as well as its adsorptive mechanisms towards cesium. Interestingly, the results revealed that changing the pH greatly influenced the sorption

capacity of cesium onto the adsorbent as a result of the changed structure. In addition, the authors mentioned that increasing the pH above 8 led to the precipitation of other compounds like iron hydroxide and nickel hydroxide.

In general, it is clear from Figure 31 that the adsorption capacity for lithium follows a similar trend for all date pits at all pH values. The adsorption capacity of lithium at all pH values is lowest for the roasted date pits and highest for RDP-FC-Cu (P-value < 0.05, appendix A). As mentioned previously in the FTIR results (section 4.2.6), the modification of roasted date pits into RDP-FC-Cu and RDP-FC-Ni gave rise to characteristic and unique functional groups to the date pits. For example, the presence of C≡N, Fe-C, C-O, and C-N bonds on the composites could have enhanced their adsorptive capabilities, functionality, structure, and characteristics towards lithium and strontium.

Lithium adsorption onto the RDP (Figure 31) shows a continuously increasing trend as the pH increases from 2 to 10 (P-value < 0.05, appendix A). The lowest adsorption capacity (44.1%) for lithium on RDP was observed at pH 2. Oppositely, the highest adsorption capacity (52.6%) for lithium on the RDP was observed at pH 10. This behavior of lithium ions adsorption is common due to the fact that at low pH (2), the solution and the adsorbent surface are highly protonated with H^+, which competes with the protonated lithium ions for the available active sites on the unmodified roasted date pits. These results in the lower adsorption capacity for lithium at pH 2 compared to higher pH values. The adsorption capacity for lithium on the unmodified roasted date pits continued to increase from pH 4 (47.8%) and 6 (51%) as the concentration of H^+ and its competing behavior decreased in the solution. The electrostatic attraction forces between the less protonated adsorbent functional groups and the protonated lithium-ion increased, which enhanced the adsorption capacity. Moreover, the adsorption capacity

slightly increased as the pH increased from 8 (52.2%) to 10 (52.6%). This could be explained by two possible scenarios. Firstly, at pH 8, the solution became less concentrated with H^+ and more concentrated with OH^-. Therefore, the electrostatic attraction forces between the negatively charged adsorbent and the positively charged lithium-ion increased with the increase of pH to 8 and 10. This led to an increase in the adsorption capacity for lithium on the RDP at pH 8 and 10. The second explanation for the observed highest adsorption of lithium-ion on the RDP at pH 10 could be due to the precipitation of the metal and the formation of metal hydroxide in the solution. This behavior corresponds to a faked adsorption behavior for metals at highly basic pH values (Su et al., 2020; Soliman and Moustafa, 2020; Zhao et al., 2020; Chen et al., 2020; Jiang et al., 2020). A recent study done by Kamran and Park (2020) revealed that lithium adsorption onto a variety of acid functionalized carbon nanofibers decorated with Mn-doped TNT-nanocomposites favored increasing pH from 2 to 14. They discussed the effect of H^+ concentration in the solution on decreasing the adsorption efficiency at low pH ranges. Another study performed by the same authors (2020) on the adsorption of lithium on composites of rice husk and coconut shell revealed the same results. Lithium adsorption was increasing with increasing the pH of the solution from pH 2 to 12. Wang and others (2017) discussed the significant effect that the solution pH plays on the adsorption efficiency of lithium onto H_xTiO_3. The results of the study showed that lithium exists as a protonated ion in the brine sample. Therefore, the adsorption was enhanced as the pH of the solution increased and the surface charge of the adsorbent decreased. However, precipitation was observed at highly basic pH values. Marthi and smith (2020) performed a study to compare the adsorption capacity of H_2TiO_3 – Diatomaceous earth composite towards lithium ions in brine and LiCl buffered solution. The results of the study revealed that lithium adsorption was

enhanced with increasing the pH. Interestingly, lithium adsorption from the buffered solution was much greater than the brine solution. The reason for that is due to the lower pH value of the brine (pH 7.5) solution and the presence of other competing ions compared to the LiCl buffer solution (pH 9.5).

Lithium adsorption onto RDP-FC-Ni at different pH values (Figure 31) shows a slight increase from pH 2 (56.1%) to 4 (56.2%) then a decrease at pH 6 (55.9%) followed by increases at pH 8 (56.1%) and 10 (57.8%) (P-value < 0.05, appendix A). The slight increase in the adsorption capacity of lithium at pH 4 compared to pH 2 could be attributed to the same explanation mentioned earlier; as the pH increases, the electrostatic repulsion forces between the positively charged adsorbent functional groups and the metal ion decrease. The H^+ concentration decreases at pH 4, which decreases its competition for the available active sites on the surface of the adsorbent. This results in an enhanced adsorption capacity for the protonated metal with an increase in the pH. However, it is important to note that, pH 4 is still acidic and the concentration of H^+ is relatively high, which explains the slight increase in the adsorption capacity from pH 2 to 4. The decrease in the adsorption capacity for lithium at pH 6 could be explained by the decrease in the available active sites on the surface of RDP-FC-Ni as the adsorption reaches equilibrium. Furthermore, the gradual increase of the adsorption capacity for lithium at the basic pH's 8 and 10 is mostly due to the formation of lithium hydroxide as the concentration of OH^- in the solution increased (Huang et al., 2020; Soliman and Moustafa, 2020; Jiang et al., 2020).

Lithium adsorption onto RDP-FC-Cu at different pH values (Figure 30) follows the same behavior as on RDP-FC-Ni. However, higher adsorption capacities are observed with RDP-FC-Cu at all pH values than RDP-FC-Ni and the RDP. The adsorption capacities for lithium on RDP-FC-Cu were 64.8%, 66.6%, 65.7%, 65.8%, and 66.5%

for pH 2, 4, 6, 8, and 10 respectively (P-value < 0.05, appendix A). The higher adsorption capacity observed for RDP-FC-Cu could be due to multiple reasons. It is evident that the electrostatic attraction forces between lithium and RDP-FC-Cu are the strongest, which led to the highest adsorption efficiency compared to the other studied adsorbents. The possible reason could be due to the fact that copper has a higher molecular weight than nickel. This makes copper take a larger space in the formed metal hexacyanoferrate complexation. Compared to copper, lithium has a much smaller molecular weight. The molecular weight of lithium is equal to 6.941 g/mol while for copper it is 63.543 g/mol. The difference in the molecular weight of lithium and copper is much higher than with nickel (58.693 g/mol). This results in the higher affinity of lithium ions to take up the smaller space left in the copper hexacyanoferrate complex to form a more stable metal complexation than with the bigger space in the nickel hexacyanoferrate complex (Guo et al., 2019; Munajad et al., 2018).

Strontium adsorption capacity onto the RDP (Figure 32) increased from pH 2 (48.9%) to pH 4 (59.5%). This increase is due to the same reasons explained earlier where the H^+ concentration decreased and led to an enhanced adsorption of the protonated strontium ion on the less protonated adsorbent surface. Moreover, the adsorption capacity decreased as the pH value increased from 4 to 6 and 8. The adsorption capacity for strontium was 59.1% and 58.9% for pH 6 and 8 respectively (P-value < 0.05, appendix A). This is typical behavior for protonated metals as more adsorption occurs, the number of the available active sites on the surface of the adsorbent decreases, and equilibrium occurs between the adsorbate and adsorbent. As a result, a decrease in the adsorption capacity takes place. Furthermore, the sudden increase in the adsorption capacity for strontium at pH 10 (65.1%) is similar to previous observations, where strontium starts to precipitate as metal hydroxide in the solution (Jiang et al., 2020;

Zhao et al., 2020; Chen et al., 2020). Similar behavior of strontium adsorption onto muscovite, biotite, and phlogopite at different pH values was observed by a study conducted by Wu and others (2020) as well as Almasri and others (2020) on the ceramic membrane. Goyal and others (2020) reported that the maximum adsorption for strontium on nanostructured chitosan/molecular sieve-4A occurs at near-neutral pH values. This is due to the precipitation of strontium hydroxides at higher pH values, which corresponds to lower adsorption. Zhang and Liu (2020) observed that the adsorption of strontium onto nanostructured layered sodium vanadosilicate favored a near-neutral pH range of 5 to 7. They explained that the lower adsorption at lower pH values is due to the competition of H^+ and sodium in the solution with the protonated strontium ions. Furthermore, Du and others (2020) observed that the adsorption of strontium onto porous media increased with the increase in the pH from 3 to 6 and was highest at pH 7. The study revealed that above pH 7, strontium adsorption decreased due to precipitation.

Strontium adsorption onto RDP-FC-Ni (Figure 32) at different pH values shows the highest adsorption capacities when compared to the unmodified roasted date pits and RDP-FC-Cu. The adsorption capacities are 59.5%, 77.5%, 74.2%, 80%, and 82.5% for pH 2, 4, 6, 8 and 10 respectively (P-value < 0.05, appendix A). It is worth noting that the increase in the adsorption capacity from pH 2 to 4 followed by a decrease at pH 6 is due to the same reasons mentioned previously. However, it can be noticed that the adsorption capacity increased from pH 6 to pH 8, which corresponds to more available active sites at the RDP-FC-Ni composite than the unmodified roasted date pits. This means that the equilibrium state for RDP-FC-Ni takes a longer time to take place than the unmodified roasted date pits. Furthermore, at pH 10, the adsorption capacity for strontium at RDP-FC-Ni is the highest due to metal hydroxide formation in the solution.

Strontium adsorption onto RDP-FC-Cu (Figure 32) follows the same trend and adsorption behavior as RDP-FC-Ni at different pH values. However, the overall adsorption capacities for RDP-FC-Ni are higher than RDP-FC-Cu (P-value < 0.05), which could indicate more functional groups for RDP-FC-Ni when compared to RDP-FC-Cu and the RDP (Soliman and Moustafa, 2020; Zhao et al., 2020; Chen et al., 2020; Jiang et al., 2020).

According to the discussed results for the adsorption of lithium and strontium onto RDP as well as RDP-FC-Cu and RDP-FC-Ni at different pH values, the pH value found to be most effective in achieving the highest real adsorption is pH 6. Also, pH 6 was chosen to be the optimum pH value for the next experiments and the recovery for the metal because preparing it does not require the addition of high amounts of harmful HCl. This means that the application of pH 6 for the recovery of the two metals could be more economically and environmentally friendly than higher pH ranges. Furthermore, the previous results for the characterization of the real reverse osmosis brine collected revealed that the pH was 7.8. This pH lies between 6 and 8, which showed relatively high adsorption capacities for the metal at the study. Therefore, the recovery of valuable metals from the real reverse osmosis brine stream involved in the study could be implemented without any pH modifications. Indeed, this would be the most environmentally safe and economically friendly approach.

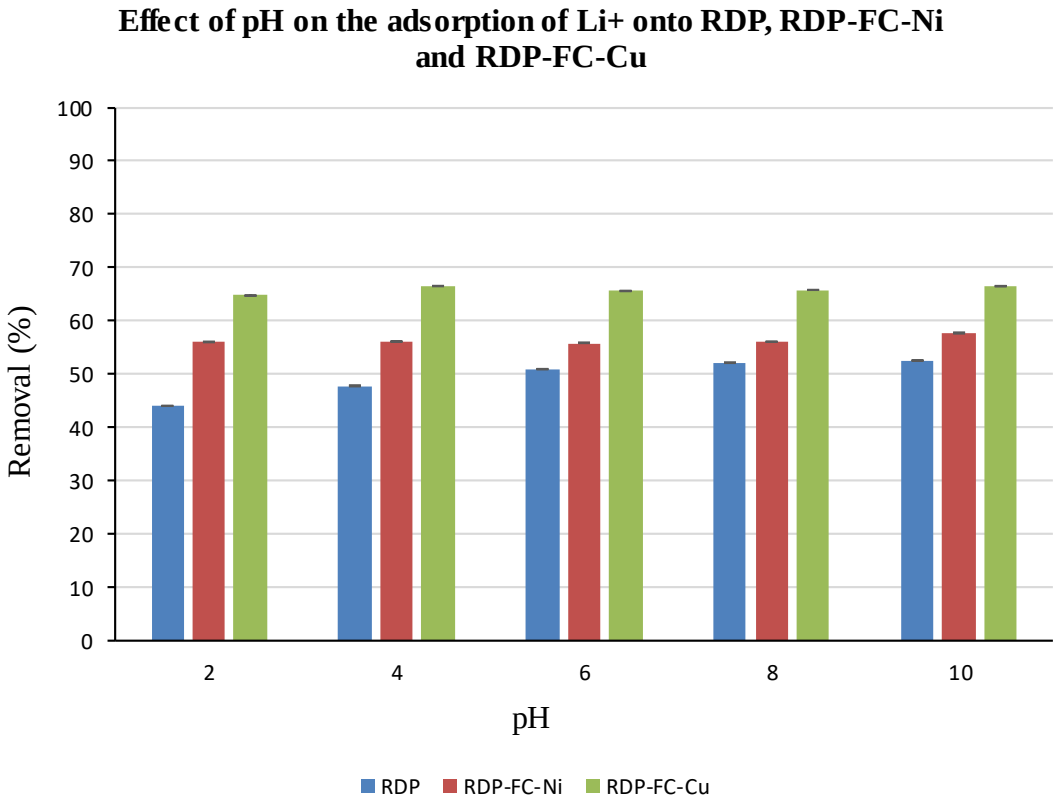

Figure 31. The effect of pH on the adsorption of lithium onto RDP, RDP-FC-Cu, and RDP-FC-Ni at a variety of pH namely: 2, 4, 6, 8, and 10. The experimental conditions were as follows: 25 °C, 50 ml volume, 100 mg/L lithium-ion concentration, shaking time of 24 hrs. at 160 rpm, and 50 g of each adsorbent. Error bars are shown on the figure.

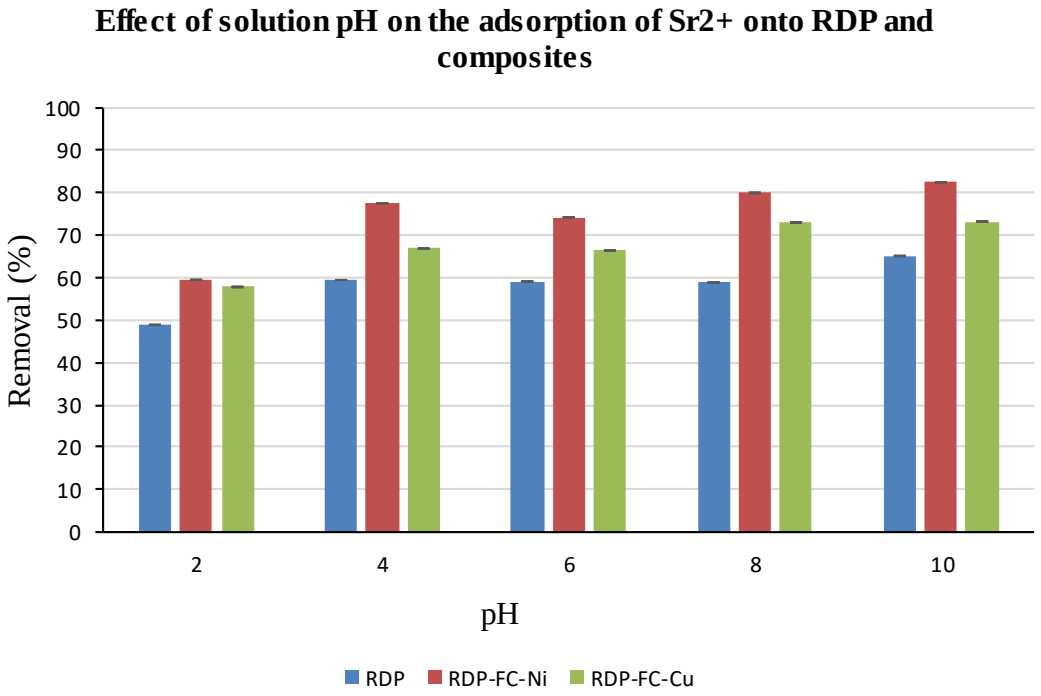

Figure 32. The effect of pH on the adsorption of strontium onto RDP, RDP-FC-Cu, and RDP-FC-Ni at a variety of pH, namely 2, 4, 6, 8, and 10. The experimental conditions were as follows: 25 °C, 50 ml volume, 100 mg/L strontium-ion concentration, shaking time of 24 hrs. at 160 rpm, and 50 g of each adsorbent. Error bars are shown on the figure.

4.3.1 The zeta potential analysis for the roasted date pits and composites

The zeta potential test was performed to study various aspects of the effect of solution pH on the adsorption of lithium and strontium onto the adsorbents involved in this study. The stability of the adsorbents in the solution as well as the determination of the charges present in the interface between the adsorbents and the liquid medium could be done through a zeta potential test. This is of great importance as the overall charges between the adsorbent's surface and the liquid medium can greatly affect the adsorption electrostatic attraction and repulsion forces which ultimately affect the adsorptive capacities of the adsorbents towards metals (Engwayu and Pawlik, 2020; Naidu et al.,

2016). Therefore, the zeta potential was determined for the three adsorbents (RDP, RDP-FC-Cu, and RDP-FC-Ni) at pH of 2, 6, and 8. The results are presented in figure 33 (A, B, and C) below. For RDP (Figure 33 (A)), the zeta potential was found to be equal to -1.67, -29.7, and -33.6 mV for pH of 2, 6, and 8, respectively. The negative values indicate that the charges in the interface between the solid adsorbent and the liquid medium that contains lithium are negative, which poses electrostatic attraction forces that support the adsorption process. It can be noticed that the zeta potential values for RDP increase with an increase in pH. Interestingly, the optimum pH was found to be 6 due to high adsorption capacities achieved as well as lower chances of metal precipitation and faked adsorption. The zeta potential value obtained for RDP at pH of 6 is relatively highly negative (-29.7 mV), which represents the stability of the adsorbent's particles as well as their high adsorptive capabilities for lithium due to opposite charges and electrostatic attraction forces. The zeta potential values obtained for RDP-FC-Cu are presented in figure 33 (B). Similar to RDP, the zeta potential values appear to negatively increase with an increase in pH from 2 to 8. However, the zeta potential values for RDP-FC-Cu are more negative than the zeta potential values for RDP. This means that RDP-FC-Cu is more stable in the adsorption solution than RDP and more electrostatically negative, which poses more electrostatic attraction forces towards the positively charged lithium ions. This is supported by the fact that RDP-FC-Cu achieved higher adsorption efficiencies than RDP at all pH values, and not just 2, 6, and 8. Moreover, RDP-FC-Ni showed similar results to RDP and RDP-FC-Cu in terms of increasing the negativity of zeta potential with raising pH. Furthermore, the zeta potential values of RDP-FC-Ni (Figure 33 (C) are closer to the values obtained for RDP-FC-Cu than RDP. However, at the optimum adsorption pH value of 6, the zeta potential value for RDP-FC-Cu was slightly higher than for RDP-FC-Ni, which shows

more stability for RDP-FC-Cu at that pH. The similarity in the zeta potential for both composites could be due to more common adsorbent characteristics between them than with the initial material (RDP). The high stability of RDP-FC-Ni is shown clearly from the overall highly negative zeta potential values obtained (Selvamani, 2019). This indicates and further confirms previous results (Effect of solution pH on the adsorption of lithium onto RDP and composites) where RDP-FC-Ni showed closer adsorptive effectiveness to RDP-FC-Cu but higher than RDP for the adsorption of lithium. The importance of studying the zeta potential for metal adsorptions has been recognized by many other studies. For example, a study done by Yuan and others (2021) examined the effect of pH on the adsorption of various heavy metals onto high nitrogen activated carbon (HNAC) based adsorbent and the zeta potential in order to understand the surface charges interactions and adsorption capacities at different pH ranges. The study showed that at a pH of below 4, the surface of the adsorbent is more positively charged, which confirmed their findings of lower adsorption efficiencies of metals at lower pH than 4. On the other hand, the zeta potential showed a significant decrease at pH ranges above 4, which further confirmed the higher adsorptions achieved for metals at higher pH values. Another study done by Lai and coworkers (2019) revealed that the adsorption of lead (Pb^{2+}) onto marmatite surface is pH-dependent through conducting a zeta potential test. The results showed that at different pH values, the adsorption of lead follows a different mechanism. At a pH of 3, it was found that lead may replace the positive ions present on the adsorbent's surface. At a pH of 6.5, lead ions seem to be chemisorbed onto the adsorbent's surface and at a pH of 11, the lead ions may have formed a partial coating onto the adsorbent's surface. These results are of significant importance for understanding and evaluating the efficiency of charged metals adsorption onto different adsorbents at different solution pH values.

(A)

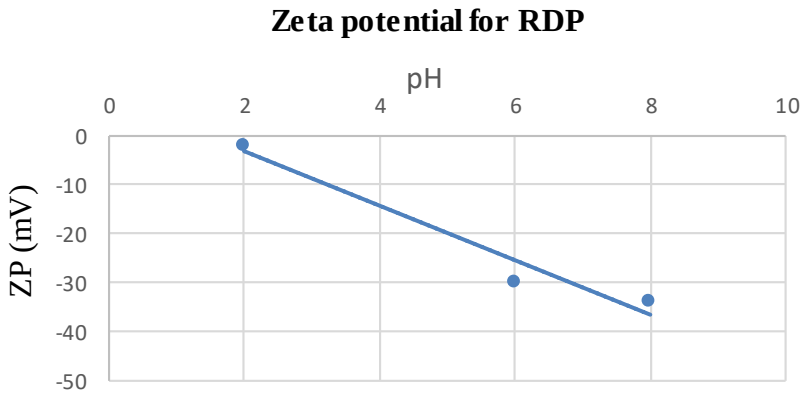

(B)

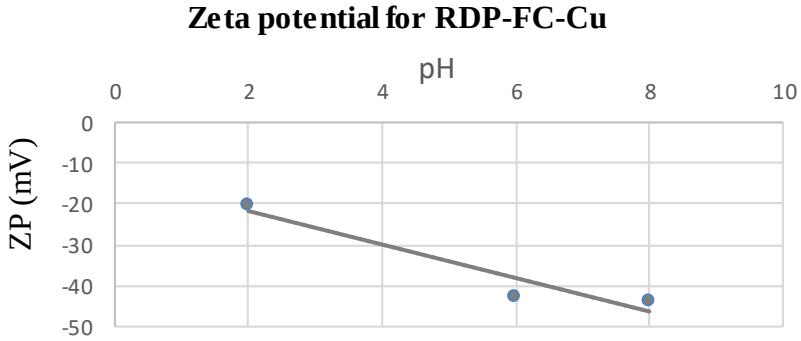

(C)

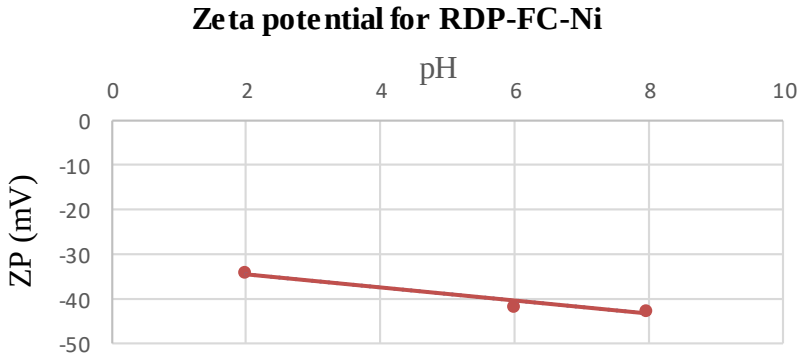

Figure 33. The zeta potential analysis for the RDP, RDP-FC-Cu, and RDP-FC-Ni at pH of 2, 6, and 8. The experimental conditions were as follows: temperature of 25 °C, 50 ml distilled water, around 0.05g of adsorbent, and shaking time of 24 hrs. at 160 rpm.

4.4 Effect of lithium and strontium ions concentration on the adsorption onto roasted date pits and two composites

Studying the effect of metal concentration on the adsorption capacities of adsorbents is vital in the optimization of metal recovery. This is because the concentration of the target metal in the solution largely affects the efficiency, capacity, and adsorption mechanism for effective recovery, adsorption, and treatment (Zhuang and Wang, 2019; Kim et al., 2017). Figure 34 (A and B) shows the adsorption capacities (mg/g) and efficiency in terms of percentage for lithium onto RDP, RDP-FC-Cu, and RDP-FC-Ni at a variety of metal concentrations. To compare, figure 35 (A and B) represents the adsorption capacity and efficiency for strontium onto the same adsorbents and concentrations. To understand and fully evaluate the capacities of the adsorbents at study in remediating lithium and strontium at a variety of concentrations, the pH, temperature, shaking time, volume and adsorbent dose was constant for all concentrations. The metal concentrations studied were 5, 10, 15, 20, 25, 30, 35, 50, 70 and 100 ppm. The pH was kept at the optimum pH of 6, the temperature of 25 °C, shaking time of 24 hours, at 160 rpm, and adsorbent dose of 0.05g.

As a general trend, figure 34 (A) shows a constant increase in adsorption capacity with increasing lithium concentration for all adsorbents. It is evident that the adsorption capacity of RDP-FC-Cu towards lithium is similar to RDP-FC-Ni while it is the lowest for RDP, especially at metal concentrations below 100 mg/L. This result is expected as it was shown previously that the adsorption efficiency of lithium at a variety of pH ranges was the highest for RDP-FC-Cu followed by RDP-FC-Ni then RDP (Section 4.3). Moreover, it can be noticed as a general trend from figure 34 (A) that the adsorption capacities of lithium onto RDP-FC-Cu and RDP-FC-Ni become very similar at metal concentrations above 5 mg/L than to RDP. As mentioned previously, the adsorption capacity (qe) provides information regarding the quantity of adsorbate that

an adsorbent can carry per unit mass. The adsorption experiments involved in this study are based on batch adsorption systems, which take into account the importance of the mass of the adsorbent. This study examined the adsorption mechanisms through the adsorption isotherm models at a variety of concentrations and temperatures (Section 4.5), which take into account the adsorption capacity concept. Therefore, the adsorption capacities for the adsorption of lithium onto RDP (Figure 34) were found to be 1.3, 7.8, 13, 14.5, 17.4, 19.2, 32, 46, 66, and 99 mg/g for metal concentrations of 5, 10, 15, 20, 25, 30, 35, 50, 70, and 100 mg/L respectively (P-value < 0.05, appendix A). As it was mentioned previously, the RDP at study had many exceptional functional groups through the FTIR analysis that were involved in the adsorption of lithium ions at a variety of concentrations (Section 4.2.6). The SEM analysis showed the smooth and porous surface morphology of RDP, which gave insights regarding the availability of sufficient amounts of adsorption active sites (Section 4.2.1). The results of this experiment are similar, where the adsorption of lithium was found to continuously increase with an increase in the initial metal concentration in the solution. The adsorption capacity of lithium onto RDP (Figure 34 (A) was found to be as high as 99 mg/g for an initial metal concentration of 100 mg/L. Moreover, the adsorption of lithium onto RDP showed relatively close adsorption capacities for metal concentrations of 5 (1.3 mg/g), 10 (7.8 mg/g), 15 (13 mg/g), 20 (14.5 mg/g), 25 (17.4 mg/g) and 30 mg/L (19.2 mg/g). The adsorption capacity can be seen to increase at a higher rate from 19.2 mg/g to 32 mg/g when the initial lithium concentration increased from 30 mg/L to 35 mg/L respectively. At lithium-ion concentrations of 35 mg/L and higher (50, 70, and 100 mg/L), the adsorption capacities of RDP maintained the same trend of highly increasing. At 50 mg/L lithium-ion concentration, the adsorption capacity was observed to be 46 mg/g while at 70 mg/L and 100 mg/L lithium

concentration, the adsorption capacities were 66 mg/g and 99 mg/g respectively. The differences in the adsorption capacities between each successive initial lithium concentration are illustrated in table 8. It is clear from the table that the adsorption capacity increased at a constant and slower pace at lower metal ion concentrations than 35 mg/L and higher.

Table 8. The differences in the adsorption capacities of lithium onto RDP at a variety of metal initial concentrations

Lithium initial concentrations (mg/L)	Difference in adsorption capacity (qe)
5 and 10	6.5
10 and 15	5.2
15 and 20	1.5
20 and 25	2.9
25 and 30	1.8
30 and 35	12.8
35 and 50	14
50 and 70	20
70 and 100	33

At low metal concentrations, the ratio of the number of the available adsorption active sites to lithium concentration is high, which means there are plenty of vacant sites for the low metal ions to bind. This facilitates the adsorption process due to the great functionality, structural morphology, and affinity of RDP towards the adsorption of lithium ions. The slower pace of increased adsorption observed for initial metal concentrations below 35 mg/L than higher concentrations could be due to less mass transfer and collision between the metal species and the binding sites (Naeimi and Faghihian, 2017; Naidu et al., 2016). The continuous increase in the adsorption capacity for lithium with increasing initial metal concentrations could be mainly attributed to enhance and increased metal mass transfer onto the available adsorption active sites on the RDP surface. In adsorption systems, the driving force for molecules

or ions onto the available active adsorption sites is internal diffusion from the highly concentrated solution to the low concentrated binding sites on the surface of the adsorbent. Therefore, at increasing initial lithium concentration in the solution, the collision and mass transfer forces dominated, which resulted in enhanced internal diffusion and adsorption capacities (Albroomi et al., 2017; Kim et al., 2017; El-Bahy et al., 2018). However, it is expected that at initial lithium concentrations above 100 mg/L the adsorption capacity to reach an equilibrium status and a maximum removal state. This is because the adsorption removal and capacity of lithium reached almost 100% (99 mg/g qe and 99% adsorption removal) at an initial metal concentration of 100 mg/L. The equilibrium and maximum pollutant removal phenomena are common in adsorption systems. This is because as the metal concentration increases, the mass transfer process would increase its adsorption onto the available active sites. However, the available active sites on any adsorbent are finite. Therefore, excess metal ions would remain in the solution and the adsorption capacity would reach a plateau (Chang et al., 2008; Naeimi and Faghihian, 2017). In other words, at higher lithium concentrations, the ratio between the available active adsorption sites and metal ions would slowly stop facilitating the mass transfer. Overall, these results reveal the extraordinary efficiency and adsorption capacity of RDP in remediating and recovering lithium metal at high concentrations. It is worth noting that the ICP results of the collected reverse osmosis brine showed a high lithium concentration of 44.2 mg/L, therefore, finding an adsorbent that can recover the metal at the highest possible concentration was the aim of this study. Several studies reported similar results where Al-Ghouti and others (2019) investigated the effect of mercury solution concentration on its adsorption capacity onto roasted date pits. The results revealed that the adsorption of mercury increased with increasing concentration due to the availability of adsorptive active sites as well as

enhanced mass transfer forces. However, a constant adsorption behavior was observed for higher mercury concentrations because of the filling of the vacant sites. Moreover, another study done by Hilal and coworkers (2012) on the adsorption of copper and cadmium metals onto roasted date pits discussed that the adsorption capacity increased as a function of metal concentrations. Samra (2014) reported that metals could have enhanced adsorption onto roasted date pits with increased concentrations because of increased metal diffusion processes onto the adsorbents. Furthermore, Al-Ghouti and others (2017) reported that the enhanced adsorption capacity of bromide ions with increased concentration is a predictable adsorption behavior. This was mainly due to the great collision and mass transfer forces between the adsorbent and the metal. The diffusion of bromide into the boundary layer of the adsorbent was enhanced when the bromide concentration was elevated per unit weight of the roasted date pits.

The adsorption of lithium onto RDP-FC-Ni and RDP-FC-Cu follows the same increasing trend with metal concentration as RDP (Figure 34 (A) and (B)). This indicates the consistency of the adsorption patterns and favorability to increasing concentrations despite the surface modifications on the RDP. From the adsorption efficiency figure 34 (B) below, the differences in the adsorption in terms of percentages are clear and significant between the three adsorbents (P-value <0.05, appendix A). It is worth noting that the adsorption capacity of RDP-FC-Cu was very similar to RDP-FC-Ni especially at higher lithium initial concentrations. This gives indications and insights regarding the enhanced high and outstanding functionality, adsorptive selectivity, and capacity of the prepared composites when compared to RDP. In fact, the adsorption capacities obtained with the adsorption of lithium onto RDP-FC-Cu were 3.55, 9.26, 14.15, 19.15, 24, 29.26, 34.26, 49.25, 69.11, and 99.15 mg/g for lithium initial concentrations of 5, 10, 15, 20, 25, 30, 35, 50, 70 and 100 respectively (P-value

< 0.05, see appendix). To compare, the achieved adsorption capacities with the adsorption of lithium onto RDP-FC-Ni are 1.83, 8.79, 13.92, 19.07, 23.94, 29.03, 33.78, 49.03, 69.07, and 99.08 mg/g (P-value < 0.05, appendix A). As mentioned previously, despite the enhanced morphological structure in terms of surface area, pore radius, and volumes as well as and cavities for RDP when compared to raw date pits, the prepared composites involved in the study showed enhanced surface area, porosity, and cavities. This could indicate the significant role of the higher surface area and adsorption active sites on the prepared composites than the RDP. The previously illustrated BET surface area analysis confirmed the increase in the total surface area for adsorption of the prepared composites from around 2.5 m^2/g for RDP to 4.7 m^2/g for RDP-FC-Cu and 5.2 m^2/g for RDP-FC-Ni (Section 4.2.3). It can also be noticed that the prepared composites resulted in similar adsorption capacities and efficiencies towards lithium at a variety of initial concentrations when compared to RDP (Figure 34). This could be because the prepared composites have more characteristic functional groups, structure, and composition in common that played significant roles in the adsorption process when compared with their starting material (RDP). This was shown in the previous FTIR results where the characteristic functional groups like C≡N and Fe-C showed altered peaks due to lithium adsorption**.** Furthermore, similar trends are observed with RDP-FC-Cu and RDP-FC-Ni as with RDP in terms of a sudden increase in the adsorption capacity towards lithium at concentrations above 35 mg/L. Moreover, it is worth noting that the adsorption capacity of lithium onto RDP, RDP-FC-Cu, and RDP-FC-Ni at an initial metal concentration of 100 mg/L is almost the same (99.04 mg/g for RDP, 99.15 mg/g for RDP-FC-Cu, and 99.08 mg/g for RDP-FC-Ni). Therefore, three main conclusions could be made from the adsorption behavior of lithium at a variety of initial concentrations and three adsorbents at study:

i. The adsorption of lithium favors increasing initial metal concentrations with an adsorption capacity as high as 99 mg/g at a metal concentration of 100 mg/L.
ii. The adsorption of lithium at a variety of concentrations proceeds increasingly until it results in constant as well as almost equal adsorption capacities for RDP, RDP-FC-Cu, and RDP at a concentration of 100 mg/L.
iii. Therefore, scientists and environmentalists could have the advantageous possibility and flexibility in selecting any of the adsorbents involved in the study in remediating lithium concentrations of 100 mg/L or above. This is because of their similar adsorptive capabilities at the mentioned lithium concentration. This provides flexibility in terms of cost expenditure as well as material and chemical utilization. For example, in countries with limited resources, RDP could be an efficient and cost-effective option for the adsorption and recovery of lithium from brines with around 100 mg/L lithium concentration. However, for optimum removal and ensured lithium recovery from less or more than 100 mg/L concentrated brines, the synthesized composites present candidate adsorbents.

As mentioned earlier, the higher adsorption capacities observed for lithium at concentrations of 35 mg/L and higher for all date pits could be mainly due to mass transfer forces. In addition, and interestingly, this could be justified by the fact that lithium ions in aqueous solutions have an ionic radius of 3.4 Ångstroms (A). Usually, in metal adsorption systems, alkali metals with the smallest ionic radius achieve the highest adsorption capacities onto adsorbents due to the shorter distance between the metal and the adsorbent's surface (Naidu et al., 2016). In the case of lithium adsorption onto the three adsorbents at higher concentrations, the lithium ions are closer to each

other and the adsorbents surfaces, which results in more collisions and confirm that mass transfer played a significant role in the sudden increases in the adsorption capacities as the concentration increased in the solution.

The high and similar adsorptive capacity of RDP-FC-Cu and RDP-FC-Ni towards lithium than RDP could be due to multiple reasons. Firstly, this adsorption behavior was more notable at high lithium initial concentrations (higher than 5 mg/L). At low initial lithium concentration (5 mg/L), the adsorption binding active sites at the three adsorbents are plenty. The ratio of the binding sites and metal concentration is high; therefore, pore filling is favorable. Despite the fact that RDP showed enhanced pores and cavities than raw date pits through the SEM analysis, the RDP-FC-Cu and RDP-FC-Ni showed more surface cavities and pores than RDP. Furthermore, the morphological and chemical characteristics of the composites explain the higher difference in adsorption capacity observed at low initial lithium concentrations between them and the RDP. At higher lithium initial concentrations, the ratio of the adsorption binding sites to the metal concentration is lower; therefore, the composites showed similar adsorption capacities due to their similar and enhanced morphological and chemical characteristics than RDP. Another reason could be due to the fact that copper has a hydrated ionic radius of 4.19 A, which is close to the ionic radius of lithium ions (3.4 A). On the other hand, the ionic radius of nickel is equal to 2 A. This could mean that during the adsorption process, higher ion exchange, and adsorption, occurred between copper followed by nickel present in the potassium hexacyanoferrate and the lithium present in the solution. This usually takes place when the target metal could replace the existing metal present in the potassium metal hexacyanoferrate due to a similar ionic radius. The somewhat similar hydrated ionic radius of lithium, copper, and nickel, explains the similar adsorption capacities between RDP-FC-Cu and RDP-FC-

Ni towards lithium. Another possible adsorption mechanism that resulted in the more favorable adsorption of lithium onto RDP-FC-Cu and RDP-FC-Ni could be due to ion exchange with potassium that is present in the complex to form a stable metal hexacyanoferrate complexation. Potassium has a hydrated ionic radius of 3.31 A, which is very close to the hydrated ionic radius of lithium (3.4 A), which favors their ionic substitution mechanism into the metal coordination cubic complexes (Hawari et al., 2014; Zhuang and Wang, 2019; Wang et al., 2018).

The slightly higher adsorption capacity of RDP-FC-Cu towards lithium when compared to RDP and RDP-FC-Ni could be due to other characteristics of the adsorbent that enhanced its selectivity towards the target metal (Figure 34 (A)). The size of the hydrated radius of lithium and copper is more similar than that of lithium and nickel, which explains the favorability of ionic exchange between lithium and copper in the metal complex. The previous BET results showed that the surface area of RDP-FC-Cu was enhanced compared to RDP (Section 4.2.3). To be exact, the surface area of RDP-FC-Cu is around 4.6 m^2/g. The pore radius of RDP-FC-Cu is equal to 138.6 A while it is equal to 39.2 A for RDP-FC-Ni. Moreover, the pore volume of RDP-FC-Cu is higher than the pore volume of RDP-FC-Ni. These characteristics of the adsorbents provide insights regarding the favorability of lithium adsorption onto RDP-FC-Cu than the other two adsorbents. RDP-FC-Cu has a higher pore radius and volume than the other two adsorbents, which provided more and deeper adsorption active binding sites for lithium. Therefore, lithium adsorption onto RDP-FC-Cu was more stable and favorable than RDP and slightly more favorable than RDP-FC-Ni. These adsorption behaviors of metals onto potassium hexacyanoferrates have been reported by many studies (Michel et al., 2015; Naidu et al., 2016). A study done by Loos-Neskovic and coworkers (2004) reported that the adsorption of cesium onto potassium copper hexacyanoferrate resulted

in the release of potassium ions in the solution as a consequence of cesium adherence onto the adsorbent's surface. The authors mentioned that copper was also released in the solution, however at much less concentrations than potassium. Interestingly, the ionic radius of cesium is equal to 2.26 A, which is closer to the ionic radius of potassium (3.31 A) than copper (4.19 A). This facilitated the ionic exchange of cesium with potassium at a higher quantity than copper. Another study was performed by Naidu and others (2016) on the adsorption of alkali metals onto laboratory synthesized and commercial potassium cobalt hexacyanoferrate adsorbent. The results of the study revealed that both adsorbents achieved higher adsorption capacities towards rubidium than cesium. This is due to the occurrence of a true ion exchange occurs between the potassium and rubidium. Also, the authors reported that the adsorbent's cavity sizes are more similar to the rubidium radius than cesium, which resulted in a greater penetration of rubidium into the adsorbent's lattice. Consequently, replacement of potassium takes place, and a higher adsorption capacity is observed. The authors also discussed that cobalt and iron were released in minute amounts into the solution, which indicates that the adsorption of the metals occurred mainly with the displacement of potassium. This is because transition metals are usually bound through strong cyano-groups bridges, which provide the hexacyanoferrate lattice with a balanced negative charge and stability. Moreover, the adsorption of cesium onto a potassium nickel hexacyanoferrate adsorbent was investigated by Michel and others (2015). The results showed that the adsorption of cesium favored the exchange with potassium more than nickel in the crystal lattice. It was reported that the amount of adsorbed cesium was more similar to the amount of potassium released than nickel. The potassium and cesium exchange proceeded at 80%, while the nickel and cesium exchange proceeded at 20%, where two ions of cesium replaced one ion of nickel in the crystal lattice.

To sum up, the adsorption of lithium at a variety of initial metal concentrations favored increasing concentrations. The adsorption capacity of RDP-FC-Cu towards lithium was the highest but similar to RDP-FC-Ni. The adsorption mechanism of lithium involved the ion exchange with potassium in the crystal lattice of the composites as well as enhanced pore fitting and filling onto RDP-FC-Cu than the other two adsorbents involved in the study. The ICP-OES analysis for the collected brine (Section 4.1.1) showed a lithium concentration of 44.2 mg/L. The RDP showed an adsorption efficiency of around 91% towards lithium while RDP-FC-Cu and RDP-FC-Ni showed efficiencies of 98% each. Therefore, applying these adsorbents for the recovery of lithium from the collected brine sample could be an effective and successful metal recovery method.

This study also investigated the adsorption capacity and efficiency of strontium ions onto RDP, RDP-FC-Cu, and RDP-FC-Ni at a variety of initial metal concentrations. Figure 35 (A and B) below represents the adsorption capacity and efficiency trends for the three adsorbents towards strontium ions. The adsorption capacities for the adsorption of strontium onto RDP were the lowest at all metal concentrations when compared to the other two adsorbents. The adsorption capacities were found to be 2.09, 5.21, 9.02, 13.31, 17.24, 23.08, 29.43, 45.36, 65.32, and 99.49 mg/g for metal concentrations of 5, 10, 15, 20, 25, 30, 35, 50, 70, and 100 mg/L respectively (P-value < 0.05, appendix A). To compare, the adsorption capacities for the adsorption of strontium onto RDP-FC-Cu were found to be slightly higher and equal to 2.92, 6.78, 10.70, 14.66, 18.56, 23.62, 30.73, 46.55, 67.79, and 99.6 mg/g for the same metal concentrations (P-value < 0.05, appendix A). On the other hand, RDP-FC-Ni showed the highest adsorption capacities for strontium (At initial metal concentrations below 100 mg/L) where they were found to be 2.99, 7.00, 12.7, 17.66, 22.66, 27.62, 32.36,

48.55, 68.75, and 99.60 mg/g for the same metal concentrations (P-value < 0.05, appendix A). As mentioned previously, the modified RDP's (RDP-FC-Cu and RDP-FC-Ni) demonstrated enhanced morphological, structural, and chemical characteristics that support higher adsorptive capabilities than RDP. For RDP two distinctive trends in adsorption capacity and efficiency towards strontium can be noticed (Figure 35 A and B):

i. The adsorption capacity and efficiency increase relatively at a slower pace at metal concentrations below 25 mg/L then increase at a higher pace for concentrations of 25 mg/L to 100 mg/L. To compare with lithium adsorption onto RDP, strontium adsorption achieved faster, and higher adsorption increases at a less starting concentration (25 mg/L for strontium and 35 mg/L for lithium).
ii. The adsorption capacity towards strontium at the mentioned concentrations was relatively higher than the adsorption capacity towards lithium (1.3, 7.8, 13, 14.5, 17.4, 19.2, 32, 46, 66, and 99 mg/g for metal concentrations of 5, 10, 15, 20, 25, 30, 35, 50, 70, and 100 mg/L respectively)

The higher adsorption capacities of RDP at all concentrations and adsorption increase at a less starting concentration for strontium when compared to lithium (25 mg/L for strontium and 35 mg/L for lithium) could be attributed to the lower hydrated ionic radius (1.18 A) and higher molecular weight of strontium (87.62 g/mol) when compared to lithium (3.4 A and 6.941 g/mol). The smaller hydrated ionic radius of strontium led to the shorter distance between the metal and the adsorbent's surface, which facilitated its higher adsorption onto the RDP than lithium (Wheeler et al., 2018; Naidu et al., 2016). Also, the heavier metal strontium facilitated the higher rate of encounter with

the surface of the adsorbent due to less suspending phenomena in the solution, which resulted in the higher rate of adsorption achieved at a lesser initial metal concentration than lithium (Dai et al., 2021).

The adsorption of strontium onto RDP-FC-Cu follows the same trend as with RDP (Figure 35 A and B) in terms of increase of adsorption with concentration, and gradual increase till a concentration of 25 mg/L followed by a higher increase at higher concentrations. However, it can be noticed that the adsorption of strontium onto RDP-FC-Ni increases more gradually and somewhat evenly than with RDP-FC-Cu. The higher adsorption capacities for strontium onto RDP-FC-Ni than the other two adsorbents could be due to many reasons. The hydrated ionic radius of strontium is equal to 1.18 A while it is equal to 1.9 A for nickel. As mentioned previously, the hydrated ionic radius of copper, potassium, and lithium are 4.19 A^o, 3.31 A^o, and 3.4 A^o, respectively (Zhuang and Wang, 2019). It is evident that the hydrated ionic radius of strontium is closest to the hydrated ionic radius of nickel than copper and potassium. on the other hand, lithium's hydrated ionic radius is closer to the radius of copper and potassium than nickel. This resulted in the more complexation, ionic exchange, and substitution between strontium and nickel in the potassium nickel hexacyanoferrate complex than the potassium copper hexacyanoferrate. However, the radius of strontium is still relatively close to potassium than copper, which may have resulted in an ionic exchange between strontium and potassium in the potassium copper hexacyanoferrate, especially at high strontium concentrations where the adsorption capacity was similar to those achieved with RDP-FC-Ni (70 mg/L and 100 mg/L). Other reasons for the higher adsorption capacities for strontium onto RDP-FC-Ni at all initial concentrations could be due to higher surface area for adsorption, more functional groups, porous structures, and chemical composition of RDP-FC-Ni that was demonstrated by previous

sections of this study. Generally, the increasing adsorption capacities for strontium onto all adsorbents with increasing initial metal concentration are due to the same reasons discussed for lithium. At low initial metal concentrations, there is less mass transfer and collision between the metal species and the binding sites. The continuous increase in the adsorption capacity for strontium with increasing initial metal concentrations could be mainly attributed to enhance and increased metal mass transfer onto the available adsorption active sites on the RDP surface (El-Bahy et al., 2018). Finally, the collected reverse osmosis brine sample showed a strontium concentration of around 447 mg/L through the ICP-OES analysis (Section 4.1.1). The adsorbents showed adsorption efficiencies of around 99% towards strontium at 100 mg/L. Therefore, applying these adsorbents for the adsorption of strontium from the brine sample could be effective remediation and metal recovery method.

(A)

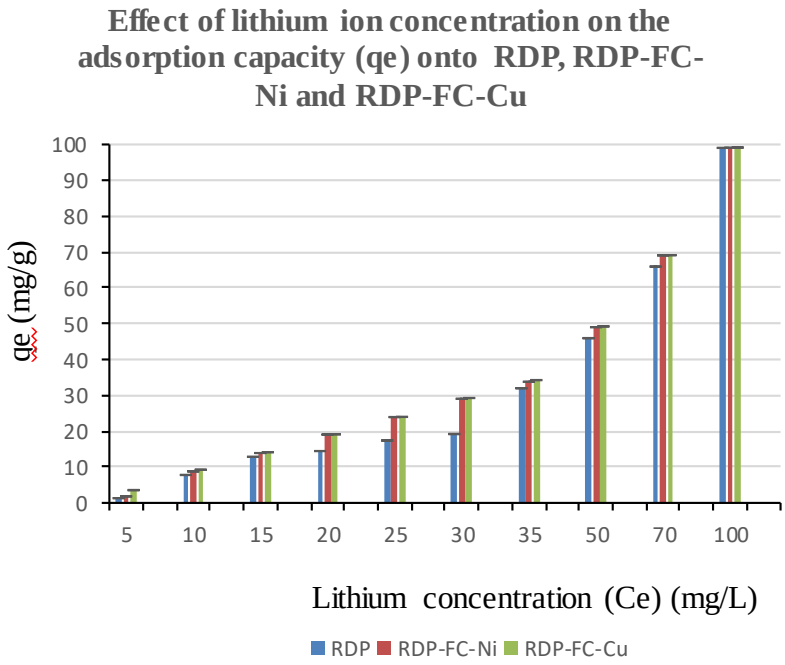

(B)

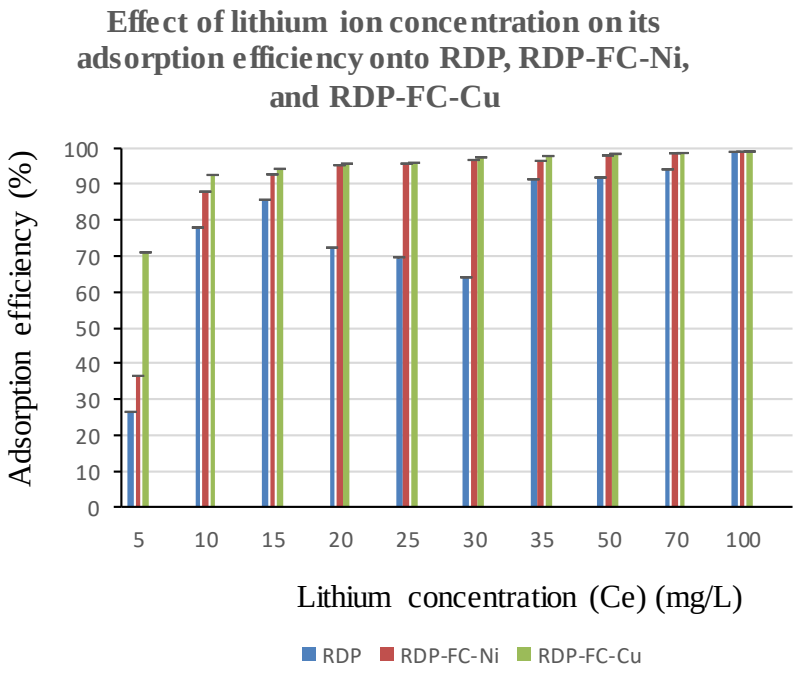

Figure 34. The effect of lithium-ion concentration on its (A) adsorption capacity and (B) efficiency onto RDP, RDP-FC-Cu and RDP-FC-Ni. The experimental conditions were as follows: the metal concentrations studied were 5, 10, 15, 20, 25, 30, 35, 50, 70, and 100 ppm. The pH was kept at the optimum pH of 6, temperature of 25 °C, shaking

time of 24 hrs. at 160 rpm, and an adsorbent dose of 0.05g. Error bars are shown in the figure.

(A)

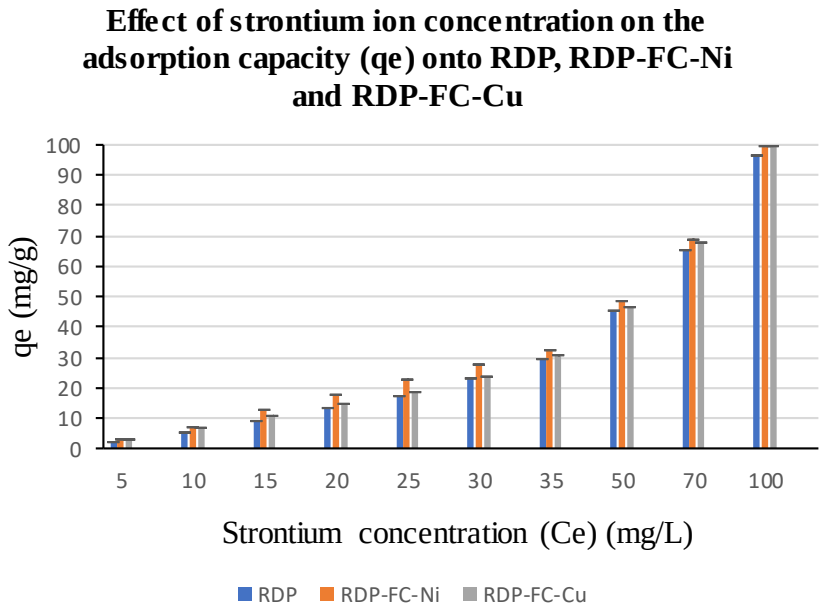

(B)

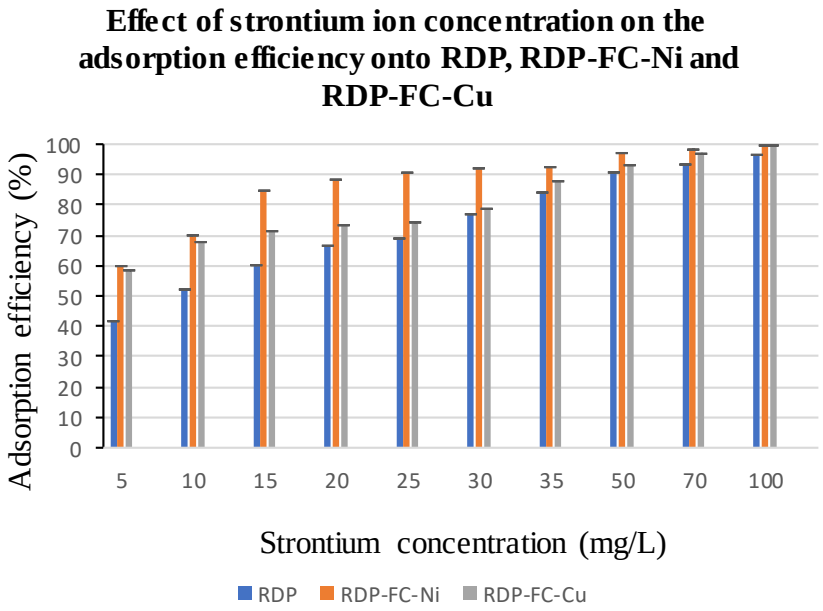

Figure 35. The effect of strontium-ion concentration on its (A) adsorption capacity and (B) efficiency onto RDP, RDP-FC-Cu and RDP-FC-Ni. The experimental conditions were as follows: the metal concentrations studied were 5, 10, 15, 20, 25, 30, 35, 50, 70, and 100 ppm. The pH was kept at the optimum pH of 6, temperature of 25 °C, shaking

time of 24 hrs. at 160 rpm, and adsorbent dose of 0.05g. Error bars are shown on the figure.

4.5 Effect of temperature and thermodynamics on the adsorption of lithium and strontium onto roasted date pits and two composites

Temperature plays a significant role in adsorption systems. The efficiency and overall removal of pollutants and recovery of metals depend largely on the surrounding temperature of a batch adsorption process. Some adsorption systems could be exothermic while others could be endothermic in nature (Rizzi et al., 2017). Exothermic adsorption processes proceed with the release of heat energy while endothermic processes take place with the requirement of heat energy. This indicates that the adsorption capacity of an adsorbent may increase or decrease with increasing temperature. Therefore, scientists interested in the recovery of valuable materials and metals from brine streams focus on optimizing the temperature for a maximum adsorption capacity (Krishnamoorthy et al., 2019; Albroomi et al., 2017). For these reasons, it was vital to study the effect of temperature on the recovery and adsorption of lithium and strontium onto RDP, RDP-FC-Cu, and RDP-FC-Ni. The adsorption batch tests of lithium onto the three adsorbents were performed at 25, 35, and 45 °C.

The figures (36, 37, and 38) show the adsorption capacities and efficiencies of lithium onto RDP, RDP-FC-Cu, and RDP-FC-Ni at a variety of temperatures. As a general trend for all adsorbents involved in the study, the adsorption of lithium is enhanced with an increase in temperature from 25 °C to 45 °C (P-value < 0.05, appendix A). Indeed, as with the effect of lithium concentration on its adsorption, the adsorption capacity and efficiency are seen to be enhanced with an increase in the metal's concentration. The results of this experiment show that the maximum lithium recovery occurred when the

initial lithium concentration was 100 ppm for the three adsorbents involved in the study. Furthermore, the highest adsorption capacities and efficiencies for lithium at a variety of temperatures were observed for RDP-FC-Cu followed by RDP-FC-Ni with similar adsorption capacities, and lastly, RDP (P-value < 0.05, appendix A). This is predictable as it was found previously that RDP-FC-Cu and RDP-FC-Ni are the most effective and selective adsorbents for the target metal at study at a variety of pH ranges and initial concentrations.

The adsorption capacity and removal of lithium at 5 mg/L onto RDP (Figure 36 A and B) is found to increase significantly from being equal to 1.33 mg/g (26.5%) at 25 °C to 2.37 mg/g (47.44%) at 35°C and 4.13 mg/g (82.64%) at 45 °C (P-value < 0.05, appendix A). Similar adsorption trends were observed for lithium metal concentrations below 35 mg/L. This is a typical adsorption behavior with the variating temperature at low metal concentrations. Under these circumstances, the adsorption active binding sites are plentiful while the metal's concentration is low, which means that mass transfer and internal diffusion forces are somewhat weak. Therefore, a higher temperature would facilitate the mass transfer process of lithium onto the internal pores of the adsorbent (Hou et al., 2020; Snyders et al., 2014; Ji et al., 2020). In other words, higher temperatures increase the rates of molecules and/or metals movements as well as pore diffusions due to an increase in the energy of the system. To illustrate further, an increase in solution temperature would mostly result in decreased viscosity, which enhances the diffusion forces of the pollutants onto the adsorption active binding sites of the adsorbent and facilitate metal complexations and coordination (Wadhawan et al., 2020). However, at lithium metal concentrations of 35 mg/L and higher, it can be noticed that the adsorption capacities and efficiencies of RDP became very similar at temperatures of 35 and 45 °C and higher than the results obtained under 25°C (P-value

< 0.05, appendix A). The adsorption capacities and efficiencies are observed to increase at a slower rate at lithium concentrations above 30 mg/L. As the concentration of lithium increases in the solution, the available active binding sites decrease. Therefore, higher temperatures than 25 °C are required to facilitate the internal diffusion of lithium ions onto the pores of the date pits. However, the adsorption binding sites are finite, which causes a slower rate of increase in adsorption despite the increasing temperature. The similarity of the adsorption capacities and efficiencies of lithium at 35°C and 45°C at higher concentrations could be due to the high collisions and mass transfer forces that dominate in the solution, which resulted in the high and similar adsorption patterns at the moderate temperature of 35°C when compared to 45°C. It is worth noting that in adsorption systems, the removal of pollutants or metals proceeds until an equilibrium state is achieved (Albatrni et al., 2020; Saad et al., 2008). This means that the adsorption binding sites become fully filled or adsorption/desorption takes place at a constant and equilibrium state. This explains that despite the increase in temperature with concentration, the achieved adsorption capacity under 35°C and 45°C were similar, but with 45°C achieving the highest adsorption at all metal concentrations. This observation is of significant importance for scientists and environmentalists because it provides flexibility when optimizing an adsorption system for lithium recovery from brines. Raising the temperature requires energy and cost expenditure, which could be not feasible for some countries. Therefore, sufficient and efficient lithium recovery could be achievable at high concentrations and moderate temperatures of between 35°C and 45°C for RDP, while the highest recovery could be obtained at 45°C. As mentioned previously, seawater reverse osmosis concentrated brine solutions are characterized by their high temperatures. Therefore, they could be utilized for metal recovery purposes on a plant or at a close point to use the advantage of their naturally high temperatures

for optimum and maximum recovery.

The adsorption of lithium onto RDP-FC-Cu (Figure 35 A and B) at a variety of temperatures (25, 35 and 45°C) and concentrations (5, 10, 15, 20, 25, 30, 35, 50, 70, and 100 mg/L) follows a similar trend to its adsorption onto RDP. However, the overall achieved adsorption capacities and removals of RDP-FC-Cu are higher than RDP. The maximum adsorption of lithium took place when the temperature was raised to 45°C for all initial metal concentrations with the highest adsorption achieved at 100 mg/L (Adsorption capacity of 99.3 mg/g). The difference between the adsorption capacities/efficiencies at different temperatures was found to be significant (P-value < 0.05, appendix A). Similar to RDP, higher differences between the adsorptions at 25, 35, and 45°C were noticed at lithium concentrations below 30 mg/L. However, these differences in the adsorption of lithium at different temperatures are less evident than the differences observed for RDP. At higher lithium concentrations than 30 mg/L, the adsorption capacities and efficiencies were very similar for 35 and 45°C. Interestingly, the RDP-FC-Cu composite showed significantly higher adsorption capacities and efficiencies for lithium at all temperatures than RDP and RDP-FC-Ni (Figure 36 A and B). This adsorption behavior and favorability could be due to the previously mentioned exceptional and selective physiochemical characteristics of the adsorbent. The RDP-FC-Ni composite shows similar adsorption trends to RDP and RDP-FC-Cu in terms of increasing adsorption with temperature, higher differences between the three temperatures in terms of adsorption at low metal concentration, and similarity between 35 and 45°C in terms of adsorption at high metal concentration. RDP-FC-Ni showed higher adsorption capacities and efficiencies for lithium than RDP and lower than RDP-FC-Cu (P-value < 0.05, appendix A). This could be due to the enhanced physicochemical characteristics for RDP-FC-Ni, however, RDP-FC-Cu shows a bigger

pore radius and volume than RDP-FC-Ni, enhanced chemical characteristics, and functional groups. Furthermore, it is worth noting that the TGA results for RDP-FC-Cu revealed remarkable insights regarding its thermal stability (Section 4.2.7). As mentioned previously, the thermal stability of adsorbents is of great importance for ensuring an optimized adsorption process. This is because temperature plays a significant role in the adsorption efficiency and capacity of numerous adsorbents. Many adsorption systems and in particular metal adsorptions require energy in terms of temperature increase to achieve high adsorption and recovery results (Albatrni et al., 2020). This study showed that the adsorption of lithium onto the three adsorbents favors increasing temperature. Therefore, the thermal stability of RDP-FC-Cu explains its constant and relatively high adsorption capabilities towards lithium despite temperature changes. Moreover, the thermal stability of RDP-FC-Ni was found to be higher than RDP. This explains its higher and similar adsorption capabilities than RDP and RDP-FC-Cu, especially at higher lithium concentrations than 30 mg/L.

As explained earlier, the temperature change in an adsorption system could greatly affect the behavior and mechanism of adsorption of metals onto different adsorbents. For that reason and as with the lithium study, the effect of temperature (25°C, 35°C, and 45 °C) on the adsorption of strontium onto RDP, RDP-FC-Cu, and RDP-FC-Ni were studied. Figures 39, 40, and 41 below represent the adsorption capacity and efficiency patterns of strontium onto RDP, RDP-FC-Cu, and RDP-FC-Ni at the mentioned temperatures and previously studied concentrations (5, 10, 15, 20, 25, 30, 35 50, 70, 100 mg/L metal concentration).

In general, from figures 39, 40, and 41, all the adsorbents show similar adsorption trends when compared to each other. That is, a noticeable increase in the adsorption capacity can be seen when the temperature was increased from 25 °C to 35 °C.

However, when the temperature further increased from 35 °C to 45 °C, the adsorption capacity of strontium increased only slightly. In other words, the differences between the adsorption capacities of strontium achieved at 35 °C and 45 °C are less evident than between 25 °C and 35°C. This gives the hint that a temperature of 35 °C would cause a significant change in the adsorption capacity of strontium onto the three adsorbents. Moreover, it must be noted that as with previous findings of this study (Section 4.4), the adsorption of strontium onto RDP-, RDP-FC-Cu, and RDP-FC-Ni enhanced significantly with an increase in the initial metal concentration from 5 mg/L to 100 mg/L.

The adsorption capacities and efficiencies of strontium onto RDP at 25°C, 35°C, and 45 °C are illustrated in Figure 39 A and B. In general, it can be seen that as the concentration of strontium increases from 5 mg/L to 100 mg/L, the difference of the achieved adsorption capacity and efficiency between 25 °C and 35 °C decreases while it becomes similar between 35 °C and 45 °C (P-value < 0.05, appendix A). This means that at low metal concentrations, raising the temperature from 25 °C to 35 °C resulted in a higher increase in the adsorption of strontium than at higher metal concentrations. Similar to the reasons explained for lithium adsorption, at low metal concentrations, the available active sites on the RDP are plentiful, while the amount of strontium ions are low. Therefore, the collisions and mass transfer forces do not play a significant role in enhancing the adsorption capacity. However, an increase in the temperature from 25 °C to 35 °C facilitated the rates of metal movements as well as pore diffusions due to an increase in the energy of the system. The similarities in the achieved adsorption of strontium onto RDP between temperatures of 35 and 45 °C (Mainly at metal concentrations above 20 mg/L) could be due to the same reasons explained for lithium.

The adsorption capacities and efficiencies of strontium onto RDP-FC-Cu are presented

in figure 40 (A and B) below. Overall, the achieved adsorption of strontium onto RDP-FC-Cu at all temperatures is higher than the adsorption that occurred onto RDP. Similar to lithium, this result is expected as the composite demonstrated exceptional adsorptive physical and chemical characteristics that could have enhanced the removal, coordination, and complexation of strontium onto its unique cubic lattice structure. In addition, and similar to previously discussed results, the adsorption of strontium onto RDP-FC-Cu favored increasing temperature from 25 °C to 45°C with more noticeable differences in adsorption between 25 °C and 35°C than between 35 °C and 45°C. However, the differences in the adsorption of strontium at different temperatures are less evident than the differences observed for RDP. At higher lithium concentrations than 20 mg/L, the adsorption capacities and efficiencies were very similar for 35 and 45°C.

The adsorption of strontium onto RDP-FC-Ni at a variety of temperatures (Figure 41 A and B) follows the same trends discussed for RDP and RDP-FC-Cu. However, RDP-FC-Ni achieved the highest adsorption capacities and efficiencies for strontium than RDP and RDP-FC-Cu (P-value < 0.05, appendix A). This result is expected due to the findings of previous experiments (Sections 4.3, 4.4, and 4.5) that in short, showed the followings:

i. The effect of pH and initial strontium concentration on the adsorption onto RDP-FC-Ni revealed the highest adsorption capacities and efficiencies when compared to RDP and RDP-FC-Cu.
ii. These high adsorption capacities and efficiencies of strontium onto RDP-FC-Ni could be mainly due to its fewer particle sizes, enhanced morphological surface area, and a porous structure with plenty of cavities that represent a variety of adsorption active sites. The SEM analysis showed that RDP-FC-Ni underwent

more structural changes upon the adsorption of strontium than RDP and RDP-FC-Cu. RDP-FC-Ni was shown to be more carbonations, highly stable with the highest number of characteristic functional groups that were shown to play a role in the adsorption processes of strontium. In addition to these characteristics, the hydrated pore radiuses of strontium and nickel are very similar which could have resulted in an enhanced, easier, and more stable ionic substitution in the cubic lattice of the adsorbent.

Similar results to the adsorption behaviors of lithium and strontium onto the three adsorbents at variating temperatures were obtained by many studies. For example, a study done by Yu and coworkers (2017) on the adsorption of gold onto chemically modified activated carbons revealed that the adsorption capacity increased with increasing temperature due to enhanced internal diffusion onto the adsorbent. Another study done by El-Bahy and coworkers (2018) showed that the adsorption of cesium ions onto a potassium copper hexacyanoferrate encapsulated carbomer favored increasing temperatures. The authors discussed the great role of temperature in the adsorption of metals from aqueous solutions. Increasing the temperature would lead to increased kinetic energy of the system, which would, in turn, increase the mobility of metals and weakens their electrostatic repulsion forces, leading to higher collisions, and adsorption capacities. Another study performed by Naeimi and Faghihian (2017) discussed that the adsorption of cesium onto a modified potassium nickel hexacyanoferrate was an endothermic process that was continuously enhanced until an equilibrium was reached with an increase in temperature.

(A)

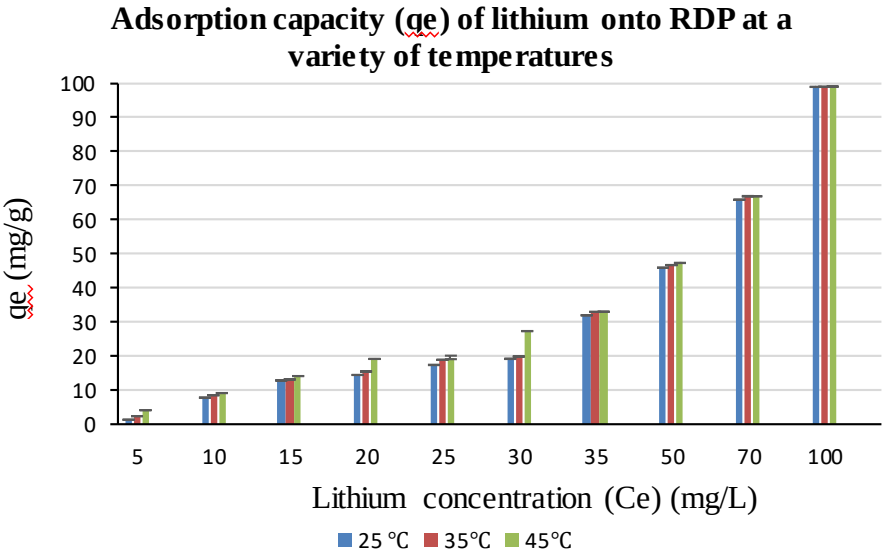

(B)

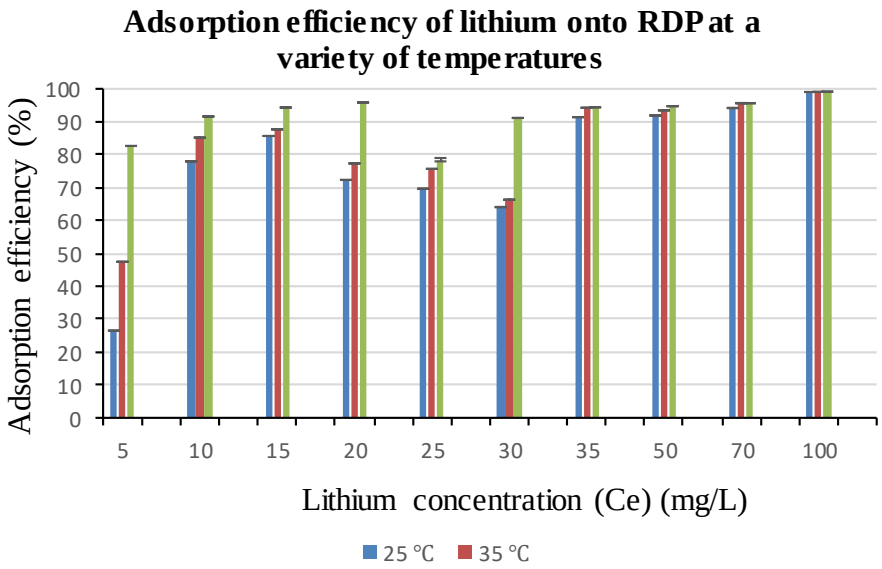

Figure 36. The effect of temperature on the adsorption (A) capacity and (B) efficiency of lithium onto RDP. The experimental conditions were as follows: the adsorption batch tests of lithium onto the adsorbents were performed at 25, 35, and 45 ℃ and shaking time of 24 hrs. at 160 rpm. Also, the adsorbent mass was constant at 0.05g, and the lithium concentrations were 2, 5, 10, 15, 20, 25, 30, 35, 50, 70, and 100 ppm in a total volume of 50 ml. The pH of the solution was kept constant at the optimum pH of 6. The error bars are shown on the figure.

(A)

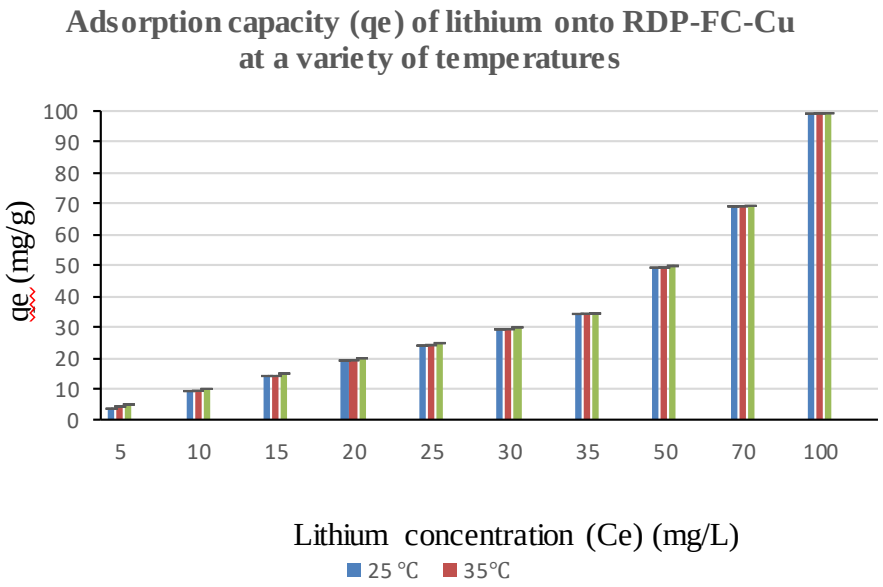

(B)

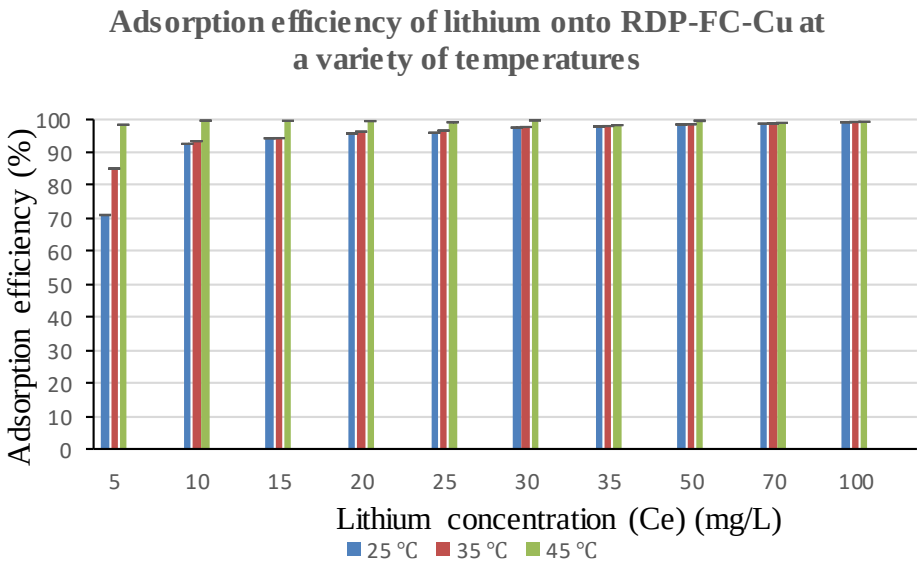

Figure 37. The effect of temperature on the adsorption (A) capacity and (B) efficiency of lithium onto RDP-FC-Cu. The experimental conditions were as follows: the adsorption batch tests of lithium onto the adsorbents were performed at 25, 35, and 45 °C and shaking time of 24 hrs. at 160 rpm. Also, the adsorbent mass was constant at 0.05g, and the lithium concentrations were 2, 5, 10, 15, 20, 25, 30, 35, 50, 70, and 100 ppm in a total volume of 50 ml. The pH of the solution was kept constant at the optimum pH of 6. The error bars are shown on the figure.

(A)

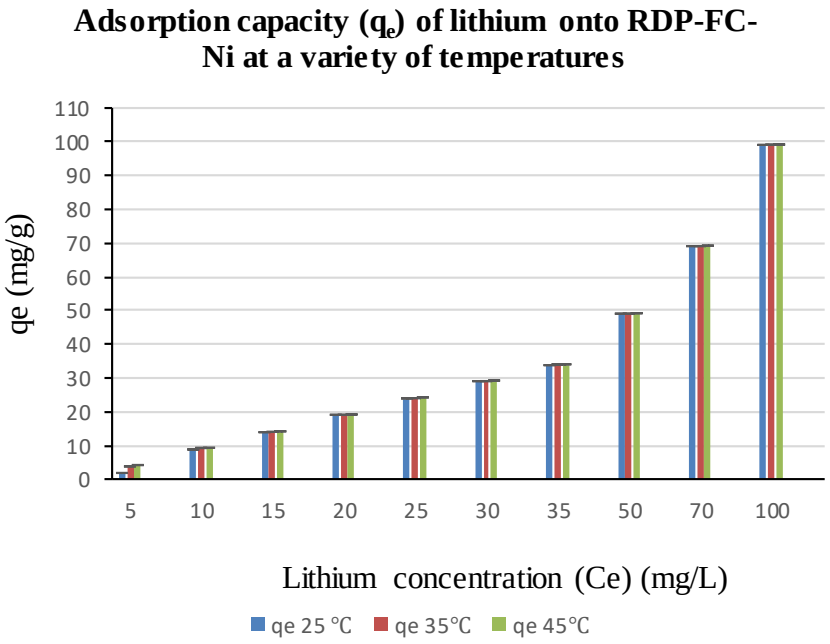

(B)

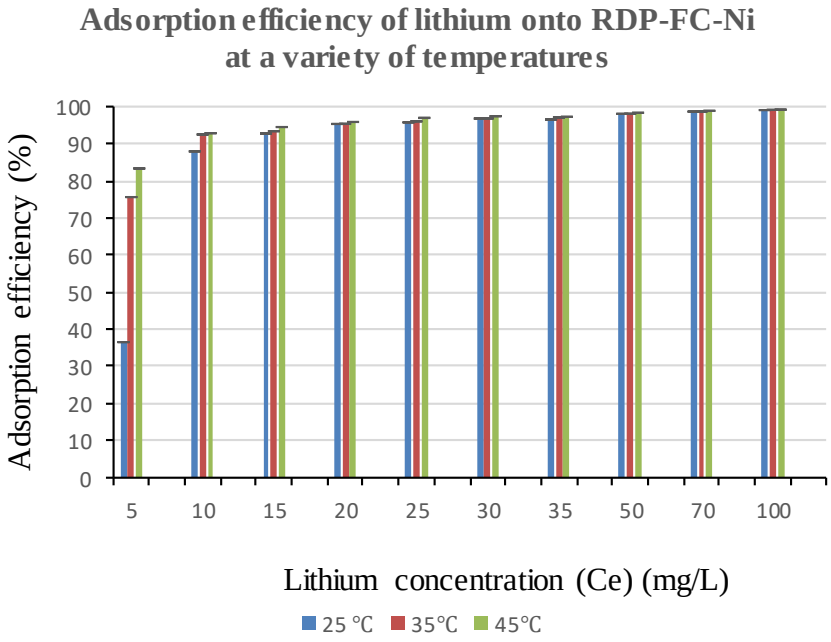

Figure 38. The effect of temperature on the adsorption (A) capacity and (B) efficiency of lithium onto RDP-FC-Ni. The experimental conditions were as follows: the adsorption batch tests of lithium onto the adsorbents were performed at 25, 35, and 45 °C and shaking time of 24 hrs. at 160 rpm. Also, the adsorbent mass was constant at 0.05g, and the lithium concentrations were 2, 5, 10, 15, 20, 25, 30, 35, 50, 70, and 100 ppm in a total volume of 50 ml. The pH of the solution was kept constant at the optimum pH of 6. The error bars are shown in the figure.

(A)

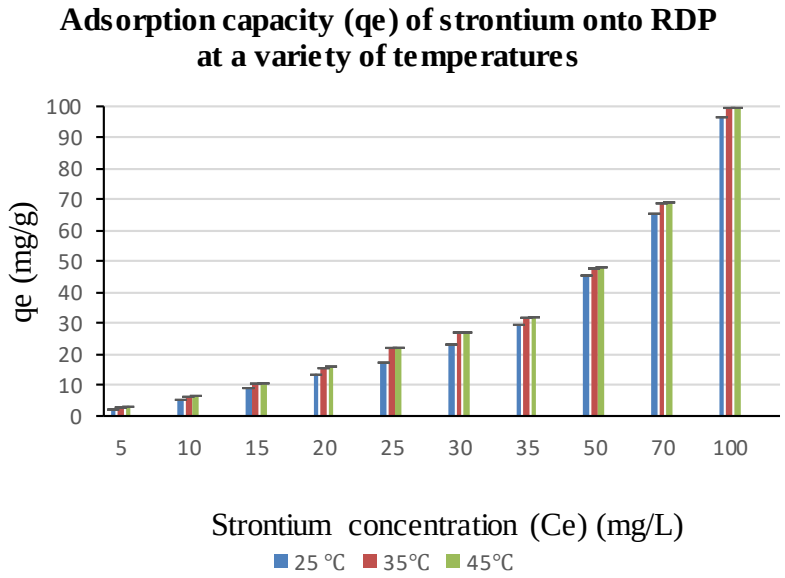

(B)

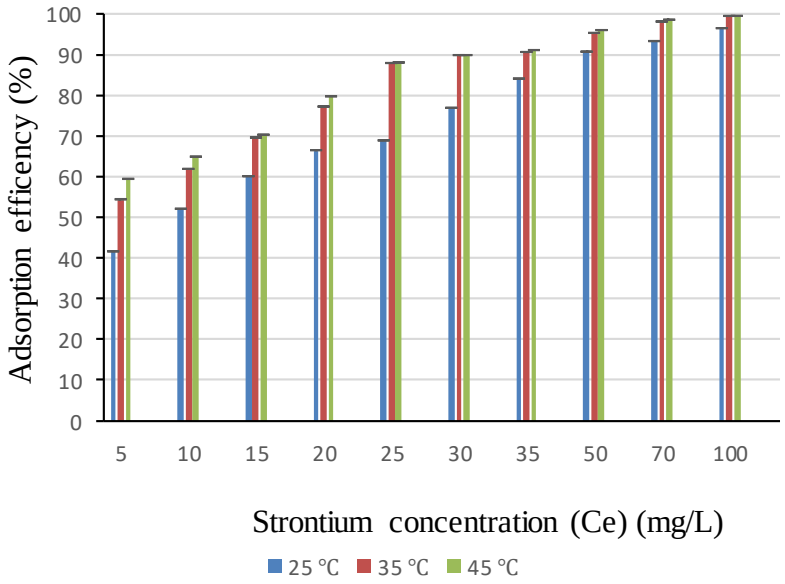

Figure 39. The effect of temperature on the adsorption (A) capacity and (B) efficiency of strontium onto RDP. The experimental conditions were as follows: the adsorption batch tests of strontium onto the adsorbents were performed at 25, 35, and 45 °C and shaking time of 24 hrs. at 160 rpm. Also, the adsorbent mass was constant at 0.05g, and the strontium concentrations were 2, 5, 10, 15, 20, 25, 30, 35, 50, 70, and 100 ppm in a total volume of 50 ml. The pH of the solution was kept constant at the optimum pH of 6. The error bars are shown on the figure.

(A)

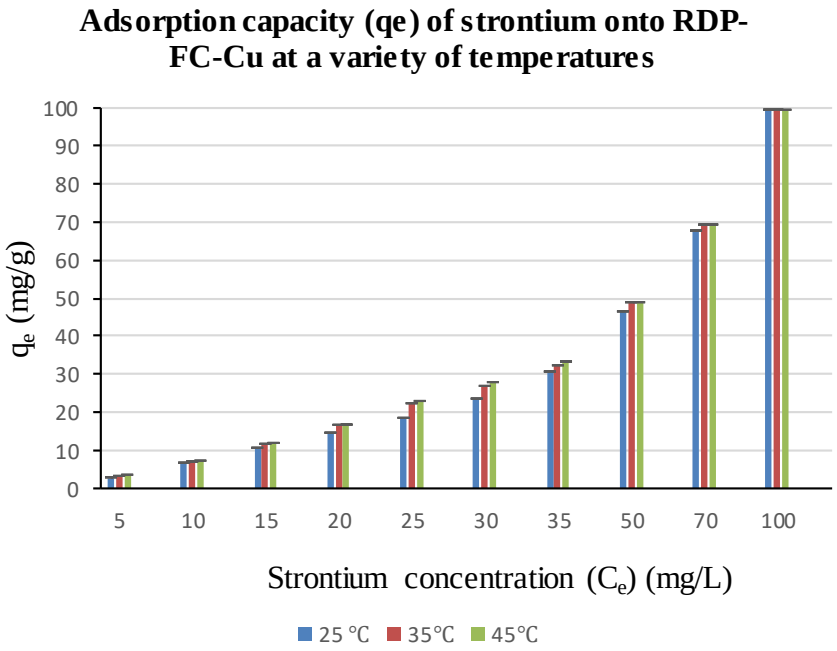

(B)

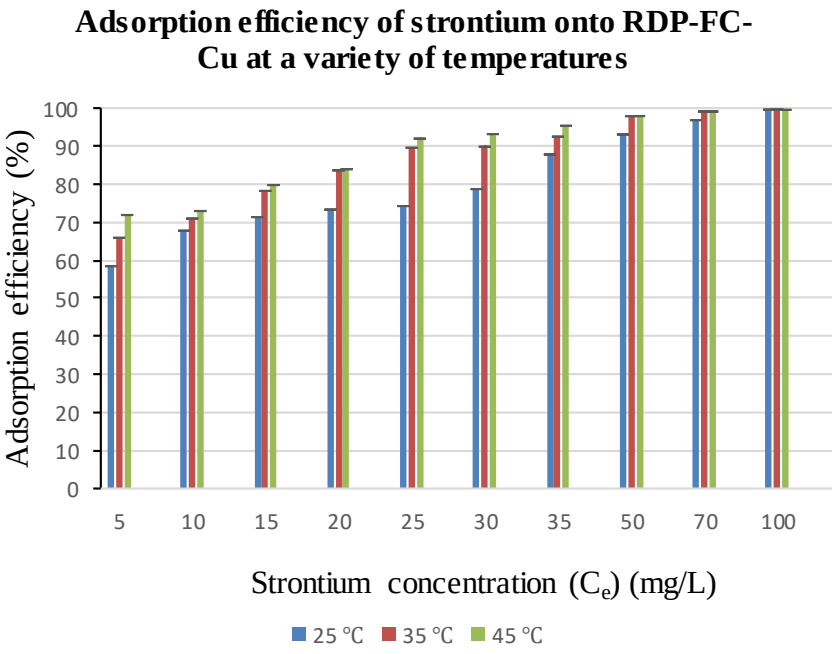

Figure 40. The effect of temperature on the adsorption (A) capacity and (B) efficiency of strontium onto RDP-FC-Cu. The experimental conditions were as follows: the adsorption batch tests of strontium onto the adsorbents were performed at 25, 35, and 45 °C and shaking time of 24 hrs. at 160 rpm. Also, the adsorbent mass was constant at 0.05g, and the strontium concentrations were 2, 5, 10, 15, 20, 25, 30, 35, 50, 70, and 100 ppm in a total volume of 50 ml. The pH of the solution was kept constant at the optimum pH of 6. The error bars are shown on the figure.

(A)

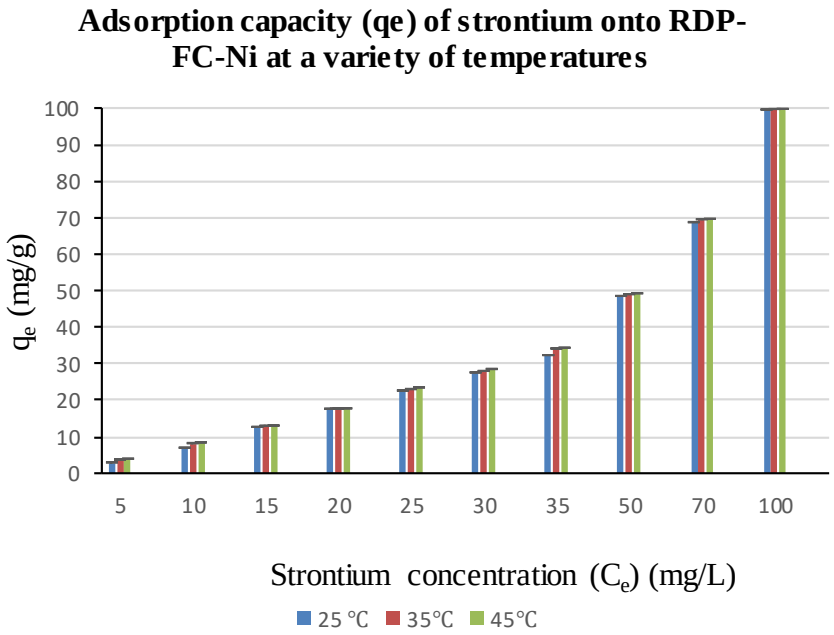

(B)

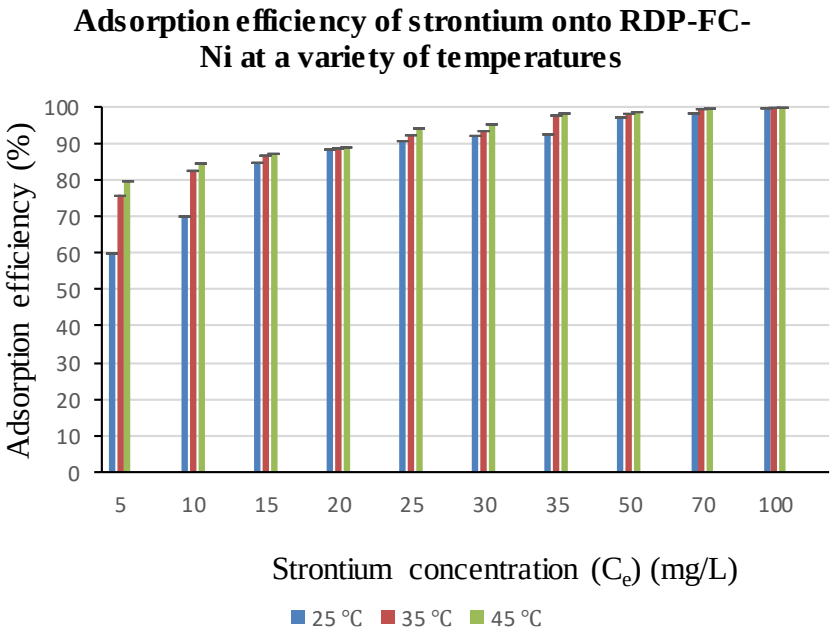

Figure 41. The effect of temperature on the adsorption (A) capacity and (B) efficiency of strontium onto RDP-FC-Ni. The experimental conditions were as follows: the adsorption batch tests of strontium onto the adsorbents were performed at 25, 35, and 45 °C and shaking time of 24 hrs. at 160 rpm. Also, the adsorbent mass was constant at 0.05g, and the strontium concentrations were 2, 5, 10, 15, 20, 25, 30, 35, 50, 70, and 100 ppm in a total volume of 50 ml. The pH of the solution was kept constant at the optimum pH of 6. The error bars are shown on the figure.

4.5.1 Adsorption thermodynamics

The adsorption capacity and efficiency provide an initial and overall understanding of adsorption systems in terms of being exothermic or endothermic (Yadav et al., 2021). As mentioned previously, temperature is one of the most important factors that affect the degree of adsorption of metals as well as many pollutants onto adsorbents. This is because the adsorption capacity could increase with increasing temperature and indicate an endothermic process, while some adsorption processes proceed by releasing energy and indicate an exothermic adsorption process (Humelnicu et al., 2020). To further confirm and characterize the adsorption patterns, behaviors, and mechanisms of lithium and strontium onto RDP, RDP-FC-Cu, and RDP-FC-Ni, the adsorption thermodynamics of the adsorption system were calculated and determined. The adsorption thermodynamics include Gibbs free energy (ΔG^o), enthalpy (ΔH^o), and entropy (ΔS^o) changes calculations, which were calculated using equations presented previously (Wadhawan et al., 2020; Abdulla et al., 2019). Moreover, the thermodynamic parameters were determined for the adsorption of lithium and strontium onto RDP, RDP-FC-Cu, and RDP-FC-Ni at a variety of initial metal concentrations (5, 10, 15, 20, 25, 30, 35, 50, 70, and 100 mg/L) and temperatures (25°C, 35°C and 45 °C). Tables 9 and 10 present the enthalpy and entropy change values obtained for all the adsorbents involved in the adsorption of lithium and strontium, respectively. Similarly, Tables 11 and 12 present Gibbs free energy values for adsorption of lithium and strontium, respectively. As the previous experiment (Effect of temperature on the adsorption of lithium onto the three adsorbents) indicated, the adsorption capacity of lithium and strontium increased with an increase of temperature from 25°C to 45°C for all adsorbents. This was confirmed by the positive values obtained for the enthalpy of all the adsorbents involved in the adsorption of lithium and strontium (Tables 9 and 10).

This indicates that the adsorption of the metals onto the adsorbents is an endothermic process that requires the addition of energy (In the form of increased temperature) (Yadav et al., 2021; Aljerf, 2018). To be more specific, the highest enthalpy value obtained for the adsorption of lithium was for RDP-FC-Cu followed by RDP then RDP-FC-Ni. This means that the adsorption of lithium onto RDP-FC-Cu requires higher energy input to proceed and achieve the high adsorption capacities. For the adsorption of strontium, the highest enthalpy value was for RDP followed by RDP-FC-Cu then RDP-FC-Ni. Furthermore, the Gibbs free energy values (Table 11 and 12) were found to be negative for all the adsorbents involved in the study. This means that the adsorption of lithium and strontium onto the adsorbents is a spontaneous and viable process. The Gibbs free energy values can be observed to decrease with increasing temperature, which indicates that the internal diffusion and adsorption of lithium and strontium are enhanced with temperature (Humelnicu et al., 2020). In addition, the adsorption of strontium onto RDP-FC-Cu and RDP-FC-Ni achieved similar Gibbs free energy values (Table 12). However, it is worth noting that for the adsorption of lithium, the decrease of Gibbs free energy with temperature is more evident than that of strontium for a given adsorbent (Table 11). Lastly, the values of ΔS^o give an understanding of the favorability of the adsorption process. The positive ΔS^o values (Table 9 and 10) obtained for all adsorbents show that the adsorption of lithium and strontium is favorable for all the adsorbents involved in this study. Also, the adsorption process of the metals onto the adsorbents takes place with increased randomness and disorder (Aljerf, 2018). A study done by Zhou and others (2017) on the adsorption of mercury onto modified graphene oxide revealed through the thermodynamic study that the process took place spontaneously and favorably with increasing temperature. On the other hand, Wadhawan and others (2020) showed that mercury adsorption onto

chitosan alginate nanoparticles decreased at temperatures above 30°C, which indicated an exothermic adsorption process. This could be justified by the fact that some adsorbed metals would de-chelate or desorb at elevated temperatures due to specific adsorbent characteristics and increased mobility of the metal ions. Moreover, the adsorption of copper ions onto different adsorbents like magnetic, activated charcoal, and Na polymer-based composite of magnetic alginate was investigated by Yadav and others (2021). Through the thermodynamic study, it was found that the adsorption process of copper was spontaneous, endothermic, and random.

Table 9. The adsorption enthalpy (ΔH^o) and entropy (ΔS^o) of lithium onto three adsorbents.

Adsorbent	ΔH^o (KJ/mol)	ΔS^o (J/K.mol)
RDP	140.12	519.00
RDP-FC-Cu	336.73	1134.86
RDP-FC-Ni	133.88	449.90

Table 10. The adsorption enthalpy (ΔH^o) and entropy (ΔS^o) of strontium onto three adsorbents.

Adsorbent	ΔH^o (KJ/mol)	ΔS^o (J/K.mol)
RDP	54.92	219.08
RDP-FC-Cu	36.26	162.00
RDP-FC-Ni	29.3	138.22

Table 11. The adsorption Gibbs free energy (ΔG) of lithium onto three adsorbents.

	ΔG (KJ/mol)		
Adsorbent	25°C/ 298.15 K	35°C/ 308.15 K	45°C/ 318.15 K
RDP	-14.62	-19.81	-25.00
RDP-FC-Cu	-1.63	-12.97	-24.32
RDP-FC-Ni	-0.26	-4.76	-9.26

Table 12. The adsorption Gibbs free energy (ΔG) of strontium onto three adsorbents.

	ΔG (KJ/mol)		
Adsorbent	25°C/ 298.15 K	35°C/ 308.15 K	45°C/ 318.15 K
RDP	-10.40	-12.60	-15.00
RDP-FC-Cu	-12.00	-14.00	-15.14
RDP-FC-Ni	-12.00	-13.30	-15.00

4.6 Adsorption isotherm models

The adsorption isotherm models can achieve an understanding of the quantity of adsorbed and non-adsorbed adsorbate molecules as well as the adsorption mechanisms of metals and pollutants onto adsorbents (Núñez-Gómez et al., 2019). Therefore, two of the most common adsorption isotherm models were conducted for the adsorption of lithium and strontium onto RDP, RDP-FC-Cu, and RDP-FC-Ni at variating temperatures (25°C, 35°C, and 45 °C) and initial metal concentrations (2, 5, 10, 15, 20, 25, 30, 35, 50, 70 and 100 mg/L). The applicability of the adsorption of lithium and strontium to Langmuir and Freundlich adsorption isotherm models was studied. The plots of the Langmuir and Freundlich adsorption isotherm models reveal the linearity of the isotherm models as well as the R^2 values obtained for the recovery of lithium and strontium onto the three adsorbents (Appendix B). Moreover, the adsorption isotherm model plots were used to calculate the isotherm-related constants for the three adsorbents involved in this study (Tables 13 - 16) (Al-Ghouti and Al-Absi, 2020). Upon general observation of table 13 and 15, both isotherm models for the three adsorbents show R^2 values of 0.6 and higher, which indicates the high possibility that the adsorption of lithium onto the adsorbents could follow both isotherm models to a good extent (Yadav et al., 2021; Magdy et al., 2018). More specifically, all the adsorbents involved in the study showed R^2 values above 0.9 under the temperatures of 25 and 35°C for the Langmuir adsorption isotherm model (Table 13). However, at 45°C, the

adsorption of lithium onto RDP-FC-Cu showed a 0.92 R^2 while the adsorption onto RDP and RDP-FC-Ni obtained lower R^2 values of 0.8 and 0.6, respectively. This means that at 25 and 35°C, the adsorption of lithium onto RDP, RDP-FC-Cu, and RDP-FC-Ni follows a monolayer adsorption while at higher temperatures (45°C), a monolayer adsorption mechanism is mainly achieved with RDP-FC-Cu (Al-Ghouti and Al-Absi, 2020). Table 13 further shows the equation parameters of Langmuir adsorption isotherm that were calculated for the three adsorbents involved in this study. The monolayer adsorption capacity (C_m) values of RDP increased continuously when the temperature increased from 25°C to 45°C. However, Langmuir's adsorption favorability constant (K_L) for RDP decreased continuously, as the temperature increased from 25°C to 45°C. This shows the great effect that temperature plays on the adsorption monolayer formations, favorability, and capacities of RDP (Zhang and Liu, 2020; Humelnicu et al., 2019). Similar trends in Langmuir's C_m values were obtained for the RDP-FC-Cu composite involved in the adsorption of lithium. Interestingly, For RDP-FC-Cu, the adsorption favorability values (K_L) continuously increased with the increase in temperature. Significant increases in the adsorption capacity and favorability values can be observed for RDP-FC-Cu when the temperature was increased to 45°C. Along with the high R^2 obtained at 45°C, this indicates that the highest and most favorable adsorption of lithium follows Langmuir's adsorption mechanism at 45°C for RDP-FC-Cu (Table 13) (Yadav et al., 2021; Al-Ghouti and Al-Absi, 2020). For RDP-FC-Ni (Table 13), the Langmuir's C_m and K_L values are found to decrease when the temperature was increased from 25°C to 35°C. However, at 45°C Langmuir's adsorption capacity and favorability can be seen to increase for the adsorption of lithium onto RDP-FC-Ni.

The adsorption of lithium onto RDP at 25°C followed Freundlich isotherm model best

with an R^2 value of 0.93 (Table 15). At 35 and 45°C, the adsorption of lithium onto RDP showed lower R^2 values of 0.89 and 0.88 respectively. It is worth noting that the adsorption of lithium at 25°C could occur with the formation of monolayers and multilayers onto the surface of RDP. As the temperature increased to 35 and 45°C, the adsorption mechanism of lithium onto RDP favored the formation of monolayers over multilayers. This is because the R^2 value obtained for RDP at 25°C and 35°C was higher for Langmuir's isotherm model (Table 13). For RDP-FC-Cu, the highest R^2 value for the Freundlich isotherm model was obtained at 45°C ($R^2 = 0.91$) followed by 25°C and then 35°C (Table 15). A similar result is obtained with the adsorption of lithium onto RDP-FC-Ni, where the highest Freundlich R^2 value can be seen at 45°C ($R^2 = 0.95$) but is followed by 35 and then 25°C. Interestingly, the adsorption of lithium onto RDP-FC-Cu favored the monolayer formation over the multilayer mechanism at lower temperatures than 45°C, with both mechanisms were obtained at 45°C. Similarly, the adsorption of lithium onto RDP-FC-Ni followed Langmuir adsorption isotherm mechanism best at 25 and 35°C with the formation of multilayer adsorption mechanism at 45°C. This shows the significant effect that temperature plays in variating the mechanism of lithium adsorption onto the studied adsorbents (Thanarasu et al., 2019). Furthermore, it is worth noting that the temperature, which showed the highest adsorption capacity for lithium (45°C) has also revealed shifts in the adsorption mechanisms. This temperature has caused the adsorption of lithium onto the adsorbents to take place as monolayer formations as well as multilayers, which indicates higher adsorption potentials and capacities due to mass transfer forces (Zhang and Liu, 2020; Borhade and Kale, 2017).

Freundlich adsorption isotherm parameters for the adsorption of lithium onto RDP, RDP-FC-Cu, and RDP-FC-Ni are shown in table 15. It is well established that the value

of n related to the Freundlich adsorption isotherm model is of great importance as it indicates the curvature of the isotherm. Generally, an n value smaller than 1 means that the adsorption is a chemical process, however, an n value bigger than 1 indicates a physical and favorable adsorption process. If the n value equal to 1 is obtained, then the adsorption process is linear. The other important parameter that could be derived from the n value of the Freundlich adsorption isotherm model is 1/n. typically, if the value of 1/n is bigger than 1, then the adsorption process is cooperative. Oppositely, a 1/n value less than 1 indicates a less cooperative adsorption process. Moreover, a decrease in the value of 1/n means that the adsorption process is becoming more heterogeneous and efficient at low adsorbate concentrations (Thanarasu et al., 2019; Zhang and Liu, 2020). According to the results of the study, the adsorption of lithium onto RDP becomes more favorable, physical, and less cooperative in terms of Freundlich's isotherm model as the temperature increased from 25°C to 45°C (Table 15). This is because the values for Freundlich's n are found to be higher than 1 and increasing with temperature. The values for 1/n are observed to be less than 1 and decreasing with increasing temperature. Freundlich's adsorption capacity parameter is known as K_f, which is seen to decrease from 8.89 mg/g at 25°C to 2.04 mg/g at 35°C then increase at 45°C to reach a value of 2.31 mg/g for RDP. To compare, the n and 1/n values for RDP-FC-Cu and RDP-FC-Ni reveal that the adsorption of lithium in terms of Freundlich's adsorption isotherm model could be a chemical cooperative process that is less efficient at low metal concentrations. Furthermore, the Freundlich adsorption capacity (K_f) values for RDP-FC-Cu are seen to continuously increase with temperature. On the other hand, the K_f values obtained for RDP-FC-Ni show that with the Freundlich isotherm mechanism, the adsorption capacity of lithium decreased as the temperature increased from 25°C to 35°C then increased as the temperature increased further to 45°C. Overall,

the applied adsorption isotherms indicate that the adsorption of lithium onto the three adsorbents at 25°C and 35°C could be more fitting to Langmuir's isotherm model than the Freundlich model. At 45°C, the adsorption of lithium onto RDP and RDP-FC-Cu could follow the Langmuir and the Freundlich adsorption mechanisms almost equally. However, the Freundlich adsorption isotherm model was found to be more fitting than Langmuir's model for the adsorption process of lithium onto RDP-FC-Ni at 45°C.

Tables 14 and 16 represent the calculated Langmuir and Freundlich adsorption isotherm constants from their respected plots for the adsorption of strontium (Appendix B). Similar to lithium, these isotherm models were done to understand the mechanisms of strontium adsorption onto the three adsorbents at a variety of temperatures (25, 35 and 45 °C) and concentrations (5, 10, 15, 20, 25, 30, 35, 50, 70, and 100 mg/L.

From the R^2 values in table 14, it can be noticed that the adsorption of strontium onto RDP fits the Langmuir's isotherm model best at a temperature of 25 °C (R^2 = 0.96) followed by 35 °C (R^2 = 0.86) then 45 °C (R^2 = 0.77). This means that at the lowest studied temperature, the adsorption of strontium onto RDP is more likely to be in the formation of monolayers than at the higher temperatures. To compare, the R^2 values obtained for RDP using Freundlich isotherm model (Table 14) showed the highest value for the temperature of 45 °C (R^2 = 0.91) followed by 35 °C (R^2 = 0.83) then 25 °C (R^2 = 0.71). This further confirms that the adsorption of strontium onto RDP is more likely to form monolayers on the surface than multilayers at lower temperatures. Furthermore, the Langmuir monolayer adsorption capacity (C_m) for the adsorption of strontium onto RDP (Table 14) is seen to increase when the temperature increased from 25 °C to 35 °C. However, at 45 °C, the C_m values are seen to decrease again. A similar trend is observed for the obtained Langmuir's K_L values for the adsorption of strontium onto RDP (Table 14). Moreover, the adsorption of strontium onto RDP-FC-Cu is seen to

follow Langmuir's isotherm model to a great extent at all the studied temperatures (R^2 values above 0.9) (Table 14). Interestingly, the high Freundlich's R^2 values obtained for the same adsorbent show that the adsorption of strontium could also follow the theory of multilayer formations, especially at temperatures of 35 °C and 45 °C (Table 16). The C_m and K_L values for the adsorption of strontium onto RDP-FC-Cu show the same trends obtained for RDP. It is of significant importance that the adsorption of strontium onto RDP-FC-Ni showed R^2 of 0.9 and higher for both adsorption isotherm models (Table 14 and 16). This means that strontium could be adsorbed onto RDP-FC-Ni in two ways: the formation of monolayers and multilayers. This further confirms the highest adsorption capacities achieved for RDP-FC-Ni towards strontium. To add, Langmuir's C_m and K_L values for RDP-FC-Ni are seen to increase with an increase in temperature.

Freundlich isotherm constants for the adsorption of strontium onto RDP, RDP-FC-Cu, and RDP-FC-Ni are represented in table 16 below. For RDP, the n values are seen to increase from 0.41 to 1.08 and 1.35 when the temperature increased from 25 to 35 and 45 °C respectively. On the other hand, the 1/n values decreased from 2.38 to 0.93 and 0.74 when the temperature increased from 25 to 35 and 45 °C, respectively. this means that at 25 °C, the adsorption of strontium onto RDP is an unfavorable, chemical and cooperative process. However, as the temperature increases to 35 and 45 °C, the adsorption process becomes physical, favorable, and less cooperative. The highest K_f value for the adsorption of strontium onto RDP is obtained at 45°C followed by 35 °C then 25 °C. For RDP-FC-Cu (Table 14), the n values are seen to decrease from 2.02 to 1.73 and 1.21 when the temperature increased from 25 to 35 and 45 °C respectively. on the other hand, the 1/n values increased slightly from 0.50 to 0.58 when the temperature increased from 25 to 35 °C then increased further to 0.82 when the temperature

increased to 45 °C. This means that according to the Freundlich model, the adsorption of strontium is a favorable and physical process at all the studied temperatures. However, the favorability decreases slightly with temperature. The adsorption process is less cooperative at the studied temperatures and is less efficient at low strontium concentrations. The K_f values are observed to decrease with temperature. Similar trends are achieved with RDP-FC-Ni when studying the Freundlich isotherm model for the adsorption of strontium at a variety of temperatures (Table 14).

Table 13. The equation parameters of the Langmuir isotherm model for the adsorption of lithium onto three adsorbents at a variety of initial metal concentrations and temperatures

	25°C			35°C			45°C		
Adsorbent	C_m (mg/g)	K_L (L/mg)	R^2	C_m (mg/g)	K_L (L/mg)	R^2	C_m (mg/g)	K_L (L/mg)	R^2
RDP	17.86	7857.14	0.95	19.61	1188.35	0.92	22.37	500.48	0.80
RDP-FC-Cu	1.78	4.24	0.96	4.24	30.43	0.97	38.91	22888.53	0.92
RDP-FC-Ni	4.97	29.71	0.94	0.96	1.00	0.95	2.70	7.88	0.60

Table 14. The equation parameters of the Langmuir isotherm model for the adsorption of strontium onto three adsorbents at a variety of initial metal concentrations and temperatures

	25°C			35°C			45°C		
Adsorbent	C_m (mg/g)	K_L (L/mg)	R^2	C_m (mg/g)	K_L (L/mg)	R^2	C_m (mg/g)	K_L (L/mg)	R^2
RDP	10.24	29.51	0.96	22.12	720.65	0.86	11.24	112.58	0.77
RDP-FC-Cu	22.03	63.51	0.92	23.09	752.27	0.95	15.22	152.51	0.94
RDP-FC-Ni	13.83	68.49	0.90	17.95	138.59	0.92	23.75	584.80	0.91

Table 15. The equation parameters of the Freundlich isotherm model for the adsorption of lithium onto three adsorbents at a variety of initial metal concentrations and temperatures

	25°C				35°C				45°C			
Adsorbent	n	1/n	K_f (L/mg)	R^2	n	1/n	K_f (L/mg)	R^2	n	1/n	K_f (L/mg)	R^2
RDP	3.09	0.32	8.89	0.93	4.98	0.20	2.04	0.89	5.08	0.20	2.31	0.88
RDP-FC-Cu	0.31	3.21	13.48	0.82	0.17	5.87	109.18	0.77	0.59	1.69	110.30	0.91
RDP-FC-Ni	0.42	2.39	35.88	0.78	0.05	20.91	16.17	0.89	0.22	4.45	39.82	0.95

Table 16. The equation parameters of the Freundlich isotherm model for the adsorption of strontium onto three adsorbents at a variety of initial metal concentrations and temperatures

	25°C				35°C				45°C			
Adsorbent	n	1/n	K_f (L/mg)	R^2	n	1/n	K_f (L/mg)	R^2	n	1/n	K_f (L/mg)	R^2
RDP	0.42	2.38	5.64	0.71	1.08	0.93	70.90	0.83	1.35	0.74	84.63	0.91
RDP-FC-Cu	2.02	0.50	72.77	0.84	1.73	0.58	53.14	0.99	1.21	0.82	49.98	0.99
RDP-FC-Ni	1.54	0.65	56.27	0.96	1.39	0.72	37.91	0.92	1.28	0.78	30.38	0.92

4.7 Desorption of lithium and strontium from the roasted date pits and two composites

Investigators are often interested in the fate of the adsorbents that were involved in adsorption processes. After the uptake of a target pollutant such as metals from solutions, the adsorbent could be regenerated and reused by performing a desorption process (Gao et al., 2020). As mentioned previously, desorption is the opposite of an adsorption process where the adsorbate is released from the adsorbent. The main purpose for carrying on a desorption process is to re-use the adsorbent material for another adsorption process. Re-using the adsorbents as many times as possible is environmentally, sustainably, and economically important. This is because it would

reduce the overall cost and waste materials in adsorption processes (Nur et al., 2018). For this reason, desorption experiments using 1M and 0.5M HCL were done for lithium and strontium from the spent RDP, RDP-FC-Cu, and RDP-FC-Ni. Tables 17 and 18 represent the percentage desorption achieved for lithium using 0.5M and 1M HCl, respectively. Similarly, Tables 19 and 20 show the percentage desorption achieved for strontium using 0.5M and 1M HCl, respectively. From tables all the tables, it is evident that all the adsorbents achieved similar adsorptions under the influence of 0.5M and 1M HCl. This shows that there is no significant effect on the desorption efficiency between the two studied HCl concentrations (P-value > 0.05, appendix A). Also, the high desorption efficiencies indicate that the adsorption of lithium onto the three adsorbents occurs due to the formations of weak and physical bonding (Ji et al., 2021; Fan et al., 2021). Moreover, the three adsorbents could be effectively regenerated and re-used as 99.9% of the metal could be desorbed after the adsorption processes. This provides scientists with the extra benefit of harnessing the full adsorptive and functionality of the adsorbents before discarding them. In addition, and from an environmentally friendly perspective, the high desorption efficiencies for lithium from the three adsorbents would help lessen date pits wastes by re-using them (Tables 17 and 18).

To compare, the desorption efficiencies for strontium under the effect of 0.5M HCl (Table 19) can be seen to be the highest and the same for RDP and RDP-FC-Cu (97%) followed by RDP-FC-Ni (91.2%). This indicates that the adsorption bonding between strontium and RDP-FC-Cu and RDP could be weaker than that of RDP-FC-Ni. It is worth noting that the adsorption of strontium was found to be the highest on RDP-FC-Ni at a variety of pH, concentrations, and temperatures than the other two adsorbents. This shows the higher stability and coordination of the strontium ions onto the

potassium nickel hexacyanoferrate complex than the other two adsorbents. For the desorption of strontium using 1M HCl (Table 20), higher desorption efficiencies were achieved for RDP (98.4%) and RDP-FC-Ni (97.12%) when compared to using 0.5M HCl. However, using 1M HCL to desorb strontium from RDP-FC-Cu resulted in a lesser desorption efficiency than using 0.5M HCl (88.32% and 96.9% desorption when using 1M and 0.5M HCl, respectively). These results demonstrate the effects of the concentrations of the acid used to desorb metals from different adsorbents (Fan et al., 2021). Overall, the results of this study showed high desorption efficiencies for lithium and strontium from all the adsorbents at both acid concentrations. Consequently, the great adsorptive capacities illustrated earlier are joined with the exceptional potential to effectively re-use these adsorbents more than once.

Table 17. Percentage desorption of lithium from three adsorbents using 0.5M HCl

Adsorbent	Average adsorbed concentration (mg/L)	% Desorption
RDP	32.56	99.94
RDP-FC-Cu	35.25	99.97
RDP-FC-Ni	35.04	99.97

Table 18. Percentage desorption of lithium from three adsorbents using 1M HCl

Adsorbent	Average adsorbed concentration (mg/L)	% Desorption
RDP	32.56	99.97
RDP-FC-Cu	35.25	99.97
RDP-FC-Ni	35.04	99.98

Table 19. Percentage desorption of strontium from three adsorbents using 0.5M HCl

Adsorbent	Average adsorbed concentration (mg/L)	% Desorption
RDP	30.66	97.04
RDP-FC-Cu	32.19	96.97
RDP-FC-Ni	33.99	91.17

Table 20. Percentage desorption of strontium from three adsorbents using 1M HCl.

Adsorbent	Average adsorbed concentration (mg/L)	% Desorption
RDP	30.66	98.36
RDP-FC-Cu	32.19	88.31
RDP-FC-Ni	33.99	97.11

4.8 Selectivity adsorption studies

4.8.1 Selective adsorption of lithium and strontium from mixture solutions

The adsorption of a target metal from solutions that contain two or more other metals could be challenging due to the effect of competing ions on the available active sites on the adsorbent. A certain adsorbent may exhibit exceptional and efficient adsorption capacities towards a specific metal and not others (Kitajima et al., 2020). Therefore, after establishing a complete understanding of the mechanisms of the RDP, RDP-FC-Cu, and RDP-FC-Ni towards a single metal, it was important to test the selectivity of the adsorbents in the presence of lithium and strontium in a single solution. Figure 43 (A and B) represent the adsorption capacity and efficiency of the three adsorbents at study towards lithium and strontium in mixture solutions. The concentration of both metals, as well as the solution pH, were kept at the optimum found concentration and

pH of 100 mg/L and pH 6, respectively. In addition, the adsorbent mass was the same as in previous experiments of 0.05 g, while the solution volume was 50 ml. the experiments lasted 24 hrs. at 160 rpm until an equilibrium was reached. From figure 42 (A and B) the differences between the achieved adsorption capacities for RDP, RDP-FC-Cu, and RDP-FC-Ni towards lithium and strontium are clearly shown (P-value < 0.05, appendix A). For the adsorption of lithium, RDP-FC-Cu achieved the highest adsorption capacity and efficiency of 99.98 mg/L and 99.91%, respectively. RDP showed the second-highest adsorption of lithium followed by RDP-FC-Ni, which achieved an adsorption capacity and efficiency of 97.03 mg/L and 80.17%, towards lithium, respectively. Interestingly, RDP-FC-Ni showed a higher capability and selectivity towards strontium (99.96 mg/L and 99.82% adsorption capacity and efficiency, respectively) than RDP and RDP-FC-Cu. These patterns and selectivity of the adsorbents towards a metal more than the other represent the significant effect that competing ions play on the adsorption capacities. It is worth noting that it was expected that RDP-FC-Cu would be slightly more selective towards lithium than strontium. In addition, it was predictable that RDP-FC-Ni would show slightly more selectivity towards strontium than lithium. However, the high selectivity of RDP towards both metals (Lithium and strontium adsorption capacities of 98.01 and 99.73 mg/L, respectively) demonstrates the high adsorptive qualities of the initial material: RDP at mixture solutions of high concentration and optimum conditions (Wei et al., 2020).

(A)

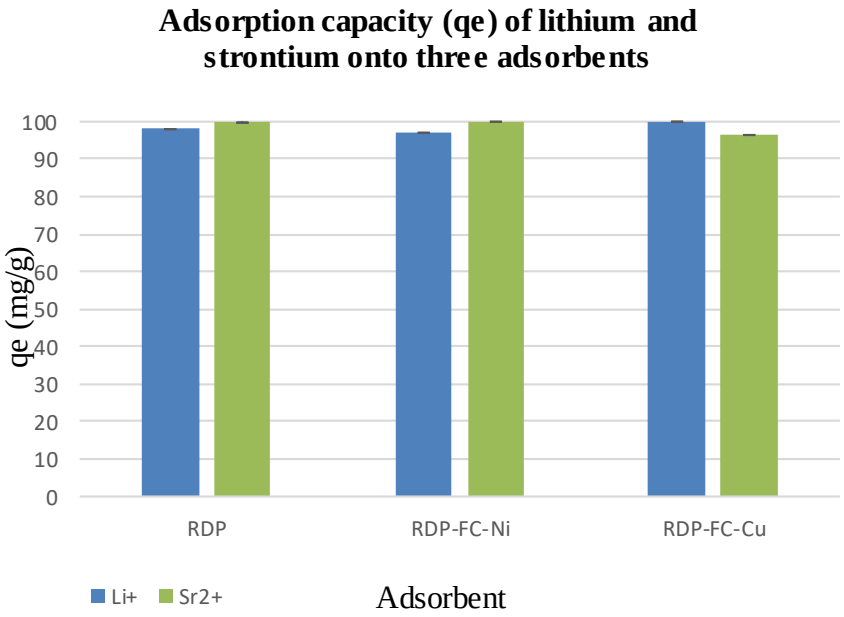

(B)

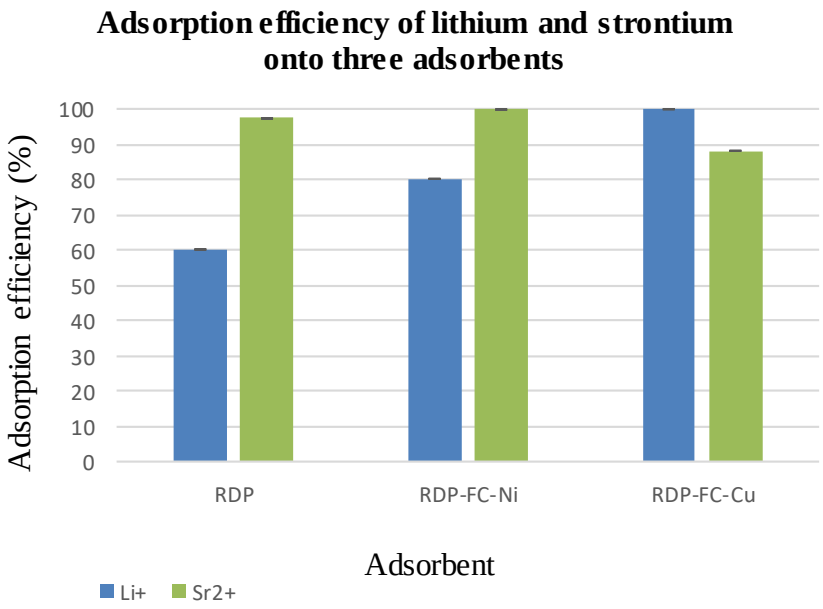

Figure 42. The adsorption (A) capacity and (B) efficiency of lithium and strontium onto RDP, RDP-FC-Cu, and RDP-FC-Ni from a mixture solution. The experimental conditions were as follows: metals concentration of 100 mg/L, solution pH of 6, volume of 50 ml, 0.05g adsorbent mass, shaking time of 24 hrs. at 160 rpm and a temperature of 25 °C. The error bars are shown on the figure.

4.8.2 Selective adsorption of metals from the collected reverse osmosis brine

The presence of various metal species in brine streams could significantly affect the adsorption capacities of adsorbents towards target metals (Ryu et al., 2020). This is because some metals could compete for the available adsorption active sites present on the adsorbents. Additionally, some adsorbents would demonstrate certain physicochemical characteristics that would favor the adsorption of certain metals (Zhong et al., 2021). Similarly, and as mentioned previously through the adsorption studies, the ionic substitution, complexation, polarity, solubility as well as the hydrated ionic radius of metals largely affect their adsorption onto different adsorbents (Rohmah et al., 2020). As the IC and ICP-OES characterization of the brine sample demonstrated, it contained various metals other than lithium and strontium (Section 4.1.1). For these reasons, it was vital to study the adsorption capabilities of the RDP, RDP-FC-Cu, and RDP-FC-Ni towards lithium and strontium from the collected reverse osmosis brine sample. The adsorption temperature was set to 35 °C because the high adsorption capacities of the adsorbents towards lithium and strontium at that temperature were shown previously. Also, brine streams are characterized by their warm temperatures, therefore, the adsorption and recovery of metals could be done as soon as the brine is rejected from a desalination plant. This would reduce the costs of energy expenditure and storing large volumes of brine streams. In addition, applying adsorption processes to brine streams directly after rejection would lessen the environmental risks of accidental leakages, or discharge into the environment. To add, this would ensure that some metals do not precipitate or leachate from the brine sample (Jiang et al., 2020). It was previously shown that the brine sample had a pH of around 7.8, which is close to the optimum pH chosen for the adsorption studies. Therefore, the real brine sample could be effectively used for the adsorption of valuable metals as soon as it is rejected

from the desalination plant, which would provide various other industries with valuable metals for their productions. Tables 21, 22, and 23 represent the adsorbed concentrations of the various metals in the collected reverse osmosis brine sample by RDP, RDP-FC-Cu, and RDP-FC-Ni, respectively. As a general observation from tables 19 – 21, all adsorbents were capable of adsorbing the whole amounts of barium, cesium, lanthanide, lead, vanadium, zinc, and strontium from the brine sample. For the other metals present in the brine sample, each metal showed unique adsorptive capabilities. For example, RDP was capable of adsorbing the highest amount of sodium and potassium followed by RDP-FC-Ni then RDP-FC-Cu. However, RDP-FC-Cu and RDP-FC-Ni achieved full recovery of calcium ions, while RDP adsorbed around 77065 mg/L of the initial amount of 77120 mg/L. Moreover, RDP-FC-Cu and RDP-FC-Ni achieved a higher and similar recovery of magnesium ions than RDP. For iron and lithium, both composites at study showed a full recovery while RDP achieved recoveries of 24.85 mg/L and 43.85 mg/L from the initial amounts of 30.5 mg/L and 44.2 mg/L respectively. Overall, RDP was capable of fully adsorbing 7 metals while RDP-FC-Cu and RDP-FC-Ni both adsorbed 10 metals of an initial amount of 13 metals. It is worth noting that both composites showed remarkable adsorption capabilities for the target metals at study: lithium and strontium. This demonstrates the great potential of the prepared composites in recovering and adsorbing various metals from the collected reverse osmosis brine sample. Consequently, it can be concluded that previous adsorption experiments are justified and proven to be successful for the aim of this study: to recover valuable metals efficiently and sustainably from reverse osmosis desalination brines.

Table 21. Comparison between the initial metal concentrations and the adsorbed concentrations from the collected reverse osmosis brine using RDP

Metal	Initial concentration (mg/L)	Concentration after adsorption (mg/L)	Adsorbed concentration (mg/L)
Na^{+}	643,50	457.00	63893.00
Ca^{2+}	77120.00	54.57	77065.43
K^{+}	151300.00	111.80	151188.20
Mg^{2+}	238800.00	135.50	238664.50
Ba^{2+}	3.30	<dl	3.30
Cs^{+}	3.40	<dl	3.40
In	4.50	<dl	4.50
Fe	30.50	5.65	24.85
Pb	10.10	<dl	10.10
Li^{+}	44.20	0.35	43.85
V	68.70	<dl	68.70
Zn^{2+}	256.40	<dl	256.40
Sr^{2+}	447.00	<dl	447.00

Table 22. Comparison between the initial metal concentrations and the adsorbed concentrations from the collected reverse osmosis brine using RDP-FC-Cu

Metal	Initial concentration (mg/L)	Concentration after adsorption(mg/L)	Adsorbed concentration
Na^{+}	643,50	673.70	63676.30
Ca^{2+}	77120.00	<dl	771,20
K^{+}	151300.00	693.55	150606.45
Mg^{2+}	238800.00	37.53	238762.47
Ba^{2+}	3.30	<dl	3.30
Cs^{+}	3.40	<dl	3.40
In	4.50	<dl	4.50
Fe	30.50	<dl	30.50
Pb	10.10	<dl	10.10
Li^{+}	44.20	<dl	44.20
V	68.70	<dl	68.70
Zn^{2+}	256.40	<dl	256.40
Sr^{2+}	447.00	<dl	447.00

Table 23. Comparison between the initial metal concentrations and the adsorbed concentrations from the collected reverse osmosis brine using RDP-FC-Ni

Metal	Initial concentration (mg/L)	Concentration after adsorption(mg/L)	Adsorbed concentration
Na^{+}	643,50	592.84	63757.16
Ca^{2+}	77120.00	<dl	771,20
K^{+}	151300.00	634.80	150665.20
Mg^{2+}	238800.00	33.62	238766.38
Ba^{2+}	3.30	<dl	3.30
Cs^{+}	3.40	<dl	3.40
In	4.50	<dl	4.50
Fe	30.50	<dl	30.50
Pb	10.10	<dl	10.10
Li^{+}	44.20	<dl	44.20
V	68.70	<dl	68.70
Zn^{2+}	256.40	<dl	256.40
Sr^{2+}	447.00	<dl	447.00

CONCLUSIONS

As a global trend, there has been a continuous increase in population and economic growths, development, urbanization, and industrialization. These are considered human-derived factors that contribute to the overall amounts of water that are available for human use in countries. As a result, water demands in the world are increasing substantially. In the semi-arid to the arid oil-rich peninsula; Qatar, water demands are accelerating substantially every year. Desalination of seawater mainly through reverse osmosis technology is the ultimate and only source of freshwater in Qatar. The desalination industry requires significant amounts of energy, cost, and specific operating conditions. In addition, desalination of seawater produces great amounts of concentrated brine, as well as pollutants like pre-treatment chemicals, detergents, and toxic wastes. These pollutants have been proven by many studies to be extremely dangerous to aquatic and wildlife as well as human beings. To add to the issue, the conventional brine management methods such as direct environmental disposal and zero discharge brine recovery technologies require energy, cost, and involve the production of many pollutants that could severely pollute the environment and cause sustainability issues. Therefore, there is an urgent need for a novel, efficient, and environmentally safe brine treatment, and recovery method. On the positive side, concentrated seawater desalination brine streams often contain various valuable metals that if extracted properly, could serve important economic and commercial purposes. For example, lithium has been reported to be found in seawater reverse osmosis brine and it could be used in the production of batteries, vehicles, and ceramics. In addition, strontium is a valuable and rare alkaline earth metal that is often used in the pharmaceutical industry and manufacturing glass and ceramics. Qatar is a home country to palm trees where the production of date pits as waste is extremely high. The

utilization of date pits in a roasted form as well as chemically modified with potassium metal hexacyanoferrates for the adsorption and recovery of lithium and strontium metals from reverse osmosis brine in Qatar has been investigated by this study. Physiochemical characterization of the reverse osmosis brine such as ICP-OES, pH, salinity, conductivity, FTIR, SEM-EDX, and XRD are the first objectives of this study in order to fully understand the characteristics of the brine solution for adsorption. In addition, extensive physiochemical characterization of the prepared RDP, RDP-FC-Cu, and RDP-FC-Ni through many analytical techniques was done. For example, SEM, particle size distribution test, Brunauer–Emmett– Teller (BET) surface area test, pore size, and volume distribution test, carbon and nitrogen elemental analysis, XRD, FTIR, and TGA were done for the three adsorbents. All the adsorbents showed great thermal stability, porosity, functional groups, chemical structure, and composition as well as other adsorptive characteristics. Unique physical and chemical changes occurred on the RDP-FC-Cu and RDP-FC-Ni such as higher surface area, functional groups as well as composition and structure. Moreover, three of the most influential factors that affect the adsorption processes were studied namely, the effect of solution pH and zeta potential, metal-ion concentration, and temperature. The adsorption of lithium and strontium onto the three adsorbents favored a pH of 6 as well as increasing metal concentration and temperature. However, it was found that generally, RDP-FC-Cu and RDP-FC-Ni achieved greater adsorption capacities and efficiencies for lithium than RDP. Interestingly, RDP-FC-Cu accounted for overall slightly higher adsorption and selectivity for lithium. On the other hand, RDP-FC-Ni achieved the highest adsorption capacity and selectivity towards strontium followed by RDP-FC-Cu and then RDP. These trends are due to many factors like higher pore radius and volumes, the cubic lattice structure, similar hydrated ionic radius of lithium, copper, and potassium, which

facilitated the metal substitution and complexation onto the RDP-FC-Cu and RDP-FC-Ni. Furthermore, the well-established adsorption isotherm models: Langmuir and Freundlich as well as the adsorption thermodynamics (Gibbs free energy, (ΔG), enthalpy ($\Delta H°$) and entropy ($\Delta S°$) were studied to examine and understand the mechanisms as well as sponeousity, and favorability of lithium adsorption onto the three adsorbents. The isotherm models revealed a variety of adsorption mechanisms for lithium unique to each adsorbent. The adsorption of lithium onto the three adsorbents was found to be endothermic, spontaneous, and favorable. The desorption study was performed to examine the possibility of regenerating and re-using the adsorbents for multiple adsorption cycles. The results revealed exceptional and high desorption percentages for both metals from all the adsorbents. Moreover, the selectivity of all the adsorbents towards lithium and strontium from a mixture solution was tested. Interestingly, RDP-FC-Cu showed the highest selectivity towards lithium with high simultaneous adsorption of strontium. RDP-FC-Ni demonstrated a similar result with the highest selectivity towards strontium. RDP revealed its great adsorptive properties through achieving high adsorption capacities towards both metals in the mixture solution. The adsorption of the real brine by the three adsorbents showed high selectivity towards both target metals as well as various other metals. The results of this study stress the main aim of this study, which is to create sustainable opportunities for the safe management of desalination brine and agricultural wastes.

REFERENCES

Abbas, K., & Marji, D. (2005). Oxidation of Triethylamine by Ferricyanide Ions in the Presence of Sodium Hydroxide and Potassium Hydroxide. *Zeitschrift Für Naturforschung A*, *60*(8-9), 667-671. doi: 10.1515/zna-2005-8-918.

Abbas, M. (2020). Modeling of adsorption isotherms of heavy metals onto Apricot stone activated carbon: Two-parameter models and equations allowing determination of thermodynamic parameters. *Materials Today: Proceedings*. doi: 10.1016/j.matpr.2020.05.320.

Abd Mutalib, M., Rahman, M., Othman, M., Ismail, A., & Jaafar, J. (2017). Scanning Electron Microscopy (SEM) and Energy-Dispersive X-Ray (EDX) Spectroscopy. *Membrane Characterization*, 161-179. doi: 10.1016/b978-0-444-63776-5.00009-7.

Abdelrazeq, H., Khraisheh, M., Al Momani, F., McLeskey, J., Hassan, M., Gad-el-Hak, M., & Tafreshi, H. (2020). Performance of electrospun polystyrene membranes in synthetic produced industrial water using direct-contact membrane distillation. *Desalination*, *493*, 114663. doi: 10.1016/j.desal.2020.114663.

Abdou, S., & Moharam, H. (2019). Characterization of table salt samples from different origins and ESR detection of the induced effects due to gamma irradiation. *Journal Of Physics: Conference Series*, *1253*, 012036. doi: 10.1088/1742-6596/1253/1/012036.

Abdullah, N., Shameli, K., Abdullah, E., & Abdullah, L. (2019). Solid matrices for fabrication of magnetic iron oxide nanocomposites: Synthesis, properties, and application for the adsorption of heavy metal ions and dyes. *Composites Part B: Engineering*, *162*, 538-568. doi: 10.1016/j.compositesb.2018.12.075.

Ahmadvand, S., Abbasi, B., Azarfar, B., Elhashimi, M., Zhang, X., & Abbasi, B. (2019). Looking Beyond Energy Efficiency: An Applied Review of Water Desalination Technologies and an Introduction to Capillary-Driven Desalination. *Water*, *11*(4), 696.

doi: 10.3390/w11040696.

Akpomie, K., Dawodu, F., & Adebowale, K. (2015). Mechanism on the sorption of heavy metals from binary-solution by a low cost montmorillonite and its desorption potential. *Alexandria Engineering Journal,* 54, 757-767.

Al-Anzi, B., Al-Rashidi, A., Abraham, L., Fernandes, J., Al-Sheikh, A., & Alhazza, A. (2020). Brine management from desalination plants for salt production utilizing high current density electrodialysis-evaporator hybrid system: A case study in Kuwait. *Desalination, 498,* 114760. doi: 10.1016/j.desal.2020.114760.

Albatrni, H., Qiblawey, H., & El-Naas, M. (2021). Comparative study between adsorption and membrane technologies for the removal of mercury. *Separation And Purification Technology, 257,* 117833. doi: 10.1016/j.seppur.2020.117833.

Albroomi, I. H., Elsayed, A. M., Baraka, A., & Abdelmaged, A. M. (2017). Batch and fixed-bed adsorption of tartrazine azo-dye onto activated carbon prepared from apricot stones. *Applied Water Science*, 7, 2063-2074.

Albroomi, I. H., Elsayed, A. M., Baraka, A., & Abdelmaged, A. M. (2017). Batch and fixed-bed adsorption of tartrazine azo-dye onto activated carbon prepared from apricot stones. *Applied Water Science*, 7, 2063-2074.

Albroomi, I. H., Elsayed, A. M., Baraka, A., & Abdelmaged, A. M. (2017). Batch and fixed-bed adsorption of tartrazine azo-dye onto activated carbon prepared from apricot stones. Applied Water Science, 7, 2063-2074. DOI 10.1007/s13201016-0387-2.

Aldawsari, A., Khan, M., Hameed, B., Alqadami, A., Siddiqui, M., Alothman, Z., & Ahmed, A. (2017). Mercerized mesoporous date pit activated carbon—A novel adsorbent to sequester potentially toxic divalent heavy metals from water. *PLOS ONE, 12*(9), e0184493. doi: 10.1371/journal.pone.0184493.

Al-Ghouti, M., & Al-Absi, R. (2020). Mechanistic understanding of the adsorption and

thermodynamic aspects of cationic methylene blue dye onto cellulosic olive stones biomass from wastewater. *Scientific Reports*, *10*(1). doi: 10.1038/s41598-020-72996-3.

Al-Ghouti, M., & Dib, S. (2020). Utilization of nano-olive stones in environmental remediation of methylene blue from water. *Journal Of Environmental Health Science And Engineering*, *18*(1), 63-77. doi: 10.1007/s40201-019-00438-y.

Al-Ghouti, M., Al Disi, Z., Al-Kaabi, N., & Khraisheh, M. (2017). Mechanistic insights into the remediation of bromide ions from desalinated water using roasted date pits. *Chemical Engineering Journal*, 308, 463-475.

Al-Ghouti, M., Da'ana, D., Abu-Dieyeh, M., & Khraisheh, M. (2019). Adsorptive removal of mercury from water by adsorbents derived from date pits. *Scientific Reports*, *9*(1). doi: 10.1038/s41598-019-51594-y.

Al-Ghouti, M., Li, J., Salamh, Y., Al-Laqtah, N., Walker, G., & Ahmad, M. (2010). Adsorption mechanisms of removing heavy metals and dyes from aqueous solution using date pits solid adsorbent. *Journal Of Hazardous Materials*, *176*(1-3), 510-520. doi: 10.1016/j.jhazmat.2009.11.059.

Ali Osman, N. (2014). Chemical Characterization, Antioxidant and Enzymatic Activity of Brines from Scandinavian Marinated Herring Products. *Journal Of Food Processing & Technology*, *05*(07). doi: 10.4172/2157-7110.1000346.

Ali, A., Quist-Jensen, C., Jørgensen, M., Siekierka, A., Christensen, M., & Bryjak, M. et al. (2020). A review of membrane crystallization, forward osmosis and membrane capacitive deionization for liquid mining. *Resources, Conservation And Recycling*, 105273. doi: 10.1016/j.resconrec.2020.105273.

Almasri, D., Kayvani Fard, A., McKay, G., Kochkodan, V., & Atieh, M. (2020). A novel adsorptive ceramic membrane for efficient strontium removal. *Journal Of Water Process Engineering*, *37*, 101538. doi: 10.1016/j.jwpe.2020.101538.

Alnouri, S., Linke, P., & El-Halwagi, M. (2018). Accounting for central and distributed zero liquid discharge options in interplant water network design. *Journal Of Cleaner Production*, *171*, 644-661. doi: 10.1016/j.jclepro.2017.09.236.

Al-Saad, K., El-Azazy, M., Issa, A., Al-Yafie, A., El-Shafie, A., Al-Sulaiti, M., & Shomar, B. (2019). Recycling of Date Pits Into a Green Adsorbent for Removal of Heavy Metals: A Fractional Factorial Design-Based Approach. *Frontiers In Chemistry*, *7*. doi: 10.3389/fchem.2019.00552.

Al-Saad, K., El-Azazy, M., Issa, A., Al-Yafie, A., El-Shafie, A., Al-Sulaiti, M., & Shomar, B. (2019). Recycling of Date Pits Into a Green Adsorbent for Removal of Heavy Metals: A Fractional Factorial Design-Based Approach. *Frontiers In Chemistry*, *7*. doi: 10.3389/fchem.2019.00552.

Al-Saad, K., El-Azazy, M., Issa, A., Al-Yafie, A., El-Shafie, A., Al-Sulaiti, M., & Shomar, B. (2019). Recycling of Date Pits Into a Green Adsorbent for Removal of Heavy Metals: A Fractional Factorial Design-Based Approach. *Frontiers In Chemistry*, *7*. doi: 10.3389/fchem.2019.00552.

Alshahri, F. (2016). Heavy metal contamination in sand and sediments near to disposal site of reject brine from desalination plant, Arabian Gulf: Assessment of environmental pollution. *Environmental Science And Pollution Research*, *24*(2), 1821-1831. doi: 10.1007/s11356-016-7961-x.

Al-Shammari, S., & Ali, L. (2018). Effect of Brine Disposal on Seawater Quality at Az-Zour Desalination Plant in Kuwait: Physical and Chemical Properties. *Journal Of Environmental Science And Engineering A*, *7*(5). doi: 10.17265/2162-5298/2018.05.001.

Alves, A., Martorano, L., Florentino, G., Lasmar, D., Miranda, Í., Lisboa, L., & da Silva Chaar, J. (2020). Thermal Diagnosis of Heat Conduction and Combustion Time of Fruits of

the Brazil Nut Tree (<i>Bertholletia excelsa</i> Bonpl.). *Advances In Bioscience And Biotechnology, 11*(02), 60-71. doi: 10.4236/abb.2020.112005.

Al-Yousef, H., Alotaibi, B., Aouaini, F., Sellaoui, L., & Bonilla-Petriciolet, A. (2021). Adsorption of ibuprofen on cocoa shell biomass-based adsorbents: Interpretation of the adsorption equilibrium via statistical physics theory. *Journal Of Molecular Liquids*, 115697. doi: 10.1016/j.molliq.2021.115697.

Amy G, Ghaffour N, Li Z, Francis L, Linares RV, Missimer T, Lattemann S (2017) Membrane-based seawater desalination: present and future prospects. *Desalination* 2(401),16–21.

Apolinário, F., & Pires, A. (2020). Oil displacement by multicomponent slug injection: An analytical solution for Langmuir adsorption isotherm. *Journal Of Petroleum Science And Engineering*, 107939. doi: 10.1016/j.petrol.2020.107939.

Ariono, D., Purwasasmita, M., & Wenten, I. (2016). Brine Effluents: Characteristics, Environmental Impacts, and Their Handling. *Journal Of Engineering And Technological Sciences, 48*(4), 367-387. doi: 10.5614/j.eng.technol.sci.2016.48.4.1.

Arslanoğlu, H. (2021). Production of low-cost adsorbent with small particle size from calcium carbonate rich residue carbonatation cake and their high performance phosphate adsorption applications. *Journal Of Materials Research And Technology, 11*, 428-447. doi: 10.1016/j.jmrt.2021.01.054.

Asyana, V., Haryanto, F., Fitri, L., Ridwan, T., Anwary, F., & Soekersi, H. (2016). Analysis of urinary stone based on a spectrum absorption FTIR-ATR. *Journal Of Physics: Conference Series, 694*, 012051. doi: 10.1088/1742-6596/694/1/012051.

Awwad, N., El-Zahhar, A., Fouda, A., & Ibrahium, H. (2013). Removal of heavy metal ions from ground and surface water samples using carbons derived from date pits. *Journal Of Environmental Chemical Engineering*, *1*(3), 416-423. doi: 10.1016/j.jece.2013.06.006.

Baalousha, H., & Ouda, O. (2017). Domestic water demand challenges in Qatar. *Arabian Journal Of Geosciences*, *10*(24). doi: 10.1007/s12517-017-3330-4.

Baalousha, H., & Ouda, O. (2017). Domestic water demand challenges in Qatar. *Arabian Journal Of Geosciences*, *10*(24). doi: 10.1007/s12517-017-3330-4.

Bagheri, H., Rezvani, O., Zeinali, S., Asgari, S., Aqda, T., & Manshaei, F. (2020). Electrospun nanofibers. *Solid-Phase Extraction*, 311-339. doi: 10.1016/b978-0-12-816906-3.00011-x.

Banat, F., Al-Asheh, S., & Al-Rousan, D. (2002). A Comparative Study of Copper and Zinc Ion Adsorption on to Activated and Non-activated Date-pits. *Adsorption Science & Technology*, *20*(4), 319-335. doi: 10.1260/026361702760295515.

Bang, J., Yoo, Y., Lee, S., Song, K., & Chae, S. (2017). CO2 Mineralization Using Brine Discharged from a Seawater Desalination Plant. *Minerals*, *7*(11), 207. doi: 10.3390/min7110207.

Belatoui, A., Bouabessalam, H., Hacene, O., de-la-Ossa-Carretero, J., Martinez-Garcia, E., & Sanchez-Lizaso, J. (2017). Environmental effects of brine discharge from two desalinations plants in Algeria (South Western Mediterranean). *DESALINATION AND WATER TREATMENT, 76*, 311-318. doi: 10.5004/dwt.2017.20812.

Berthomieu, C., & Hienerwadel, R. (2009). Fourier transform infrared (FTIR) spectroscopy. *Photosynthesis Research*, *101*(2-3), 157-170. doi: 10.1007/s11120-009-9439-x.

Berthomieu, C., & Hienerwadel, R. (2009). Fourier transform infrared (FTIR) spectroscopy. *Photosynthesis Research*, *101*(2-3), 157-170. doi: 10.1007/s11120-009-9439-x.

Borhade, V. A., & Kale, S. A. (2017). Calcined eggshell as a cost effective material for removal of dyes from aqueous solution. *Applied Water Sciences*, 7(8), 4255—4268.

Borja-Urzola, A., García-Gómez, R., Bernal-González, M., & Durán-Domínguez-de-Bazúa,

M. (2021). Chitosan-calcite from shrimp residues: A low-cost adsorbent for three triazines removal from aqueous media. *Materials Today Communications*, *26*, 102131. doi: 10.1016/j.mtcomm.2021.102131.

Brine Treatment ZLD. (2020). Retrieved 27 March 2020, from https://www.lenntech.com/processes/brine-treatment-ZLD.htm.

Bruckner, M. Z. (2020). Ion Chromatography. Retrieved from: https://serc.carleton.edu/microbelife/research_methods/biogeochemical/ic.html.

Burakov, A., Galunin, E., Burakova, I., Kucherova, A., Agarwal, S., Tkachev, A., et al. (2017). Adsorption of heavy metals on conventional and nanostructured materials for wastewater treatment purposes: a review. Ecotoxicol. Environ. Saf. 148, 702–712. doi: 10.1016/j.ecoenv.2017.11.034.

Buthiyappan, A., Gopalan, J., & Abdul Raman, A. (2019). Synthesis of iron oxides impregnated green adsorbent from sugarcane bagasse: Characterization and evaluation of adsorption efficiency. *Journal Of Environmental Management*, *249*, 109323. doi: 10.1016/j.jenvman.2019.109323.

Buyang, S., Yi, Q., Cui, H., Wan, K., & Zhang, S. (2019). Distribution and adsorption of metals on different particle size fractions of sediments in a hydrodynamically disturbed canal. *Science Of The Total Environment*, *670*, 654-661. doi: 10.1016/j.scitotenv.2019.03.276.

Cámara-Martos, F., & Moreno-Rojas, R. (2016). Zinc: Properties and Determination. *Encyclopedia Of Food And Health*, 638-644. doi: 10.1016/b978-0-12-384947-2.00768-6.

Can, N., Ömür, B., & Altındal, A. (2016). Modeling of heavy metal ion adsorption isotherms onto metallophthalocyanine film. *Sensors And Actuators B: Chemical*, *237*, 953-961. doi: 10.1016/j.snb.2016.07.026.

Castro, M., Alcanzare, M., Esparcia, E., & Ocon, J. (2020). A Comparative Techno-Economic Analysis of Different Desalination Technologies in Off-Grid Islands. *Energies*, *13*(9), 2261. doi: 10.3390/en13092261.

Chan, W., Warren, J., Krieger, S., Vestal, B., & Harrison, R. (2020). Separation and preconcentration of perrhenate from ionic solutions by ion exchange chromatography. *Journal Of Chromatography A*, *1631*, 461588. doi: 10.1016/j.chroma.2020.461588.

Chang, C., Chau, L., Hu, W., Wang, C., & Liao, J. (2008). Nickel hexacyanoferrate multilayers on functionalized mesoporous silica supports for selective sorption and sensing of cesium. *Microporous And Mesoporous Materials*, *109*(1-3), 505-512. doi: 10.1016/j.micromeso.2007.05.057.

Cha-umpong, W., Li, Q., Razmjou, A., & Chen, V. (2021). Concentrating brine for lithium recovery using GO composite pervaporation membranes. *Desalination*, *500*, 114894. doi: 10.1016/j.desal.2020.114894.

Chen, M., Dollar, O., Shafer-Peltier, K., Randtke, S., Waseem, S., & Peltier, E. (2020). Boron removal by electrocoagulation: Removal mechanism, adsorption models and factors influencing removal. *Water Research*, *170*, 115362. doi: 10.1016/j.watres.2019.115362.

Chong, S., Wu, Y., Guo, S., Liu, Y., & Cao, G. (2019). Potassium nickel hexacyanoferrate as cathode for high voltage and ultralong life potassium-ion batteries. *Energy Storage Materials*, *22*, 120-127. doi: 10.1016/j.ensm.2019.07.003.

Chowdhury, A., Kumari, S., Khan, A., Chandra, M., & Hussain, S. (2020). Activated carbon loaded with Ni-Co-S nanoparticle for superior adsorption capacity of antibiotics and dye from wastewater: Kinetics and isotherms. *Colloids And Surfaces A: Physicochemical And Engineering Aspects*, 125868. doi: 10.1016/j.colsurfa.2020.125868.

Comparison of ICP-OES and ICP-MS for Trace Element Analysis. (2020). Retrieved from: https://www.thermofisher.com/qa/en/home/industrial/environmental/environmental-learning-center/contaminant-analysis-information/metal-analysis/comparison-icp-oes-icp-ms-trace-element-analysis.html.

Cui, J., Sun, T., Chen, L., & Zhang, W. (2020). Engineering salt tolerance of photosynthetic cyanobacteria for seawater utilization. *Biotechnology Advances*, *43*, 107578. doi: 10.1016/j.biotechadv.2020.107578.

D'Odorico, P., Carr, J., Dalin, C., Dell'Angelo, J., Konar, M., & Laio, F. et al. (2019). Global virtual water trade and the hydrological cycle: patterns, drivers, and socio-environmental impacts. *Environmental Research Letters*, *14*(5), 053001. doi: 10.1088/1748-9326/ab05f4.

Dai, L., Nudelman, F., Chu, C., Lo, E., & Mei, M. (2021). The effects of strontium-doped bioactive glass and fluoride on hydroxyapatite crystallization. *Journal Of Dentistry*, *105*, 103581. doi: 10.1016/j.jdent.2021.103581.

Damkjaer, S., & Taylor, R. (2017). The measurement of water scarcity: Defining a meaningful indicator. *Ambio*, *46*(5), 513-531. doi: 10.1007/s13280-017-0912-z.

Das, D., Jaya Sre Varshini, C., & Das, N. (2014). Recovery of lanthanum(III) from aqueous solution using biosorbents of plant and animal origin: Batch and column studies. *Minerals Engineering*, *69*, 40-56. doi: 10.1016/j.mineng.2014.06.013.

Dawoud, M. (2012). Environmental Impacts of Seawater Desalination: Arabian Gulf Case Study. *International Journal Of Environment And Sustainability*, *1*(3). doi: 10.24102/ijes.v1i3.96.

Deliyanni Eleni, A., Kyzas George, Z., Triantafyllidis Kostas, S., and Matis Kostas, A. (2015). Activated carbons for the removal of heavy metal ions: a systematic review of recent literature focused on lead and arsenic ions. In Open Chem. 13, 699–708. doi:

10.1515/chem-2015-0087.

Díaz Nieto, C., Palacios, N., Verbeeck, K., Prévoteau, A., Rabaey, K., & Flexer, V. (2019). Membrane electrolysis for the removal of Mg2+ and Ca2+ from lithium rich brines. *Water Research, 154*, 117-124. doi: 10.1016/j.watres.2019.01.050

Dou, W., Liu, J., & Li, M. (2021). Competitive adsorption of Cu2+ in Cu2+, Co2+ and Ni2+ mixed multi–metal solution onto graphene oxide (GO)–based hybrid membranes. *Journal Of Molecular Liquids, 322*, 114516. doi: 10.1016/j.molliq.2020.114516.

Dovidauskas, S., Okada, I., & dos Santos, F. (2020). Validation of a simple ion chromatography method for simultaneous determination of glyphosate, aminomethylphosphonic acid and ions of Public Health concern in water intended for human consumption. *Journal Of Chromatography A, 1632*, 461603. doi: 10.1016/j.chroma.2020.461603.

Du, C., Zuo, R., Chen, M., Wang, J., Liu, X., Liu, L., & Lin, Y. (2020). Influence of colloidal Fe(OH)3 on the adsorption characteristics of strontium in porous media from a candidate high-level radioactive waste geological disposal site. *Environmental Pollution, 260*, 113997. doi: 10.1016/j.envpol.2020.113997.

Du, C., Zuo, R., Chen, M., Wang, J., Liu, X., Liu, L., & Lin, Y. (2020). Influence of colloidal Fe(OH)3 on the adsorption characteristics of strontium in porous media from a candidate high-level radioactive waste geological disposal site. *Environmental Pollution, 260*, 113997. doi: 10.1016/j.envpol.2020.113997.

Du, C., Zuo, R., Chen, M., Wang, J., Liu, X., Liu, L., & Lin, Y. (2020). Influence of colloidal Fe(OH)3 on the adsorption characteristics of strontium in porous media from a candidate high-level radioactive waste geological disposal site. *Environmental Pollution, 260*, 113997. doi: 10.1016/j.envpol.2020.113997.

El-Azazy, M., El-Shafie, A., Issa, A., Al-Sulaiti, M., Al-Yafie, J., Shomar, B., & Al-Saad, K.

(2019). Potato Peels as an Adsorbent for Heavy Metals from Aqueous Solutions: Eco-Structuring of a Green Adsorbent Operating Plackett–Burman Design. *Journal Of Chemistry*, *2019*, 1-14. doi: 10.1155/2019/4926240.

El-Bahy, S., Fadel, D., El-Bahy, Z., & Metwally, A. (2018). Rapid and highly efficient cesium removal by newly synthesized carbomer encapsulated potassium copper hexacyanoferrate composite. *Journal Of Environmental Chemical Engineering*, *6*(2), 1875-1885. doi: 10.1016/j.jece.2018.02.030.

El-Bahy, S., Fadel, D., El-Bahy, Z., & Metwally, A. (2018). Rapid and highly efficient cesium removal by newly synthesized carbomer encapsulated potassium copper hexacyanoferrate composite. *Journal Of Environmental Chemical Engineering*, *6*(2), 1875-1885. doi: 10.1016/j.jece.2018.02.030

Elsaid, K., Sayed, E., Abdelkareem, M., Baroutaji, A., & Olabi, A. (2020). Environmental impact of desalination processes: Mitigation and control strategies. *Science Of The Total Environment*, *740*, 140125. doi: 10.1016/j.scitotenv.2020.140125.

Engwayu, J., & Pawlik, M. (2020). Adsorption of anionic polymers on hematite – a study of zeta potential distributions. *Minerals Engineering*, *148*, 106225. doi: 10.1016/j.mineng.2020.106225.

Erabee, I., Ahsan, A., Nik Daud, N., Idrus, S., Shams, S., Md Din, M., & Rezania, S. (2017). Manufacture of Low-cost Activated Carbon Using Sago Palm Bark and Date Pits by Physiochemical Activation. *Bioresources*, *12*(1). doi: 10.15376/biores.12.1.1916-1923.

Ezzati, R. (2020). Derivation of Pseudo-First-Order, Pseudo-Second-Order and Modified Pseudo-First-Order rate equations from Langmuir and Freundlich isotherms for adsorption. *Chemical Engineering Journal*, *392*, 123705. doi: 10.1016/j.cej.2019.123705.

Fallah, N., & Taghizadeh, M. (2020). Continuous fixed-bed adsorption of Mo(VI) from aqueous solutions by Mo(VI)-IIP: Breakthrough curves analysis and mathematical modeling. *Journal Of Environmental Chemical Engineering*, *8*(5), 104079. doi: 10.1016/j.jece.2020.104079.

Fan, X., Ma, Z., Zou, Y., Liu, J., & Hou, J. (2021). Investigation on the adsorption and desorption behaviors of heavy metals by tire wear particles with or without UV ageing processes. *Environmental Research*, *195*, 110858. doi: 10.1016/j.envres.2021.110858.

Faustino, P., Brown, A., Lowry, B., Yang, Y., Wang, Y., & Khan, M. et al. (2019). Quantitative evaluation of the thallium binding of soluble and insoluble Prussian blue hexacyanoferrate analogs: A scientific comparison based on their critical quality attributes. *International Journal Of Pharmaceutics*, *569*, 118600. doi: 10.1016/j.ijpharm.2019.118600.

Flexer, V., Baspineiro, C., & Galli, C. (2018). Lithium recovery from brines: A vital raw material for green energies with a potential environmental impact in its mining and processing. *Science Of The Total Environment*, *639*, 1188-1204. doi: 10.1016/j.scitotenv.2018.05.223.

Forghani, M., Azizi, A., Livani, M., & Kafshgari, L. (2020). Adsorption of lead(II) and chromium(VI) from aqueous environment onto metal-organic framework MIL-100(Fe):

Fotoohi, B., & Mercier, L. (2014). Recovery of precious metals from ammoniacal thiosulfate solutions by hybrid mesoporous silica: 1-Factors affecting gold adsorption. *Separation And Purification Technology*, *127*, 84-96. doi: 10.1016/j.seppur.2014.02.024.

Gao, X., Liu, J., Li, M., Guo, C., Long, H., Zhang, Y., & Xin, L. (2020). Mechanistic study of selective adsorption and reduction of Au (III) to gold nanoparticles by ion-imprinted porous alginate microspheres. *Chemical Engineering Journal*, *385*, 123897. doi:

10.1016/j.cej.2019.123897.

Gao, X., Liu, J., Li, M., Guo, C., Long, H., Zhang, Y., & Xin, L. (2020). Mechanistic study of selective adsorption and reduction of Au (III) to gold nanoparticles by ion-imprinted porous alginate microspheres. *Chemical Engineering Journal*, *385*, 123897. doi: 10.1016/j.cej.2019.123897.

Gao, Z., Bandosz, T., Zhao, Z., Han, M., & Qiu, J. (2009). Investigation of factors affecting adsorption of transition metals on oxidized carbon nanotubes. *Journal Of Hazardous Materials*, *167*(1-3), 357-365. doi: 10.1016/j.jhazmat.2009.01.050.

Gao, Z., Bandosz, T., Zhao, Z., Han, M., & Qiu, J. (2009). Investigation of factors affecting adsorption of transition metals on oxidized carbon nanotubes. *Journal Of Hazardous Materials*, *167*(1-3), 357-365. doi: 10.1016/j.jhazmat.2009.01.050.

Gaztañaga, F., Sandoval, M., Luna, C., & Jasen, P. (2020). Theoretical study about alkali metal adsorption on pristine and defective (8,0) SWCNT: Geometrical, magnetic and electronic changes. *Applied Surface Science*, *513*, 145769. doi: 10.1016/j.apsusc.2020.145769.

Ghaffour, N., Missimer, T., & Amy, G. (2012). Combined desalination, water reuse, and aquifer storage and recovery to meet water supply demands in the GCC/MENA region. *Desalination And Water Treatment*, *51*(1-3), 38-43. doi: 10.1080/19443994.2012.700034.

Gibert, O., Valderrama, C., Peterkóva, M., & Cortina, J. L. (2010). *Solvent Extr. Ion Exch*., 28, 543–562.

Giwa, A., Dufour, V., Al Marzooqi, F., Al Kaabi, M., & Hasan, S. (2017). Brine management methods: Recent innovations and current status. *Desalination*, 407, 1-23. http://dx.doi.org/10.1016/j.desal.2016.12.008.

Goyal, N., Gao, P., Wang, Z., Cheng, S., Ok, Y., Li, G., & Liu, L. (2020). Nanostructured

chitosan/molecular sieve-4A an emergent material for the synergistic adsorption of radioactive major pollutants cesium and strontium. *Journal Of Hazardous Materials, 392,* 122494. doi: 10.1016/j.jhazmat.2020.122494.

Goyal, N., Gao, P., Wang, Z., Cheng, S., Ok, Y., Li, G., & Liu, L. (2020). Nanostructured chitosan/molecular sieve-4A an emergent material for the synergistic adsorption of radioactive major pollutants cesium and strontium. *Journal Of Hazardous Materials, 392,* 122494. doi: 10.1016/j.jhazmat.2020.122494.

Gude, V. (2017). Desalination and water reuse to address global water scarcity. *Reviews In Environmental Science And Bio/Technology*, *16*(4), 591-609. doi: 10.1007/s11157-017-9449-7.

Guo, X., Jiang, X., Zhu, Y., & Zhuang, S. (2019). Unified description on principles of fourier transform infrared spectroscopy and terahertz time-domain spectroscopy. *Infrared Physics & Technology, 101,* 105-109. doi: 10.1016/j.infrared.2019.06.005.

Guo, X., Jiang, X., Zhu, Y., & Zhuang, S. (2019). Unified description on principles of fourier transform infrared spectroscopy and terahertz time-domain spectroscopy. *Infrared Physics & Technology, 101,* 105-109. doi: 10.1016/j.infrared.2019.06.005.

Habiyaremye, A. (2020). Water innovation in South Africa: Mapping innovation successes and diffusion constraints. *Environmental Science & Policy, 114,* 217-229. doi: 10.1016/j.envsci.2020.08.011.

Hawari, A., Khraisheh, M., & Al-Ghouti, M. (2014). Characteristics of olive mill solid residue and its application in remediation of Pb2+, Cu2+ and Ni2+ from aqueous solution: Mechanistic study. Chemical Engineering Journal, 251, 329-336.

Henrique, A., Rodrigues, A., & Silva, J. (2020). Fixed bed dynamics of single and multicomponent adsorption of pentane and hexane isomers in ZIF-8. *Separation And Purification Technology, 238,* 116419. doi: 10.1016/j.seppur.2019.116419.

Hilal, N., Ahmed, I. & El-Sayed, R. (2012). Activated and Nonactivated Date Pits Adsorbents for the Removal of Copper(II) and Cadmium(II) from Aqueous Solutions. *Int. Sch. Res. Notices Phys. Chem.*, 1–11.

Holder, C., & Schaak, R. (2019). Tutorial on Powder X-ray Diffraction for Characterizing Nanoscale Materials. *ACS Nano, 13*(7), 7359-7365. doi: 10.1021/acsnano.9b05157.

Höllriegl, V. (2019). Other Environmental Health Issues: Strontium in the Environment and Possible Human Health Effects. *Encyclopedia Of Environmental Health*, 797-802. doi: 10.1016/b978-0-12-409548-9.11195-9.

Honarparvar Ramlow, H., Ferreira, R., Marangoni, C., & Machado, R. (2019). Ceramic membranes applied to membrane distillation: A comprehensive review. *International Journal Of Applied Ceramic Technology*, *16*(6), 2161-2172. doi: 10.1111/ijac.13301.

Hong, H., Ryu, J., Park, I., Ryu, T., Chung, K., & Kim, B, J. (2016). *Environ. Manage.*, 165, 263–270.

Hosseini Abbandanak, M., Taghizadeh, M., & Fallah, N. (2021). High-purity hydrogen production by sorption-enhanced methanol steam reforming over a combination of Cu–Zn–CeO2–ZrO2/MCM-41 catalyst and (Li–Na–K)NO3·MgO adsorbent. *International Journal Of Hydrogen Energy*, *46*(10), 7099-7112. doi: 10.1016/j.ijhydene.2020.11.250

Hou, Q., Zhou, H., Zhang, W., Chang, Q., Yang, J., Xue, C., & Hu, S. (2021). Boosting adsorption of heavy metal ions in wastewater through solar-driven interfacial evaporation of chemically-treated carbonized wood. *Science Of The Total Environment*, *759*, 144317. doi: 10.1016/j.scitotenv.2020.144317.

Huang, D., Zheng, H., Liu, Z., Bao, A., & Li, B. (2018). Extraction of rubidium and cesium from brine solutions using a room temperature ionic liquid system containing 18-crown-6. *Polish Journal of Chemical Technology*, 20(2), 40-46.

Huang, D., Zheng, H., Liu, Z., Bao, A., & Li, B. (2018). Extraction of rubidium and cesium

from brine solutions using a room temperature ionic liquid system containing 18-crown-6. *Polish Journal Of Chemical Technology*, *20*(2), 40-46. doi: 10.2478/pjct-2018-0021.

Huang, X., Zemlyanov, D., Diaz-Amaya, S., Salehi, M., Stanciu, L., & Whelton, A. (2020). Competitive heavy metal adsorption onto new and aged polyethylene under various drinking water conditions. *Journal Of Hazardous Materials*, *385*, 121585. doi: 10.1016/j.jhazmat.2019.121585.

Humelnicu, D., Lazar, M., Ignat, M., Dinu, I., Dragan, E., & Dinu, M. (2020). Removal of heavy metal ions from multi-component aqueous solutions by eco-friendly and low-cost composite sorbents with anisotropic pores. *Journal Of Hazardous Materials*, *381*, 120980. doi: 10.1016/j.jhazmat.2019.120980.

Ibrahim, H., Xue, P., & Eltahir, E. (2020). Multiple Salinity Equilibria and Resilience of Persian/Arabian Gulf Basin Salinity to Brine Discharge. *Frontiers In Marine Science*, *7*. doi: 10.3389/fmars.2020.00573.

Jeong, S., Naidu, G., Leiknes, T., & Vigneswaran, S. (2017). 4.3 Membrane Biofouling: Biofouling Assessment and Reduction Strategies in Seawater Reverse Osmosis Desalination. *Comprehensive Membrane Science And Engineering*, 48-71. doi: 10.1016/b978-0-12-409547-2.12261-9.

Ji, C., Wu, D., Lu, J., Shan, C., Ren, Y., & Li, T. et al. (2021). Temperature regulated adsorption and desorption of heavy metals to A-MIL-121: Mechanisms and the role of exchangeable protons. *Water Research*, *189*, 116599. doi: 10.1016/j.watres.2020.116599.

Ji, C., Wu, D., Lu, J., Shan, C., Ren, Y., & Li, T. et al. (2021). Temperature regulated adsorption and desorption of heavy metals to A-MIL-121: Mechanisms and the role of exchangeable protons. *Water Research*, *189*, 116599. doi:

10.1016/j.watres.2020.116599.

Jiang, H., Yang, Y., Lin, Z., Zhao, B., Wang, J., Xie, J., & Zhang, A. (2020). Preparation of a novel bio-adsorbent of sodium alginate grafted polyacrylamide/graphene oxide hydrogel for the adsorption of heavy metal ion. *Science Of The Total Environment*, *744*, 140653. doi: 10.1016/j.scitotenv.2020.140653.

Jiménez-Arias, D., Morales-Sierra, S., García-Machado, F., García-García, A., Luis, J., & Valdés, F. et al. (2020). Rejected brine recycling in hydroponic and thermo-solar evaporation systems for leisure and tourist facilities. Changing waste into raw material. *Desalination*, *496*, 114443. doi: 10.1016/j.desal.2020.114443.

Jones, E., Qadir, M., van Vliet, M., Smakhtin, V., & Kang, S. (2019). The state of desalination and brine production: A global outlook. *Science Of The Total Environment*, *657*, 1343-1356. doi: 10.1016/j.scitotenv.2018.12.076.

Kamil, M., Ramadan, K., Ghenai, C., Olabi, A., & Nazzal, I. (2019). Emissions from Combustion of Second-Generation Biodiesel Produced from Seeds of Date Palm Fruit (Phoenix dactylifera L.). *Applied Sciences*, *9*(18), 3720. doi: 10.3390/app9183720.

Kaminski, P. (2020). The application of FTIR in situ spectroscopy combined with methanol adsorption to the study of mesoporous sieve SBA-15 with cerium-zirconium oxides modified with gold and copper species. Arabian Journal of Chemistry, 13, 851-862.

Kamran, U., & Park, S. (2020). Functionalized titanate nanotubes for efficient lithium adsorption and recovery from aqueous media. *Journal Of Solid State Chemistry*, *283*, 121157. doi: 10.1016/j.jssc.2019.121157.

Kamran, U., & Park, S. (2020). Microwave-assisted acid functionalized carbon nanofibers decorated with Mn doped TNTs nanocomposites: Efficient contenders for lithium adsorption and recovery from aqueous media. *Journal Of Industrial And Engineering Chemistry*, *92*, 263-277. doi: 10.1016/j.jiec.2020.09.014.

Kamran, U., & Park, S. (2020). MnO2-decorated biochar composites of coconut shell and rice husk: An efficient lithium ions adsorption-desorption performance in aqueous media. *Chemosphere*, *260*, 127500. doi: 10.1016/j.chemosphere.2020.127500.

Kara, k. G., & Rabbani, M. (2019). Experimental Study of Methylene Blue Adsorption from Aqueous Solutions onto Fe3 O4 /NiO Nano Mixed Oxides Prepared by Ultrasonic Assisted Co-precipitation. *J Nanostruct*, 9(2), 287-300. DOI: 10.22052/JNS.2019.02.011.

Kasedde, H., Kirabira, J., Bäbler, M., Tilliander, A., & Jonsson, S. (2014). Characterization of brines and evaporites of Lake Katwe, Uganda. *Journal Of African Earth Sciences*, *91*, 55-65. doi: 10.1016/j.jafrearsci.2013.12.004.

Kaur, S., Rani, S., & Mahajan, R. (2013). Adsorption Kinetics for the Removal of Hazardous Dye Congo Red by Biowaste Materials as Adsorbents. *Journal of chemistry*, 2013, 1-12. http://dx.doi.org/10.1155/2013/628582.

Kiener, J., Limousy, L., Jeguirim, M., Le Meins, J., Hajjar-Garreau, S., Bigoin, G., & Ghimbeu, C. (2019). Activated Carbon/Transition Metal (Ni, In, Cu) Hexacyanoferrate Nanocomposites for Cesium Adsorption. *Materials*, *12*(8), 1253. doi: 10.3390/ma12081253.

Kim, C. Y., & Min, T. (2020). Influence of osmotic mediation on permeation of water in reverse osmosis: Experimental and numerical analysis. *Journal Of Membrane Science*, *595*, 117574. doi: 10.1016/j.memsci.2019.117574.

Kim, Y., Kim, Y., Kim, S., Harbottle, D., & Lee, J. (2017). Nanostructured potassium copper hexacyanoferrate-cellulose hydrogel for selective and rapid cesium adsorption. *Chemical Engineering Journal*, 313, 1042-1050. http://dx.doi.org/10.1016/j.cej.2016.10.136 1385-894.

Kim, Y., Kim, Y., Kim, S., Harbottle, D., & Lee, J. (2017). Nanostructured potassium copper

hexacyanoferrate-cellulose hydrogel for selective and rapid cesium adsorption. Chemical Engineering Journal, 313, 1042-1050.

Kitajima, A., Ogawa, H., Kawamoto, T., Kobayashi, T., Kawasaki, T., Kawatsu, Y., & Tanaka, H. (2020). Cesium uptake ability of a nonwoven fabric supporting iron hexacyanoferrate nanoparticles from solutions of coexisting alkali metal ions. *Inorganica Chimica Acta*, *503*, 119401. doi: 10.1016/j.ica.2019.119401.

Konicki, W., Aleksandrzak, M., & Mijowska, E. (2017). Equilibrium, Kinetic and Thermodynamic Studies on Adsorption of Cationic Dyes from Aqueous Solutions Using Graphene Oxide. *Chemical Engineering Research and Design*, 123, 35-49.

Koutu, V., Shastri, L., & Malik, M. (2016). Effect of NaOH concentration on optical properties of zinc oxide nanoparticles. *Materials Science-Poland*, *34*(4), 819-827. doi: 10.1515/msp-2016-0119.

Krishnamoorthy, R., Govindan, B., Banat, F., Sagadevan, V., Purushothaman, M., & Show, P. (2019). Date pits activated carbon for divalent lead ions removal. *Journal Of Bioscience And Bioengineering*, *128*(1), 88-97. doi: 10.1016/j.jbiosc.2018.12.011.

Kumar, A., & Jena, H. (2016). Preparation and characterization of high surface area activated carbon from Fox nut (Euryale ferox) shell by chemical activation with H 3 PO 4. *Results In Physics*, *6*, 651-658. doi: 10.1016/j.rinp.2016.09.012.

Kummu, M., Guillaume, J., de Moel, H., Eisner, S., Flörke, M., & Porkka, M. et al. (2016). The world's road to water scarcity: shortage and stress in the 20th century and pathways towards sustainability. *Scientific Reports*, *6*(1). doi: 10.1038/srep38495.

Lahlou, F., Mackey, H., McKay, G., Onwusogh, U., & Al-Ansari, T. (2020). Water planning framework for alfalfa fields using treated wastewater fertigation in Qatar: An energy-water-food nexus approach. *Computers & Chemical Engineering*, *141*, 106999. doi: 10.1016/j.compchemeng.2020.106999.

Lai, H., Deng, J., Wen, S., & Liu, Q. (2019). Elucidation of lead ions adsorption mechanism

on marmatite surface by PCA-assisted ToF-SIMS, XPS and zeta potential. *Minerals Engineering*, *144*, 106035. doi: 10.1016/j.mineng.2019.106035.

Lakherwal, D. (2014). Adsorption of heavy metals: A review. *International Journal of Environmental Research and Development*, 4(1), 41-48.

Li, J., Li, H., Li, J., Wu, G., Shao, Y., & Li, Y. et al. (2018). A single-walled carbon nanotubes/poly(3,4-ethylenedioxythiophene)-poly(styrenesulfonate)/copper hexacyanoferrate hybrid film for high-volumetric performance flexible supercapacitors. *Journal Of Power Sources*, *386*, 96-105. doi: 10.1016/j.jpowsour.2018.03.046.

Li, J., Zhang, L., Wang, T., Chang, J., Song, Z., & Ma, C. (2021). Study on sulfur migration in activated carbon adsorption-desorption cycle: Effect of alkali/alkaline earth metals. *Journal Of Environmental Sciences*, *99*, 119-129. doi: 10.1016/j.jes.2020.06.009.

Li, K., Yu, L., Cai, J., & Zhang, L. (2021). Removal of dyes from aqueous solution using novel C@C composite adsorbents. *Microporous And Mesoporous Materials*, *313*, 110840. doi: 10.1016/j.micromeso.2020.110840.

Li, P., & Qian, H. (2018). Water resources research to support a sustainable China. *International Journal Of Water Resources Development*, *34*(3), 327-336. doi: 10.1080/07900627.2018.1452723.

Li, Q., Shi, W., & Yang, Q. (2021). Polarization induced covalent bonding: A new force of heavy metal adsorption on charged particle surface. *Journal Of Hazardous Materials*, *412*, 125168. doi: 10.1016/j.jhazmat.2021.125168.

Li, W., Nan, Y., You, Q., & Jin, Z. (2020). CO2 solubility in brine in silica nanopores in relation to geological CO2 sequestration in tight formations: Effect of salinity and pH. *Chemical Engineering Journal*, 127626. doi: 10.1016/j.cej.2020.127626.

Li, W., Nan, Y., You, Q., & Jin, Z. (2020). CO2 solubility in brine in silica nanopores in relation to geological CO2 sequestration in tight formations: Effect of salinity and pH. *Chemical Engineering Journal*, 127626. doi: 10.1016/j.cej.2020.127626.

Lin, Z., Li, J., Luan, Y., & Dai, W. (2020). Application of algae for heavy metal adsorption: A 20-year meta-analysis. *Ecotoxicology And Environmental Safety*, *190*, 110089. doi: 10.1016/j.ecoenv.2019.110089.

Liu, G., Zhao, Z., & Ghahreman, A. (2019). Novel approaches for lithium extraction from salt-lake brines: A review. *Hydrometallurgy*, *187*, 81-100. doi: 10.1016/j.hydromet.2019.05.005.

Liu, J., Martin, P., & Peter McGrail, B. (2020). Rare-earth element extraction from geothermal brine using magnetic core-shell nanoparticles-techno-economic analysis. *Geothermics*, *89*, 101938. doi: 10.1016/j.geothermics.2020.101938.

Liu, K., & Gao, X. (2019). Adsorption and fractionation of Pt, Pd and Rh onto inorganic microparticles and the effects of macromolecular organic compounds in seawater. *Environmental Pollution*, *255*, 113192. doi: 10.1016/j.envpol.2019.113192.

Loganathan, P., Naidu, G., & Vigneswaran, S. (2017). Mining valuable minerals from seawater: a critical review. *Environmental Science: Water Research & Technology*, *3*(1), 37-53. doi: 10.1039/c6ew00268d.

Long, X., Chen, R., Tan, J., Lu, Y., Wang, J., Huang, T., & Lei, Q. (2020). Electrochemical recovery of cobalt using nanoparticles film of copper hexacyanoferrates from aqueous solution. *Journal Of Hazardous Materials*, *384*, 121252. doi: 10.1016/j.jhazmat.2019.121252.

Long, X., Chen, R., Tan, J., Lu, Y., Wang, J., Huang, T., & Lei, Q. (2020). Electrochemical recovery of cobalt using nanoparticles film of copper hexacyanoferrates from aqueous solution. *Journal Of Hazardous Materials*, *384*, 121252. doi:

10.1016/j.jhazmat.2019.121252.

Loos-Neskovic, C., Ayrault, S., Badillo, V., Jimenez, B., Garnier, E., & Fedoroff, M. et al. (2004). Structure of copper-potassium hexacyanoferrate (II) and sorption mechanisms of cesium. *Journal Of Solid State Chemistry*, *177*(6), 1817-1828. doi: 10.1016/j.jssc.2004.01.018.

Ma, X., Jia, W., Wang, J., Zhou, J., Wu, Y., & Wei, Y. et al. (2019). Synthesis of copper hexacyanoferrate nanoflake as a cathode for sodium-ion batteries. *Ceramics International*, *45*(1), 740-746. doi: 10.1016/j.ceramint.2018.09.238.

Madejová, J. (2003). FTIR techniques in clay mineral studies. *Vibrational Spectroscopy*, *31*(1), 1-10. doi: 10.1016/s0924-2031(02)00065-6.

Magdy, Y., Altaher, H. & ElQada, E. (2018). Removal of three nitrophenols from aqueous solutions by adsorption onto char ash: equilibrium and kinetic modeling. *Applied Water Science*, 8(1), 2-15.

Mahjabin, T., Mejia, A., Blumsack, S., & Grady, C. (2020). Integrating embedded resources and network analysis to understand food-energy-water nexus in the US. *Science Of The Total Environment*, *709*, 136153. doi: 10.1016/j.scitotenv.2019.136153.

Mallesh, D., Anbarasan, J., Mahesh Kumar, P., Upendar, K., Chandrashekar, P., Rao, B., & Lingaiah, N. (2020). Synthesis, characterization of carbon adsorbents derived from waste biomass and its application to CO2 capture. *Applied Surface Science*, *530*, 147226. doi: 10.1016/j.apsusc.2020.147226.

Maneechakr, P., & Mongkollertlop, S. (2020). Investigation on adsorption behaviors of heavy metal ions (Cd2+, Cr3+, Hg2+ and Pb2+) through low-cost/active manganese dioxide-modified magnetic biochar derived from palm kernel cake residue. *Journal Of Environmental Chemical Engineering*, *8*(6), 104467. doi: 10.1016/j.jece.2020.104467.

Mangwandi, C., Kurniawan, T., & Albadarin, A. (2020). Comparative biosorption of

chromium (VI) using chemically modified date pits (CM-DP) and olive stone (CM-OS): Kinetics, isotherms and influence of co-existing ions. *Chemical Engineering Research And Design*, *156*, 251-262. doi: 10.1016/j.cherd.2020.01.034.

Mangwandi, C., Kurniawan, T., & Albadarin, A. (2020). Comparative biosorption of chromium (VI) using chemically modified date pits (CM-DP) and olive stone (CM-OS): Kinetics, isotherms and influence of co-existing ions. *Chemical Engineering Research And Design*, *156*, 251-262. doi: 10.1016/j.cherd.2020.01.034.

Mannan, M., Alhaj, M., Mabrouk, A., & Al-Ghamdi, S. (2019). Examining the life-cycle environmental impacts of desalination: A case study in the State of Qatar. *Desalination*, *452*, 238-246. doi: 10.1016/j.desal.2018.11.017.

Margenot, A., Calderón, F., Goyne, K., Mukome, F., & Parikh, S. (2017). IR Spectroscopy, Soil Analysis Applications. *Encyclopedia Of Spectroscopy And Spectrometry*, 448-454. doi: 10.1016/b978-0-12-409547-2.12170-5.

Marthi, R., & Smith, Y. (2020). Application and limitations of a H2TiO3 – Diatomaceous earth composite synthesized from titania slag as a selective lithium adsorbent. *Separation And Purification Technology*, *254*, 117580. doi: 10.1016/j.seppur.2020.117580.

Martin, I., Patapy, C., Boher, C., & Cyr, M. (2019). Investigation of caesium retention by potassium nickel hexacyanoferrate (II) in different pH conditions and potential effect on the selection of storage matrix. *Journal Of Nuclear Materials*, *526*, 151764. doi: 10.1016/j.jnucmat.2019.151764.

Martin, I., Patapy, C., Boher, C., & Cyr, M. (2019). Investigation of caesium retention by potassium nickel hexacyanoferrate (II) in different pH conditions and potential effect on the selection of storage matrix. *Journal Of Nuclear Materials*, *526*, 151764. doi: 10.1016/j.jnucmat.2019.151764

Mavukkandy, M., Chabib, C., Mustafa, I., Al Ghaferi, A., & AlMarzooqi, F. (2019). Brine

management in desalination industry: From waste to resources generation. *Desalination*, *472*, 114187. doi: 10.1016/j.desal.2019.114187

Maxwell, B., Díaz-García, C., Martínez-Sánchez, J., & Álvarez-Rogel, J. (2020). Increased brine concentration increases nitrate reduction rates in batch woodchip bioreactors treating brine from desalination. *Desalination*, *495*, 114629. doi: 10.1016/j.desal.2020.114629.

Mbonyiryivuze, A., Mwakikunga, B., Dhlamini, M. S., & Maaza, M. (2015). Fourier Transform Infrared Spectroscopy for Sepia Melanin. *Physics and Materials Chemistry*, 3(2), 25-29. doi: 10.12691/pmc-3-2-2.

Michel, C., Barré, Y., de Dieuleveult, C., Grandjean, A., & De Windt, L. (2015). Cs ion exchange by a potassium nickel hexacyanoferrate loaded on a granular support. *Chemical Engineering Science*, 137, 904-913.

Michel, C., Barré, Y., de Dieuleveult, C., Grandjean, A., & De Windt, L. (2015). Cs ion exchange by a potassium nickel hexacyanoferrate loaded on a granular support. *Chemical Engineering Science*, 137, 904-913.

Misra, N., Rawat, S., Goel, N., Shelkar, S., & Kumar, V. (2020). Radiation grafted cellulose fabric as reusable anionic adsorbent: A novel strategy for potential large-scale dye wastewater remediation. *Carbohydrate Polymers*, *249*, 116902. doi: 10.1016/j.carbpol.2020.116902.

Mohamed, A., Maraqa, M., & Al Handhaly, J. (2005). Impact of land disposal of reject brine from desalination plants on soil and groundwater. *Desalination*, *182*(1-3), 411-433. doi: 10.1016/j.desal.2005.02.035.

Moloney, M., Massoni, N., & Grandjean, A. (2020). Tuning the thermal stability of copper(II) hexacyanoferrate(II) nanoparticles. *Journal Of Thermal Analysis And Calorimetry*. doi: 10.1007/s10973-020-09823-4.

Mqehe-Nedzivhe, K., Makhado, K., Olorundare, O., Arotiba, O., Makhatha, E., Nomngongo, P., & Mabuba, N. (2018). Bio-adsorbents for the Removal of Heavy Metals from Water. *Arsenic - Analytical And Toxicological Studies*. doi: 10.5772/intechopen.73570.

Mudalige, T., Qu, H., Van Haute, D., Ansar, S., Paredes, A., & Ingle, T. (2019). Characterization of Nanomaterials. *Nanomaterials For Food Applications*, 313-353. doi: 10.1016/b978-0-12-814130-4.00011-7.

Müller, A., Avellán, T., & Schanze, J. (2020). Risk and sustainability assessment framework for decision support in 'water scarcity – water reuse' situations. *Journal Of Hydrology*, *591*, 125424. doi: 10.1016/j.jhydrol.2020.125424.

Munajad, A., Subroto, C., & Suwarno. (2018). Fourier Transform Infrared (FTIR) Spectroscopy Analysis of Transformer Paper in Mineral Oil-Paper Composite Insulation under Accelerated Thermal Aging. *Energies*, 11(364). doi:10.3390/en11020364.

Munajad, A., Subroto, C., & Suwarno. (2018). Fourier Transform Infrared (FTIR) Spectroscopy Analysis of Transformer Paper in Mineral Oil-Paper Composite Insulation under Accelerated Thermal Aging. *Energies*, 11(364). doi:10.3390/en11020364.

Mvulirwenande, S., & Wehn, U. (2020). Dynamics of water innovation in African cities: Insights from Kenya, Ghana and Mozambique. *Environmental Science & Policy*, *114*, 96-108. doi: 10.1016/j.envsci.2020.07.024.

Naeimi, S., & Faghihian, H. (2017). Performance of novel adsorbent prepared by magnetic metal-organic framework (MOF) modified by potassium nickel hexacyanoferrate for removal of Cs + from aqueous solution. *Separation And Purification Technology*, *175*, 255-265. doi: 10.1016/j.seppur.2016.11.028.

Naeimi, S., & Faghihian, H. (2017). Performance of novel adsorbent prepared by magnetic

metal-organic framework (MOF) modified by potassium nickel hexacyanoferrate for removal of Cs + from aqueous solution. *Separation and Purification Technology*, 175, 225-265. http://dx.doi.org/10.1016/j.seppur.2016.11.028.

Naidu, G., Jeong, S., Choi, Y., Song, M., Oyunchuluun, U., & Vigneswaran, S. (2018). Valuable rubidium extraction from potassium reduced seawater brine. *Journal Of Cleaner Production*, *174*, 1079-1088. doi: 10.1016/j.jclepro.2017.11.042.

Naidu, G., Loganathan, P., Jeong, S., Johir, M., To, V., Kandasamy, J., & Vigneswaran, S. (2016). Rubidium extraction using an organic polymer encapsulated potassium copper hexacyanoferrate sorbent. *Chemical Engineering Journal*, 306, 31-42.

Naidu, G., Loganathan, P., Jeong, S., Johir, M., To, V., Kandasamy, J., & Vigneswaran, S. (2016). Rubidium extraction using an organic polymer encapsulated potassium copper hexacyanoferrate sorbent. Chemical Engineering Journal, 306, 31-42.

Naidu, G., Nur, T., Loganathan, P., Kandasamy, J., & Vigneswaran, S. (2016). Selective sorption of rubidium by potassium cobalt hexacyanoferrate. *Separation and Purification Technology*, 163, 238-246.

Nanakoudis, A. (2019). EDX Analysis - SEM - EDS Analysis - Accelerating Microscopy. Retrieved 6 February 2021, from https://www.thermofisher.com/blog/microscopy/edx-analysis-with-sem-how-does-it-work/.

Nanakoudis, A. (2019). EDX Analysis With SEM: How Does it Work?. Retrieved from: https://www.thermofisher.com/blog/microscopy/edx-analysis-with-sem-how-does-it-work/.

Nannarone, A., Toro, C., & Sciubba, E. (2017). Multi-Stage Flash Desalination Process: Modeling and Simulation. PROCEEDINGS OF ECOS 2017 - THE 30TH INTERNATIONAL CONFERENCE ON EFFICIENCY, COST, OPTIMIZATION, SIMULATION AND ENVIRONMENTAL IMPACT OF ENERGY SYSTEMS JULY

2-JULY 6, 2017, SAN DIEGO, CALIFORNIA, USA.

Nasrazadani, S., & Hassani, S. (2016). Modern analytical techniques in failure analysis of aerospace, chemical, and oil and gas industries. *Handbook Of Materials Failure Analysis With Case Studies From The Oil And Gas Industry*, 39-54. doi: 10.1016/b978-0-08-100117-2.00010-8.

Nasrollahzadeh, M., Atarod, M., Sajjadi, M., Sajadi, S., & Issaabadi, Z. (2019). Plant-Mediated Green Synthesis of Nanostructures: Mechanisms, Characterization, and Applications. *Interface Science And Technology*, 199-322. doi: 10.1016/b978-0-12-813586-0.00006-7.

Nassrullah, H., Anis, S., Hashaikeh, R., & Hilal, N. (2020). Energy for desalination: A state-of-the-art review. *Desalination*, *491*, 114569. doi: 10.1016/j.desal.2020.114569.

Nesterenko, P., & Paull, B. (2017). Ion chromatography. *Liquid Chromatography*, 205-244. doi: 10.1016/b978-0-12-805393-5.00009-9.

Ngueagni, P., Woumfo, E., Kumar, P., Siéwé, M., Vieillard, J., Brun, N., & Nkuigue, P. (2020). Adsorption of Cu(II) ions by modified horn core: Effect of temperature on adsorbent preparation and extended application in river water. *Journal Of Molecular Liquids*, *298*, 112023. doi: 10.1016/j.molliq.2019.112023.

Nguyen, H., Chen, S., Nguyen, N., Ngo, H., Guo, W., & Li, C. (2015). Exploring an innovative surfactant and phosphate-based draw solution for forward osmosis desalination. *Journal Of Membrane Science*, *489*, 212-219. doi: 10.1016/j.memsci.2015.03.085.

Nnadozie, E., & Ajibade, P. (2020). Data for experimental and calculated values of the adsorption of Pb(II) and Cr(VI) on APTES functionalized magnetite biochar using Langmuir, Freundlich and Temkin equations. *Data In Brief*, *32*, 106292. doi: 10.1016/j.dib.2020.106292.

Núñez-Gómez, D., Rodrigues, C., Lapolli, F., & Lobo-Recio, M. (2019). Adsorption of heavy

metals from coal acid mine drainage by shrimp shell waste: Isotherm and continuous-flow studies. *Journal Of Environmental Chemical Engineering*, *7*(1), 102787. doi: 10.1016/j.jece.2018.11.032.

Nur, T., Loganathan, P., Johir, M., Kandasamy, J., & Vigneswaran, S. (2018). Removing rubidium using potassium cobalt hexacyanoferrate in the membrane adsorption hybrid system. *Separation And Purification Technology*, *191*, 286-294. doi: 10.1016/j.seppur.2017.09.048.

Ogungbenro, A., Quang, D., Al-Ali, K., & Abu-Zahra, M. (2017). Activated Carbon from Date Seeds for CO2 Capture Applications. *Energy Procedia*, *114*, 2313-2321. doi: 10.1016/j.egypro.2017.03.1370.

Oliveira, P., Kalinke, C., Mangrich, A., Marcolino-Junior, L., & Bergamini, M. (2018). Copper hexacyanoferrate nanoparticles supported on biochar for amperometric determination of isoniazid. *Electrochimica Acta*, *285*, 373-380. doi: 10.1016/j.electacta.2018.08.004.

Omer, A., Elagib, N., Zhuguo, M., Saleem, F., & Mohammed, A. (2020). Water scarcity in the Yellow River Basin under future climate change and human activities. *Science Of The Total Environment*, *749*, 141446. doi: 10.1016/j.scitotenv.2020.141446.

Onwuka, O., Umar, N., Omonona, O., & Idris, I. (2019). Heavy metals and rare earth elements distribution in the brine fields of awe, keana and giza, central benue trough, Nigeria. *Journal Of African Earth Sciences*, *157*, 103514. doi: 10.1016/j.jafrearsci.2019.103514.

Pal, P., Shittu, I., Othman, I., Sengupta, A., Voleti, L., & Banat, F. (2020). Removal of the total organic acid anions from an industrial lean diglycolamine solvent using a calcium alginate carbon adsorbent, and molecular modeling studies. *Journal Of Natural Gas Science And Engineering*, *82*, 103516. doi: 10.1016/j.jngse.2020.103516.

Panagopoulos, A., Haralambous, K., & Loizidou, M. (2019). Desalination brine disposal

methods and treatment technologies - A review. *Science Of The Total Environment*, *693*, 133545. doi: 10.1016/j.scitotenv.2019.07.351.

Pangarkar, B., Sane, M., & Guddad, M. (2011). Reverse Osmosis and Membrane Distillation for Desalination of Groundwater: A Review. *ISRN Materials Science*, *2011*, 1-9. doi: 10.5402/2011/523124.

Pantapasis, K., & Grumezescu, A. (2017). Gold nanoparticles: advances in water purification approaches. *Water Purification*, 447-477. doi: 10.1016/b978-0-12-804300-4.00013-7.

Park, J., Park, C., Lee, K., & Suh, S. (2020). Effect of NaOH and precursor concentration on size and magnetic properties of FeCo nanoparticles synthesized using the polyol method. *AIP Advances*, *10*(11), 115220. doi: 10.1063/5.0024622.

Pelalak, R., Heidari, Z., Khatami, S., Kurniawan, T., Marjani, A., & Shirazian, S. (2021). Oak wood ash/GO/Fe3O4 adsorption efficiencies for cadmium and lead removal from aqueous solution: Kinetics, equilibrium and thermodynamic evaluation. *Arabian Journal Of Chemistry*, *14*(3), 102991. doi: 10.1016/j.arabjc.2021.102991.

Petersen, K., Paytan, A., Rahav, E., Levy, O., Silverman, J., & Barzel, O. et al. (2018). Impact of brine and antiscalants on reef-building corals in the Gulf of Aqaba – Potential effects from desalination plants. *Water Research*, *144*, 183-191. doi: 10.1016/j.watres.2018.07.009.

Petersková, M., Valderrama, C., Gibert, O., & Cortina, J. (2012). Extraction of valuable metal ions (Cs, Rb, Li, U) from reverse osmosis concentrate using selective sorbents. *Desalination*, *286*, 316-323. doi: 10.1016/j.desal.2011.11.042.

Petersková, M., Valderrama, C., Gibert, O., & Cortina, J. (2012). Extraction of valuable metal ions (Cs, Rb, Li, U) from reverse osmosis concentrate using selective sorbents. *Desalination*, *286*, 316-323. doi: 10.1016/j.desal.2011.11.042.

Pires, B., Nunes, W., Freitas, B., Oliveira, F., Katic, V., & Rodella, C. et al. (2021).

Characterization of porous cobalt hexacyanoferrate and activated carbon electrodes under dynamic polarization conditions in a sodium-ion pseudocapacitor. *Journal Of Energy Chemistry*, *54*, 53-62. doi: 10.1016/j.jechem.2020.05.045.

Pramanik, B., Asif, M., Roychand, R., Shu, L., Jegatheesan, V., Bhuiyan, M., & Hai, F. (2020). Lithium recovery from salt-lake brine: Impact of competing cations, pretreatment and preconcentration. *Chemosphere*, *260*, 127623. doi: 10.1016/j.chemosphere.2020.127623.

Pramanik, B., Shu, L., & Jegatheesan, V. (2017). A review of the management and treatment of brine solutions. *Environmental Science: Water Research & Technology*, *3*(4), 625-658. doi: 10.1039/c6ew00339g.

Preez, C., & van Huyssteen, C. (2020). Threats to soil and water resources in South Africa. *Environmental Research*, *183*, 109015. doi: 10.1016/j.envres.2019.109015.

Prussian blue - American Chemical Society. (2017). Retrieved from https://www.acs.org/content/acs/en/molecule-of-the-week/archive/p/prussian-blue.html.

Quilaqueo, M., Duizer, L., & Aguilera, J. (2015). The morphology of salt crystals affects the perception of saltiness. Food Research International, 76, 675-681. http://dx.doi.org/10.1016/j.foodres.2015.07.004.

Rahman, H., & Zaidi, S. J. (2018). Desalination in Qatar: Present Status and Future Prospects. *Civil Engineering Research Journal*, *6*(5). doi: 10.19080/cerj.2018.06.555700.

Rasoulpoor, K., Poursattar Marjani, A., & Nozad, E. (2020). Competitive chemisorption and physisorption processes of a walnut shell based semi-IPN bio-composite adsorbent for lead ion removal from water: Equilibrium, Kinetic and Thermodynamic studies. *Environmental Technology & Innovation*, *20*, 101133. doi:

10.1016/j.eti.2020.101133.

Reverse Osmosis - Lenntech. (2020). Retrieved 27 March 2020, from https://www.lenntech.com/systems/reverse-osmosis/ro/rosmosis.htm?gclid=EAIaIQobChMI9IaM1MG26AIV2aqWCh2n_QFdEAAYASAAEgLhR_D_BwE.

Rizzi, V., D'Agostino, F., Fini, P., Semeraro, P., & Cosma, P. (2017). An interesting environmental friendly cleanup: The excellent potential of olive pomace for disperse blue adsorption/desorption from wastewater. *Journal of Dyes and Pigments*, 140, 480-490.

Rodríguez-Rojas, F., López-Marras, A., Celis-Plá, P., Muñoz, P., García-Bartolomei, E., & Valenzuela, F. et al. (2020). Ecophysiological and cellular stress responses in the cosmopolitan brown macroalga Ectocarpus as biomonitoring tools for assessing desalination brine impacts. *Desalination*, *489*, 114527. doi: 10.1016/j.desal.2020.114527

Rohmah, M., Hanum Lalasari, L., Chrisayu Natasha, N., Sulistiyono, E., Firdiyono, F., & Wahyuadi Soedarsono, J. (2021). Adsorption Behavior of Alkali Metal (Na+, Li+, and K+) from Bledug Kuwu brine by Resin Adsorbent for Purification: pH and Flow Rate Parameter. Oriental Journal of Chemistry, 36(2), 273-279.

Rohrer, J. (2019). Monitoring Water Contaminants With Ion Chromatography. *Advances In Water Purification Techniques*, 115-134. doi: 10.1016/b978-0-12-814790-0.00005-3.

Rojas-Mayorga, C., Aguayo-Villarreal, I., Moreno-Pérez, J., Muñiz-Valencia, R., Montes-Morán, M., & Ocampo-Pérez, R. (2020). Influence of calcium species on SO2 adsorption capacity of a novel carbonaceous materials and their ANN modeling. *Journal Of Environmental Chemical Engineering*, 104810. doi: 10.1016/j.jece.2020.104810.

Ruan, S., Yang, E., & Unluer, C. (2021). Production of reactive magnesia from desalination reject brine and its use as a binder. *Journal Of CO2 Utilization*, *44*, 101383. doi: 10.1016/j.jcou.2020.101383.

Ryu, J., Hong, J., Park, I., Ryu, T., & Hong, H. (2020). Recovery of strontium (Sr2+) from seawater using a hierarchically structured MnO2/C/Fe3O4 magnetic nanocomposite. *Hydrometallurgy*, *191*, 105224. doi: 10.1016/j.hydromet.2019.105224.

Ryu, J., Hong, J., Park, I., Ryu, T., & Hong, H. (2020). Recovery of strontium (Sr2+) from seawater using a hierarchically structured MnO2/C/Fe3O4 magnetic nanocomposite. *Hydrometallurgy*, *191*, 105224. doi: 10.1016/j.hydromet.2019.105224.

Ryu, T., Lee, D., Ryu, J., Shin, J., Chung, K., & Kim, Y. (2019). A lithium selective adsorption composite by coating adsorbent on PVC plate using epoxy-silica hybrid binder. *Hydrometallurgy*, *183*, 118-124. doi: 10.1016/j.hydromet.2018.11.011.

Saad, E., Mansour, R., El-Asmy, A., & El-Shahawi, M. (2008). Sorption profile and chromatographic separation of uranium (VI) ions from aqueous solutions onto date pits solid sorbent. *Talanta*, *76*(5), 1041-1046. doi: 10.1016/j.talanta.2008.04.065.

Samra, S. (2014). Biosorption of Pb2+ from Natural Water using Date Pits: A Green Chemistry Approach. *Mod. Chem. Appl.*, 2.

Scanning Electron Microscopy Working Principle. (2019). Thermofisher. Retrieved from: https://assets.thermofisher.com/TFS-Assets/MSD/Reference-Materials/WP0016-scanning-electron-microscopy-working-principle.pdf.

Schorr, M. (2011). *Desalination, trends and technologies*. Rijeka: InTech.

SeaWater Desalination - Key Issues. (2020). Retrieved 27 March 2020, from https://www.lenntech.com/processes/desalination/general/desalination-key-issue.htm.

Seekaew, Y., Arayawut, O., Timsorn, K., & Wongchoosuk, C. (2019). Synthesis, Characterization, and Applications of Graphene and Derivatives. *Carbon-Based Nanofillers And Their Rubber Nanocomposites*, 259-283. doi: 10.1016/b978-0-12-813248-7.00009-2.

Selvamani, V. (2019). Stability Studies on Nanomaterials Used in Drugs. *Characterization And Biology Of Nanomaterials For Drug Delivery*, 425-444. doi: 10.1016/b978-0-12-814031-4.00015-5.

Shahmansouri, A., Min, J., Jin, L., & Bellona, C. (2015). Feasibility of extracting valuable minerals from desalination concentrate: a comprehensive literature review. Journal of Cleaner Production, 100, 4-16. https://doi.org/10.1016/j.jclepro.2015.03.031.

Shen, L., Jiang, Y., Liu, Y., Ma, J., Sun, T., & Zhu, N. (2020). High-stability monoclinic nickel hexacyanoferrate cathode materials for ultrafast aqueous sodium ion battery. *Chemical Engineering Journal*, *388*, 124228. doi: 10.1016/j.cej.2020.124228.

Shi, Y., Zhang, M., Zhang, H., Yang, F., Tang, C., & Dong, Y. (2020). Recent development of pressure retarded osmosis membranes for water and energy sustainability: A critical review. *Water Research*, *189*, 116666. doi: 10.1016/j.watres.2020.116666.

Snyders, C., Bradshaw, S., Akdogan, G., & Eksteen, J. (2014). The effect of temperature, cyanide and base metals on the adsorption of Pt, Pd and Au onto activated carbon. *Hydrometallurgy*, 149, 132-142.

Soliman, N., & Moustafa, A. (2020). Industrial solid waste for heavy metals adsorption features and challenges; a review. *Journal Of Materials Research And Technology*, *9*(5), 10235-10253. doi: 10.1016/j.jmrt.2020.07.045.

Su, X., Hu, J., Zhang, J., Liu, H., Yan, C., & Xu, J. et al. (2020). Investigating the adsorption behavior and mechanisms of insoluble Humic acid/starch composite microspheres for metal ions from water. *Colloids And Surfaces A: Physicochemical And Engineering*

Aspects, 125672. doi: 10.1016/j.colsurfa.2020.125672.

Sun, S., Zhou, X., Liu, H., Jiang, Y., Zhou, H., Zhang, C., & Fu, G. (2021). Unraveling the effect of inter-basin water transfer on reducing water scarcity and its inequality in China. *Water Research, 194*, 116931. doi: 10.1016/j.watres.2021.116931.

Suresh Kumar, P., Korving, L., Keesman, K., van Loosdrecht, M., & Witkamp, G. (2019). Effect of pore size distribution and particle size of porous metal oxides on phosphate adsorption capacity and kinetics. *Chemical Engineering Journal, 358*, 160-169. doi: 10.1016/j.cej.2018.09.202.

Synthesis, kinetics, equilibrium and thermodynamics. *Journal Of Solid State Chemistry*, *291*, 121636. doi: 10.1016/j.jssc.2020.121636.

Tang, L., Gou, S., He, Y., Liu, L., Fang, S., Duan, W., & Liu, T. (2021). An efficient chitosan-based adsorption material containing phosphoric acid and amidoxime groups for the enrichment of Cu (II) and Ni (II) from water. *Journal Of Molecular Liquids*, 115815. doi: 10.1016/j.molliq.2021.115815.

Terangpi, P., & Chakraborty, S. (2017). Adsorption kinetics and equilibrium studies for removal of acid azo dyes by aniline formaldehyde condensate. (2016). *Applied Water Science*, 7(7), 3661-3671.

Thanarasu, A., Periyasamy, K., Manickam Periyaraman, P., Devaraj, T., Velayutham, K., & Subramanian, S. (2020). Comparative studies on adsorption of dye and heavy metal ions from effluents using eco-friendly adsorbent. *Materials Today: Proceedings*. doi: 10.1016/j.matpr.2020.07.001.

Thanarasu, A., Periyasamy, K., Manickam Periyaraman, P., Devaraj, T., Velayutham, K., & Subramanian, S. (2020). Comparative studies on adsorption of dye and heavy metal ions from effluents using eco-friendly adsorbent. *Materials Today: Proceedings*. doi: 10.1016/j.matpr.2020.07.001.

Thanarasu, A., Periyasamy, K., Manickam Periyaraman, P., Devaraj, T., Velayutham, K., & Subramanian, S. (2020). Comparative studies on adsorption of dye and heavy metal ions from effluents using eco-friendly adsorbent. *Materials Today: Proceedings*. doi: 10.1016/j.matpr.2020.07.001.

Thompson, B., Leshy, J., Abrams, R., & Zellmer, S. (2018). *Legal control of water resources*. St. Paul: West Academic.

Touriño, I., Barrrios-Bermúdez, N., Cerpa-Naranjo, A., & Rojas-Cervantes, M. (2019). Molecular dynamics simulation of the adsorption of alkali metal cations on carbon nanotubes surfaces. *Computational Condensed Matter, 18*, e00357. doi: 10.1016/j.cocom.2018.e00357.

Touriño, I., Barrrios-Bermúdez, N., Cerpa-Naranjo, A., & Rojas-Cervantes, M. (2019). Molecular dynamics simulation of the adsorption of alkali metal cations on carbon nanotubes surfaces. *Computational Condensed Matter*, *18*, e00357. doi: 10.1016/j.cocom.2018.e00357.

Uddin, T., Rahman, A., Rukanuzzaman, & Islam, A. (2017). A potential low cost adsorbent for the removal of cationic dyes from aqueous solutions. Applied Water Sciences, 7, 2831-2842. DOI 10.1007/s13201-017-0542-4.

Vanderheyden, S., Yperman, J., Carleer, R., & Schreurs, S. (2018). Enhanced cesium removal from real matrices by nickel-hexacyanoferrate modified activated carbons. *Chemosphere*, *202*, 569-575. doi: 10.1016/j.chemosphere.2018.03.096.

Vardhan, K., Kumar, P., & Panda, R. (2019). A review on heavy metal pollution, toxicity and remedial measures: Current trends and future perspectives. *Journal Of Molecular Liquids*, *290*, 111197. doi: 10.1016/j.molliq.2019.111197.

Vengatesh, G., & Sundaravadivelu, M. (2019). Non-toxic bisacodyl as an effective corrosion inhibitor for mild steel in 1 M HCl: Thermodynamic, electrochemical, SEM, EDX,

AFM, FT-IR, DFT and molecular dynamics simulation studies. *Journal Of Molecular Liquids*, *287*, 110906. doi: 10.1016/j.molliq.2019.110906.

Ventura, S., Bhamidi, S., Hornbostel, M., & Nagar, A. (2020). Selective Recovery of Lithium from Geothermal Brines. California Energy Commission. Retrieved from: https://ww2.energy.ca.gov/2020publications/CEC-500-2020-020/CEC-500-2020-020.pdf.

Villaescusa, I., Fiol, N., Martínez, M., Miralles, N., Poch, J., & Serarols, J. (2004). Removal of copper and nickel ions from aqueous solutions by grape stalks wastes. *Water Research*, *38*(4), 992-1002. doi: 10.1016/j.watres.2003.10.040.

Vincent, J., Neggers, Y., & McClung, J. (2019). Roles of Chromium(III), Vanadium, Iron, and Zinc in Sports Nutrition. *Nutrition And Enhanced Sports Performance*, 653-664. doi: 10.1016/b978-0-12-813922-6.00056-4.

Vincent, T., Vincent, C., & Guibal, E. (2015). Immobilization of Metal Hexacyanoferrate Ion-Exchangers for the Synthesis of Metal Ion Sorbents—A Mini-Review. *Molecules*, *20*(11), 20582-20613. doi: 10.3390/molecules201119718.

Wadhawan, S., Jain, A., Nayyar, J., & Mehta, S. (2020). Role of nanomaterials as adsorbents in heavy metal ion removal from waste water: A review. *Journal Of Water Process Engineering*, *33*, 101038. doi: 10.1016/j.jwpe.2019.101038.

Wang, B., Zhang, Q., Hong, J., & Li, L. (2018). Highly effective iron–carbon–bentonite–alginate beads (Fe°/C-BABs) as catalyst to treat benzalkonium chloride in fixed-bed column systems. *Process Safety And Environmental Protection*, *119*, 75-86. doi: 10.1016/j.psep.2018.07.018.

Wang, H., Luo, W., Tian, Z., & Ouyang, C. (2019). First principles study of alkali and alkaline earth metal ions adsorption and diffusion on penta-graphene. *Solid State Ionics*, *342*, 115062. doi: 10.1016/j.ssi.2019.115062.

Wang, J., Yang, S., Long, X., Li, Z., Tan, J., Wang, X., & Chen, R. (2020). Electrochemical recovery of low concentrated platinum (Pt) on nickel hexacyanoferrate nanoparticles film. *Journal Of The Taiwan Institute Of Chemical Engineers*, *111*, 246-251. doi: 10.1016/j.jtice.2020.05.004.

Wang, J., Zhuang, S., & Liu, Y. (2018). Metal hexacyanoferrates-based adsorbents for cesium removal. *Coordination Chemistry Reviews*, *374*, 430-438. doi: 10.1016/j.ccr.2018.07.014.

Wang, J., Zhuang, S., & Liu, Y. (2018). Metal hexacyanoferrates-based adsorbents for cesium removal. *Coordination Chemistry Reviews*, *374*, 430-438. doi: 10.1016/j.ccr.2018.07.014.

Wang, S., Chen, X., Zhang, Y., Zhang, Y., & Zheng, S. (2018). Lithium adsorption from brine by iron-doped titanium lithium ion sieves. *Particuology*, *41*, 40-47. doi: 10.1016/j.partic.2018.02.001.

Wang, S., Chen, X., Zhang, Y., Zhang, Y., & Zheng, S. (2018). Lithium adsorption from brine by iron-doped titanium lithium ion sieves. *Particuology*, *41*, 40-47. doi: 10.1016/j.partic.2018.02.001.

Wang, S., Li, P., Zhang, X., Zheng, S., & Zhang, Y. (2017). Selective adsorption of lithium from high Mg-containing brines using H x TiO 3 ion sieve. Hydrometallurgy, 174, 21-28.

Wang, S., Li, P., Zhang, X., Zheng, S., & Zhang, Y. (2017). Selective adsorption of lithium from high Mg-containing brines using H x TiO 3 ion sieve. Hydrometallurgy, 174, 21-28. https://doi.org/10.1016/j.hydromet.2017.09.009.

Wellner, N. (2013). Fourier transform infrared (FTIR) and Raman microscopy: principles and applications to food microstructures. *Food Microstructures*, 163-191. doi: 10.1533/9780857098894.1.163.

Wenten, I., Khoiruddin, K., Reynard, R., Lugito, G., & Julian, H. (2020). Advancement of forward osmosis (FO) membrane for fruit juice concentration. *Journal Of Food Engineering*, *290*, 110216. doi: 10.1016/j.jfoodeng.2020.110216.

Wessells, C., Huggins, R., & Cui, Y. (2011). Copper hexacyanoferrate battery electrodes with long cycle life and high power. *Nature Communications*, *2*(1). doi: 10.1038/ncomms1563.

Wheeler, O., Carl, D., & Armentrout, P. (2018). Second–shell thermochemistry for hydration of strontium dications as determined by threshold collision-induced dissociation and computations. *International Journal Of Mass Spectrometry*, *429*, 76-89. doi: 10.1016/j.ijms.2017.05.009.

Wu, C., Klemes, M., Trang, B., Dichtel, W., & Helbling, D. (2020). Exploring the factors that influence the adsorption of anionic PFAS on conventional and emerging adsorbents in aquatic matrices. *Water Research*, *182*, 115950. doi: 10.1016/j.watres.2020.115950.

Wu, H., Lin, S., Cheng, X., Chen, J., Ji, Y., Xu, D., & Kang, M. (2020). Comparative study of strontium adsorption on muscovite, biotite and phlogopite. *Journal Of Environmental Radioactivity*, *225*, 106446. doi: 10.1016/j.jenvrad.2020.106446.

Wu, M., Lyu, L., & Syu, J. (2015). Copper and nickel hexacyanoferrate nanostructures with graphene-coated stainless steel sheets for electrochemical supercapacitors. *Journal of Power Sources*, 297, 75-82. http://dx.doi.org/10.1016/j.jpowsour.2015.07.101.

Wu, M., Lyu, L., & Syu, J. (2015). Copper and nickel hexacyanoferrate nanostructures with graphene-coated stainless steel sheets for electrochemical supercapacitors. *Journal of Power Sources*, 297, 75-82.

Xing, H., Hu, P., Li, S., Zuo, Y., Han, J., & Hua, X. et al. (2021). Adsorption and diffusion of oxygen on metal surfaces studied by first-principle study: A review. *Journal Of Materials Science & Technology*, *62*, 180-194. doi: 10.1016/j.jmst.2020.04.063.

X-ray Powder Diffraction (XRD). (2020). Retrieved 8 February 2021, from https://serc.carleton.edu/research_education/geochemsheets/technique.

Xu, Z., Rong, M., Meng, Q., Yao, H., Ni, S., & Wang, L. et al. (2020). Fabrication of hypercrosslinked hydroxyl-rich solid phase extractants for cesium separation from the salt lake brine. *Chemical Engineering Journal*, *400*, 125991. doi: 10.1016/j.cej.2020.125991.

Yadav, S., Asthana, A., Singh, A., Chakraborty, R., Vidya, S., Susan, M., & Carabineiro, S. (2021). Adsorption of cationic dyes, drugs and metal from aqueous solutions using a polymer composite of magnetic/β-cyclodextrin/activated charcoal/Na alginate: Isotherm, kinetics and regeneration studies. *Journal Of Hazardous Materials*, *409*, 124840. doi: 10.1016/j.jhazmat.2020.124840.

Yahya, M., Yohanna, I., Auta, M., & Obayomi, K. (2020). Remediation of Pb (II) ions from Kagara gold mining effluent using cotton hull adsorbent. *Scientific African*, *8*, e00399. doi: 10.1016/j.sciaf.2020.e00399.

Yang, S., Zhang, F., Ding, H., He, P., & Zhou, H. (2018). Lithium Metal Extraction from Seawater. *Joule*, *2*(9), 1648-1651. doi: 10.1016/j.joule.2018.07.006.

Yang, W., Wang, Z., Song, S., Han, J., Chen, H., & Wang, X. et al. (2019). Adsorption of copper(II) and lead(II) from seawater using hydrothermal biochar derived from Enteromorpha. *Marine Pollution Bulletin*, *149*, 110586. doi: 10.1016/j.marpolbul.2019.110586.

Yi, H., Qin, R., Ding, S., Wang, Y., Li, S., Zhao, Q., & Pan, F. (2020). Structure and Properties of Prussian Blue Analogues in Energy Storage and Conversion Applications. *Advanced Functional Materials*, *31*(6), 2006970. doi: 10.1002/adfm.202006970.

Yin, X., Bai, J., Tian, W., Li, S., Wang, J., & Wu, X. et al. (2017). Uranium sorption from saline lake brine by amidoximated silica. *Journal Of Radioanalytical And Nuclear*

Chemistry, *313*(1), 113-121. doi: 10.1007/s10967-017-5283-1.

Yu, H., Zi, F., Hu, X., Nie, Y., Chen, Y., & Cheng, H. (2017). Adsorption of gold from thiosulfate solutions with chemically modified activated carbon. *Adsorption Science & Technology*, *36*(1-2), 408-428. doi: 10.1177/0263617417698864.

Yu, H., Zi, F., Hu, X., Nie, Y., Chen, Y., & Cheng, H. (2017). Adsorption of gold from thiosulfate solutions with chemically modified activated carbon. *Adsorption Science & Technology*, *36*(1-2), 408-428. doi: 10.1177/0263617417698864.

Yuan, Y., An, Z., Zhang, R., Wei, X., & Lai, B. (2021). Efficiencies and mechanisms of heavy metals adsorption on waste leather-derived high-nitrogen activated carbon. *Journal Of Cleaner Production*, *293*, 126215. doi: 10.1016/j.jclepro.2021.126215.

Zaman, M., Birkett, G., Pratt, C., Stuart, B., & Pratt, S. (2015). Downstream processing of reverse osmosis brine: Characterisation of potential scaling compounds. *Water Research*, *80*, 227-234. doi: 10.1016/j.watres.2015.05.004.

Zhang, B., & Chen, Y. (2020). Particle size effect on pore structure characteristics of lignite determined via low-temperature nitrogen adsorption. *Journal Of Natural Gas Science And Engineering*, *84*, 103633. doi: 10.1016/j.jngse.2020.103633.

Zhang, H., Kim, Y., Hunter, T., Brown, A., Lee, J., & Harbottle, D. (2017). Organically modified clay with potassium copper hexacyanoferrate for enhanced Cs+ adsorption capacity and selective recovery by flotation. *Journal Of Materials Chemistry A*, *5*(29), 15130-15143. doi: 10.1039/c7ta03873a.

Zhang, J., Gao, J., Chen, Y., Hao, X., & Jin, X. (2017). Characterization, preparation, and reaction mechanism of hemp stem based activated carbon. *Results In Physics*, *7*, 1628-1633. doi: 10.1016/j.rinp.2017.04.028.

Zhang, W., Miao, M., Pan, J., Sotto, A., Shen, J., Gao, C., & der Bruggen, B. (2017). Separation of divalent ions from seawater concentrate to enhance the purity of coarse salt by electrodialysis with monovalent-selective membranes. *Desalination*, *411*, 28-37. doi:

10.1016/j.desal.2017.02.008.

Zhang, W., Miao, M., Pan, J., Sotto, A., Shen, J., Gao, C., & der Bruggen, B. (2017). Separation of divalent ions from seawater concentrate to enhance the purity of coarse salt by electrodialysis with monovalent-selective membranes. *Desalination*, *411*, 28-37. doi: 10.1016/j.desal.2017.02.008.

Zhang, X., & Liu, Y. (2020). Ultrafast removal of radioactive strontium ions from contaminated water by nanostructured layered sodium vanadosilicate with high adsorption capacity and selectivity. *Journal Of Hazardous Materials*, *398*, 122907. doi: 10.1016/j.jhazmat.2020.122907.

Zhang, X., & Liu, Y. (2020). Ultrafast removal of radioactive strontium ions from contaminated water by nanostructured layered sodium vanadosilicate with high adsorption capacity and selectivity. *Journal Of Hazardous Materials*, *398*, 122907. doi: 10.1016/j.jhazmat.2020.122907.

Zhang, X., & Liu, Y. (2020). Ultrafast removal of radioactive strontium ions from contaminated water by nanostructured layered sodium vanadosilicate with high adsorption capacity and selectivity. *Journal Of Hazardous Materials*, *398*, 122907. doi: 10.1016/j.jhazmat.2020.122907.

Zhang, Y., Xu, S., Zhou, H., Qi, H., & Wang, H. (2020). Adsorption of organic pollutants and heavy metal by Co-doped core-shell MoO2/Mo2C adsorbent. *Journal Of Solid State Chemistry*, *293*, 121801. doi: 10.1016/j.jssc.2020.121801.

Zhao, J., Temimi, M., & Ghedira, H. (2017). Remotely sensed sea surface salinity in the hyper-saline Arabian Gulf: Application to landsat 8 OLI data. *Estuarine, Coastal And Shelf Science*, *187*, 168-177. doi: 10.1016/j.ecss.2017.01.008.

Zhao, L., Duan, X., Azhar, M., Sun, H., Fang, X., & Wang, S. (2020). Selective adsorption of rare earth ions from aqueous solution on metal-organic framework HKUST-

1. *Chemical Engineering Journal Advances*, *1*, 100009. doi: 10.1016/j.ceja.2020.100009.

Zheng, X., Wen, J., Shi, L., Cheng, R., & Zhang, Z. (2020). A top-down approach to estimate global RO desalination water production considering uncertainty. *Desalination*, *488*, 114523. doi: 10.1016/j.desal.2020.114523.

Zhong, J., Lin, S., & Yu, J. (2021). Lithium recovery from ultrahigh Mg2+/Li+ ratio brine using a novel granulated Li/Al-LDHs adsorbent. *Separation And Purification Technology*, *256*, 117780. doi: 10.1016/j.seppur.2020.117780.

Zhou, X., Liu, D., Bu, H., Deng, L., Liu, H., & Yuan, P. et al. (2018). XRD-based quantitative analysis of clay minerals using reference intensity ratios, mineral intensity factors, Rietveld, and full pattern summation methods: A critical review. *Solid Earth Sciences*, *3*(1), 16-29. doi: 10.1016/j.sesci.2017.12.002.

Zhuang, S., & Wang, J. (2019). Removal of cesium ions using nickel hexacyanoferrates-loaded bacterial cellulose membrane as an effective adsorbent. *Journal Of Molecular Liquids*, *294*, 111682. doi: 10.1016/j.molliq.2019.111682.

APPENDIX

Appendix (A) Statistical analysis

Table A-1. ANOVA of the effect of solution pH on the adsorption of lithium onto RDP, RDP-FC-Cu and RDP-FC-Ni

Source of Variation	*SS*	*df*	*MS*	*F*	*P-value*	*F crit*
Sample	0.051735	4	0.012934	5.682968	0.011904	3.47805
Columns	0.476381	1	0.476381	209.3167	4.94E-08	4.964603
Interaction	0.05979	4	0.014947	6.567766	0.007362	3.47805
Within	0.022759	10	0.002276			
Total	0.610665	19				

Table A-2. ANOVA of the effect of solution pH on the adsorption of strontium onto RDP, RDP-FC-Cu and RDP-FC-Ni

Source of Variation	*SS*	*df*	*MS*	*F*	*P-value*	*F crit*
Sample	1.18285	4	0.295713	96.72064	1.6E-10	3.055568
Columns	1.3533307	2	0.676665	221.3214	7.36E-12	3.68232
Interaction	0.0936289	8	0.011704	3.827977	0.012124	2.640797
Within	0.0458608	15	0.003057			
Total	2.6756705	29				

Table A-3. ANOVA of the effect of lithium-ion concentration on the adsorption onto RDP, RDP-FC-Cu and RDP-FC-Ni

Source of Variation	*SS*	*df*	*MS*	*F*	*P-value*	*F crit*
Sample	52.32406	9	5.813784	4504.152	1.96711E-44	2.210697
Columns	137.5064	2	68.75321	53265.64	5.5313E-54	3.31583
Interaction	122.4297	18	6.80165	5269.488	1.54379E-47	1.960116
Within	0.038723	30	0.001291			

	312.298	5				
Total	9	9				

Table A-4. ANOVA of the effect of strontium-ion concentration on the adsorption onto RDP, RDP-FC-Cu and RDP-FC-Ni

Source of Variation	*SS*	*df*	*MS*	*F*	*P-value*	*F crit*
Sample	93.02871	9	10.33652352	46874.11467	1.09481E-59	2.210697
Columns	111.3369	2	55.66847465	252445.6563	4.05941E-64	3.31583
Interaction	27.79023	18	1.543901465	7001.291504	2.17875E-49	1.960116
Within	0.006615	30	0.000220517			
Total	232.1625	59				

Table A-5. ANOVA of the effect of temperature on the adsorption of lithium onto RDP

Source of Variation	*SS*	*df*	*MS*	*F*	*P-value*	*F crit*
Sample	273.4029785	9	30.37811	3039.753	7.12234E-42	2.210697
Columns	58.7476501	2	29.37383	2939.26	3.84271E-35	3.31583
Interaction	69.73126063	18	3.873959	387.6436	1.41188E-30	1.960116
Within	0.29980833	30	0.009994			
Total	402.1816975	59				

Table A-6. ANOVA of the effect of temperature on the adsorption of lithium onto RDP-FC-Cu

Source of Variation	*SS*	*df*	*MS*	*F*	*P-value*	*F crit*
Sample	0.779763991	9	0.08664	39.22792	3.57119E-14	2.210696983

Columns	4.140585782	2	2.070293	937.3601	9.10649E-28	3.315829501
Interaction	1.566753521	18	0.087042	39.40967	4.7826E-16	1.960115912
Within	0.066259236	30	0.002209			
Total	6.553362473	59				

Table A-7. ANOVA of the effect of temperature on the adsorption of lithium onto RDP-FC-Ni

Source of Variation	*SS*	*df*	*MS*	*F*	*P-value*	*F crit*
Sample	3.784655	9	0.420517248	685.1677422	3.37609E-32	2.210696 98
Columns	1.950716	2	0.975358 06	1589.194933	3.65184E-31	3.315829 5
Interaction	5.010625	18	0.278368037	453.5576133	1.35794E-31	1.960115 91
Within	0.018412	30	0.000613744			
Total	10.76441	59				

Table A-8. ANOVA of the effect of temperature on the adsorption of strontium onto RDP

Source of Variation	*SS*	*df*	*MS*	*F*	*P-value*	*F crit*
Sample	83.81012	9	9.312236	38993.24	1.73133E-58	2.210697
Columns	88.1363	2	44.06815	184527.1	4.46619E-62	3.31583
Interaction	18.7032	18	1.039067	4350.897	2.7276E-46	1.960116
Within	0.007164	30	0.000239			
Total	190.6568	59				

Table A-9. ANOVA of the effect of temperature on the adsorption of strontium onto RDP-FC-Cu

Source of Variation	*SS*	*df*	*MS*	*F*	*P-value*	*F crit*
Sample	82.53441	9	9.17049	99685.74	1.33E-64	2.210697
Columns	45.60457	2	22.80228	247867.1	5.34E-64	3.31583
Interaction	24.67321	18	1.370734	14900.25	2.63E-54	1.960116
Within	0.00276	30	9.2E-05			
Total	152.8149	59				

Table A-10. ANOVA of the effect of temperature on the adsorption of strontium onto RDP-FC-Ni

Source of Variation	*SS*	*df*	*MS*	*F*	*P-value*	*F crit*
Sample	24.21536	9	2.690596	3839.869	2.15E-43	2.210697
Columns	7.98837	2	3.994185	5700.279	1.93E-39	3.31583
Interaction	3.931804	18	0.218434	311.7362	3.62E-29	1.960116
Within	0.021021	30	0.000701			
Total	36.15655	59				

Table A-11. ANOVA of the effect of 1M HCL and 0.5M HCL on the desorption of lithium from RDP, RDP-FC-Cu and RDP-FC-Ni

Source of Variation	*SS*	*df*	*MS*	*F*	*P-value*	*F crit*
Between Groups	0.000196	1	0.000196	1.099852	0.353483	7.708647
Within Groups	0.000714	4	0.000179			
Total	0.000911	5				

Table A-12. ANOVA of the effect of 1M HCL and 0.5M HCL on the desorption of strontium from RDP, RDP-FC-Cu and RDP-FC-Ni

Source of Variation	*SS*	*df*	*MS*	*F*	*P-value*	*F crit*
Between Groups	0.328886	1	0.328886	0.015895	0.905754	7.708647
Within Groups	82.7627	4	20.69068			
Total	83.09159	5				

Table A-13. ANOVA of the effect of the presence of lithium and strontium as competing ions on the adsorption onto RDP, RDP-FC-Cu and RDP-FC-Ni

Source of Variation	*SS*	*df*	*MS*	*F*	*P-value*	*F crit*
Sample	0.418791	1	0.418791	8820.644	9.82E-11	5.987378
Columns	0.88343	2	0.441715	9303.481	3.35E-11	5.143253
Interaction	23.73007	2	11.86503	249903.5	1.73E-15	5.143253
Within	0.000285	6	4.75E-05			
Total	25.03257	11				

APPENDIX (B): Adsorption isotherm model plots

(A)

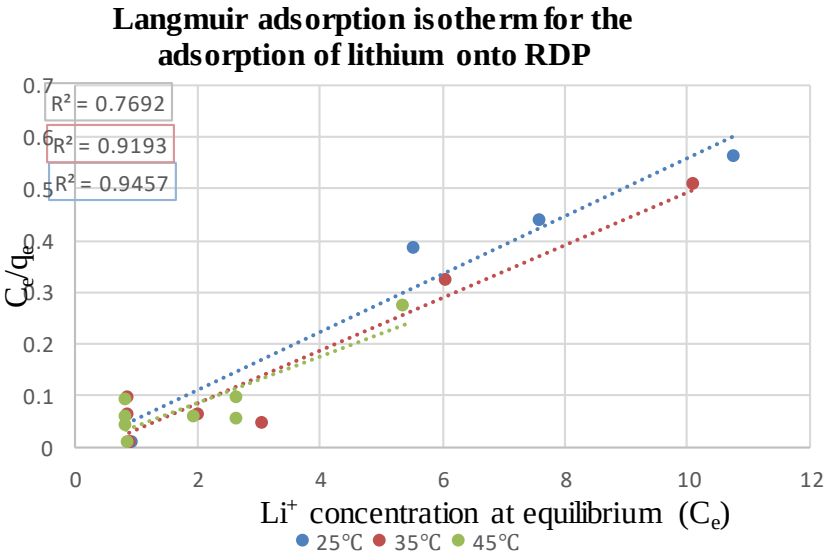

(B)

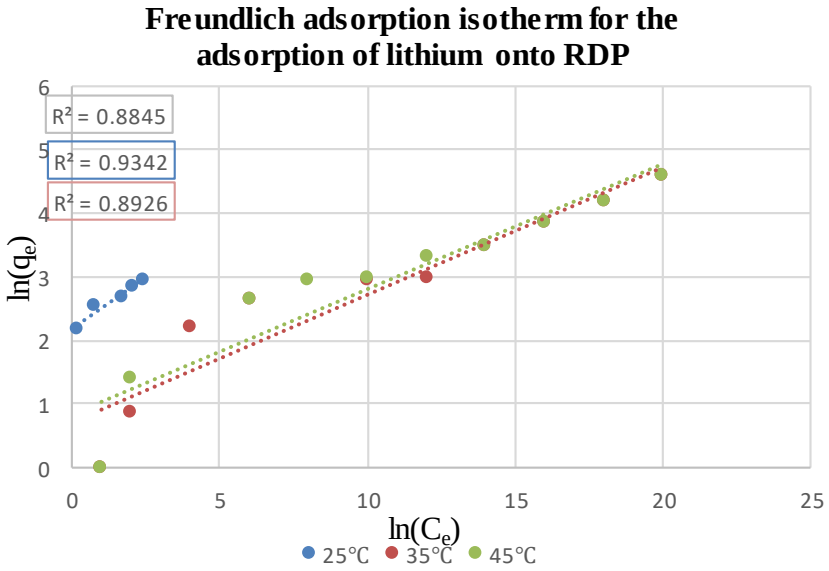

Figure B-1. (A) Langmuir and (B) Freundlich adsorption isotherm model plots for the adsorption of lithium onto RDP.

(A)

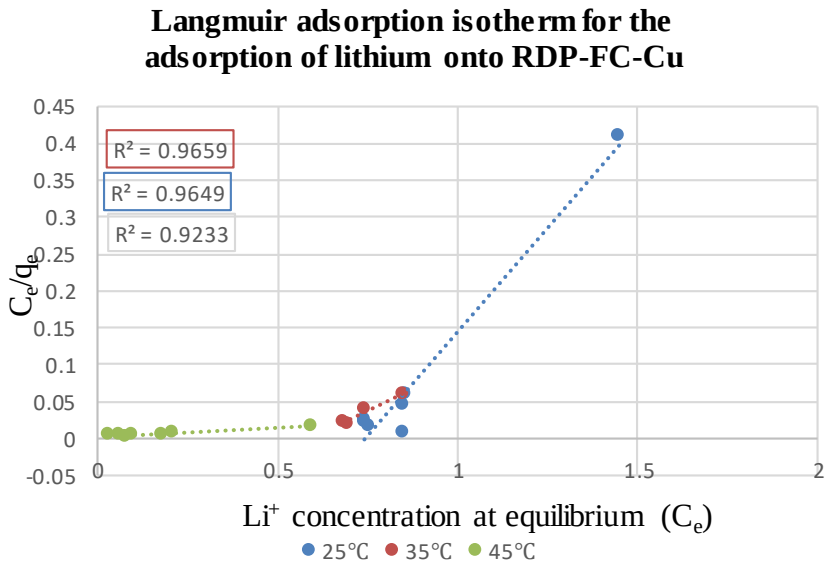

(B)

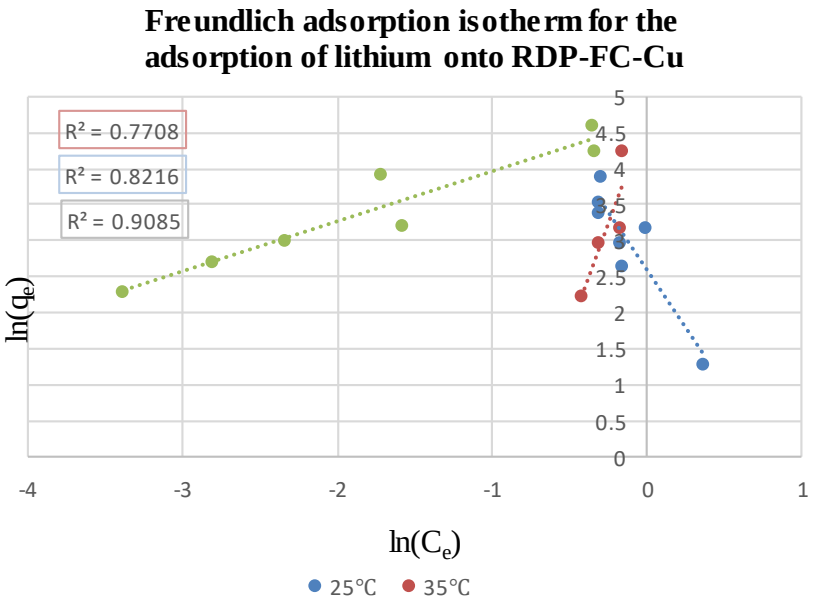

Figure B-2. (A) Langmuir and (B) Freundlich adsorption isotherm model plots for the adsorption of lithium onto RDP-FC-Cu.

(A)

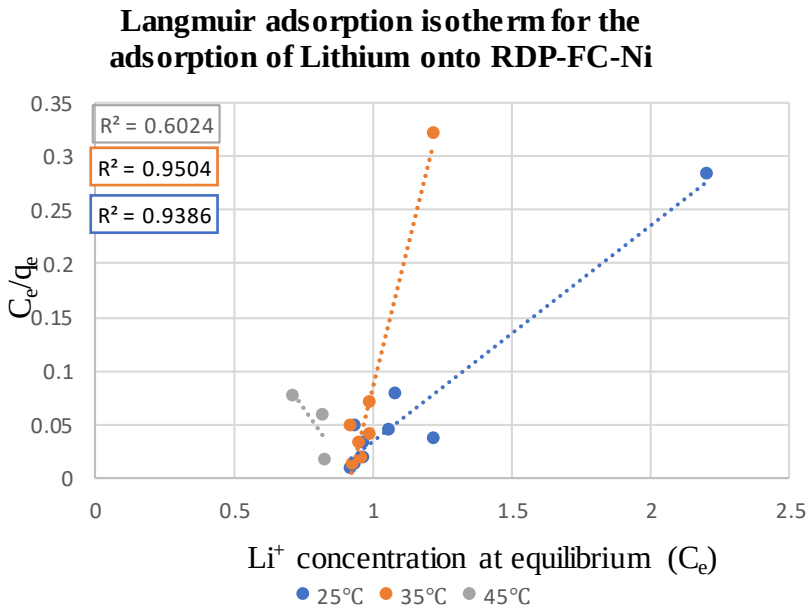

(B)

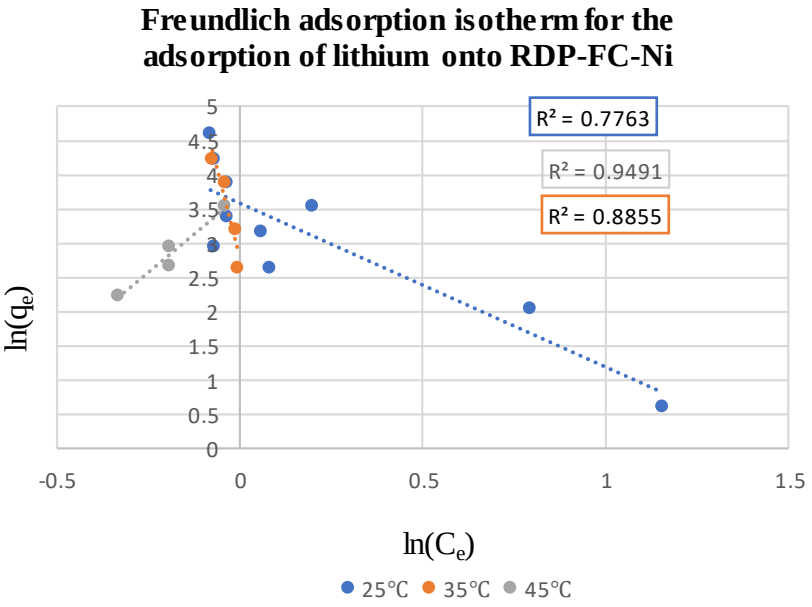

Figure B-3. Langmuir and (B) Freundlich adsorption isotherm model plots for the adsorption of lithium onto RDP-FC-Ni.

(A)

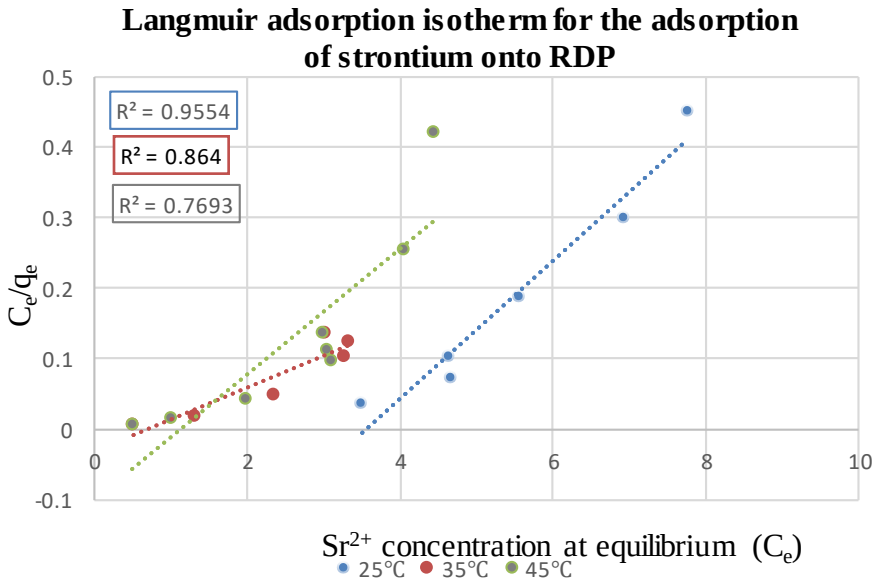

(B)

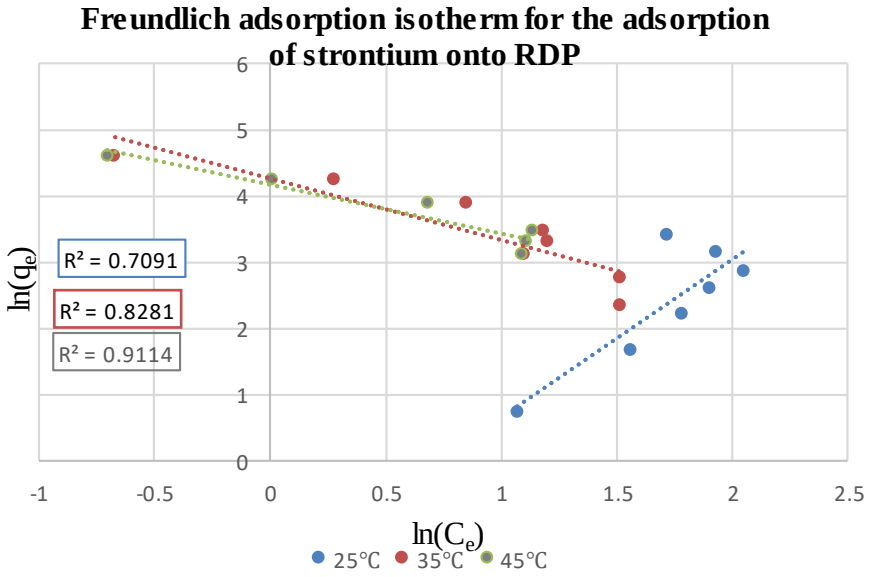

Figure B-4. Langmuir and (B) Freundlich adsorption isotherm model plots for the adsorption of strontium onto RDP.

(A)

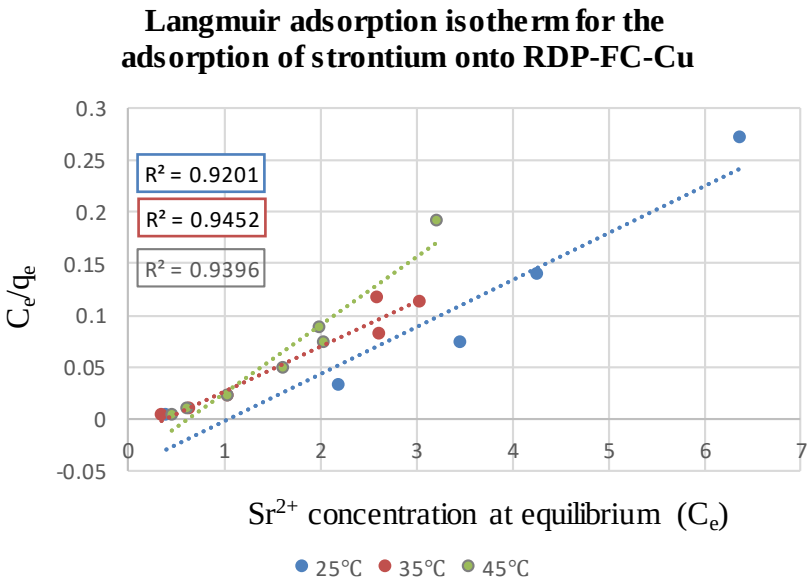

(B)

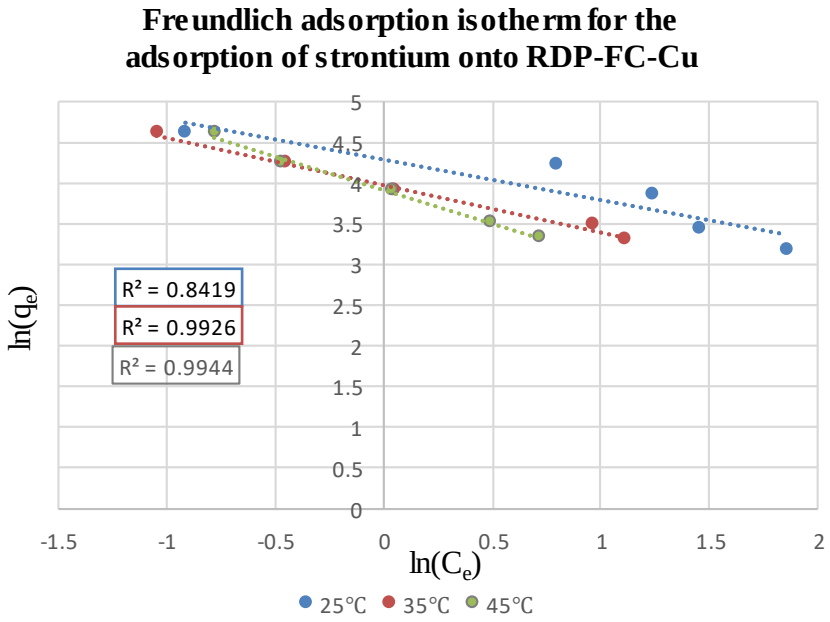

Figure B-5. Langmuir and (B) Freundlich adsorption isotherm model plots for the adsorption of strontium onto RDP-FC-Cu.

(A)

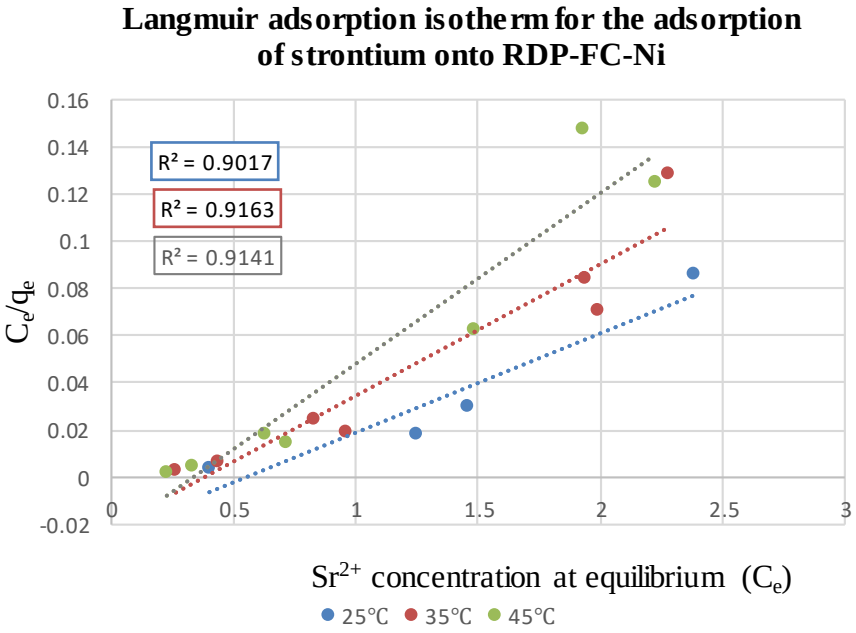

(B)

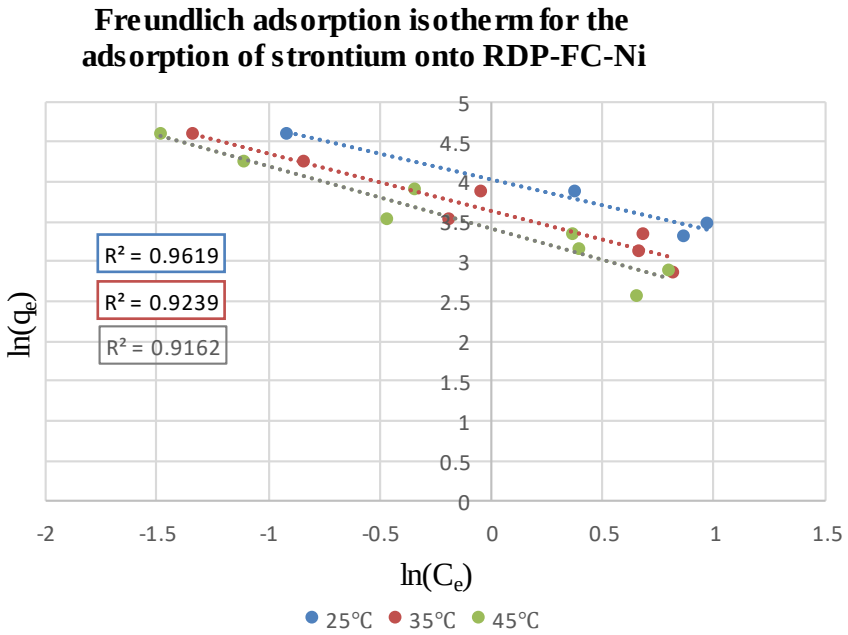

Figure B-6. Langmuir and (B) Freundlich adsorption isotherm model plots for the adsorption of strontium onto RDP-FC-Ni.